

NATIONAL COOPERATIVE HIGHWAY RESEARCH PROGRAM  
REPORT

**105**

**DYNAMIC PAVEMENT LOADS OF  
HEAVY HIGHWAY VEHICLES**

HIGHWAY RESEARCH BOARD  
NATIONAL RESEARCH COUNCIL  
NATIONAL ACADEMY OF SCIENCES—NATIONAL ACADEMY OF ENGINEERING



## HIGHWAY RESEARCH BOARD 1970

### *Officers*

D. GRANT MICKLE, *Chairman*  
CHARLES E. SHUMATE, *First Vice Chairman*  
ALAN M. VOORHEES, *Second Vice Chairman*  
W. N. CAREY, JR., *Executive Director*

### *Executive Committee*

F. C. TURNER, *Federal Highway Administrator, U. S. Department of Transportation (ex officio)*  
A. E. JOHNSON, *Executive Director, American Association of State Highway Officials (ex officio)*  
ERNST WEBER, *Chairman, Division of Engineering, National Research Council (ex officio)*  
DAVID H. STEVENS, *Chairman, Maine State Highway Commission (ex officio, Past Chairman, 1968)*  
OSCAR T. MARZKE, *Vice President, Fundamental Research, U. S. Steel Corporation (ex officio, Past Chairman, 1969)*  
DONALD S. BERRY, *Department of Civil Engineering, Northwestern University*  
CHARLES A. BLESSING, *Director, Detroit City Planning Commission*  
JAY W. BROWN, *Director of Road Operations, Florida Department of Transportation*  
J. DOUGLAS CARROLL, JR., *Executive Director, Tri-State Transportation Commission, New York*  
HOWARD A. COLEMAN, *Consultant, Missouri Portland Cement Company*  
HARMER E. DAVIS, *Director, Institute of Transportation and Traffic Engineering, University of California*  
WILLIAM L. GARRISON, *School of Engineering, University of Pittsburgh*  
SIDNEY GOLDIN, *Consultant, Witco Chemical Company*  
WILLIAM J. HEDLEY, *Consultant, Program and Policy, Federal Highway Administration*  
GEORGE E. HOLBROOK, *E. I. du Pont de Nemours and Company*  
EUGENE M. JOHNSON, *President, The Asphalt Institute*  
JOHN A. LEGARRA, *State Highway Engineer and Chief of Division, California Division of Highways*  
WILLIAM A. MCCONNELL, *Director, Operations Office, Engineering Staff, Ford Motor Company*  
JOHN J. MCKETTA, *Executive Vice Chancellor for Academic Affairs, University of Texas*  
J. B. McMORRAN, *Consultant*  
D. GRANT MICKLE, *President, Highway Users Federation for Safety and Mobility*  
R. L. PEYTON, *Assistant State Highway Director, State Highway Commission of Kansas*  
CHARLES E. SHUMATE, *Executive Director-Chief Engineer, Colorado Department of Highways*  
R. G. STAPP, *Superintendent, Wyoming State Highway Commission*  
ALAN M. VOORHEES, *Alan M. Voorhees and Associates*

## NATIONAL COOPERATIVE HIGHWAY RESEARCH PROGRAM

### *Advisory Committee*

D. GRANT MICKLE, *Highway Users Federation for Safety and Mobility (Chairman)*  
CHARLES E. SHUMATE, *Colorado Department of Highways*  
ALAN M. VOORHEES, *Alan M. Voorhees and Associates*  
F. C. TURNER, *U. S. Department of Transportation*  
A. E. JOHNSON, *American Association of State Highway Officials*  
ERNST WEBER, *National Research Council*  
DAVID H. STEVENS, *Maine State Highway Commission*  
OSCAR T. MARZKE, *United States Steel Corporation*  
W. N. CAREY, JR., *Highway Research Board*

### *General Field of Design*

#### *Area of General Design*

#### *Advisory Panel C15-5*

JOHN E. MEYER, *Michigan Department of Highways (Chairman)*  
J. L. BEATON, *California Division of Highways*  
H. T. DAVIDSON, *Connecticut Department of Transportation*  
W. B. DRAKE, *Kentucky Department of Highways*  
M. D. GRAHAM, *New York Department of Transportation*  
D. L. HAWKINS, *Texas Highway Department*  
E. M. LAURSEN, *University of Arizona*  
P. C. SKEELS, *Retired*  
F. W. THORSTENSON, *Minnesota Department of Highways*  
W. H. COLLINS, *Federal Highway Administration*  
L. F. SPAINE, *Highway Research Board*

### *Program Staff*

K. W. HENDERSON, JR., *Program Director*  
W. C. GRAEUB, *Projects Engineer*  
J. R. NOVAK, *Projects Engineer*  
H. A. SMITH, *Projects Engineer*  
W. L. WILLIAMS, *Projects Engineer*

HERBERT P. ORLAND, *Editor*  
ROSEMARY S. MAPES, *Editor*  
CATHERINE B. CARLSTON, *Editorial Assistant*  
L. M. MacGREGOR, *Administrative Engineer*



NATIONAL COOPERATIVE HIGHWAY RESEARCH PROGRAM  
REPORT **105**

## DYNAMIC PAVEMENT LOADS OF HEAVY HIGHWAY VEHICLES

ALLAN P. WHITTEMORE, JOHN R. WILEY,  
PHILLIP C. SCHULTZ, AND DONALD E. POLLOCK  
GENERAL MOTORS CORPORATION  
MILFORD, MICHIGAN

RESEARCH SPONSORED BY THE AMERICAN ASSOCIATION  
OF STATE HIGHWAY OFFICIALS IN COOPERATION  
WITH THE FEDERAL HIGHWAY ADMINISTRATION

NAS-NAE

DEC 21 1970

LIBRARY

SUBJECT CLASSIFICATIONS:  
PAVEMENT PERFORMANCE  
ROAD USER CHARACTERISTICS

HIGHWAY RESEARCH BOARD  
DIVISION OF ENGINEERING      NATIONAL RESEARCH COUNCIL  
NATIONAL ACADEMY OF SCIENCES—NATIONAL ACADEMY OF ENGINEERING      1970

## **NATIONAL COOPERATIVE HIGHWAY RESEARCH PROGRAM**

Systematic, well-designed research provides the most effective approach to the solution of many problems facing highway administrators and engineers. Often, highway problems are of local interest and can best be studied by highway departments individually or in cooperation with their state universities and others. However, the accelerating growth of highway transportation develops increasingly complex problems of wide interest to highway authorities. These problems are best studied through a coordinated program of cooperative research.

In recognition to these needs, the highway administrators of the American Association of State Highway Officials initiated in 1962 an objective national highway research program employing modern scientific techniques. This program is supported on a continuing basis by funds from participating member states of the Association and it receives the full cooperation and support of the Federal Highway Administration, United States Department of Transportation.

The Highway Research Board of the National Academy of Sciences-National Research Council was requested by the Association to administer the research program because of the Board's recognized objectivity and understanding of modern research practices. The Board is uniquely suited for this purpose as it maintains an extensive committee structure from which authorities on any highway transportation subject may be drawn, it possesses avenues of communications and cooperation with federal, state, and local governmental agencies, universities, and industry, its relationship to its parent organization, the National Academy of Sciences, a private, nonprofit institution, is an insurance of objectivity, it maintains a full-time research correlation staff of specialists in highway transportation matters to bring the findings of research directly to those who are in a position to use them.

The program is developed on the basis of research needs identified by chief administrators of the highway departments and by committees of AASHO. Each year, specific areas of research needs to be included in the program are proposed to the Academy and the Board by the American Association of State Highway Officials. Research projects to fulfill these needs are defined by the Board, and qualified research agencies are selected from those that have submitted proposals. Administration and surveillance of research contracts are responsibilities of the Academy and its Highway Research Board.

The needs for highway research are many, and the National Cooperative Highway Research Program can make significant contributions to the solution of highway transportation problems of mutual concern to many responsible groups. The program, however, is intended to complement rather than to substitute for or duplicate other highway research programs.

### **NCHRP Report 105**

Project 15-5 FY '68  
ISBN 0-309-01893-5  
L C Card No. 73-608741

**Price: \$5.00**

This report is one of a series of reports issued from a continuing research program conducted under a three-way agreement entered into in June 1962 by and among the National Academy of Sciences-National Research Council, the American Association of State Highway Officials, and the Federal Highway Administration. Individual fiscal agreements are executed annually by the Academy-Research Council, the Federal Highway Administration, and participating state highway departments, members of the American Association of State Highway Officials.

This report was prepared by the contracting research agency. It has been reviewed by the appropriate Advisory Panel for clarity, documentation, and fulfillment of the contract. It has been accepted by the Highway Research Board and published in the interest of effective dissemination of findings and their application in the formulation of policies, procedures, and practices in the subject problem area.

The opinions and conclusions expressed or implied in these reports are those of the research agencies that performed the research. They are not necessarily those of the Highway Research Board, the National Academy of Sciences, the Federal Highway Administration, the American Association of State Highway Officials, nor of the individual states participating in the Program.

Published reports of the

### **NATIONAL COOPERATIVE HIGHWAY RESEARCH PROGRAM**

are available from:

Highway Research Board  
National Academy of Sciences  
2101 Constitution Avenue  
Washington, D. C. 20418

(See last pages for list of published titles and prices)



# FOREWORD

*By Staff*

*Highway Research Board*

This report is recommended primarily to researchers interested in defining the dynamic loads that can be expected from heavy vehicles excited by pavement irregularities. General Motors Corporation has successfully described techniques for the measurement and computation of dynamic tire-road interface forces of heavy vehicles, but the techniques have been applied to only three vehicles. Because some of the research findings are based on only the test vehicles, caution should be exercised in drawing broad conclusions.

---

As vehicles pass over highway pavements and structures they impose loads at the tire-road interface that are a combination of vehicle static weight and induced dynamic forces. The dynamic forces result from the motions imparted to the vehicle by road surface irregularities, and their magnitude depends on vehicle characteristics, vehicle speed, and the nature of the road surface irregularities.

The dynamic forces influence the life expectancy of bridges and pavements by an unknown amount. Bridges may be particularly susceptible to damage for the case of a vehicle loaded at or above the legal limit and the vehicle dynamic characteristics producing large impact factors. The variable nature of dynamic responses of heavy vehicles may severely complicate the problem of predicting pavement performance over its design life.

In line with this need, General Motors Corporation undertook a review of the state of the art; development of techniques to obtain the required information by the design and construction of equipment and instrumentation; measurement of the pertinent characteristics of different types of heavy vehicles, including static and dynamic axle loads, suspension effects, and sizes and dimensions; and development and experimental verification of a method to predict the dynamic loads that will appear at the tire-road interface.

This report deals with the measurement and prediction of dynamic tire-road interface forces of heavy trucks. The development of equipment to provide a continuous, accurate measurement of tire-road interface forces is discussed, and pavement loads from three test vehicles—under a variety of speed, load, and road conditions—are presented in several different data analysis forms. Also presented is a time domain analog simulation technique for predicting dynamic pavement loads based on measured road profiles and known vehicle characteristics. The simulation is used to determine the relative effects of vehicle parameters on dynamic pavement loading, and correlation between measured and predicted loads is discussed. Two other pavement load prediction techniques are also discussed.

Now that techniques, equipment, and methodology for predicting dynamic loads at the tire-road interface from pavement profiles and vehicle characteristics have been developed, there remains the monumental task of empirically verifying the methodology. This requires determination of the responses of a sufficiently large sampling of heavy vehicles to produce the large body of data necessary to support conclusions that can bear on design specifications, maintenance policies, and prediction of pavement and structure performance.



# CONTENTS

1	SUMMARY
	<b>PART I</b>
1	CHAPTER ONE Introduction and Research Approach History Objectives Research Plan
2	CHAPTER TWO Findings Literature Survey Survey of Highway Vehicle Types and Their Dynamic Pavement Loads Test Road Selection and Profile Study Pavement Load Measurement Systems Development Identification of Factors Affecting Dynamic Pavement Loads Pavement Load Measurements Pavement Load Prediction Techniques Dynamic Pavement Load Prediction Using Analog Computation Techniques Variation of Parameters Study
25	CHAPTER THREE Appraisal and Applications Dynamic Pavement Load Data Dynamic Pavement Load Measurement Systems Pavement Load Prediction Technique
26	CHAPTER FOUR Suggested Research Pavement Loads Related to Wheel Rotation Pavement Load Studies of Tandem-Axle Vehicles Pavement Load Prediction Techniques The Effect of Vehicle Properties on Dynamic Pavement Loading Study of Tire/Road Interface Shear Loads Data Presentation Techniques Pavement Surveillance
27	REFERENCES
	<b>PART II</b>
28	APPENDIX A Literature Survey, Bibliography and Abstracts
33	APPENDIX B Vehicle Type Designation
34	APPENDIX C Test Vehicle Specifications
35	APPENDIX D Test Road Section Specifications
36	APPENDIX E GM Profilometer and Its Use on This Project



38	APPENDIX F	Computation of Power Spectral Density Functions: Techniques and Errors
41	APPENDIX G	Road Profile Power Spectral Density Functions
44	APPENDIX H	Tire Pressure Transducer System
46	APPENDIX I	Strain-Gaged Axle Housing Transducer System
50	APPENDIX J	Wheel Force Transducer System
62	APPENDIX K	Hydraulic Shaker Tests
63	APPENDIX L	Initial Road Tests
69	APPENDIX M	Study of Pavement Loads Related to Wheel Rotation
73	APPENDIX N	Deterministic Profile Tests
74	APPENDIX O	Repeatability Studies
75	APPENDIX P	Pavement Load Data—Strip Charts and Probability Densities
77	APPENDIX Q	Frequency Domain Prediction Techniques
78	APPENDIX R	Simulation of Tire Enveloping
81	APPENDIX S	Development of a Quarter-Vehicle Analog Simulation
87	APPENDIX T	Correlation Data for Measured and Computed Pavement Loads
90	APPENDIX U	Factors That Limited Prediction Technique Accuracy
91	APPENDIX V	Variation of Parameters Study

## ACKNOWLEDGMENTS

The research reported herein was performed under NCHRP Project 15-5 by General Motors Corporation. Contract negotiation, program administration, and the literature survey were done by Ralph W Hawkins and the Principal Investigator, Donald E Pollock, of the Military Projects Group, Engineering Staff. Experimental and analytical studies were conducted by the following staff members of the General Motors Proving Ground, Noise and Vibration Laboratory. Planning and coordination, H W Larsen and A P Whittemore, experimental measurements, J R Wiley, analog computation, P. C Schultz and H D Stewart, digital computation, D M Briggs, data processing, K D Spietz, road profiling, C A Teal; technical assistance, R B Hayward, P M Majernik, R. E. Ruckert, and L W Slagle.

The General Motors Truck and Coach Division contributed test vehicles for this project on a loan basis. This conserved

funds for other facets of the program and resulted in increased findings.

The considerable advisory assistance of Professor Bayard E Quinn of Purdue University, project consultant, is gratefully acknowledged. His expertise in the field of frequency domain analysis and his broad experience in highway engineering practices were invaluable.

The opportunity to repeatedly use the Embedded Electronic Scale Facility of the Michigan Department of State Highways permitted important preliminary work and greatly contributed to the success of this project. Paul Milliman arranged for use of the scale facility. Gale Otto and John Darlington of the Physical Research Section assisted with the scale load measurements. Mr. Milliman also recommended suitable roads of specified roughness to be used as test roads during this project.



# DYNAMIC PAVEMENT LOADS OF HEAVY HIGHWAY VEHICLES

## SUMMARY

- Two reliable, accurate, instantaneous, on-board systems for measuring dynamic pavement load on a long-term, continuous basis were developed for heavy highway vehicles and were used extensively during this project.
  - Dynamic reactions of vehicles to road surface irregularities common to public highways can produce variable pavement loads that are more than double the static loads.
  - A data set of the measured pavement loads for heavy vehicles traversing various public highways is presented.
  - Dynamic loads related to wheel rotation were measured and were judged to be of sufficient magnitude to warrant further study.
  - An analog computer simulation of a heavy highway vehicle predicted pavement loads from recorded road profiles with an over-all accuracy of 85%.
  - Tire stiffness, tire enveloping properties, and the weight of the unsprung mass were computed to have a major influence on the magnitude of pavement loads.
- 

## CHAPTER ONE

### INTRODUCTION AND RESEARCH APPROACH

#### HISTORY

One element of the criteria used in the design of bridges and pavements is the loading to be expected—both magnitude and number of applications—during the lifetime of the structure. Of highest interest and concern is the loading applied to these structures by heavy highway vehicles. Traditionally, the loading element of the design criteria has been accounted for through use of specified truck dimensions and weights, with the addition of overload factors calculated as a percentage of the specified weight. These loads are equivalent, respectively, to vehicle static weight and dynamic load. The latter has been considered a variable and largely unknown quantity.

Although it is assumed that the life expectancy of pavement and bridge structures is influenced by dynamic vehicle loads, the degree of influence has been a point of

conjecture, because of their unknown nature. Because of this, a complete and comprehensive study and subsequent understanding of the nature and magnitude of heavy vehicle dynamic loads has been considered a desirable goal.

To gain an understanding of dynamic pavement loading, a study of the factors that influence it is necessary. These factors are. (1) pavement surface profile (roughness), (2) certain characteristics of the vehicle(s), and (3) the mode of vehicle operation. Pavement surface profile is that profile which is traversed by the rolling tire of the vehicle under consideration. Important vehicle characteristics are weight and weight distribution, method of distributing that weight to the pavement (wheels and tires), and the nature of the elastic suspension system. The important vehicle operating mode that must be considered is speed.

## OBJECTIVES

In view of these considerations, the following research objectives were formulated as part of this project:

1. To examine the dynamic pavement loads inflicted on pavements and bridges by heavy highway vehicles, especially as influenced by pavement roughness characteristics and by certain vehicle characteristics.
2. To learn and specify which, and to what degree, vehicle characteristics influence peak dynamic pavement loads.
3. To develop a technique whereby the dynamic pavement loads can be predicted from a measured road profile and knowledge of vehicle characteristics.

## RESEARCH PLAN

An examination of the project objectives led to the conclusion that good measuring techniques were a critical requirement if success was to be attained. Accurate road profile data would be essential as a simulation input for the prediction of dynamic pavement loads. The accurate measurement of vehicle properties, such as tire and suspension spring rates, axle mass, etc., would be required if the relationship between vehicle characteristics and their influence on dynamic pavement load was to be determined. The need for means to accurately measure the tire/road interface force was foremost, as accurate data would be an essential requirement for prediction technique verification.

The GM road profilometer, an existing tool for measurement of geometric profiles of road surfaces, was available for use by the researchers. Methods of measuring certain vehicle characteristics were common practice in the automotive industry. It was believed that although some techniques for measurement of the tire/road interface force had been investigated, results had been inconclusive and considerable effort would have to be devoted to investigation and development of accurate and usable force-measuring equipment.

The research plan developed from these objectives divided the work into three phases: (1) survey, (2) experi-

mental, and (3) simulation and prediction. A general description of the tasks to be performed in each phase is outlined as follows:

1. *Literature and field surveys* consisted of:
  - a. A literature search relating to dynamic vehicle loadings of highways and bridges to provide background, and to assure that the work would be complementary and additional to related projects.
  - b. A vehicle survey to determine which vehicles, and vehicle characteristics, produce the largest dynamic loads and which would be pertinent for further analysis and test.
2. The *experimental phase* was designed to include:
  - a. The development of a tire/road force measuring device. This included the investigation of the tire pressure transducer method and, if necessary, the design and construction of an instrumented wheel or other device.
  - b. The selection of highway test sections. Three roughness grades for each of rigid, flexible, and overlay road surfaces (total of nine test sections) were to be selected in cooperation with highway consultants.
  - c. Operation of the selected instrumented vehicles and the GM profilometer over local and selected road surfaces. The resulting experimental data would be used in the simulation and prediction phase for dynamic load prediction technique verification.
3. *Simulation and prediction* was divided into three tasks.
  - a. To develop a simulation model based on the masses, moments of inertia, and suspension system characteristics of the selected vehicle.
  - b. To compare the theoretical results with the data obtained from the experimental phase.
  - c. To develop a dynamic load prediction technique based on experimental data and vehicle simulation results.

## CHAPTER TWO

# FINDINGS

## LITERATURE SURVEY

A literature survey was conducted to determine the applicability of previous work to the objectives of this project and to ensure that the work would be complementary to past accomplishments. Techniques previously applied and the

results obtained were examined to aid in planning the course of this project.

Of primary interest in the literature survey were methods of measuring dynamic tire/road interface forces, means of presenting dynamic pavement load data which would pro-



vide maximum usefulness to highway designers, and the character and influence of various vehicle parameters on dynamic loads

Of secondary interest were reports on highway or runway roughness measurements, vehicle displacement response characteristics to road profile input, and highway and bridge reactions to vehicle dynamic loads.

A bibliography of the selected literature appears in Appendix A. An abstract of each article of primary interest is included

An examination of the listed literature revealed that a great deal of related work has been accomplished and reported. Also, several suggested methods of predicting dynamic vehicle/highway loads have been presented, but detailed verification of the methods is lacking.

Following completion of the literature survey, it was believed that a successful conclusion of the planned research would provide a valuable addition to the state of the art in the understanding of dynamic tire/road interface forces.

#### SURVEY OF HIGHWAY VEHICLE TYPES AND THEIR DYNAMIC PAVEMENT LOADS

Project objectives required the selection of three test vehicles for dynamic tire/road interface force measurements. The selection of these test vehicles and their specifications was based on the magnitude of tire/road interface forces (pavement loads) and the popularity of vehicle types and suspensions. Considerable investigation was required to make the selection.

As a first step in selecting these vehicles, a highway vehicle survey and pavement load study was conducted by directing 171 vehicles through the Michigan Department of State Highways' I-94 weigh station near Grass Lake, Mich. The preliminary data taken at this facility were invaluable to this project because they provided information for project direction without the usual delays required for instrumentation preparation.

#### I-94 Truck Traffic Survey

The survey involved recording as much information about the vehicles as possible without delaying traffic. Vehicle manufacture, suspension type for each axle, tire size, tire type, and tire pressure were among the vehicle properties of interest. The vehicle designation was recorded for every vehicle and the axle suspension type was recorded for the more popular vehicle types.

#### Vehicle and Axle Types

The axle configuration of the 171 vehicles was noted in order to determine the prevalence of the various vehicle types. Four of the most common vehicle types were separately counted. Table 1 gives this popularity information. Appendix B is a complete list of vehicle types.

#### Suspension Types

The tractor axle suspension types for 171 vehicles and the trailer axle suspension types for 90 semitrailer combinations were counted and are given in Table 2. Most surveyed trucks used leaf spring suspensions. The majority of vehicles used  $10.00 \times 20$  bias ply tires.

#### Electronic Scale Pavement Load Studies

#### I-94 Truck Traffic Study

Pavement loads were studied by directing 171 vehicles over two 3-ft-long embedded electronic scales. The first scale measured the tire/road interface force as each axle passed over the smooth electronic scale. Previous researchers have called this "electronic weight." The other scale measured the peak pavement load of each axle during traverse of a step bump bonded to the leading end of the scale.

Single step bumps were selected for this study for several reasons:

1. A preliminary computer study comparing several

TABLE 1  
VEHICLE AND AXLE TYPE SURVEY






Vehicle Type Survey		Tractor Axle Survey		Semitrailer Axle Survey			
Type	No.	Type	No.	Type	No.		
 	2-D	19	Single	} = 62	Single	19	
	2S1	19	Single		} = 71	Tandem	
	2S2	24	Single			Tandem	
	3S2	47	Tandem	47	Tandem		
Common Vehicles	109				Semitrailers	90	
Other Vehicles	62						
All Vehicles	171						

TABLE 2  
AXLE SUSPENSION-TYPE SURVEY

SUSPENSION TYPE	AXLE TYPES	
	TRACTOR	TRAILER
Leaf spring	140	64
Coil spring	1	0
Torsion bar	5	5
Air	8	10
Unidentified	17	11
All	171	90

bumps showed that a step bump caused loads that were equal to or greater than loads caused by any other shape bump of the same height.

2. The computer study also showed that the maximum dynamic load occurred during initial compression of the tire.

3. A step bump contains components of all frequencies and therefore would not show a preference for any particular vehicle speed and/or characteristics.

A 3/4-in-high × 18-in.-long plywood bump was used for the first 135 vehicles and a similar 3/8-in. bump was used for the remaining 36 vehicles. Vehicle speed, rolling electronic weight per axle, and peak pavement load per axle were measured and recorded for all vehicles. The portion

TABLE 3  
MEASURED PEAK PAVEMENT LOAD STATISTICS  
FOR VARIOUS AXLE TYPES

AXLE TYPE	SAMPLE SIZE	PEAK PAVEMENT LOAD (KIPS)	
		MEAN	RANGE
(a) Step bump height: 3/4 in.			
Steer	72	13.6	5.0-19.5
Single tractor	33	26.7	15.0-37.0
Tandem tractor:	39	—	—
Forward axle	—	21.9	12.8-30.3
Aft axle	—	16.1	6.5-30.0
Single trailer	16	24.2	14.0-35.0
Tandem trailer:	56	—	—
Forward axle	—	19.3	9.0-34.5
Aft axle	—	18.0	5.0-30.3
(b) Step bump height: 3/8 in.			
Steer	18	11.4	5.0-15.5
Single tractor	10	20.5	14.0-31.0
Tandem tractor:	8	—	—
Forward axle	—	16.0	10.0-24.0
Aft axle	—	13.8	9.5-21.0
Single trailer	3	18.0	13.0-26.0
Tandem trailer:	15	—	—
Forward axle	—	15.1	8.0-26.0
Aft axle	—	14.2	8.0-24.0

of the peak pavement load attributable to the step bump (dynamic pavement load) was approximated\* by subtracting the electronic weight from the peak pavement load (Fig. 1).

### Suspension Types

These data were first inspected for differences in dynamic load magnitude between the popular leaf spring suspension and other suspension types (coil spring, torsion bar, or air). No differences in dynamic loads relating to the various suspension types were observed. However, in view of the small sample size of suspension types other than leaf spring, it is likely that minor differences would not be recognized.

### Axle Types

The data were then analyzed to reflect the relative peak pavement load magnitudes of steer axles, single and tandem tractor axles, and single and tandem trailer axles. The mean and range of the peak pavement loads for the 7 axle types for the 90 common semitrailer combinations that passed over the step bumps are given in Table 3. From these data one can select the types of axles that produce large peak pavement loads.

### Electronic Weight and Vehicle Speed

The first drive axle pavement load data for all 171 vehicles were analyzed by studying pavement load variations with respect to electronic weight and vehicle speed. Graphs of both peak pavement load and dynamic pavement load versus electronic weight and vehicle speed were plotted for the 3/4-in. bump (Fig. 2) and the 3/8-in. bump (Fig. 3).

The following observations may be made from these plots:

1. In general, dynamic loads were measured to be an appreciable percentage of static axle weights; therefore, they warrant further investigation.
2. The dynamic loads measured with this group of trucks traversing a step bump apparently are not related to the electronic weight.
3. The largest peak pavement loads were caused by heavily loaded axles.
4. Faster-moving vehicles tend to exhibit somewhat greater dynamic and peak pavement loads.
5. The plotted data exhibit a great deal of scatter; there-

\* The electronic weight may differ from the static weight for several reasons, which are discussed later.

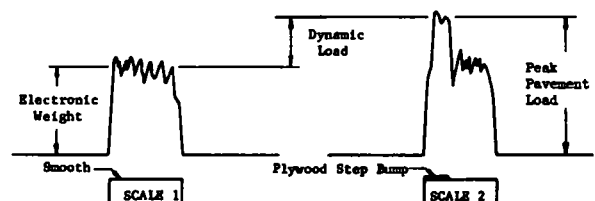


Figure 1 Pavement load nomenclature



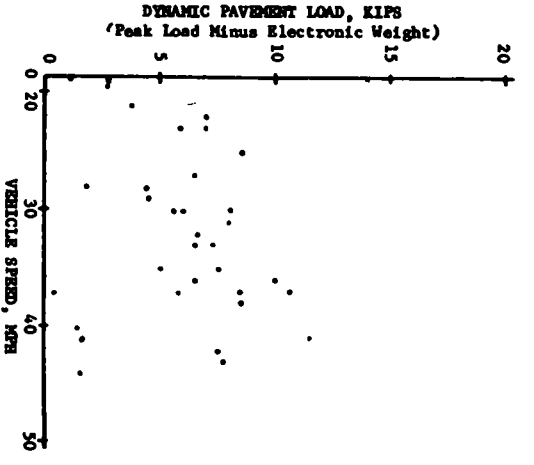
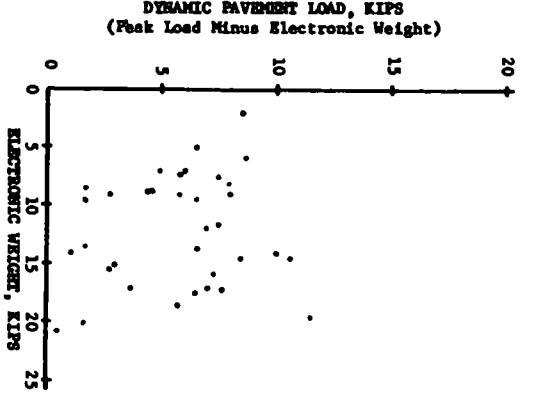
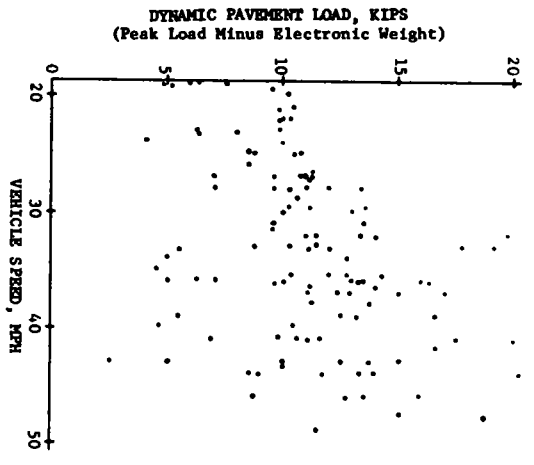
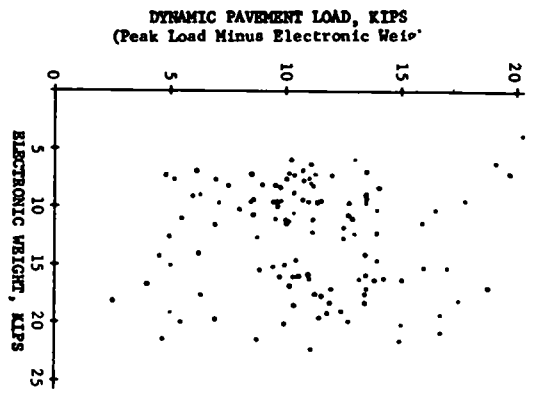
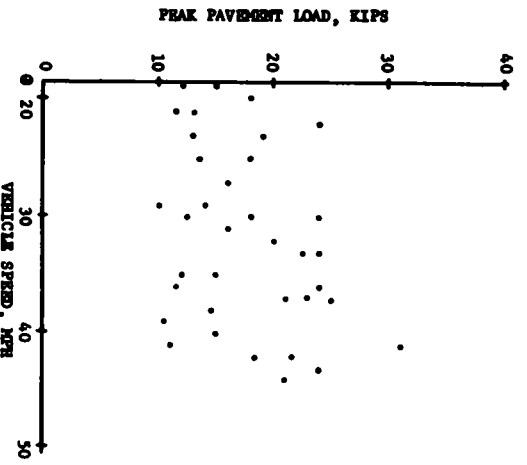
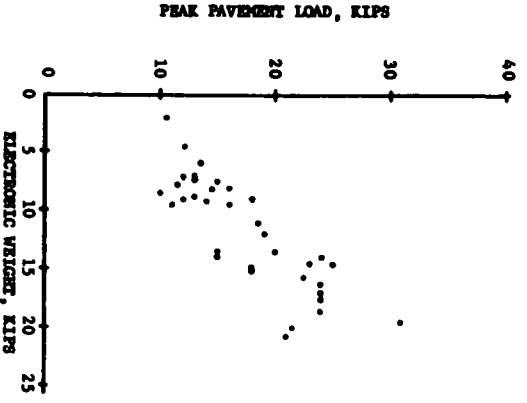
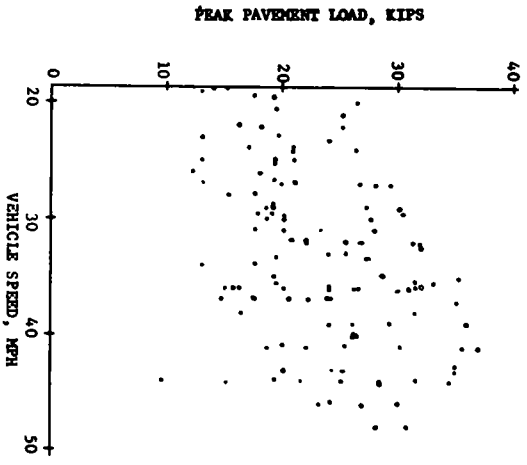
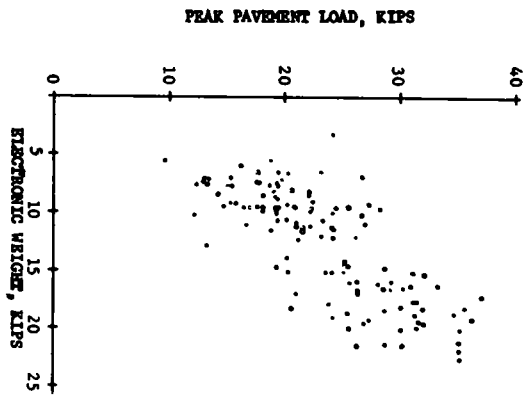


Figure 2. Peak and dynamic pavement load versus electronic weight and vehicle speed for first drive axles

Figure 3. Peak and dynamic pavement load versus electronic weight and vehicle speed for first drive axles.

fore, electronic weight and vehicle speed were not considered to be the only factors affecting pavement load magnitude

#### Rolling Electronic Weight Variations

When the smooth-surfaced electronic scale is traversed by a moving vehicle, the measured load varies during the time each axle is on the scale (Fig. 1). These variations are caused by pavement irregularities in the approach to the scale and by vehicle disturbances such as tire and driveline excitations

Because of these variations, electronic weight could be considered only an estimate of the static weight (1). Inasmuch as the dynamic load was determined by subtracting the electronic weight from the peak load, this uncertainty is part of the dynamic load also.

#### Additional Pavement Load Measurements

In an effort to more accurately measure the dynamic pavement load resulting from a step bump, a modified test procedure was established. A 1/2-in.-high  $\times$  18-in.-long step bump was bonded to the trailing end of a 9-ft-long scale. The peak pavement load was measured when the vehicle contacted the leading edge of the step bump. The instantaneous pavement load immediately prior to encountering the step bump was measured and subtracted from the peak pavement load to yield the dynamic pavement load attributable to the step bump.

The visual average of the electronic scale load record over the 7 1/2 ft of scale prior to the step bump was recorded as the electronic weight. The static (parked) weight of each axle was measured by mechanical scales.

The longer scale permitted meaningful measurements to be taken only on single axles because the aft axle of a tandem set loaded the scale before the forward axle hit the

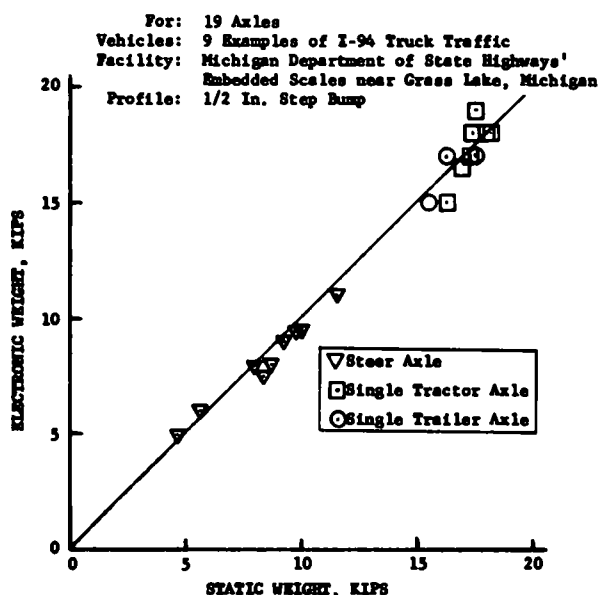


Figure 4 Electronic weight versus static weight

step bump. Therefore, a sample of nine common vehicles was studied. Of these vehicles, 9 steer axles, 7 single tractor axles, and 3 trailer axles were recorded. Figure 4 is a plot of electronic weight versus static (parked) weight for these 19 axles. The electronic weight agreed with the static weight within  $\pm 8\%$ . This was about the maximum reading resolution possible from electronic scale records.

Graphs of both peak pavement load and dynamic pavement load were plotted versus static weight and vehicle speed (Fig. 5). These data support the observations made from the earlier load measurements for 3/4- and 3/8-in. step bumps (Figs. 2 and 3). Initial observation of the dynamic pavement load versus static weight graph (Fig. 5) would lead one to believe that a relationship exists between the two variables. However, the difference between steer axle dynamic loads and tractor drive axle and trailer axle loads may be due to other characteristic differences rather than static weight. For example, tire spring rates on steer axles are typically one-half of the rates on tractor drive axles and trailer axles. When only the 7 tractor and 3 trailer axles are considered, no relationship between dynamic load and static weight is evident.

#### Pavement Load Measurements—Tire Study

Measurements were made at the General Motors Proving Ground Embedded Scale Facility to study differences in pavement load with respect to tire type (bias ply vs radial ply), tire wear, and tire pressure. A 3/4-in.-high  $\times$  18-in.-long step bump was bonded to the trailing end of the embedded scale. The right dual wheels of a 2-D vehicle were driven over the scale at several speeds for each test condition. Figure 6 shows dynamic pavement loads plotted versus vehicle speed for the tire variations. Figure 6 also compares the dynamic and peak pavement loads for this particular vehicle loaded and empty.

1. There are no significant pavement load differences between new and worn bias ply tires.
2. Bias ply tires cause somewhat greater dynamic pavement loads than do radial ply tires.
3. Pavement loads increase with tire pressure.
4. Pavement loads increase slightly with vehicle speed [also shown by measurements made on I-94 truck traffic (Figs. 2 and 3)].
5. Dynamic pavement loads (right side only) are somewhat greater for the unloaded test vehicle, but the peak pavement loads are much greater for the loaded test vehicle.
6. The measured peak pavement loads are representative of vehicles measured during previous work done on I-94 truck traffic (Table 3 and Figs. 2 and 3).

#### Test Vehicle Selection

The selected test vehicles and axles are shown in Figure 7. Detailed vehicle specifications are listed in Appendix C. All vehicles were furnished by General Motors Truck and Coach Division. All three test vehicles had leaf spring suspensions, 7-in. rims, and 10 00  $\times$  20 bias ply tires inflated to 75 psi-cold. All three were loaded to near the legal limit.

Vehicles: 9 Examples of I-94 Truck Traffic  
 Facility: Michigan Department of State Highways'  
 Embedded Scales near Grass Lake, Michigan  
 Profile: 1/2 In. Step Bump

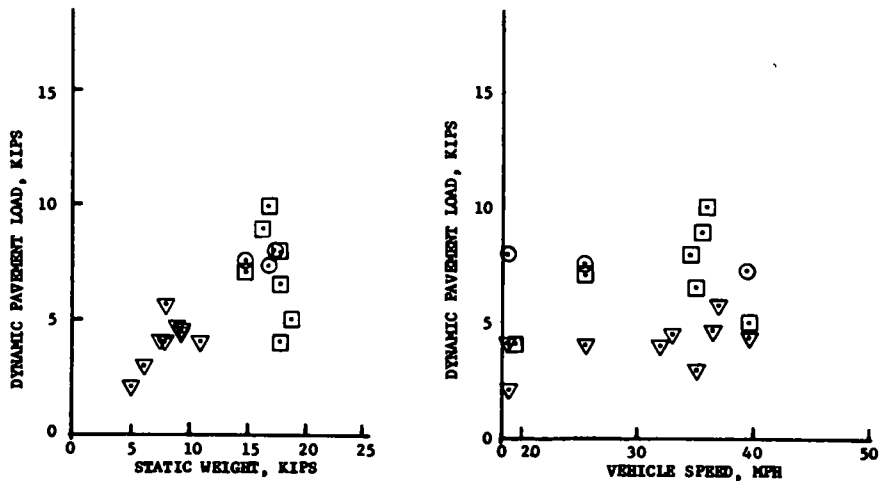
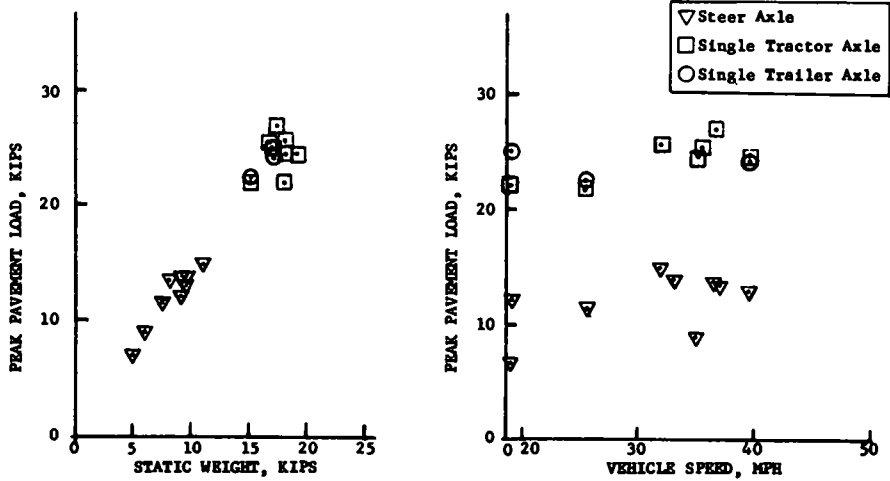


Figure 5. Peak and dynamic pavement load versus static weight and vehicle speed for 19 axles.

Vehicle Axle 2-D, Right Side of the Rear Axle  
 Tire Size 10.00 x 20  
 Profile 3/4-In. Step Bump

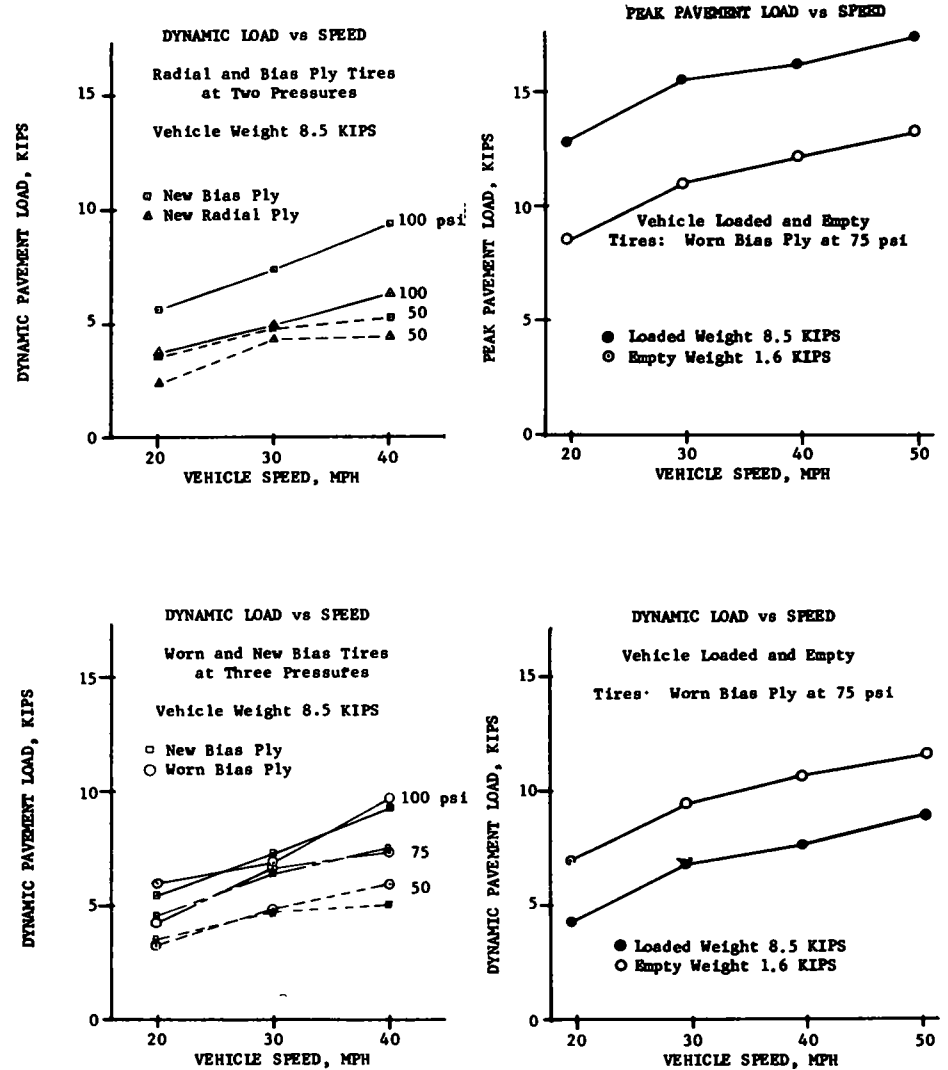
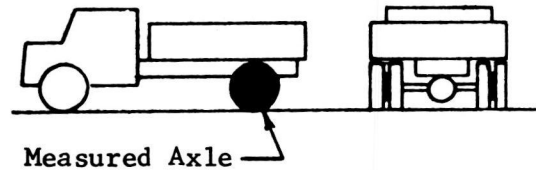


Figure 6. Pavement load measurements—tire study



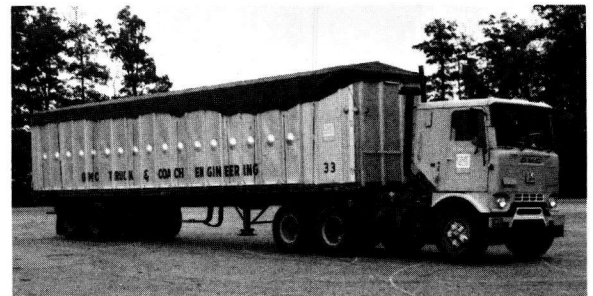
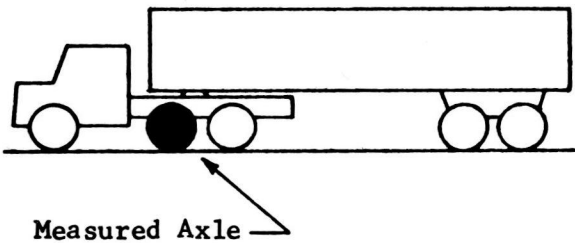
## TEST VEHICLE NO. 1

Single Drive Axle  
 Designation: 2-D Drive  
 Schematic Representation:



## TEST VEHICLE NO. 2

Forward Axle of a Tandem Drive Set  
 Designation: 3S2 Forward Drive  
 Schematic Representation:



## TEST VEHICLE NO. 3

Single Axle Trailer  
 Designation: 3S1 Trailer  
 Schematic Representation:

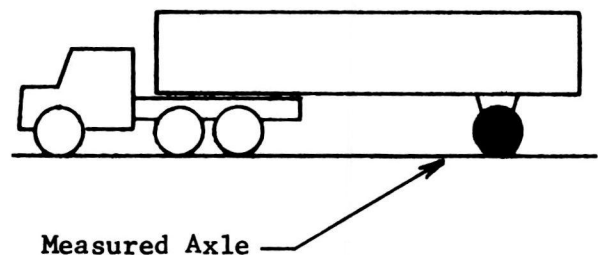


Figure 7. Test vehicle and axle selection.

1. *Test Vehicle No. 1* was selected because the largest peak pavement loads were recorded when single tractors traversed the step bumps (Table 3). This vehicle also was selected for its popularity (Table 1). The vehicle was designated the prime test vehicle for prediction technique development.

2. *Test Vehicle No. 2* was selected to represent tandem-axle suspensions. Tandem-axle tractors are popular (Table 1) and they were associated with significantly large pavement loads (Table 3).

3. *Test Vehicle No. 3* was selected to represent trailer axles. The single-axle trailer was chosen because of large

measured pavement loads (Table 3). The tandem tractor of Test Vehicle No. 2 was used to pull the trailer; thus, Test Vehicle No. 3 was a 3S1 vehicle.

## TEST ROAD SELECTION AND PROFILE STUDY

### Test Road Selection

The Michigan Department of State Highways identified nine 1-mile test road sections to represent good, fair, and poor grades of rigid, flexible, and overlay pavement. The condition of the road sections had been previously graded using a Bureau of Public Roads roughometer. Less than 130 in./mi was specified a good road; 130 to 175 in./mi a fair road, and more than 175 in./mi a poor road. The selected test road sections are described in Appendix D.

### Road Profile Measurements

Road profile inputs were needed for the development of a dynamic pavement load prediction technique. The GM profilometer was used to measure the elevation profiles of all nine test road sections. Appendix E describes the profilometer and its use on this project.

Profiles were first recorded with the profilometer towed behind Test Vehicle No. 1 (Fig. E-2) so that the road profile and pavement load functions would be generated from the same highway track. This technique also permitted exact time correlation of the profile and load signals.

Preliminary observation of the profiles revealed that they contained extraneous signals resulting from profilometer wheel bounce at high profilometer vehicle speeds. This situation was overcome by recording profiles at low vehicle and tape recorder speeds, and then playing back the profiles at a higher tape speed corresponding to the vehicle speed at which dynamic loads were recorded.

### Road Profile Analysis

Digital computer techniques were used to compute power spectral density (PSD) functions for the nine test road sections. A short discussion of PSD functions follows.

When a time-varying quantity such as a road profile or pavement load measurement is analyzed, it is often convenient to treat the particular data signal as a time-varying voltage and apply electrical circuit analysis techniques. One such technique is power spectral density analysis.

Obviously, the total power contained in a time-varying electrical signal can have components at many wavelengths. The power spectral density function shows the distribution of power density (in volts<sup>2</sup>/cps) as a function of frequency or, inversely, wavelength.

When voltage is converted to physical units (such as feet of road profile) the dimensions of the PSD function become ft<sup>2</sup>/cps as shown in Figure 8. This same notion is used later in the report for PSD analysis of pavement load data.

Appendix F contains an explanation of the techniques used, a discussion of the errors encountered during computation, and a discussion of the over-all accuracy of the computation. Figure 8 is a sample PSD plot. Appendix G includes a complete set of these plots.

The PSD functions of all nine test sections had very similar shapes and were generally void of dominant wavelengths. The magnitude of the PSD functions generally increased with increasing wavelengths (increasing wavelength corresponds to decreasing cycles per foot, cpf). The power input to a vehicle at any particular time-based frequency (cps) will therefore be greater for higher vehicle speeds, because higher vehicle speeds correspond to longer wavelengths which have greater PSD ordinate values. For example, the road profile excitation at 10 cps is typically three times greater at 68 mph (10-ft wavelength, 0.1 cpf) than at 34 mph (5-ft wavelength, 0.2 cpf).

The nine test road profiles were ranked for roughness by comparing the PSD functions in the range of wavelengths from 1.67 to 20 ft (0.60 to 0.05 cpf). Table 4 lists the test roads in order of increasing roughness. The Bureau of Public Roads roughness indices also are listed for comparison.

## PAVEMENT LOAD MEASUREMENT SYSTEMS DEVELOPMENT

The force at the tire/road interface can be measured either in the pavement or on the vehicle. Many systems of both types have been developed by previous researchers. Embedded-scale systems measure dynamic pavement loads over the scale length, and are useful for studying loads

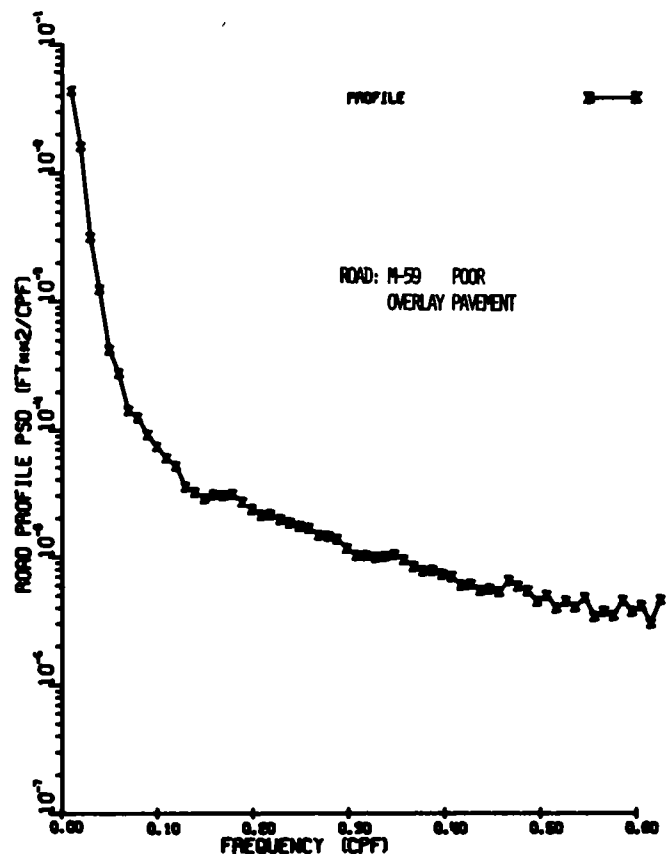


Figure 8 Road profile power spectral density

TABLE 4  
ROUGHNESS ORDERING OF THE TEST ROAD SECTIONS  
BASED ON THE PSD CURVES

ROAD SECTION	COMMENTS	BPR ROUGH-OMETER ROUGHNESS (IN./MI)
M-52	Smoothest test road section	92
M-53 NB <sup>a</sup>	Same as M-52	128
I-75	Slightly rougher than M-53 NB for wavelengths less than 6.7 ft (greater than 0.15 cpf)	118
I-696	Significantly rougher than I-75 at all wavelengths considered	149
M-50	Same as I-696	176
M-247	Rougher than I-696 for wavelengths from 5 to 10 ft (0.2 to 0.1 cpf), otherwise identical	169
M-53 SB <sup>a</sup>	Somewhat rougher than I-696, M-50, M-247 for wavelengths less than 3 ft (greater than 0.3 cpf), otherwise very similar	154
M-59	At least as rough as any preceding road at all wavelengths and considerably rougher at shorter (less than 5 ft) wavelengths (greater than 0.2 cpf)	225
M-138	Somewhat rougher than M-59 for wavelengths from 6.7 to 20 ft (0.15 to 0.05 cpf), otherwise identical	249

<sup>a</sup> The two different test sections on M-53 are differentiated by noting the direction of travel, NB = northbound, SB = southbound

developed by many vehicles over short pavement lengths. On-board vehicle systems measure dynamic pavement loads on a long-term, continuous basis and are useful for studying loads developed by vehicles over many highways.

Pavement load measurements over a variety of road sections required an on-board measurement system. Three devices were considered for these measurements:

1. A differential tire pressure transducer.
2. A strain-gaged axle housing transducer.
3. A wheel force transducer.

Measurement systems using these devices were evaluated by comparing the on-board pavement load signal to a corresponding embedded-scale signal.

The tire pressure system showed nonlinearities and phase shifts in the relationship between the differential tire pressure and the embedded-scale load. A plot of both these parameters versus time shows the differences (Fig. H-4).

Both the strain-gaged axle housing and the wheel force transducer systems accurately measured dynamic loads. Figures I-7 and J-18 show the remarkably good correlation of the analog signals of these systems with the embedded scale analog signal. Both measurement systems were used extensively during this study.

#### Tire Pressure Transducer System

##### Description

A differential tire pressure measurement system provides a simple and convenient pavement load measurement system. Because of the attractive simplicity, a tire pressure

system similar to systems previously reported (2, 3) was fabricated and evaluated. The details of this system appear in Appendix H.

##### Evaluation

The time responses of the tire pressure transducer and an embedded scale to ½-in. step bumps were compared. The traces indicated a definitely nonlinear and phase shifted relationship between the two variables. The observed nonlinearities and frequency response limitations were not considered acceptable for a precision pavement load measurement system; therefore, work on this system was discontinued.

##### Features and Applications

Because the tire pressure system is simple and conveniently adapted to any vehicle, it is appealing and might adequately provide pavement load data in limited frequency and amplitude ranges under specific test conditions.

#### Strain-Gaged Axle Housing Transducer System

##### Description

The strain-gaged axle housing system differed from previously reported strain-gaged axle housing systems (4) in that an inertial force component was added to the force measured in the axle housing to obtain pavement load. This system was an adaptation of a General Motors Proving Ground automotive pavement load measurement technique. Both sides of the rear axle housing of Test Vehicle No. 1

were strain gaged to measure the vertical shear force transmitted through those sections of the axle housing. Two accelerometers were mounted on the axle housing to measure the vertical plane accelerations of the axle assembly (Fig. I-1).

The lateral position of the accelerometers with respect to the wheels was used in the computation of accelerations at the two wheel assembly center lines. An inertial force component for each wheel was computed by multiplying the wheel center line acceleration by the mass of the suspension components outboard of the strain-gage location. The product was added to the axle housing shear force to obtain pavement load. This "outboard mass" included the tires, rims, wheels, brakes, and part of the axle housing. The details of this system are documented in Appendix I.

### *Evaluation*

The vertical shear force, the inertial force, and the computed dynamic pavement load were recorded as the vehicle passed over a ½-in. step bump on a 9-ft embedded scale. These signals were compared to the embedded scale pavement load (Fig. I-7). As shown, the comparison between the strain-gaged axle housing system and the embedded scales was very good. The significance of the inertial force component in determining the pavement load is also clearly demonstrated.

### *Features and Applications*

The strain-gaged axle housing system supplies right side, left side, and total pavement loads. As a result the system is very useful for extensively studying the relationships between various characteristics of one vehicle. Each different vehicle requires a completely new installation and calibration must be performed. The performance of the system is a function of the configuration of the particular test axle; therefore, some axles may not be suitable for strain-gage measurement of axle housing shear forces.

Although very good correlation with embedded scale measurements was obtained, the system did have some deficiencies. The sensitivity of the vertical shear force strain gage bridges was low. The resulting low signal-to-noise ratio limited the maximum potential accuracy of the pavement load measurements. Some machining of the axle housing would have increased the bridge sensitivity. Errors in the inertial force measurement could have been introduced by inaccurate determination of the mass and/or the center of mass of the outboard assembly, or by accelerations resulting from axle bending.

### **Wheel Force Transducer System**

#### *Description*

A truck wheel force transducer system, incorporating principles of operation similar to the strain-gaged axle housing system was developed (Fig. 9). The system consisted of three components.

1. A strain-gaged wheel transducer.
2. A set of accelerometers.
3. Electronic summing networks.

A hub adaptor (Fig. J-10) and the force measurement transducer (Fig. J-1) replaced the conventional cast wheel. The inner ring of the transducer was bolted to the hub adaptor and dual tires and rims were clamped to the outer ring of the transducer. The inner and outer rings were connected by eight laterally oriented beam-type sensing elements (Fig. J-2). These strain-gaged sensing elements, designed for high sensitivity and minimum crosstalk, measured two orthogonal components of the vector force transmitted from the outer to the inner rings in the plane of the wheel.

A set of accelerometers, mounted on the adaptor, measured two orthogonal wheel acceleration components along the force measurement axes. An instrumentation slip ring was mounted on the accelerometer mount base to allow both the force and acceleration signals to be taken from the rotating wheel system (Fig. J-15).

The product of each acceleration component and the mass between the strain-gaged beams and the tire/road interface yielded orthogonal inertial force components of the pavement load. Electronic summing of the inertial force components and the strain-gaged force components gave two orthogonal radial components of the pavement load.

These radial load components rotated with the wheel and neither was referenced to a stationary axis. The instantaneous vector sum of the two components was therefore computed electronically. This vector sum was the resultant pavement load in the plane of the wheel. In practice, this resultant may be treated as vertical with less than 1% error for steady-speed runs with little acceleration or braking. Even under conditions of hard braking or fore-and-aft acceleration, this vector sum represents the maximum force between the pavement and tire, although it may not be vertical. The details of this system appear in Appendix J.

### *Evaluation*

An initial dynamic laboratory evaluation of the wheel force transducer system was accomplished by setting the rear axle of Test Vehicle No. 1 on four electro-hydraulic servo rams, on top of two reference transducers (Fig. 10). "Pavement" loads were recorded while the truck was excited through the rear tires with sinusoidal and step inputs. Correlation between the two transducers was very good. A detailed discussion of this evaluation appears in Appendix K.

A rolling evaluation was performed at the Grass Lake weigh station embedded scales. The resultant dynamic pavement load measured by the wheel force transducer system caused by a ½-in.-high by 3-ft-long haversine bump was compared to corresponding measurements made by the strain-gaged axle housing system and embedded scales. Good correlation between the wheel force transducer system and the embedded scale is shown in Figure J-18.

### *Features and Applications*

This system measures the pavement load at one wheel location only. It permits high-sensitivity, low-crosstalk



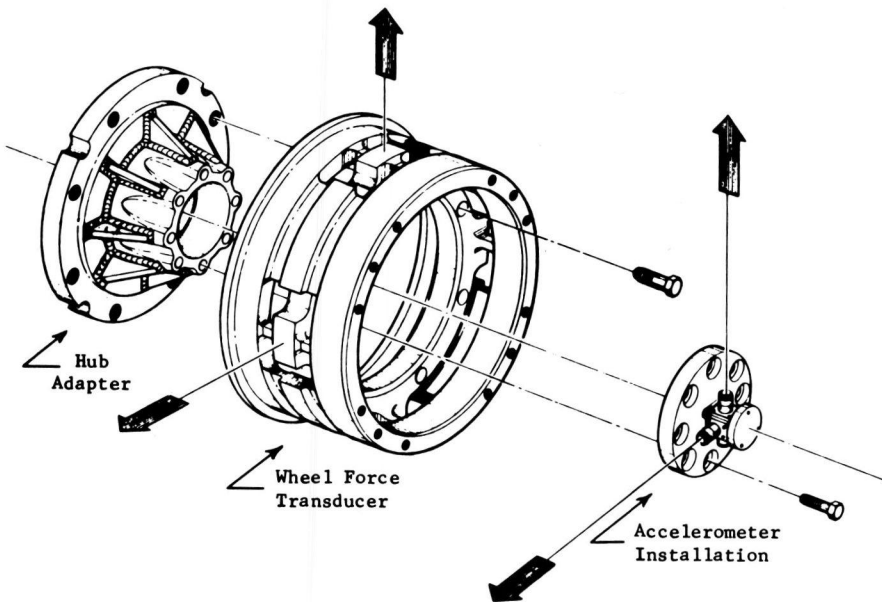


Figure 9. Wheel force transducer system.

pavement load measurements on a number of vehicles without requiring strain gaging and calibration for each vehicle. The system, designed to fit any vehicle with 20-in. or larger rims, is a bolt-on assembly with operating properties that are not affected by individual vehicle characteristics. A great deal of the experimental data on this project, including all of the data on Test Vehicles Nos. 2 and 3, was taken using the wheel force transducer.

#### On-Board Signal Conditioning Instrumentation

The force, acceleration, and pressure transducers all used strain-gaged sensing elements. Bridge excitation voltages, output amplification, and signal conditioning were provided by a carrier amplifier system. The carrier amplifier also included circuitry for applying 100K-ohm shunt calibra-

tions to each bridge. Carrier amplifier outputs were recorded on a Leach, Model MTR 3200, 14-channel instrumentation tape recorder. Power for the carrier amplifier system and the tape recorder was obtained from the test vehicle's electrical system. A vehicle installation is shown in Figure 11.

#### IDENTIFICATION OF FACTORS AFFECTING DYNAMIC PAVEMENT LOADS

Prior to recording pavement loads on the nine test road sections, studies were conducted to evaluate the effects of several factors on pavement loading and to establish procedures for future testing. Factors investigated were:

1. Loads related to wheel rotation.



Figure 10. Test Vehicle No. 1 on hydraulic servo rams.



Figure 11. On-board instrumentation.

2. The relative magnitude of fore-and-aft loads compared to vertical loads.
3. Front and rear axle interaction (vehicle pitch effects).
4. Right wheel to left wheel interaction (e.g., axle tramp effects).
5. Repeatability of load measurements.

These studies were conducted on Test Vehicle No. 1; therefore, the findings should be generally representative of 2-D vehicles. The vehicle was instrumented with strain-gaged axle housing systems to measure vertical pavement loads at all four wheel locations and fore-and-aft loads at the right rear wheel location.

#### Pavement Loads Related to Wheel Rotation

Rear wheel loads measured on a smooth road (Fig. M-1) show that variations of considerable magnitude occurred at first order of wheel rotation frequency (Appendix L). Such loads are commonly associated with tire-rim unbalance, tire nonuniformity, and rim assembly installation misalignment.

A detailed study of these variations was made by running the vehicle on the very smooth roll surface of a chassis dynamometer (Fig. M-3). The study revealed that the load variations were caused primarily by radial runout resulting from rim assembly installation misalignment. This misalignment also causes lateral runout, producing the familiar wheel "wobble."

Loads on each rear wheel varied from a maximum of 2,800 lb peak-to-peak (at 20 mph) to about 1,100 lb peak-to-peak (at 40 mph). At 20 mph, wheel rotation frequency coincided approximately with the bounce resonant frequency of the loaded truck body. The peak amplitudes at a fixed speed were not constant, but varied slowly as the phase relationship between excitations at the right and left wheels changed, causing the excitation to change from hop to tramp.

These loads were considered typical of heavy trucks;

however, in this test program it was not desirable to measure loads generated by the truck system independent of the road surface. A very careful custom installation, involving monitoring of runout during the clamp-tightening procedure, improved rim installation alignment enough to reduce the loads to a maximum of 1,600 lb peak-to-peak at 20 mph and a maximum of less than 800 lb peak-to-peak at speeds over 30 mph. Further details of this study are included in Appendix M.

#### Relative Magnitudes of Vertical and Fore-and-Aft Loads

On a rough road at steady speeds, maximum fore-and-aft pavement loads at the right rear wheel were less than 1,000 lb, or 10% of corresponding vertical loads (Appendix L). Because the fore-and-aft loads are small compared to the vertical loads, the difference between the vertical load and the resultant load in the plane of the wheel is less than 1%. This is an important consideration because throughout this study both resultant loads and loads in the vertical direction were used interchangeably. The strain-gaged axle housing transducer measured vertical load and the wheel force transducer measured the resultant load in the radial plane.

#### Comparison of Front and Rear Pavement Loads

Road tests showed that front axle dynamic pavement loads never exceeded 30% of comparable rear axle dynamic pavement loads (Appendix L). When abrupt obstructions were encountered at the rear axle, simultaneous front axle loads never exceeded 5% of rear axle loads. Rear axle loads occurring simultaneously with abrupt obstructions at the front axle never exceeded 2% of maximum rear axle loads. Figure 12 shows the degree of front-to-rear interaction. These results showed that vehicle pitch motions did not contribute significantly to front or rear axle pavement loads and that rear axle loads could be studied without considering front axle effects. Front axle loads were considered too low to merit further study.

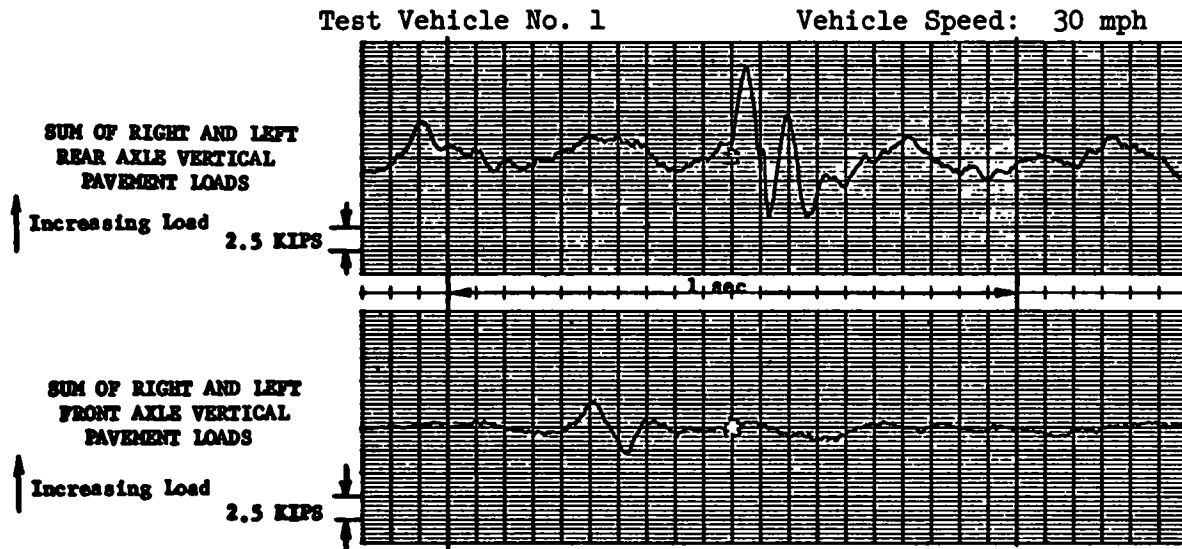


Figure 12. Simultaneous front and rear axle pavement loads

#### Effects of Axle Tramp on Rear Wheel Dynamic Pavement Loads

Significant tramp components were observed in the rear axle pavement load data (Appendix L). This indicated that consideration of total pavement loads for the axle may be misleading. That is, one-side wheel loads are not always equal to one-half of total axle loads.

The degree of tramp coupling was determined by measuring rear axle loads (right and left sides) as the right side of the vehicle was driven over a series of step, ramp, haversine, and impact bumps (Appendix N).

Left wheel dynamic loads measured when only the right wheels traversed the bumps were typically 30% of the dynamic loads developed at the right wheel. Right wheel dynamic loads developed when only the right wheels traversed the bumps were 70% to 85% of the right wheel dynamic loads developed when both wheels traversed the bumps (Fig. N-1). This corresponded to a difference in peak pavement load of less than 12%.

#### Repeatability of Pavement Load Measurements

An estimate of pavement load measurement repeatability was obtained by driving the vehicle over a step bump several times under identical conditions of vehicle speed, vehicle load, and tire pressure (Appendix O). It was found that measurements of peak pavement load were repeatable within  $\pm 3\%$ , and measurements of dynamic pavement load were repeatable within  $\pm 10\%$ .

#### PAVEMENT LOAD MEASUREMENTS

One important objective of the experimental work on this project involved the measurement, analysis, and publication of pavement load data that are representative of heavy highway vehicles. Three test vehicles, representing the majority of heavy highway vehicles, were selected for this purpose (Fig. 7 and Appendix C). Nine test road

sections, representing a variety of pavement types and conditions, were also selected (Appendix D). All of the measurements in this portion of the test program were made using the wheel force transducer system; therefore, the reported pavement loads are for one wheel set only. For consistency, right-wheel loads were measured.

#### Test Conditions

##### Vehicle Speed

I-94 truck traffic monitoring failed to indicate a definite relationship between peak pavement loads and vehicle speed when traversing step bumps (Figs. 2 and 3); therefore, the following test speeds were selected to further study the effect of vehicle velocity:

1. 34 mph (50 fps).
2. 55 mph (80 fps).
3. A speed sweep from 15 to 55 mph.

Thirty-four mph was selected as a convenient moderate speed. Fifty-five mph was selected as a realistic maximum for the test roads. On some of the roads 55 mph could not be attained. The speed sweep was run to aid in detecting any large pavement loads that might result from vehicle sensitivities to specific speeds.

##### Static Axle Weight

Because preliminary tests showed that maximum pavement loads occurred with maximum static weight (Figs. 2 and 3), each test vehicle was loaded to near its legal static weight limit.

##### Additional Measurements

To obtain pavement load data for an unloaded vehicle, Test Vehicle No. 1, with a 6.1-kip static axle weight, was

run at 34 and 65 mph on a "good" test road (I-75) and a "poor" test road (M-59).

To obtain pavement load data for vehicle speeds in excess of 55 mph, Test Vehicle No. 1 (loaded) was run at 65 mph on these two test roads.

#### Data Presentation

A review of pertinent literature on analysis of pavement and highway structure life revealed that because of the variety of analytical techniques employed, it would be presumptive to choose any "best way" to present dynamic pavement load data. Therefore, it was decided that several methods of data presentation would be beneficial. These methods required both analog and digital data processing.

#### Analog Computer Equipment

An EAI analog computer, Model 231R; a Sangamo 14-channel magnetic tape recorder, Model 471-RB; a Brush pen recorder; 20 electronic counters; and provisions for transmitting analog data to the digital computer were used to aid the analysis and presentation of the pavement load data (Fig. 13).

#### Digital Computer Equipment

An IBM System/360 Model 30 digital computer, an IBM 1827 Data Control Unit (analog-to-digital conversion equipment), and a California Computer Products plotter also were used for analysis and presentation of the pavement load data (Fig. 14).

#### Presentation Techniques

The scaled pavement load measurements for each run were rerecorded on a master data tape. This master was used for the subsequent data presentations.

#### Pavement Load versus Time Graphs

Pavement load versus time was recorded at two chart speeds for all test runs. The low-speed charts (1 or 2 mm/sec) compress entire 1-mi runs into strips about 5 in. long, showing maximum loads and defining the general envelope of the measured pavement load. High-speed strip charts (50 mm/sec) clearly show the frequency content of the peak load of each run. Figure 15 is a sample of these strip charts. Appendix P contains the data for each run. Table



Figure 13. Analog computer equipment.



Figure 14. Digital computer equipment.



**Test Vehicle No. 1, 2-D**  
**Instrumented Wheel: Right Side of Drive Axle**  
**Static Weight on Wheel: 9.4 KIPS**  
**Road: M-59, Poor-Overlay**  
**Speed: 34 mph**

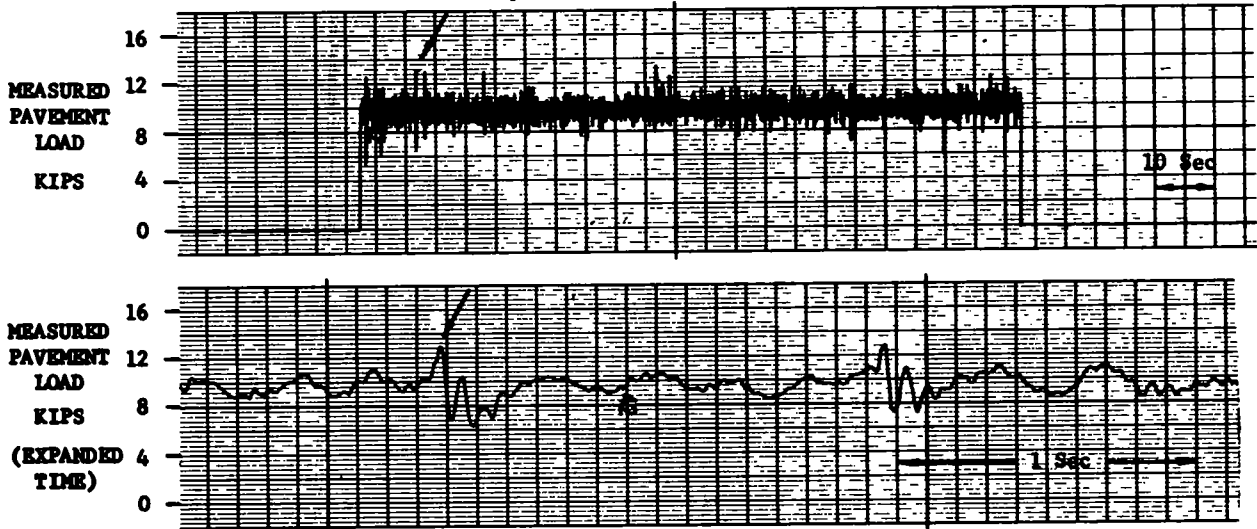


Figure 15 Measured pavement load

5 gives the maximum pavement load for each test condition Table 6 gives the predominant frequency of the load peak

*Probability Density Analysis*

Pavement load probability density functions were made using analog computer techniques Figure 16 is a sample of these analyses Appendix P contains a probability density plot for each run

*Number of Peak Load Occurrences*

The 20 counters at the analog computation facility were used to count the number of times the pavement load peaked in each of 20 consecutive pavement "load win-

dows" Each load window is a 1,000-lb load increment This analysis was made for all Test Vehicle No. 1 runs Figure 17 is a sample of these analyses. Appendix T contains a representative plot of these analyses.

*Power Spectral Density (PSD)*

Pavement load power spectral density plots were made for several test conditions of Test Vehicle No. 1. Figure 18 is a sample of these analyses Appendix T contains a representative plot of these PSD functions. Appendix F discusses the digital techniques used to compute the PSD functions

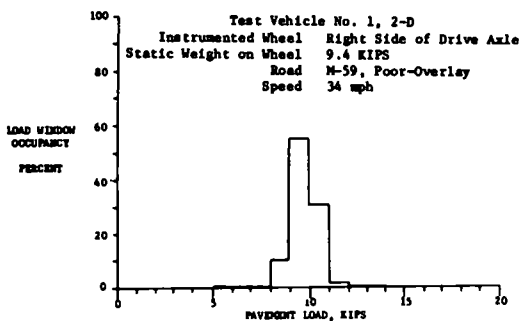


Figure 16 Pavement load probability density analysis

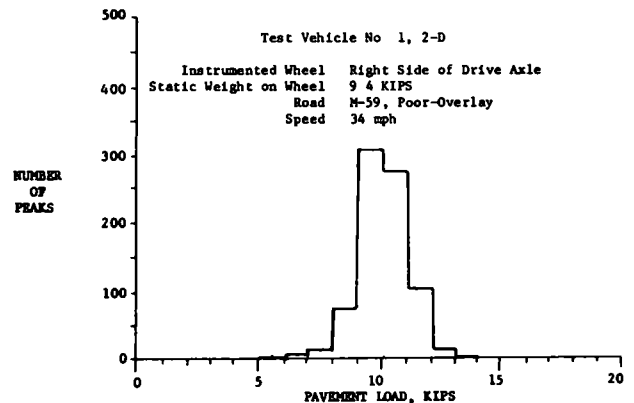


Figure 17 Number of peak load occurrences.

TABLE 5  
MAXIMUM MEASURED PAVEMENT LOADS

TEST SPEED (MPH)	MAXIMUM MEASURED PAVEMENT LOADS (KIPS), BY TEST ROAD SECTIONS.								
	RIGID PAVEMENT			FLEXIBLE PAVEMENT			OVERLAY PAVEMENT		
	GOOD I-75	FAIR I-696	POOR M-50	GOOD M-52	FAIR M-247	POOR M-138	GOOD M-53 NB	FAIR M-53 SB	POOR M-59
(a) Test Vehicle No. 1, static load=9.4 kips									
34	11.6	12.8	11.8	12.8	14.2	14.5	13.0	13.6	13.5
Near 55	12.0	12.5	13.5	13.5	17.5	14.2	13.0	14.5	16.2
Sweep	12.3	13.2	13.2	13.2	15.6	14.4	13.0	14.2	15.1
65	13.0								15.5
34, empty	5.2								7.7
65, empty	5.8								7.5
(b) Test Vehicle No. 2, static load=7.7 kips									
34	11.1	11.5	11.4	10.2	13.8	14.0	12.1	11.0	12.7
Near 55	11.9	15.2	13.6	12.0	19.5 <sup>a</sup>	N.A.	17.5	17.5	16.5
Sweep	11.7	14.2	14.1	11.1	20.4 <sup>a</sup>	15.0	17.0	14.2	16.0
(c) Test Vehicle No. 3, static load=8.8 kips									
34	13.8	14.0	14.0	12.6	19.6 <sup>a</sup>	16.1	15.2	14.0	16.0
Near 55	14.9	12.8	13.5	12.5	16.5	16.8	12.8	14.1	15.9
Sweep	13.8	12.8	15.2	12.6	17.0	17.4	13.2	15.0	14.5

<sup>a</sup> Exceeded strip chart scaling, value determined from computer voltage readings

TABLE 6  
PREDOMINANT FREQUENCIES OF MAXIMUM LOAD PEAKS

TEST SPEED (MPH)	PREDOMINANT FREQUENCIES (CPS) OF MAXIMUM LOAD PEAKS, BY TEST ROAD SECTIONS								
	RIGID PAVEMENT			FLEXIBLE PAVEMENT			OVERLAY PAVEMENT		
	GOOD I-75	FAIR I-696	POOR M-50	GOOD M-52	FAIR M-247	POOR M-138	GOOD M-53 NB	FAIR M-53 SB	POOR M-59
(a) Test Vehicle No. 1, static load=9.4 kips									
34	3.0	2.6	2.6	2.6	2.6	15	15	12	20
	17	17	17	17	17				
Near 55	2.6	2.3	16	2.6	12	15	12	17	12
		16		17					
Sweep	2.6	5.0	17	2.6	12	13	12	20	13
	12	16		17					
65	2.6								14
	25								
34, empty	17								10
65, empty	2.5								10
	17								
(b) Test Vehicle No. 2, static load=7.7 kips									
34	2.8	3.2	3.0	8.0	3.0	11	6.5	9.5	3.0
	15			15					
55	3.0	11	11	3.0	11	11	11	11	3.0
				11					11
Sweep	3.0	11	11	11	11	11	11	11	11
(c) Test Vehicle No. 3, static load=8.8 kips									
34	3.0	3.0	3.0	3.0	3.0	3.0	3.0	3.0	3.0
									17
55	2.8	3.0	3.0	3.0	3.0	3.0	3.0	3.0	3.0
			17			17	15	17	
Sweep	3.0	3.0	3.0	3.0	3.0	3.0	3.0	3.0	3.0
						17	12	17	

## Discussion of Results

The true usefulness and applicability of the various analyzed forms of the measured pavement loads will best be determined during applications by users of highway load data. Some observations relative to these data were made, and it is appropriate that they be included here. Most importantly, the maximum pavement loads measured on public roads on all three test vehicles (Table 5) show that dynamic loads are appreciable. In fact, the loads imposed on a pavement (and imposed on the vehicle) under dynamic conditions can be double the static loads.

### Test Vehicle No. 1

The pavement loads developed with Test Vehicle No. 1 varied greatly in amplitude and frequency content with changing road roughness, but only slightly with changes in vehicle speed. Low-frequency loads, near 3 cps, were observed on all roads, but on the rougher roads larger amplitude, high-frequency (12 to 20 cps) loads were dominant. The low-frequency loads may be associated with the bounce resonant frequency of the body on the tire and suspension springs, whereas the higher-frequency loads probably involve resonant vibration of the rear suspension excited by short-wavelength "impact" bumps.

### Test Vehicle No. 2

Pavement loading with Test Vehicle No. 2 varied slightly with changes in road conditions, but the amplitude and frequency of the loads varied greatly with changes in vehicle speed. Although low-amplitude, low-frequency loads were produced by this vehicle at 34 mph, at 55 mph very high-amplitude (19.5 kips), higher-frequency (11 cps) loads were observed. Several cycles of large oscillatory loading following "impact" bumps at 55 mph suggest the presence of a lightly damped resonance in the tandem suspension.

The very high dynamic loads of Test Vehicle No. 2 (Table 5) would seem to be contradicted by traffic survey results in Table 3. Inasmuch as the survey includes statistical data from many test vehicles, one might conclude that Test Vehicle No. 2 was not very representative of tandem axle suspensions. It should be noted, however, that Test Vehicle No. 2 produced high loads only at high vehicle speeds (near 55 mph), whereas the vehicles in the traffic survey rarely crossed the scales at speeds over 45 mph. Possibly the time delay between the front and rear tandem axles encountering an obstruction at 55 mph is such that both inputs reinforce. Apparently, dynamic loads with tandem suspensions can be significantly affected by vehicle speed.

### Test Vehicle No. 3

Pavement loading with Test Vehicle No. 3 did not vary significantly in amplitude or frequency with vehicle speed or road condition. The nearly constant amplitude loads occurred primarily at low frequencies (2.6 to 3.0 cps). The absence of loads at suspension wheel bounce frequencies is of interest.

## Effects of Vehicle Load (Test Vehicle No. 1 Only)

Dynamic loads of Test Vehicle No. 1 were not significantly affected by a change in static rear axle weight from 6.1 kips (unloaded) to 18.8 kips (loaded). Total pavement loads were therefore much higher with the loaded vehicle.

### Ranking of Test Roads

Comparison of Bureau of Public Roads roughometer readings, road profile PSD's, pavement load PSD's, and maximum loads produced different roughness orderings of the roads (Table 7). The differences between the various orderings are slight, reflecting variations in the measurement techniques. For example, a generally rough road might not produce a particularly high maximum load, whereas a relatively smooth road with one bad bump could produce a high maximum load. It is interesting to note that the two most similar methods, profile and load PSD functions, produce nearly identical orderings.

### Average Pavement Load versus Static Weight

The strip charts and the probability density analyses indicate average pavement loads that differed from the static wheel weight. This difference ranged from about -100 lb to +1,000 lb and was due to load transfer from one wheel to another. Some possible reasons for this load transfer are as follows:

1. Crown in the test roads.
2. Wind resistance.
3. Drive torque reaction.

### Pavement Load Frequency Spectrum

Several interesting features of the PSD plots indicated the primary mechanisms causing repetitive pavement loads. On smooth roads loading at body mode frequency is predominant, but loads at 2nd, 3rd, 4th, and 5th orders of wheel rotation frequency dominate the spectrum above 8 cps (Fig. M-8). Loads at first order of wheel rotation frequency are completely masked by loads at body mode frequency. On rougher roads, loads at body mode and wheel hop frequencies are dominant, with wheel rotation frequency modes masked (Fig. 18).

## PAVEMENT LOAD PREDICTION TECHNIQUES

The concept of predicting pavement loads from road profiles requires definition of a vehicle transfer function, as follows:



Three methods of defining the transfer function and, hence, three prediction techniques were considered for this project:

1. Frequency domain prediction using digital computation.
2. Time domain prediction using convolution theory.
3. Time domain prediction using analog simulation.

TABLE 7  
ROUGHNESS ORDERING OF THE TEST ROAD SECTIONS

RANK	ROUGHNESS ORDERING			
	BPR ROUGHOMETER	PROFILE PSD	TEST VEHICLE NO. 1, 34 MPH	
			LOAD PSD	MAX. LOAD
1 (Smoothest)	M-52	M-52	M-52	M-50
2	I-75	M-53 NB	M-53 NB	I-75
3	M-53 NB	I-75	I-75	M-52
4	I-696	I-696	I-696	I-696
5	M-53 SB	M-50	M-50	M-53 NB
6	M-247	M-247	M-53 SB	M-53 SB
7	M-50	M-53 SB	M-247	M-59
8	M-59	M-59	M-59	M-247
9 (Roughest)	M-138	M-138	M-138	M-138

NB = northbound, SB = southbound

#### Frequency Domain Prediction Using Digital Computation

The frequency domain prediction using digital computation computes a vehicle frequency response function by dividing a frequency representation of a road profile by a frequency representation of the corresponding pavement load. The vehicle frequency response function can then be multiplied by any road profile power spectral density (PSD) to predict a pavement load power spectral density. This technique is established only for linear systems excited by stationary, random inputs. The details of this technique are described in Appendix Q.

#### Time Domain Prediction Using Convolution Theory

The time domain prediction using convolution theory predicts pavement loads by solving the equation:

$$P(t) = \int_0^t V(t) Z(t - \tau) d\tau \quad (1)$$

in which

$P(t)$  = predicted pavement load time function;  
 $V(t)$  = vehicle impulse load response time function; and  
 $Z(t)$  = road profile time function.

The vehicle impulse response can be obtained by computation of the Fourier transform of the vehicle complex frequency response function (Appendix Q) or by experimental measurement of the vehicle's response to a unit displacement impulse. This technique is established for linear systems only.

#### Time Domain Prediction Using Analog Simulation

The time domain prediction using analog simulation predicts pavement loads by solving a set of time-dependent, differential equations that describe the dynamic response of a vehicle analog simulation to road profile inputs. This simulation is an idealized mathematical model of the vehicle which includes those vehicle parameters judged significant to the problem. Analog computation conveniently allows the programming of nonlinearities where necessary for accurate simulation. Accuracy of this tech-

nique is limited mainly by the ability to include all significant parameters in a program of manageable size.

The time domain prediction technique using analog computation was used during this project for two reasons. First, experimental measurements on Test Vehicle No. 1 revealed the nonlinearity of its rear suspension. Second,

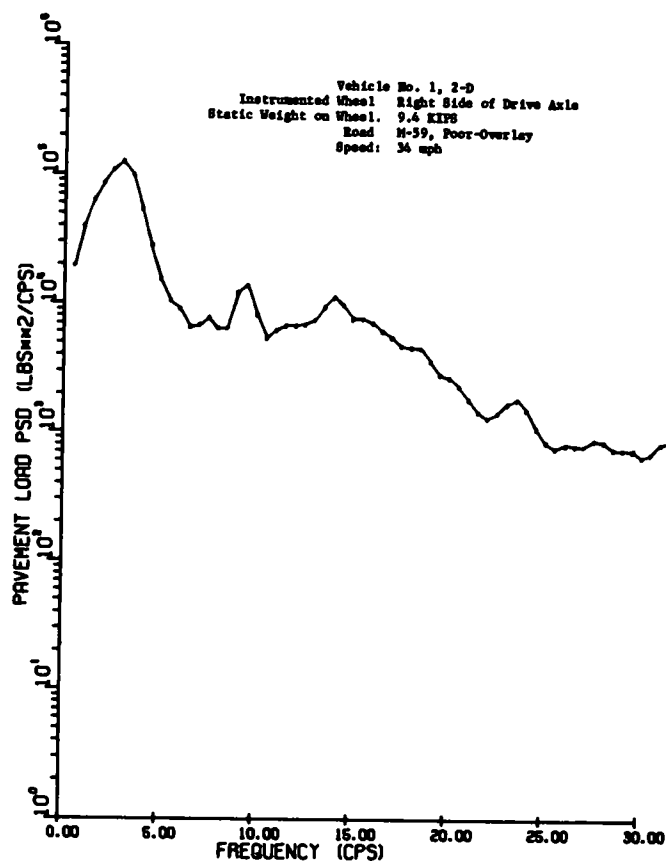


Figure 18. Pavement load power spectral density.

the analog computer simulation of the vehicle could easily be used to study the effect of each of the simulated parameters on the dynamic pavement load.

### DYNAMIC PAVEMENT LOAD PREDICTION USING ANALOG COMPUTATION TECHNIQUES

A time domain pavement load prediction technique was developed using analog simulation techniques. This required an analog computer simulation that accurately predicted dynamic tire/road interface loads caused by a truck traveling over highways of various roughness. The simulation included significant vehicle properties such as body mass, suspension configuration, tire spring rate, and suspension mass. Experimental measurements were used to verify the simulation accuracy.

#### General Features of Computer Simulation

The computer simulation predicted dynamic pavement loads for only one test vehicle, however, this simulation could be adapted to predict loads for other trucks, as discussed in the following. The truck chosen for this study was Test Vehicle No. 1 (Fig. 7). The simulation included a nonlinear friction model of suspension spring damping. Attempts at using only linear viscous damping are discussed in Appendix S.

Input data for the simulation were road profiles of 1-mi road sections (Appendix D) as measured by the GM profilometer. These profiles were recorded on magnetic tape. Output from the simulation was an analog, time-varying voltage proportional to dynamic pavement load. Total pavement load was computed by summing dynamic and static loads. When both the input and output data were plotted versus time (Fig. 19), pavement loads result-

ing from each road irregularity were studied. Other processing of computed load data included load versus number-of-occurrences data, probability density functions, and power spectral density functions. These are discussed in detail in the earlier section entitled "Pavement Load Measurements."

#### Use of a Quarter-Vehicle Model in the Prediction Technique

The prediction technique was confined to computing pavement loads for the right rear wheel set only. This is referred to as a quarter-vehicle model (Fig. 20).

The rear axle was chosen for study because tests showed that the highest pavement loads were associated with the rear axle. Also, rear axle dynamic loads were essentially independent of front wheel loads (Appendix L).

Tramp coupling effects between right and left rear wheels are not included in a quarter-vehicle model. Omission of these effects was justified for two reasons. First, road profile records showed that many large highway bumps occurred simultaneously at the right and left wheels. Second, tests discussed in the earlier section entitled "Identification of Factors Affecting Dynamic Pavement Loads" indicated that a simulation without tramp coupling would compute peak pavement loads conservatively higher than measured loads (about 12% in some cases). Conservative load predictions might be acceptable in estimating loads for pavement and bridge designs.

#### Vehicle Properties Included in Computer Simulation

Table 8 gives the vehicle properties included in the quarter-vehicle model simulation and the tests performed to determine their magnitudes.

A schematic diagram of the quarter-vehicle model and

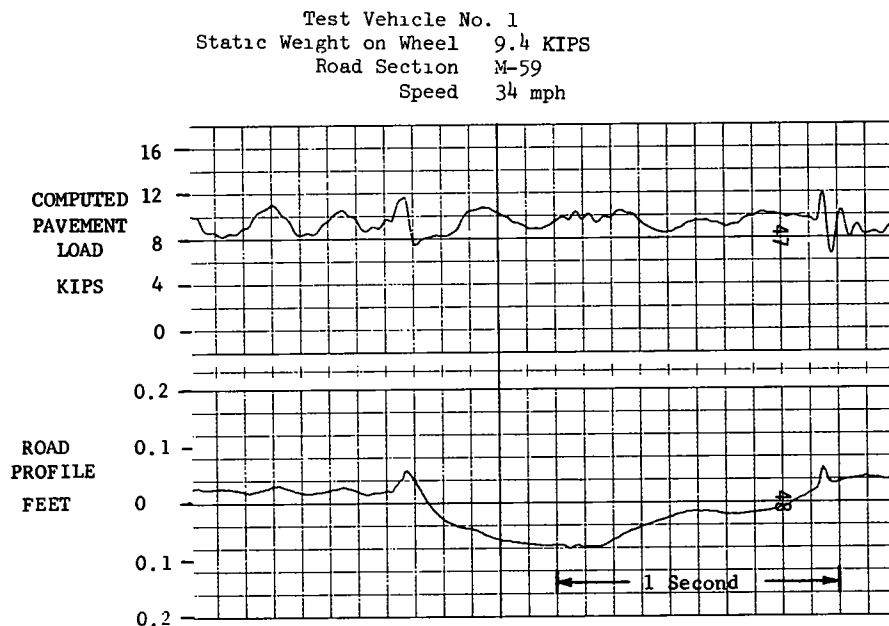


Figure 19 Sample traces of road profile and computed pavement load versus time



TABLE 8  
TESTS REQUIRED FOR PARAMETER DEFINITION

VEHICLE PROPERTY	METHOD OF DETERMINATION
Mass supported by rear suspension	Static weight measurement
Mass of rear axle and wheels	Static weight measurement
Spring rate of rear tires	Static load-deflection test
Spring rate of rear suspension	Static load-deflection test and dynamic test
Damping in rear springs	Dynamic test
Enveloping quality of tires	Dynamic test

a listing of the parameters determined for Test Vehicle No 1 are shown in Figure S-6. As shown, the quarter-vehicle model is a two-mass system with each mass having a single, vertical degree of freedom. A complete discussion of this simulation appears in Appendix S.

#### Comparison of Measured and Computed Load Data

The accuracy of the prediction technique was evaluated by comparing computed pavement loads to corresponding measured pavement loads. Only the 34-mph runs on Test Vehicle No. 1 were simulated on the computer.

Several methods of comparing the measured and computed pavement load data were used to evaluate the prediction technique. The methods and a sample figure for each are as follows:

1. Load versus time strip charts (Fig. 21).
2. Number of occurrences of peak loads (Fig. 22).
3. Probability density analyses (Fig. 22).
4. Power spectral density analyses (Fig. 23).

Representative data for all nine road sections appear in Appendix T.

#### Discussion of Prediction Technique Accuracy

Several observations regarding the accuracy of the pavement load prediction technique were made from a study of the many comparative graphs discussed in Appendix T.

1. *Peak Pavement Load Predictions.* Comparisons of load versus time records showed that peak loads measured on each 1-m road section were predicted with an average error of 2%. Maximum error was 12%. The load peaks selected for comparison were maximums or near-maximums for each test road section.

To illustrate the prediction accuracy for two roads of widely varying roughness, the following examples are drawn from the data:

- a. On M-52, a smooth road, the maximum measured load was 11.2 kips, compared to a computed load of 10.8 kips. These are within 3.6%.
- b. On M-59, a rough road, the measured peak value was 13.6 kips, compared to a computed value of 13.2 kips. These agree within 2.9%.

This indicates that the accuracy of the predictions provides adequate resolution to delineate the dynamic forces resulting from various grades of road roughness.

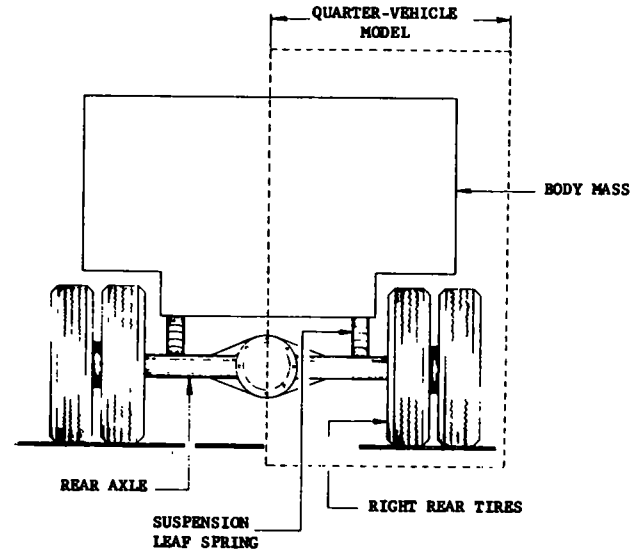


Figure 20. Rear view of Test Vehicle No. 1, outlining the quarter-vehicle computer model.

2. *Number of Peak Load Occurrence Predictions:* Peak pavement loads were predicted within 1.0 kip of measured loads for all nine roads using peak load occurrence data. However, rather large differences between the number of computed and measured peak load occurrences were noted in some 1.0-kip "load windows."

3. *Probability Density Analyses:* Peak pavement loads above 10.0 kips (dynamic loads above 0.6 kip) were predicted for all nine roads within 2.0 kips on the basis of probability density analyses. This was considered good correlation inasmuch as the analyses defined loads within only 1.0 kip. Better correlation would have resulted if loads had been defined with greater resolution.

4. *Power Spectral Density (PSD) Analyses.* Over-all agreement between measured and computed PSD functions for the nine road sections was very good. Logarithms of PSD functions for the vehicle bounce frequency (about 3 cps) and wheel hop frequency (about 19 cps) were predicted for all roads with an average error of 7%. Maximum error was 17%.

Several noticeable peaks in measured PSD functions corresponded to 2nd through 5th orders of wheel rotation frequency (first order approximately 5 cps @ 34 mph). Computed pavement load PSD functions cannot, of course, be compared with the measured PSD functions containing the peaks at orders of wheel rotation frequency. Therefore, the measured pavement load PSD was redrawn for a smooth road (I-75) and a rough road (M-59) with the wheel rotation peaks removed (Fig. 24). The corresponding computed pavement load PSD functions were traced on the same figure.

The following observations were made from this figure:

- a. The most significant road-to-road variations occurred in the 5- to 30-cps range. In this range, the rough road measured pavement load PSD values were

Vehicle No. 1, 2-D  
 Instrumented Wheel: Right Side of Drive Axle  
 Static Weight on Wheel: 9.4 KIPS  
 Road: M-59, Poor-Overlay  
 Speed: 34 mph

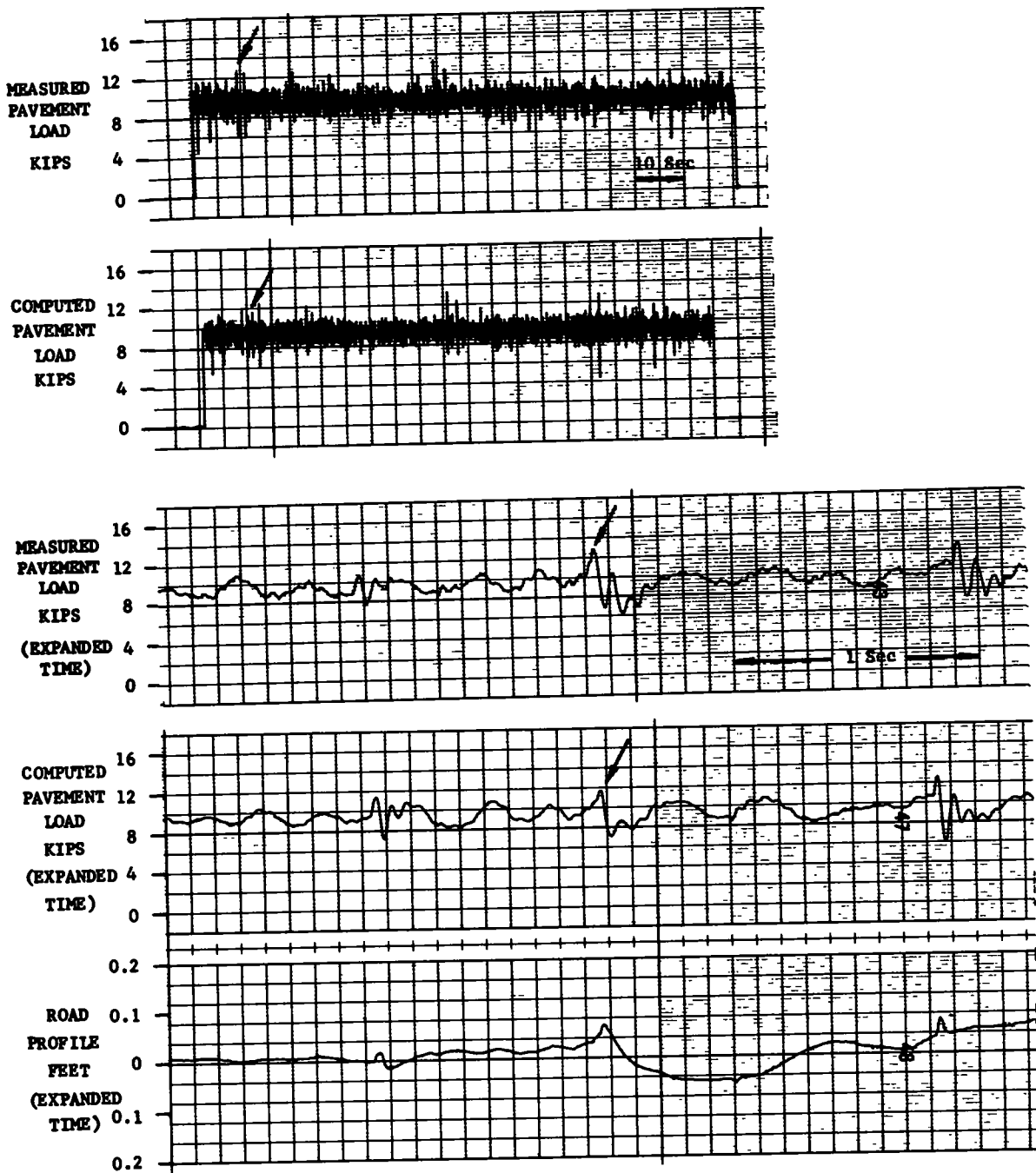


Figure 21. Load versus time comparisons

greater than the corresponding smooth road PSD values by an average factor of 6:1.

- b The computed PSD function showed peaks at about 19 cps, whereas the measured PSD functions showed a more even distribution in the 5- to 30-cps range

This was possibly due to differences in suspension damping between the real vehicle and the computer model. Also, measured loads contained *both* rear axle tramp and wheel hop frequencies, whereas the computed loads included *only* wheel hop frequencies.

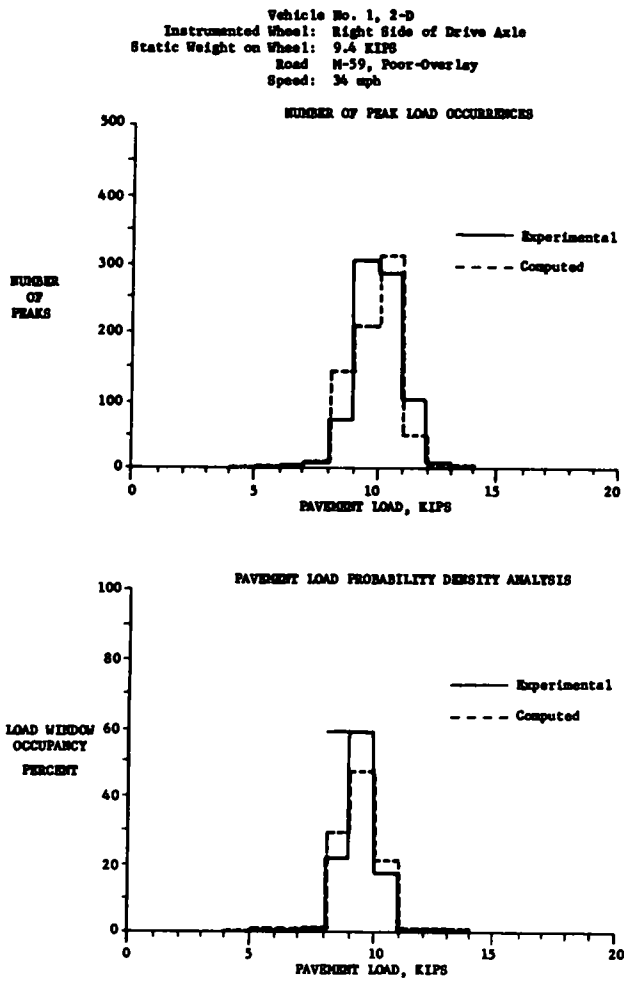


Figure 22. Statistical comparisons.

- c. The *average* of PSD values in the 5- to 30-cps range of the measured and computed functions shows good correlation for both the smooth and the rough road.

**Simulation of Additional Vehicle Operating Conditions**

In addition to the fixed test conditions, the following additional conditions were simulated:

1. An unloaded vehicle was simulated by reducing the body mass of the quarter-vehicle model from 8.2 kips to 2.0 kips. Pavement loads were then computed for the M-59 and I-75 road sections, with all other parameters held constant.
2. A vehicle speed of 65 mph was simulated on the analog computer, and pavement loads were computed for the same two road sections with all other parameters held constant.

On the basis of these comparisons, the following observations were made:

1. Correlation between computed and measured loads diminished for the unloaded condition. This indicated that some vehicle properties measured on the *loaded* vehicle were significantly changed when the vehicle was *unloaded*.

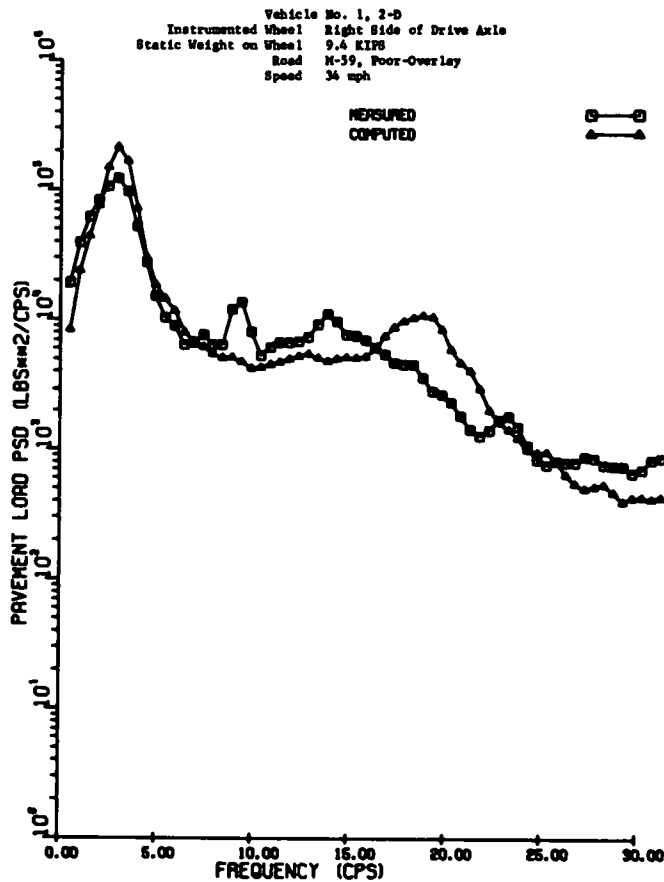


Figure 23. Pavement load power spectral density.

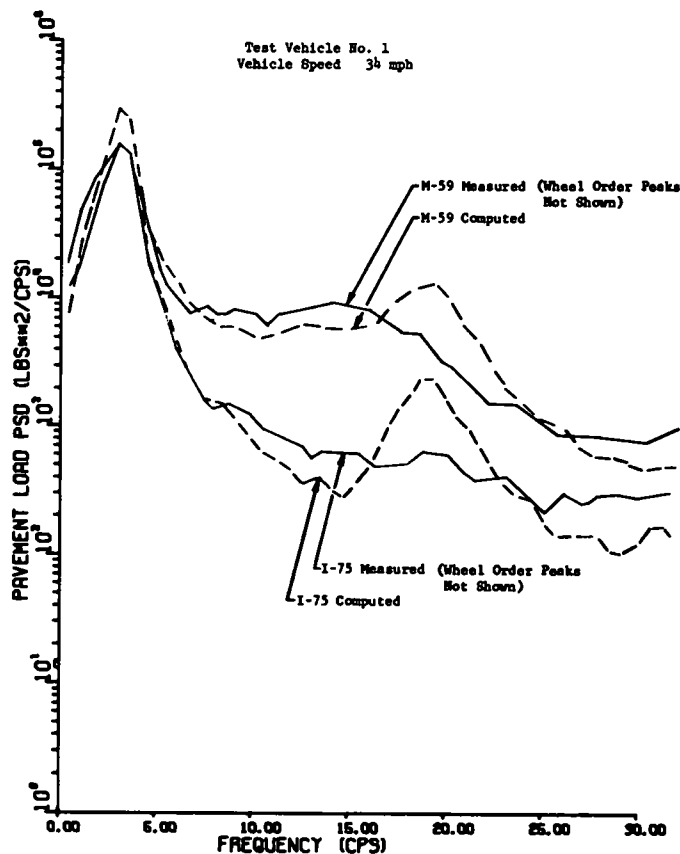


Figure 24. Pavement load power spectral density.

This emphasizes the importance of measuring vehicle properties and pavement loads under the same conditions.

2. Correlation between measured and computed loads for the 34-mph and 65-mph conditions was nearly the same, indicating that this model is adequate for at least the speed range from 34 to 65 mph

**Factors Affecting Prediction Technique Accuracy**

The degree of correlation between measured and computed loads is considered adequate for many purposes. However, some future application may require even better correlation. This could be achieved by considering the following items which are discussed in detail in Appendix U.

*Potential Refinements in Computer Simulation*

The following potential refinements could be included to improve the accuracy of the computer simulation:

1. A more detailed model of the tire spring and tire enveloping
2. A more detailed model of suspension spring and damping (this would have a negligible effect on peak dynamic loads but would have considerable effect on decay of the loads)
3. A half-vehicle model, including wheel hop and axle tramp effects

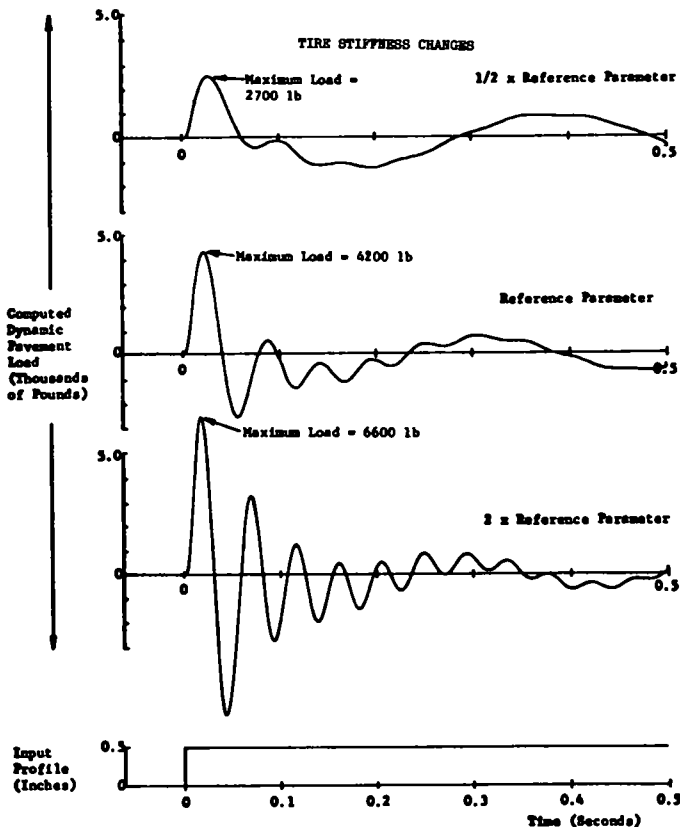


Figure 25 Computed effects of parameter variations.

*Repeatability of Experimental Pavement Load Measurements*

Pavement loads were measured on Test Vehicle No. 1 as it was driven over a step bump (Appendix O). There were differences in *dynamic* load measurements of about  $\pm 10\%$  between tests that were conducted under the same conditions. This degree of nonrepeatability probably resulted from the effects of vehicle pitch and roll, rim assembly runout, and tire nonuniformity. Pavement load data for the nine test roads also were subject to these nonrepeatability effects, thus, some disagreement between measured and computed data was inevitable.

*Effects of Lateral Road Variations on Road Profile Measurements*

Two aspects of the road profile data created differences between real road inputs to the test vehicle and inputs to the computer simulation. First, the total tread width of a rear dual tire set is much greater than the 2-in. width of the profilometer following wheel. Another difference was due to lateral misalignment between wheel paths of the test vehicle and the profile vehicle. This resulted because neither vehicle traveled a fixed distance from the edge of the road but wandered slightly from side to side in its traffic lane. Both of these problems could be corrected if the test vehicle itself was instrumented as a profiling device.

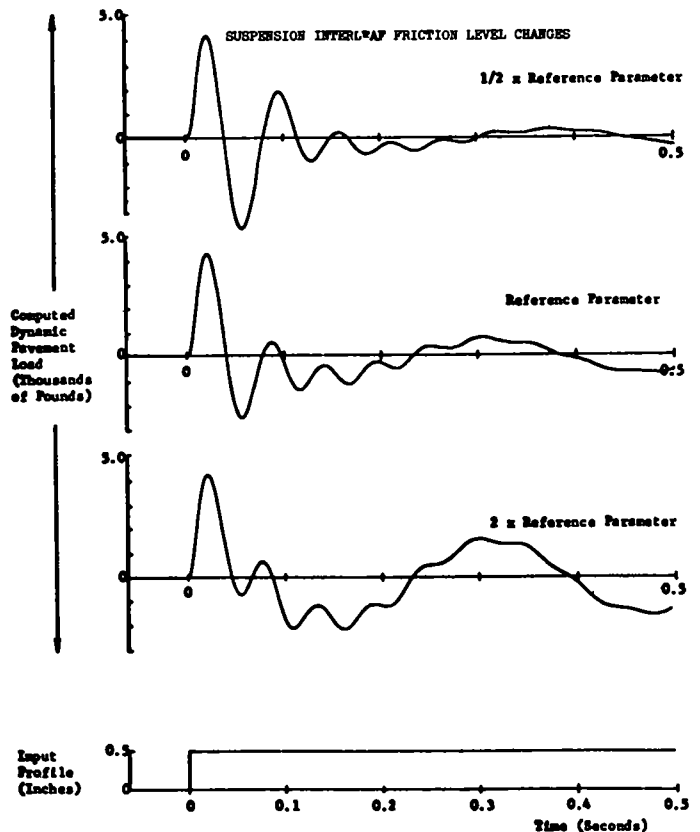


Figure 26 Computed effects of parameter variations

### Applicability of This Simulation to Other Vehicles

The quarter-vehicle model (Fig S-6) should be applicable to other vehicles, provided the following limitations are observed.

1. The vehicle must be fairly free of front-to-rear and side-to-side suspension interaction
2. Individual vehicle parameters for the simulation must be determined for each vehicle
3. Other suspension systems such as coil spring, torsion bar, and air bag probably could be simulated using this model with slightly different spring and damping representations.

### VARIATION OF PARAMETERS STUDY

Insight into the relative influence of various vehicle parameters on dynamic pavement loads is a byproduct of the analog simulation prediction technique. A parameter study on the quarter-vehicle simulation of Test Vehicle No. 1 (Fig. S-6) consisted of varying each parameter independently by a factor of one-half and a factor of two while observing the pavement loads generated by a ½-in.-high step bump. These loads were plotted versus time as shown in Figure 25, a typical example. Details of this study and pavement load records for each parameter appear in Appendix V.

The effects of parameter changes were evaluated by

comparing percentage changes in the maximum dynamic load (Table V-1).

From this summary, the following parameters appear most significant to *maximum* dynamic loading.

1. Tire stiffness.
2. Tire enveloping
3. Suspension mass

Figure 26, also taken from Appendix V, shows that the *decay of dynamic loading* can be affected by parameter variations even when the changes in maximum dynamic load are small. Parameters that produced this effect are:

1. Suspension interleaf friction level.
2. Suspension spring stiffness.
3. Body mass.
4. Suspension viscous damping.

Although variations in these parameters showed little effect on maximum dynamic loads, the effect they have on the decay of dynamic loads makes them important in correlating experimental and computed forces for real road inputs. It should be pointed out that variations in the other parameters *also* affected decay of dynamic loading (e.g., Fig 25)

An extension of this work, including experimental parameter variation, would contribute further to the understanding of vehicle responses to parameter changes and lead to refinement of the time domain prediction of dynamic pavement loads.

## CHAPTER THREE

# APPRAISAL AND APPLICATIONS

The value of an extended understanding of dynamic pavement loads is apparent. A few applications of the findings of this project are discussed

### DYNAMIC PAVEMENT LOAD DATA

Measurements made during this project verified that dynamic tire/road interface forces are an appreciable percentage of corresponding static loads. These forces (dynamic pavement loads) were measured for three test vehicles over a variety of public roads and several speed conditions. Because the vehicles, roads, and test conditions were so chosen, these test data are representative of a majority of heavy-vehicle highway mileage.

These experimental data should permit better interpretation of road profile measurements that might aid in the evaluation of various pavement roughness criteria. The data should also be useful for pavement loading fatigue studies

### DYNAMIC PAVEMENT LOAD MEASUREMENT SYSTEMS

Two reliable, accurate, instantaneous, on-board systems for measuring dynamic pavement load on a long-term, continuous basis were developed for heavy highway vehicles. These systems, a strain-gaged axle housing transducer and a wheel force transducer, were used extensively during this project. The strain-gaged axle housing system is best applied when requirements are for considerable testing with one or a few vehicles. The wheel force transducer system is most applicable when testing a large number of vehicles.

The two measurement systems could be used to measure periodically the pavement loading of a "standard" vehicle on highways of interest. This information, taken several times over the life of a highway, should aid the pavement maintenance decision.

These two pavement load measurement systems could



also be used to measure fore-and-aft shear forces at the tire/road interface. Some forms of pavement deterioration may be a function of these shear loads.

#### **PAVEMENT LOAD PREDICTION TECHNIQUE**

The analog computer simulation, developed during this project, of a heavy highway vehicle predicted pavement loads from recorded road profiles with an over-all accuracy of 85%. The vehicle model included properties most significant to pavement-induced dynamic loading. This simulation could be extended to predict pavement loading of representative vehicles over any profiled highway. These

predicted pavement loads can be applied in the same manner as measured pavement loads.

In conclusion, the objectives of this program have been met by the following achievements:

1. Development of two pavement load measurement systems.
2. Identification of vehicle properties affecting dynamic pavement load.
3. Presentation of a diverse pavement load data set representative of a majority of heavy-vehicle highway mileage.
4. Development of a pavement load prediction technique.

#### **CHAPTER FOUR**

### **SUGGESTED RESEARCH**

Some additional knowledge of the nature of heavy highway vehicle pavement loads was gained in this program and, of course, questions arise related to that new knowledge. Several of these questions suggest objectives for additional research.

#### **PAVEMENT LOADS RELATED TO WHEEL ROTATION**

Work during this project revealed that imperfectly mounted tire-rim assemblies can cause substantial pavement loading, regardless of pavement smoothness. A complete investigation of loads caused by wheel rotation should include: the identification of all sources of wheel rotation excitation, a study of the severity of each source throughout the truck population, and consideration of means to minimize these loads if warranted.

#### **PAVEMENT LOAD STUDIES OF TANDEM-AXLE VEHICLES**

Large dynamic pavement loads were measured on a tandem axle at 55 mph. The mechanism that caused these large loads was not investigated. The pavement load measurement systems and an extension of the analog computer simulation developed for this project could be used to study the dynamic loading of tandem-axle suspensions. These studies should include the effects of axle interaction, tramp action, and a variety of excitations.

#### **PAVEMENT LOAD PREDICTION TECHNIQUES**

The analog simulation technique developed for this project predicted pavement loads with 85% accuracy. If future applications require a higher degree of correlation, the following refinements should be considered:

1. Rear axle tramp effects.
2. More accurate road profile measurement.
3. More detailed tire and suspension simulation.
4. Wheel rotation excitation.

The simulation prediction technique was evaluated for one vehicle. The task of extending the prediction technique to a variety of vehicles remains.

The frequency domain and convolution concepts that are discussed in the section entitled "Pavement Load Prediction Techniques," but not used on this project, could be evaluated as possible pavement load prediction techniques.

#### **THE EFFECT OF VEHICLE PROPERTIES ON DYNAMIC PAVEMENT LOADING**

The variation of parameters study performed on the analog simulation indicated several vehicle properties that influence dynamic pavement loads. An experimental evaluation of the pertinent vehicle properties is needed to verify the results of the parameter study. Also, the effect of vehicle speed should be studied experimentally for a wide range of vehicles and operating conditions.

#### **STUDY OF TIRE/ROAD INTERFACE SHEAR LOADS**

Some forms of pavement deterioration may depend on the shear loads at the tire/road interface. Techniques for measurement of fore-and-aft shear loads have been demonstrated during this project. A study of shear loads during braking, turning, and acceleration would provide highway researchers with shear load information.

## DATA PRESENTATION TECHNIQUES

The pavement load data measured during this project were presented in several different formats because the exact applications of these data are uncertain. A comprehensive study that considers which of the numerous pavement load data formats are most useful for each of many applications would increase the usefulness of subsequent measurements.

## PAVEMENT SURVEILLANCE

If pavement load information were obtained at intervals over a period of time and plotted versus time, it would be possible to study pavement deterioration. Experience with several such graphs might help highway engineers to forecast maintenance needs on the basis of maximum economy. Such observations may also provide guidance in establishing seasonal load regulation practices.

---

## REFERENCES

1. MILLIMAN, P., "Automatic Weighing of Vehicles in Motion and Collection of Traffic Data by Electronic Methods." *Res. Report No. R-498*, Mich. State Highway Dept., Lansing, Research Lab. Div., Office of Testing and Research (Feb 1965).
2. FISHER, J. W., and HUCKINS, H. C., "Measuring Dynamic Vehicle Loads." *HRB Spec. Report 73* (1962) pp. 138-148.
3. BODE, O., ET AL., "Comparison of Different Methods of Determining the Dynamic Wheel Load." *Deutsche Kraft* (German), No. 131, 33 pp. (1959). M.I.R.A. trans. No. 1/63, *Monthly Summary of Automobile Eng. Lit.*, pp. 35-36 (Jan. 1963).
4. HOPKINS, R. C., and BOSWELL, H. H., "Methods for Measuring Load Transfer Through Vehicle Tires to the Road Surface." *Proc. HRB*, Vol. 36 (1957) pp. 240-252.
5. SPANGLER, E. B., and KELLY, W. J., "GMR Road Profilometer—A Method for Measuring Road Profile." *Hwy. Res. Record No. 121* (1965) pp. 27-54.
6. BENDAT, J. S., and PIERSOL, A. G., *Measurement and Analysis of Random Data*. Wiley (1966) pp. 182-295.
7. BLACKMAN, R. B., and TUKEY, J. W., *The Measurement of Power Spectra*. Dover Publications, N.Y. (1958) pp. 21-23.
8. JENKINS, G. M., and WALTERS, D. G., *Spectral Analysis and its Applications*. Holden-Day, San Francisco (1968) p. 422.
9. LIPPMANN, S. A., PICCIN, W. A., and BARKER, T. P., "Enveloping Characteristics of Truck Tires, A Laboratory Evaluation." *Trans. SAE*, Vol. 74 (1966).
10. SETO, W. W., *Theory and Problems of Mechanical Vibrations*. Schaum Pub. Co., N.Y. (1964) pp. 34-35.

## APPENDIX A

### LITERATURE SURVEY, BIBLIOGRAPHY AND ABSTRACTS

The list of literature, 33 articles, as selected during the survey phase of this project is presented in this appendix. Eighteen of the articles which were considered to be of primary interest to this project are indicated with an asterisk, and an abstract is included.

Of primary interest in the literature survey were methods of measuring dynamic tire/road interface forces, means of presenting dynamic pavement load data that would provide maximum usefulness to highway designers, and the character and influence of various vehicle parameters on dynamic loads.

Of secondary interest were reports on highway or runway roughness measurements, vehicle response characteristics to road profile input, and highway and bridge reactions to dynamic vehicle loads.

#### SELECTED LITERATURE

- ALBERT, C J., "A Method of Simulating Tire Enveloping Power in Calculations of Vehicle Ride Performance." *Report No YM-1424-V-300*, Cornell Aeronautical Lab. (Nov. 18, 1961)
- \*BLYTHE, D K, DEARINGER, J A, and PUCKETT, R. E., "Variations in Axle Weights of Moving Trucks." *Soc. of Automotive Eng Preprint 65015* (May 1965).
- \*BODE, O., ET AL., "Comparison of Different Methods of Determining the Dynamic Wheel Load." *Deutsche Kraft* (German), No. 131, 33 pp. (1959). M.I.R.A. trans No 1/63, *Monthly Summary of Automobile Eng Lit*, pp. 35-36 (Jan. 1963).
- \*EDWARDS, S G, "Dynamic Measurement of Front Wheel Loads Using a Special Purpose Transducer." *General Motors Eng J*, Vol. 11, No. 4, pp 15-18 (4th Quarter, 1964).
- \*ESSERS, KOTITSCHKE, "Masstechnische Bestimmung der dynamischen Radkrafte von Kraftfahrzeugen (Measurement Techniques to Determine the Dynamic Wheel Loads of Vehicles)" *Strasse und Autobahn*, Vol. 6, No. 2, pp. 55-56 (Feb. 1966).
- \*FINNEY, E. A., "Dynamic Aspects of Vehicle Size and Weight." *Res Report No R-517*, Mich State Highway Comm (May 1965).
- \*FISHER, J. W, and HUCKINS, H. C., "Measuring Dynamic Vehicle Loads." *HRB Spec Report 73* (1962) pp 138-148
- \*FREITAG, D. R, GREEN, A J, and MURPHY, N R, JR., "Normal Stresses at Tire-Soil Interface in Yielding Soils" *Hwy. Res. Record No. 74* (1965) pp. 1-18.
- \*GINN, J L, MILLER, R. F., MARLOWE, R L., and HEIMOVICS, J. F., "B. F. Goodrich Tire Dynamics Machine" *Soc. of Automotive Eng. Paper 490 B* (Mar. 1962).
- HEUKELOM, W, and FOSTER, C. R, "Dynamic Testing of Pavements." *Proc ASCE*, Vol. 86, *J. Soil Mechanics & Foundations Div*, No. SM1, Part 1, Paper No 2368, pp 1-28 (Feb. 1960).
- "The WASHO Road Test—Part 1: Design, Construction and Testing Procedures" *HRB Spec. Report 18* (1954) pp. 1-121.
- "Road Test One-MD, Final Report. Effect of Controlled Truck Axle Loadings on Concrete Pavement." *HRB Spec. Report 4* (1952) pp 1-179.
- "Bridge Dynamics and Deflections, and Fatigue in Welded Members." *HRB Bull. 315* (1962) pp. 1-62.
- \*HOPKINS, R C, and BOSWELL, H. H, "Methods for Measuring Load Transfer Through Vehicle Tires to the Road Surface" *Proc HRB*, Vol 36 (1957) pp 240-252.
- HOUBOLT, J C., WALLS, J. H., and SMILEY, R. F., "On Spectral Analysis of Runway Roughness and Loads Developed During Taxiing" *Nat Advisory Committee for Aeronautics Tech. Note 3484*, Langley Aero. Lab., Langley Field, Va (July 1955).
- HUDSON, W R, "Comparison of Concrete Pavement Load-Stresses at AASHO Road Test with Previous Work." *Hwy. Res. Record No 42* (1963) pp. 57-98.
- \*LIPPMAN, S. A, and NANNY, J D, "A Quantitative Analysis of the Enveloping Forces of Passenger Tires." *Soc. of Automotive Eng. Preprint No. 657174* (Jan 1967).
- \*LIPPMAN, S. A., PICCIN, W. A., and BAKER, T. P, "Evaluating Characteristics of Truck Tires—A Laboratory Evaluation" *Tran Soc. of Automotive Eng*, Vol. 74 (1966)
- \*MILLIMAN, P, "Automatic Weighing of Vehicles in Motion and Collection of Traffic Data by Electronic Methods." *Res. Report No. R-498*, Mich. State Highway Dept., Lansing, Research Lab. Div, Office of Testing and Research (Feb 1965).
- \*MITSCHKE, M., "Influence of Road and Vehicle Dimensions on the Amplitude of Body Motions and Dynamic Wheel Loads (Theoretical and Experimental Vibration Investigations)" *Soc. of Automotive Eng Preprint 310 C* (Jan 1961).
- MORRIS, G. J, "Response of a Jet Trainer Aircraft to Roughness of Three Runways." *NASA TN D-2203* (May 1964).
- \*QUINN, B. E, and THOMPSON, D. R, "Effect of Pavement Condition in Dynamic Vehicle Reactions." *HRB Bull. 328* (1962) pp. 24-32.
- \*QUINN, B. E., and VAN WYK, R., "A Method for Introducing Dynamic Vehicle Loads into Design of Highways" *Proc. HRB*, Vol. 40 (1961) pp. 111-124.

- \*QUINN, B. E., and WILSON, C. C., "Can Dynamic Tire Forces be Used as a Criterion of Pavement Condition?" *Hwy. Res. Record No. 46* (1964) pp. 88-100.
- "Road Tests on Controlled Truck Axle Loadings." *Civil Eng. (London)*, Vol. 49, No. 571, pp. 52-53 (Jan 1954).
- SILSBY, N. S., "An Analytical Study of Effects of Some Airplane and Landing Gear Factors on the Response to Runway Roughness with Application to Supersonic Transports." *NASA Tech Note D-1492*, Langley Res Center, Langley Station, Hampton, Va. (Dec 1962)
- \*SPANGLER, E. B., and KELLY, W. J., "GMR Road Profilometer—A Method for Measuring Road Profile" *Hwy. Res. Record No. 121* (1965) pp. 27-54.
- SUTHERLAND, E. C. and CASHELL, H. D., "Structural Effects of Heavy-Duty Trailer on Concrete Pavement. A Supplemental Investigation to Road Test One-MD." *HRB Spec Report 14* (1953) pp. 1-32.
- TARAGIN, A., "Evaluation of Performance of an Existing Concrete Pavement Under Accelerated Load Application." *HRB Bull. 187* (1958) pp. 67-69.
- THOMPSON, W. E., "Measurements and Power Spectra of Runway Roughness at Airports in Countries of the North Atlantic Treaty Organization." *Nat'l. Advisory Committee for Aeronautics Tech. Note 4303*, Langley Aero Lab, Langley Field, Va (July 1957).
- \*TRABBI, G. W., LASK, K. V., and BUCHELE, W. F., "Measurement of Soil-Tire Interface Pressures." *Agric. Eng.*, Vol. 40, No. 11, 678-681 (Nov. 1959)
- "Traffic Keeps Going on AASHO Road Test." *Better Roads*, Vol. 29, pp. 33-34 (Feb. 1959).
- WALLS, J. H., HOUBOLT, J. C., and PRESS, H., "Some Measurements and Power Spectra of Runway Roughness" *Nat'l Advisory Committee for Aeronautics Tech. Note 3305* (Aug. 13, 1954).
- ZUBE, E., and FORSYTH, R., "Investigation of Destructive Effect of Flotation Tires on Flexible Pavement." *Hwy. Res. Record No. 71* (1965) pp. 129-150.

#### ABSTRACTS, LITERATURE OF PRIMARY INTEREST

- BLYTHE, D. K., DEARINGER, J. A., and PUCKETT, R. E., "Variations in Axle Weights of Moving Trucks."

This paper presents an analysis of axle weight data collected during the performance testing of the Broken Bridge dynamic electronic highway scale. Test results are analyzed by comparing the in-motion axle weights as measured by the Broken Bridge scale with the corresponding static values for an instrumented two-axle test vehicle and for a sample of trucks diverted from an Interstate Highway. Analysis of the two-axle test truck data shows that the actual loads applied to the highway surface by the wheels of a moving vehicle vary above and below the static equivalents in a manner that is typical for a specific location and range of speeds.

For a random selection of different types of trucks, the variation of dynamic from static axle

weight is further affected by axle position (front, third, etc.) and spacing. It is generally concluded that dynamic scales should be used to collect large samples of axle weight data at various locations in the highway system and that such information should be evaluated and used in formulating future pavement design criteria. It is also suggested that further research be conducted in the field of vehicle dynamics to consider the variations in axle loads due to vehicular, driver, and environmental characteristics.

- BODE, O., ET AL., "Comparison of Different Methods of Determining the Dynamic Wheel Load."

Because of the growing importance of the dynamic forces between wheel and road, several German engineering colleges have developed methods of measuring the dynamic wheel loads of motor vehicles. The methods compared in the first part of the present study are those of the Aachen, Brunswick, and Hanover Colleges. Aachen determines the wheel loads by measuring the accelerations of axle and superstructure. The Brunswick method uses the tire as a measuring spring. The variations in the distance between axle and road surface resulting from tire deflections are measured by a capacitance technique. With the help of the load/deflection curve of the tire, the wheel loads can be calculated. The Hanover method is based on the relationship between the dynamic wheel loads and the resulting elastic deformations of the axle housing. Details of the test equipment, calibration, and methods of evaluation used by the three institutes are given.

To compare the three methods, wheel-load measurements were made simultaneously on the same vehicle (a 10-ton truck) by the test teams of the three institutes, each using its own method of measurement and evaluation. The test runs were made on a good and a bad road and on a roadway. The results are given in tables and diagrams. A second series of tests was made as just described, except that the test data were all evaluated by the same statistical method, and additional measurements were made during travel over sewer covers and transit lines. Potential sources of errors inherent in the test methods are discussed.

Part 2 of the study compares the wheel-load measuring techniques of the Darmstadt, Munich, and Brunswick Institutes. Darmstadt measures the bending stresses at two points in the rim base of a special test wheel. As the correct load is indicated only twice per wheel revolution (viz., each time one of the strain gages is vertically above the tire-ground contact center) no continuous wheel-load trace is obtained, and the method is statistical in character. In the Munich method, the transverse bulging of the tire resulting from

vertical tire deflection is used as a measure of the wheel load. The bulging is scanned by two mechanical feelers which are so connected that the effects of side forces are largely eliminated. The Brunswick method was as described previously.

The results were again evaluated statistically. The inherent sources of error are mentioned, and the advantages and disadvantages of the methods are compared. In Part 3, three methods are compared, all of which use the tire as a measuring spring. These are the Brunswick and Munich methods mentioned previously and another method developed at Brunswick which also measures tire bulging, but by means of electric scanners. These tests were evaluated by direct comparison of the traces.

**EDWARDS, S. G., "Dynamic Measurement of Vehicle Front Wheel Loads Using a Special Purpose Transducer."**

Engineers at the General Motors Proving Ground Noise and Vibration Laboratory are engaged in a variety of engineering testing activities to detect, reduce, and eliminate noise and vibration problems in vehicles. To assist in the basic measurements of front suspension loads, Proving Ground engineers have designed a special-purpose transducer to provide dynamic measurement of the forces and moments imposed on the front wheel. This transducer, with a modified knuckle, replaces the production knuckle-spindle assembly of the front wheel.

Strain gages pick up stresses created by forces and moments at the wheel and send signals through an amplifying system to be recorded by instrumentation in the vehicle in forms suitable for data reduction. The spindle transducer has proven to be a valuable development and research tool.

**ESSERS, KOTITSCHKE, "Masstechnische Bestimmung der dynamischen Radkrafte von Kraftfahrzeugen (Measurement Technique to Determine the Dynamic Wheel Loads of Vehicles)."**

Test methods for determination of dynamic wheel force of motor vehicles, new method applied by Technische Hochschule Aachen for determination of impact by accelerated measurements on axle of heavy motor vehicles

**FINNEY, E. A., "Dynamic Aspects of Vehicle Size and Weight."**

This discussion gives dynamic axle load data in support of Professor Blythe's general statements that such data should be collected, evaluated, and used in formulating future pavement design criteria, and that further research should be conducted in vehicle dynamics, considering variations in axle loads due to vehicular, driver, and environmental characteristics.

Factors relating to weighing vehicles in motion to determine static weight are covered, as well as those associated with the dynamic aspects of vehicle size and weight. The magnitude and frequency of impact loads determined from current Michigan studies are included for further illustration of the problems related to dynamic load determinations.

**FISHER, J. W. and HUCKINS, H. C., "Measuring Dynamic Vehicle Loads."**

This paper describes the development of a differential tire pressure system for the measurement of dynamic vehicle loads on the pavement. The differential tire pressure existing between the vehicle tire and an air storage tank was measured. This allowed the use of a sensitive pressure gage with a range of 0 to  $\pm 1.5$  psi. The changes in pressure caused movement in a steel diaphragm which produced changes in voltage across a steel-core induction coil. An extension of the tire valve stem was connected to a revolving joint which rotated with the wheel. The revolving joint was connected to the pressure gage, thus eliminating the need for an electrical slip ring assembly. Differential tire pressure measurements were correlated with dynamic vehicle loads. The relationship between differential pressure and load is reasonably linear. The differential pressure-load relationship is affected by the tire pressure and the tire volume.

**FREITAG, D. R., GREEN, A. J., and MURPHY, N. R., JR., "Normal Stresses at Tire-Soil Interface in Yielding Soils."**

Small diaphragm-type pressure-sensitive cells were set flush with outer surface of smooth pneumatic tire; tests were run to determine magnitude and distribution of normal pressures at tire-soil interface of driven and towed tire at several loads and inflation pressures; tests were conducted on both cohesive and noncohesive soils; tire deflection measurements were made to determine shape of deformed tire and to locate position of cells; typical patterns are shown and some general relations between patterns observed and test variables are presented.

**GINN, J. L., MILLER, R. F., MARLOWE, R. L., and HEIMOVICS, J. F., "B. F. Goodrich Tire Dynamics Machine."**

Features of new machine to measure forces exerted by loads, speeds, and other operating characteristics. Forces and torques developed by tire under normal operating conditions are: normal load, axial force, drag, self-aligning torque, overturning moment, drag torque. Forces are transmitted through axle bearings to load-resolving cells. Road wheel test shows sensitivity of machine to tire properties depending on cornering response.



HOPKINS, R. C., and BOSWELL, H. H., "Methods for Measuring Load Transfer Through Vehicle Tires to the Road Surface."

Three different methods for obtaining a continuous record of the magnitude and variations in the weight transferred by the tires to the road surface were developed and tested. The three measurement systems investigated were. (1) axle-housing strain near the spring mounting; (2) the change of bulge or spread of the tire sidewall directly above the center of contact with the pavement surface, and (3) changes in air pressure within the tire. Simultaneous measurements were recorded and compared. Each system is discussed.

LIPPMANN, S. A., and NANNY, J. D., "A Quantitative Analysis of the Enveloping Forces of Passenger Tires."

The forces generated by tires when traveling over irregular roads are related to the structure of the tire and to the geometry of the road surface in a useful mathematical relationship. Linearity and superposition principles allow an idealized and synthetic road irregularity to represent the response of a tire to realistic kinds of road irregularities. The association of the enveloping forces with factors related to the structure of tires facilitates the understanding of the enveloping responses. The analysis of the forces for the idealized road irregularity, coupled with the Fourier integral analysis of road surfaces, produces the spectrum of outputs for exciting modes of vibration in the tire itself and in vehicles.

LIPPMANN, S. A., PICCIN, W. A., and BAKER, T. P., "Enveloping Characteristics of Truck Tires—A Laboratory Evaluation."

The paper describes the enveloping properties of truck tires as consisting of two components of force, one in the vertical direction and another in the direction of travel. The responses to irregular surfaces are mathematically accountable in terms of the response to a step in pavement elevation. Tires may therefore be readily characterized, in general, through their reactions to step functions. Curves display the differences in enveloping properties available in the  $10.00 \times 20$  size on the open market.

MILLIMAN, P., "Automatic Weighing of Vehicles in Motion and Collection of Traffic Data by Electronic Methods."

An interim experimental program is reported, conducted to improve accuracy and durability of the existing system, as installed at the test site for weight and dimension measurement of moving vehicles. In addition to extensive modifications of the system and thorough refurbishing, weight tests were conducted to determine the results of the alterations. Accuracy was significantly improved, when determined by the same method as

in Part A, and even further improved when using multiple regression analysis. Platform surface switches and traffic control continue to present problems, but solutions are being evolved.

MITSCHE, M., "Influence of Road and Vehicle Dimensions on the Amplitude of Body Motions and Dynamic Wheel Loads (Theoretical and Experimental Vibration Investigations)."

The relationship between selected body and chassis parameters and dynamic wheel loads is presented along with techniques to obtain and present dynamic wheel load data. The effect of changes in spring and damping rates, wheelbase, and coupling mass on vehicle body motions is examined. The relationship of parameter changes to vehicle ride is discussed.

QUINN, B. E., and THOMPSON, D. R., "Effect of Pavement Condition on Dynamic Vehicle Reactions"

A vehicle traveling over a highway containing surface irregularities experiences vertical motion as well as horizontal motion. Associated with the vertical motion are forces between the highway and the vehicle that are developed in addition to the static weight of the vehicle. These forces are frequently referred to as the dynamic reactions or the dynamic forces. They depend on the vehicle suspension characteristics, the condition of the pavement, and the velocity of the vehicle.

Laboratory tests were conducted to determine the frequencies of vibration at which passenger vehicles would develop large forces between the tires and the pavement. The relationship between force exerted by the tire and vertical displacement of the tire tread was measured at all frequencies at which any appreciable force was developed. The vehicle characteristic thus obtained included the actual effects of all components of the vehicle suspension system.

A criterion of pavement condition was established by making power spectral density analyses of highway elevation measurements. A brief description of the physical significance of this criterion is included.

A procedure is discussed for combining the vehicle characteristics with an elevation power spectrum (pavement condition criterion) at a selected vehicle velocity to obtain a dynamic force power spectrum. The usefulness of this result is discussed and curves for the root mean squared value of the dynamic force versus vehicle velocity are included for three different pavement conditions.

By using the criterion of pavement condition as defined in this paper, it is possible to estimate the dynamic force that one wheel of a vehicle will exert on a highway.

QUINN, B. E. and VAN WYK, R., "A Method for Introducing Dynamic Vehicle Loads into Design of Highways"

To predict the dynamic load of a vehicle on a pavement, suitable methods are necessary for characterizing the highway profile and the vehicle suspension system. Highway profiles have been described by using Fourier series approximations or power spectral density techniques, and the resulting frequency domain descriptions indicate that a similar description of the vehicle would be useful.

The ratio of wheel reaction to wheel displacement ( $F/X$ ) versus frequency is therefore investigated for several vehicles. Effects of shock absorbers and tire pressure are observed. The prediction of the dynamic load using the proposed vehicle characteristics is used to obtain significant vehicle parameters

Estimation of the dynamic vehicle load indicates that a study of the significance of this quantity in highway design is desirable, as well as experimental verification of the predicted values.

QUINN, B. E., and WILSON, C. C., "Can Dynamic Tire Forces Be Used as a Criterion of Pavement Condition?"

A moving vehicle exerts a fluctuating component of force on the highway due to vertical motion induced in the vehicle by unevenness of the pavement. This force, superimposed on the static wheel load, is frequently called the dynamic wheel force or the dynamic tire force. This paper includes a brief description of instrumentation used to determine the dynamic tire force by measuring the fluctuation of the air pressure in a tire of a moving vehicle. Actual force records that were taken on several sections of pavement are included. From these records the corresponding root mean squared value of the dynamic force is determined, and the possible use of this quantity as a criterion of pavement condition is suggested. In addition, for certain pavement sections the frequency of occurrence of various magnitudes of the dynamic tire force is determined. The influence of speed on dynamic force is investigated by operating the test vehicle over the same length of pavement at different velocities. In like manner the influence of tire inflation pressure on dynamic force is studied by conducting tests in which only the inflation pressure was varied.

SPANGLER, E. B. and KELLY, W. J., "GMR Road Profilometer—A Method for Measuring Road Profile."

Accurate road profiles are often required for the analytical study of vehicle ride and vibration phenomena induced by road irregularities. The desire to bring profiles of existing roads into the laboratory has led to the development of a road profilometer for the rapid measurement of such

road profiles. The continued interest in this device by persons engaged in highway design, construction and maintenance encouraged the authors to further develop and simplify this instrument and to make it available to these highway groups. This paper discusses the basic operating principle of the GMR profilometer, describes the unit supplied to the Michigan Department of State Highways, and presents some typical test results.

TRABIC, G. W., LASK, K. V., and BUCHELE, W. F., "Measurement of Soil-Tire Interface Pressures."

Diaphragm-type pressure transducers instrumented with strain gages were designed and built to measure soil-tire interface pressures. The interface pressure was measured on the undertread, lug face leading-lug side of a tire.

Drawbar load and tire-inflation pressures were the controlled variables in this investigation. The tests were run with drawbar loads of 40, 446, 928, 1,374, and 1,783 lb and tire-inflation pressures of 10, 14, and 18 psi. Three replications were run for each condition. The results were averaged for each cell position and plotted. The plotted data showed that high drawbar loads increased the interface pressure on the undertread and leading-lug side and reduced the interface pressure on the lug face and trailing-lug side. These plots also show that, as tire inflation pressure was increased, the soil-tire interface pressure increased at the center of the tire and decreased at the edges.

Slip was measured during each run with two microswitches electrically connected to event marker pens on the oscillograph. One of the microswitches measured actual forward travel and the other measured theoretical travel. Percentage of slip was calculated from the data thus obtained and the results were plotted against drawbar load for each tire-inflation pressure.

The torque measured on the rear axle was plotted against drawbar load and percentage of slip for each tire-inflation pressure. The plot of torque versus drawbar load showed that torque increased linearly with drawbar load with a tire-inflation pressure of 10 psi. With tire-inflation pressures of 14 and 18 psi, the torque increased linearly up to 1,374- and 928-lb drawbar loads, respectively, and then increased at an increasing rate. The plot of torque versus percentage of slip showed that percentage of slip increased slowly up to a torque of approximately 1,500 lb-ft and then increased more rapidly, especially with the 14- and 18-psi tire pressures. This plot also showed that with a tire pressure of 10 psi, a torque of 2,655 lb-ft in the right rear axle was required to develop a 1,783-lb drawbar pull. With an inflation pressure of 18 psi, 3,506 lb-ft were required to develop the same pull.

# APPENDIX B

## VEHICLE TYPE DESIGNATION

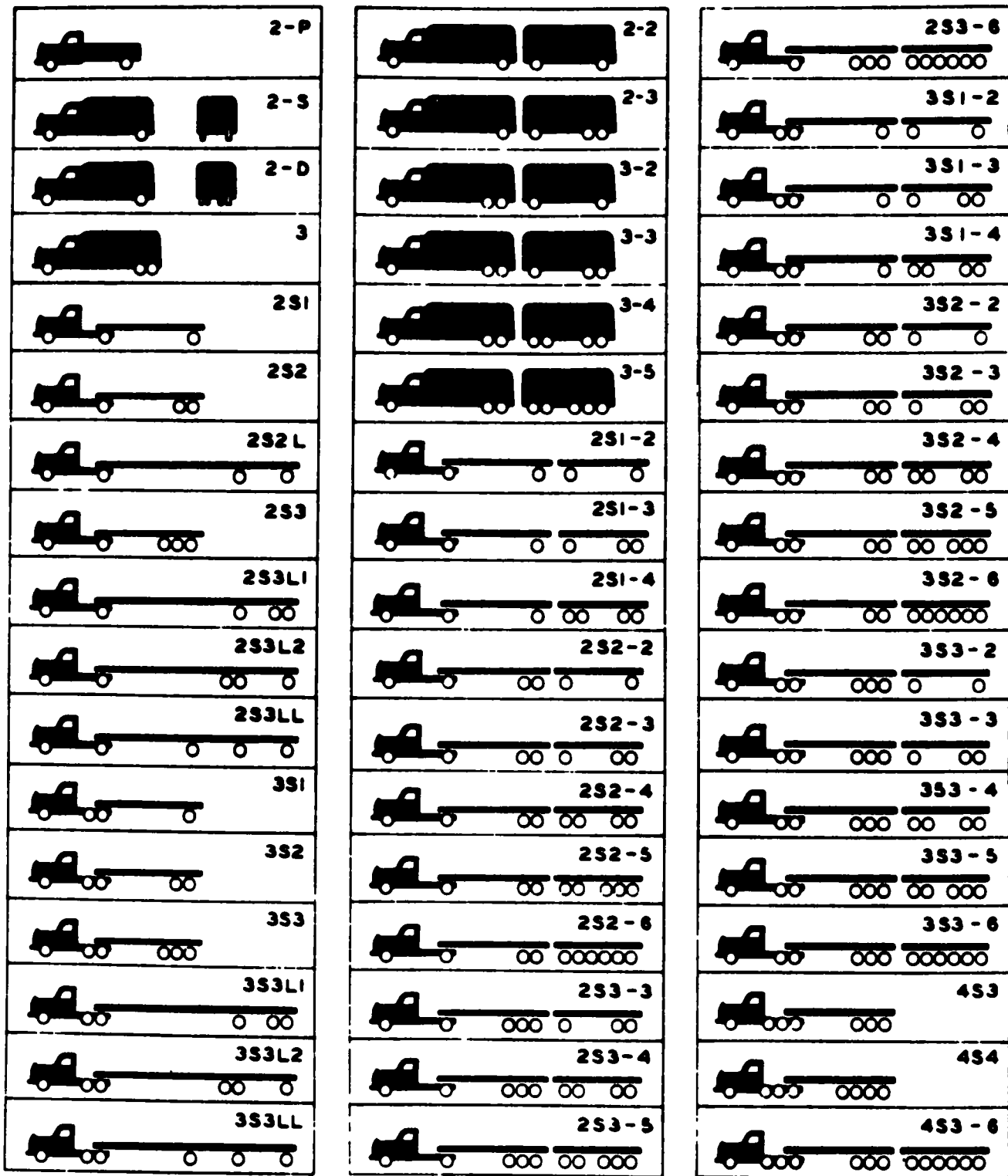
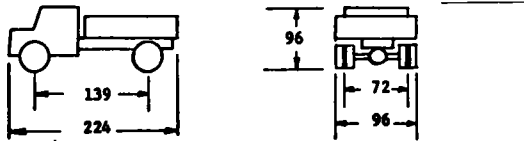


Figure B-1. Vehicle type designation.

## APPENDIX C

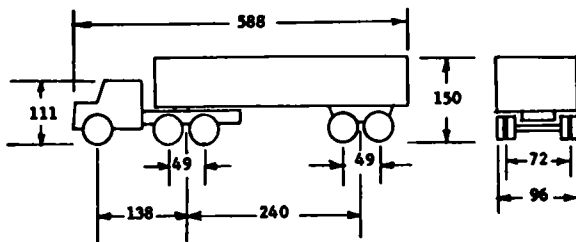
### TEST VEHICLE SPECIFICATIONS

#### VEHICLE NO. 1 2-D



**Chassis.** GMC model HM 7620  
**Body** Gar-Wood dump box  
**Engine** GMC 478-cu in V-6, gasoline  
**Transmission:** New process model 541GL, 5-speed  
**Suspension, steer**  
 Type Simple leaf spring  
 Axle GMC F-070 Rating, 7,000 lb  
 Springs 55 in  $\times$  3 in, 6-leaf Rating 3,500 lb each  
 Shocks Yes  
**Suspension, drive**  
 Type: Simple leaf spring  
 Axle: Eaton 16221, 2-speed Rating: 17,000 lb  
 Springs 46 to 51 in.  $\times$  3 in., 10-leaf Rating 8,750 lb each  
 Shocks. No  
**Wheels**  
 Type: Cast steel spoke  
 Rims: 20 in.  $\times$  7 in., 4-in spacer  
 Tires 10 00  $\times$  20 bias ply, 12-ply rating  
**Brakes.**  
 Front 15 in.  $\times$  3 in., air  
 Rear: 15 in  $\times$  6 in., air  
**Test axle weights**  
 Steer. 5,000 lb  
 Drive. 18,800 lb

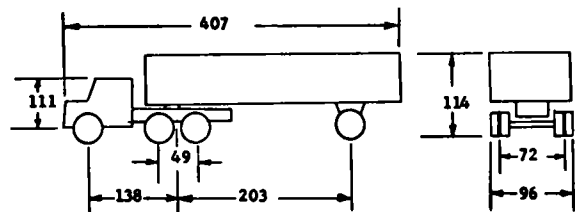
#### VEHICLE NO. 2 3S2



**Tractor.** GMC model DH-9690 (with sleeper cab)  
**Trailer** Trailmobile model P31T75AHB  
**Engine** Detroit diesel 8V-71 NE, diesel  
**Transmission:** Fuller RT 910, 10-speed progressive  
**Suspension, steer**

Type Simple leaf spring  
 Axle. GMC F-090 Rating 9,000 lb  
 Springs 55 in  $\times$  3 in., 8-leaf Rating 4,500 lb each  
 Shocks Yes  
**Suspension, drive.**  
 Type Hendrickson RT-340 with steel equalizer beams  
 Axles. Rockwell Timken SLHD Rating: 34,000 lb  
 Springs. 34 in.  $\times$  4 in, 11-leaf Rating: 17,000 lb each  
 Shocks: No  
**Suspension, trailer.**  
 Type Simple leaf spring, tandem  
 Axles: Fruehauf  
 Springs Leaf Rating 8,500 lb each  
 Shocks No  
**Wheels**  
 Type. Cast steel spoke  
 Rims: 20 in  $\times$  7 in, 4 in. spacer  
 Tires. 10 00  $\times$  20 bias ply, 12-ply rating  
**Brakes.**  
 Steer 15 in.  $\times$  3½ in., air  
 Drive. 15 in.  $\times$  6 in., air  
 Trailer 16½ in.  $\times$  5 in., air  
**Test axle weights**  
 Steer 7,000 lb  
 Drive 30,790 lb  
 Trailer 31,030 lb

#### VEHICLE NO. 3 3S1



**Tractor.** GMC model DH-9690 (with sleeper cab)  
**Trailer.** Fruehauf model JA 2082 FW (#12)  
**Engine:** Detroit diesel 8V-71NE, diesel  
**Transmission** Fuller RT 910, 10-speed progressive  
**Suspension, steer:**  
 Type Simple leaf spring  
 Axle. GMC F-090 Rating. 9,000 lb  
 Springs 55 in  $\times$  3 in, 8-leaf Rating: 4,500 lb each  
 Shocks. Yes  
**Suspension, drive.**  
 Type. Hendrickson RT-340 with steel equalizer beams  
 Axles: Rockwell Timken SLDH Rating: 34,000 lb  
 Springs 34 in  $\times$  4 in., 11-leaf Rating: 17,000 lb each  
 Shocks: No

*Suspension, trailer.*

Type: Simple leaf spring  
 Axle Fruehauf I-Beam, 1960 Rating 18,000 lb  
 Springs Leaf Rating 9,000 lb each  
 Shocks No

*Wheels.*

Type: Cast steel spoke, 20 in.  
 Rims. 20 in. × 7 in., 4-in. spacer  
 Tires 10 00 × 20 bias ply, 12-ply rating

*Brakes:*

Steer. 15 in. × 2½ in., air  
 Drive 15 in. × 6 in., air  
 Trailer. 16½ in. × 7 in., air

*Test axle weights.*

Steer: 7,000 lb  
 Drive. 21,605 lb  
 Trailer: 17,670 lb

**APPENDIX D****TEST ROAD SECTION SPECIFICATIONS**

The Michigan Department of State Highways identified nine 1-mi test road sections to represent good, fair, and poor grades of rigid, flexible, and overlay pavement. The condition of the road sections previously had been graded with a Bureau of Public Roads roughometer. Less than 130 in./mi was specified a good road, 130 to 175 in./mi a fair road, and more than 175 in./mi a poor road. The selected sections were

DESCRIPTION	ROUGHNESS (IN./MI)
<b>Rigid Pavement</b>	
Good—I-75 southbound in Oakland Co., beginning at Walton Boul, thence 1 mi south	118 (1965) <sup>a</sup>
Fair—I-696 eastbound in Oakland Co., beginning at the 6-mi marker 300 yd east of Middlebelt Road, thence 1 mi east.	149 (1965)
Poor—M-50 eastbound in Lenawee Co. between US 23 and Britton, Mich., beginning at Downing Highway, thence 1 mi east	176 (1963)
<b>Flexible Pavement.</b>	
Good—M-52 northbound, beginning at the Jackson-Washtenaw Co. line, approximately 0.3 mi south of Leeke Road, thence 1 mi north	92 (1968)
Fair—M-247 northbound in Bay Co., beginning at the first "M-247" sign north of the Kawkawlin River, thence 1 mi north.	169 (1968)
Poor—M-138 eastbound in Bay Co., beginning at the "M-138 Ends" sign on the north side of the roadway near M-15, thence 1 mi east	249 (1968)
<b>Overlay Pavement.</b>	
Good—M-53 northbound in Lapeer Co., beginning at the "M-53" sign north of Hollow Corners Road, thence 1 mi north.	128 (1968)
Fair—M-53 southbound in Lapeer Co., beginning at the "Dryden Road" sign on the east side of the roadway, south of Dryden Road, thence 1 mi south.	154 (1968)
Poor—M-59 eastbound in Oakland Co., beginning at the "M-59" sign just east of Centerline Drive, thence 1 mi east	225 (1968)

<sup>a</sup> Figures in parentheses are measurement dates

## APPENDIX E

### GM PROFILOMETER AND ITS USE ON THIS PROJECT

#### THEORY OF PROFILOMETER OPERATION

The GM profilometer (5) was developed by the General Motors Research Laboratories during the period 1961 to 1964. Profilometers based on the same principle have been used extensively by state highway departments and General Motors since that time. The profilometer produces a continuous record of elevation profile within the wavelength limits established by its design.

A schematic of the profilometer is shown in Figure E-1. The GM profilometer is a seismic mass device in which the body of the truck is the mass on its suspension springs and shock absorbers. Because there is motion of the truck body, a 2g servo accelerometer is used to measure its motion relative to an inertial reference. A 14-in. travel linear potentiometer measures the relative displacement of the road-following wheels to the truck. The acceleration of the truck body is then double-integrated and summed with the truck to road-following wheel displacement. This results in the measurement of the road profile with respect to an inertial reference. The high-amplitude, long-wavelength elevation changes are rejected with a high-pass filter to improve the resolution of detail.

The profilometer vehicle carries self-monitoring strip chart recorders and a 14-channel instrumentation tape recorder. Vehicle speed, voice, raw data, and finished profiles are all recorded on magnetic tape.

#### HIGH-SPEED PROFILES

The original intent was to measure road profiles simultaneously with the measurement of test truck dynamic loads. This was accomplished by towing the profilometer vehicle with the truck being tested (Fig. E-2). As the truck was

driven along the pavement section, the profilometer would measure profile along the same wheel path and under the same road conditions that the truck measurements were being made. Owing to the fixed distance between the truck wheels and the road-following wheels of the profilometer, time correlation of measured and computed pavement loads to road profile would be simplified.

Early in the testing, high-amplitude, short-wavelength components were present in the recorded profile data to a greater extent than in the actual road profile. This was detected during early attempts to correlate the dynamic load predicted by the model with load measurements made on the test vehicle. The profile error was due to road-following wheel bounce. The following wheel has an acceleration limit in the down direction due to the limited preload force and the mass of the following arm and wheel. Whenever this acceleration level is exceeded, the road-following wheel leaves the road surface.

There are several methods by which wheel bounce may be reduced:

1. Use higher preloads and/or a lower mass for the trailing arm and wheel assembly.
2. Develop a noncontacting profiling system.
3. Reduce the speed of the profilometer.

The third method was used for this project.

#### LOW-SPEED PROFILES

Road-following wheel bounce was essentially eliminated by decreasing the speed of the profilometer vehicle. Because pavement load measurements were made at 34 mph, it was necessary to speed up the profile tape recordings

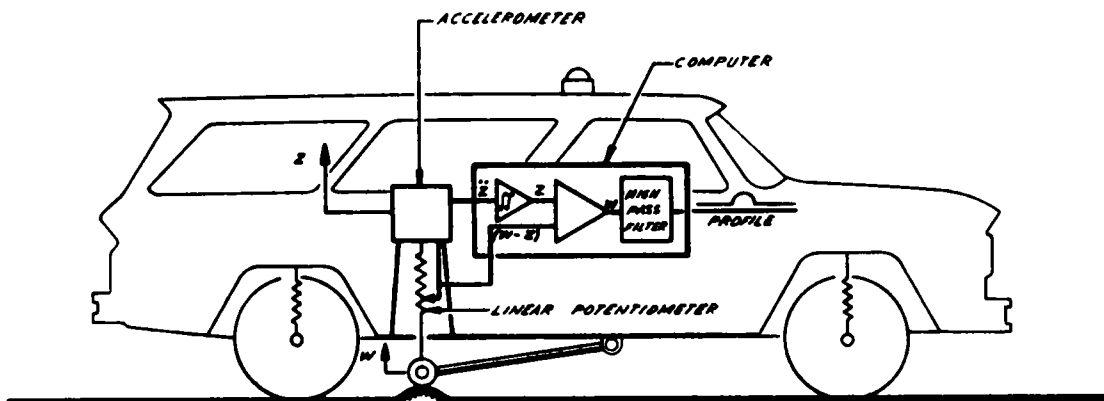


Figure E-1. Schematic of GM profilometer



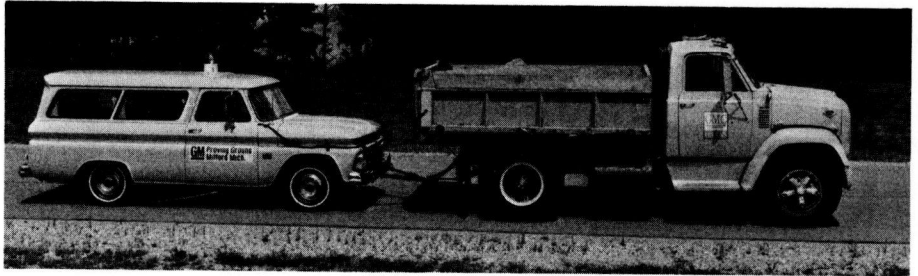


Figure E-2. Test Vehicle No. 1 towing the GM profilometer.

when recorded profiles were used as an input to a computer simulation for pavement load predictions. A speed change of 8:1 was readily available with equipment on hand, so the road profiles were measured at a profilometer speed of  $4\frac{1}{4}$  mph and a tape recording speed of  $3\frac{3}{4}$  ips. The data were then played back at 30 ips to be equivalent

to 34 mph. A 0.3-rad/sec high-pass filter was used during profile recording (Fig. E-3).

Low-speed profiling did not provide simultaneous road profile and pavement load measurements, nor were the profiles recorded in this manner of the exact same wheel path as that followed by the test vehicle.

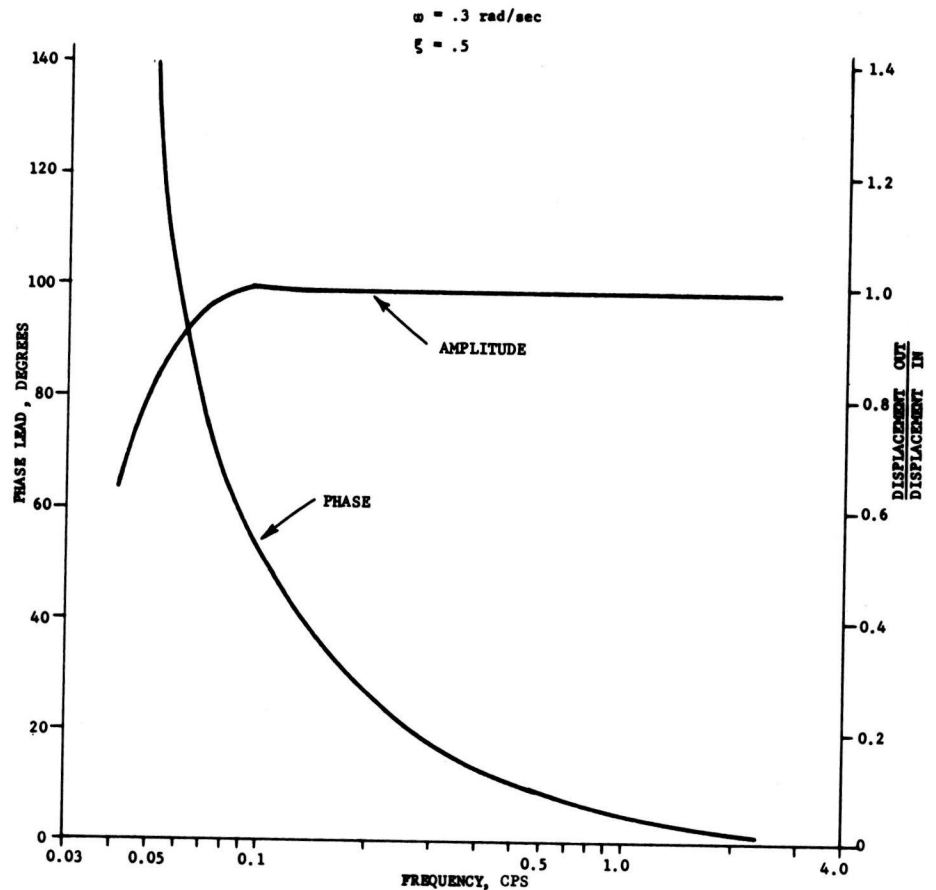


Figure E-3. Filter frequency response characteristics.

## APPENDIX F

### COMPUTATION OF POWER SPECTRAL DENSITY FUNCTIONS: TECHNIQUES AND ERRORS

This appendix describes the processing procedures used to compute power spectral density functions of road profile and pavement load data. The description includes processing the data from the time it is recorded on the road until the power spectral density functions are generated. Some errors that are encountered during the computations are also discussed.

#### COMPUTATION PROCEDURES

Analog voltages proportional to road profile and pavement load were recorded on FM magnetic tape. The tape was then played back in the laboratory to an analog-to-digital conversion facility that converted the analog voltages to digital numbers and generated a digital magnetic tape. The digital tape was used for further data processing by an IBM System/360 Model 30 computer

The digital processing consisted of all the computations necessary for the determination of a power spectral density function. The Blackman-Tukey method of computing power spectral densities was used (6). A brief description of this method follows:

First, the average of all the data points describing the input curve (the original time series) was computed and subtracted from the original time series. Then, the autocorrelation was calculated using the lagged products method (Fig. F-1). The Fourier transform of the autocorrelation, which is a raw estimate of the power spectral density function, was then calculated. Because the autocorrelation is an even function, only the cosine terms of the Fourier series were calculated. The raw estimate of the power spectral density was then smoothed to produce a refined estimate of the PSD. The smoothing was performed after the Fourier transformation and used the Hanning spectral window (Fig. F-2). The refined estimates of the PSD were then plotted using the program shown in Figure F-3.

#### COMPUTATIONAL ERRORS

Certain errors involved in calculating the power spectral density function are discussed in many references (6). These errors are listed and discussed in the following, and an estimate is made of the amount of error in the PSD's in this report.

1. Leakage Error. The Hanning spectral window, which was used to smooth the raw estimate of the PSD, has small side lobes that extend over a wide frequency range. This means that large components of the PSD at frequencies far removed from the frequency being smoothed can have some effect on the latter frequency. If the component

being smoothed is very small compared to the large component far away, the large component can have considerable influence on the small component. This appears on certain road profile PSD's at very low levels at higher frequencies, where the PSD functions seem to oscillate. To further compound the leakage problem, alternate side lobes of the Hanning window are negative, which leads to the possibility of negative estimates of PSD. This phenomenon was observed on one pavement load PSD and one road profile PSD. Leakage can be reduced by decreasing the spacing along the abscissa, effectively reducing the frequency range of the side lobes of the Hanning window

2. Truncation Error. Random analysis requires an infinite time series for theoretical accuracy in the estimation of statistical properties. Any random analysis performed with a truncated (not infinite) time series will result in some error being introduced.

3. Stationarity Errors: In addition to an infinite time series, other conditions necessary in this method of calculation of PSD's are that the road profile and pavement load data be stationary and ergodic; that is, the statistics of the

```

DIMENSION A(5000),R(600),X(600),VABS(10),VORD(10),VPAGE(10)
DIMENSION WORK(250)
CALL PLOTS(WORK(1),1000,9)
RFAD(1,10)NCURVE
10 FORMAT(315)
15 FORMAT(10A4/10A4/10A4)
DO 100 N=1,NCURVE
  READ(1,10)NPTS,NLAGS,NPLT
  READ(8,1)(A(M),M=1,NPTS)
  1 FORMAT(20(1PE13.4))
  SUM=0.
  DO 18 M=1,NPTS
    18 SUM=SUM+A(M)
  AVG=SUM/NPTS
  DO 19 M=1,NPTS
    19 A(M)=A(M)-AVG
  IF(NLAGS-1)100,100,20
  20 CALL AUTO(A,NPTS,NLAGS,R)
  READ(1,25)XNCRE
  25 FORMAT(F10.4)
  XA=0.
  DO 30 M=1,NLAGS
    X(M)=XA
    XA=XA+XNCRE
  30 CONTINUE
  WRITE(9,1)(R(I),I=1,NLAGS)
  IF(NPLT)50,40,50
  40 READ(1,15)VABS,VORD,VPAGE
  READ(1,10)NCA,NCO,NCP
  CALL GRAPH(X,R,VABS,VORD,VPAGE,NCA,NCO,NCP,NLAGS,0,0)
  50 CALL PDUMP(A(1),A(NPTS),5)
100 CONTINUE
CALL TAPECO(7,5)
CALL PLOT(15.0,0.0,999)
END

```

Figure F-1 Autocorrelation computation program

```

      DIMENSION A(1028),          INV(256),S(256)
      DIMENSION          COEF(2,512),ORD(514),ABC(514),VABS(10),VORD(10),
1VPAGE(10)
      DIMENSION WORK(100)
      EQUIVALENCE (A(1),COEF(1,1))
      CALL PLOTS(WORK(1),400 ,9)
      READ(1,1) NCURVE
1  FORMAT(2I4,F8.6,E12.6,I4)
      DO 500 NCURV=1,NCURVE
      DO 11 I=1,1028
11 A(I)=0.
      READ (1,1) NPTS,NSKIP,TIME,FAC,NPL
30 IFERR=0
100 READ(8,21)(A(J),J=1,NPTS)
21 FORMAT(20(1PE13.4))
      NS=NPTS-1

      MAKE UP FREQUENCY ARRAY FOR THE ABSCISSA

      ABC(1)=0.
      H=1./(2.*TIME*NS*FAC)
      DO 40 J=2,NPTS
40 ABC(J)=ABC(J-1)+H
3  FORMAT(3F15.6)
      AO=A(1)
      ANSIZE=A(NPTS)
      CALL PDUMP(A(1),A(NPTS),5,NPTS,NPTS,4)

      FOURIER TRANSFORM THE AUTOCOVARIANCE, AN EVEN FUNCTION

      T=3.14159265/NPTS
      DO 101 J=1,NPTS
      SUM=0.
      T2=T*(J-1)
      DO 99 I=2,NS
99 SUM=SUM+A(I)*COS(T2*(I-1))
      WRITE(3,5)SUM
5  FORMAT(E15.6)
101 ORD(J)=2.*TIME*(AO+2.*SUM+ANSIZE*COS((J-1)*3.14159265))
      WRITE(3,4)H,AO,ANSIZE,NPTS,TIME
4  FORMAT(' H=',E12.4,5X,'AO=',E12.4,5X,'ANSIZE=',E12.4,5X,'NPTS=',
1  I12,5X,'TIME=',E12.4)
      CALL PDUMP(ABC(1),ABC(NPTS), 5)
20 FORMAT(10A4/10A4/10A4)
10 FORMAT(4I4)
      CALL PDUMP(ORD(1),ORD(NPTS),5)

      PERFORM HANNING SMOOTHING

      A(1)=0.5*ORD(1)+0.5*ORD(2)
      DO 90 J2=2,NPTS
90 A(J2)=0.25*ORD(J2-1)+.50*ORD(J2)+0.25*ORD(J2+1)
      A(NPTS )=0.5*ORD(NPTS -1)+0.5*ORD(NPTS )

      PUT SMOOTHED PSD BACK IN ORD ARRAY

      DO 91 J2=1,NPTS
91 ORD(J2)=A(J2)*FAC
      CALL PDUMP(ORD(1),ORD(NPTS), 5)
      WRITE(9,21)(ABC(IA),IA=1,NPTS)
      WRITE(9,21)(ORD(IA),IA=1,NPTS)
      IF(NPL)450,450,460
450 READ(1,20)VABS,VORD,VPAGE
      READ(1,10)NCA,NCO,NCP
      CALL GRAPH(ABC,ORD,VABS,VORD,VPAGE,NCA,NCO,NCP,NPTS,0,0)

      INTEGRATE UNDER PSD CURVE. THIS VALUE IS THE MEAN
      SQUARE, SHOULD EQUAL THE ZERO-LAG AUTOCOVARIANCE.

460 HH=0.5*H
      SUM2=0.
      DO 470 I=2,NPTS
      SUM1=SUM2
      SUM2=SUM2+HH*(ORD(I)+ORD(I-1))
470 ORD(I-1)=SUM1
      WRITE(3,12)SUM2
12 FORMAT(' INTEGRATED VALUE=',E14.5,/)
500 CONTINUE
      CALL EXIT
      END

```

Figure F-2. Power spectral density computation program

data should not change with time or with repeated measurements. Errors are introduced where the data are non-stationary or nonergodic

4. Sampling Errors. Digital processing requires that continuous data be sampled at intervals of time. Errors are introduced if the intervals are not small enough to

THIS PROGRAM READS TWO ARRAYS FROM A TAPE GENERATED BY A PROGRAM IN DLS CALLED POWER. THE FIRST ARRAY CONTAINS EQUALLY SPACED FREQUENCIES. THE SECOND ARRAY CONTAINS ORDINATES OF POWER SPECTRAL DENSITY. THIS PROGRAM PLOTS THE ARRAYS IN A SEMI-LOG FORMAT (LOG ON THE ORDINATE, LINEAR ON THE ABSCISSA). IT CAN PLOT UP TO 5 CURVES ON ONE GRAPH.

```

DIMENSION ABC(514),GRD(514),VABS(10),VORD(10),VPAGE(6),WORK(100)
DIMENSION HEAD(10),C1(6),C2(6),C3(6)
REAL LABEL,LIBEL
1 FORMAT(4I4)
2 FORMAT(10A4/10A4)
3 FORMAT(2L12.5,11L2,F12.8)
4 FORMAT(6A4,2I4)
5 FORMAT(10A4,12)
6 FORMAT(1(6A4,12))
7 FORMAT(20(1PE13.4))

```

NPLOTS--NO. PLOTS TO BE MADE

NLINES--NO. LINES ON THE PRESENT PLOT

```
CALL PLOTS(FORPK(1),400,9)
```

READ NO. GRAPHS TO BE GENERATED

```

REAL(1,1)NPLOTS
DO 1000 NPLIT=1,NPLOTS
  LABEL=7.6
  CALL PLOT(0.,0.02,23)

```

DRAW A LINE, GET THE PEN WRITING

```

CALL PLOT(0.,11.0,2)
CALL PLOT(0.,0.,2)
CALL PLOT(2.5,1.5,23)

```

READ NO. CURVES ON THIS GRAPH, NO. POINTS PER CURVE

```

READ(1,1)NLINES,NPTS
READ(1,2)VABS,VGRD
READ(1,3)NCA,NCU
READ(1,5)HLAL,NH
READ(1,6)C1,NC1,C2,NC2,C3,NC3
READ(1,3)STLIN,UNITS,ILOG,CYCLES

```

Figure F-3. Power spectral density plotting program.

COMPUTE MAXIMUM VALUE ON 8 IN. Y-AXIS

```

YSTART=10.**ILOG
IF(ILOG)100,110,110
100 ILOG=ILOG+1
110 NEXP=8.*CYCLES
IFXP=ILOG+NEXP
YMAX=10.**IFXP
YMIN=10.**ILOG

```

DRAW THE AXES

```

CALL LGAXIS(0.,0.,VORD,NCU,8.0,90.0, YMIN,CYCLES)
CALL AXIS(0.,0.,VABS,-NCA,6.,0.,STLIN,UNITS,10.)

```

WRITE HEADER INFORMATION ON PLOT

```

CALL SYMBOL(-.18,8.7,0.20,HEAD,0.,NH)
CALL SYMBOL(3.0,8.0,0.10,C1,0.,NC1)
CALL SYMBOL(3.0,7.8,0.10,C2,0.,NC2)
CALL SYMBOL(3.0,7.6,0.10,C3,0.,NC3)

```

START LOOP THAT PLOTS THE LINES

```

DO 300 NLINE=1,NLINES
  READ(1,4)VPAGE,NCP,NSYM
  PEAC(H,8)(ABC(I),I=1,NPTS)
  READ(1,8)(GRD(I),I=1,NPTS)
  GRD(NPTS+1)=YSTART
  GRD(NPTS+2)=CYCLES
  ABC(NPTS+1)=STLIN
  ABC(NPTS+2)=UNITS

```

FIND ANY POINTS OUTSIDE Y LIMITS, SET THEM EQUAL TO THE LIMITS

```

DO 200 I=1,NPTS
  IF(OPD(I)-YMAX)160,160,150
150 ORD(I)=YMAX
  GO TO 200
160 IF(ORD(I)-YSTART)170,200,200
170 ORD(I)=YSTART
200 CONTINUE

```

PLOT THE CURVE

```
CALL LGLINE(ABC,GRD,NPTS,1,1,NSYM,1)
```

DRAW THE LEGEND FOR THIS CURVE

```

LABEL=LABEL-0.2
LIBEL=LABEL+0.05
CALL SYMBOL(3.0,LABEL,0.1,VPAGE,0.,NCP)
CALL SYMBOL(5.5,LABEL,0.1,NSYM,0.,-1)
CALL SYMBOL(6.0,LABEL,0.1,NSYM,0.,-2)
300 CONTINUE
CALL PLOT(8.5,-2.0,-3)
1000 CONTINUE
CALL PLOT(2.0,0.0,999)
CALL EXIT
STOP
END

```

recover all the frequencies in the continuous data (aliasing error). Also, some small error is introduced when a digital number is assigned to a continuous value (quantization error).

Evaluation of the statistical errors is, in general, difficult because a prior knowledge of the PSD is necessary. An approximate method has been suggested (7) to determine confidence levels of the computed PSD. The approximation consists of assuming the distribution of several estimates of one point on the PSD curve to be a chi-square distribution. For the approximation to be valid, the original time series must be Gaussian distributed. This assumption was not checked on all load and profile data; however, spot checks indicate that the probability densities have at least the same general shape as the

Gaussian curve. Using the chi-square method of estimating errors, 80% of the computed PSD ordinates fall within  $\pm 15\%$  of the true value of the ordinate. The true value of a point on the PSD is defined here to be the average of many estimates of the point resulting from many test runs.

The chi-square approximation to error includes only the effects of leakage and truncation. Therefore, an upward adjustment of the error estimate should be made to compensate for stationarity errors, sampling errors, and other errors not included in the chi-square approximation. Also, because the distributions are not perfectly normal, the error figure should be further adjusted upward to arrive at a final error estimate. It should be emphasized that the final estimate of error magnitude would be approximate.

## APPENDIX G

### ROAD PROFILE POWER SPECTRAL DENSITY FUNCTIONS

This appendix contains the power spectral density functions (Fig. G-1) of the elevation profiles of the 1-mi test road sections given in Table G-1.

During computation of these PSD's some errors became apparent at small magnitudes of the functions. Appendix F contains a discussion of sources of computational error, the resulting accuracy of the PSD's, and the techniques used to compute the PSD's.

TABLE G-1  
CONDITIONS OF TEST ROAD SECTIONS

ROAD SECTION	PAVEMENT	ROUGHNESS	BPR ROUGHOMETER ROUGHNESS (IN./MI)
I-75	Rigid	Good	118
I-696	Rigid	Fair	149
M-50	Rigid	Poor	176
M-52	Flexible	Good	92
M-247	Flexible	Fair	169
M-138	Flexible	Poor	249
M-53 NB	Overlay	Good	128
M-53 SB	Overlay	Fair	154
M-59	Overlay	Poor	225

NB = northbound; SB = southbound

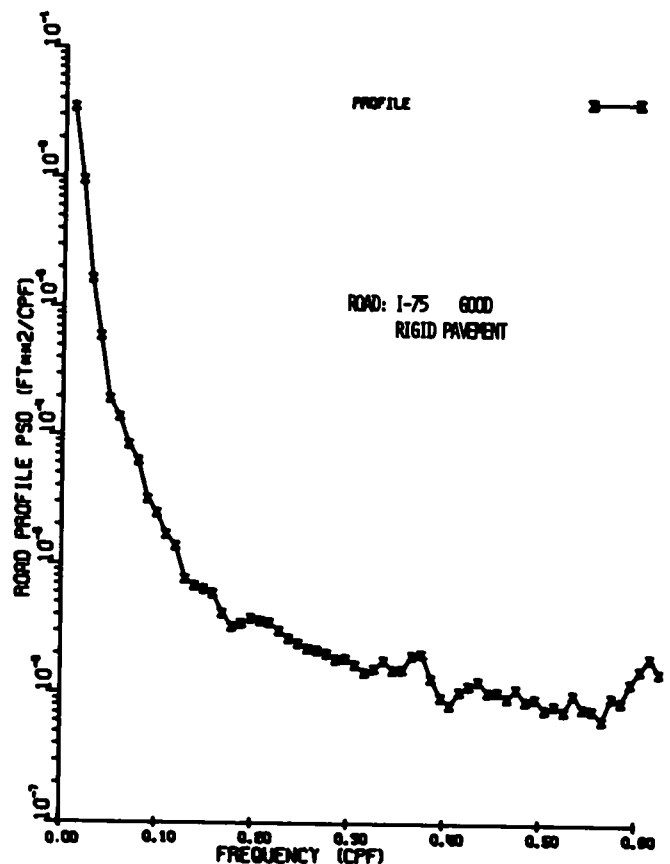


Figure G-1. Road profile power spectral density.

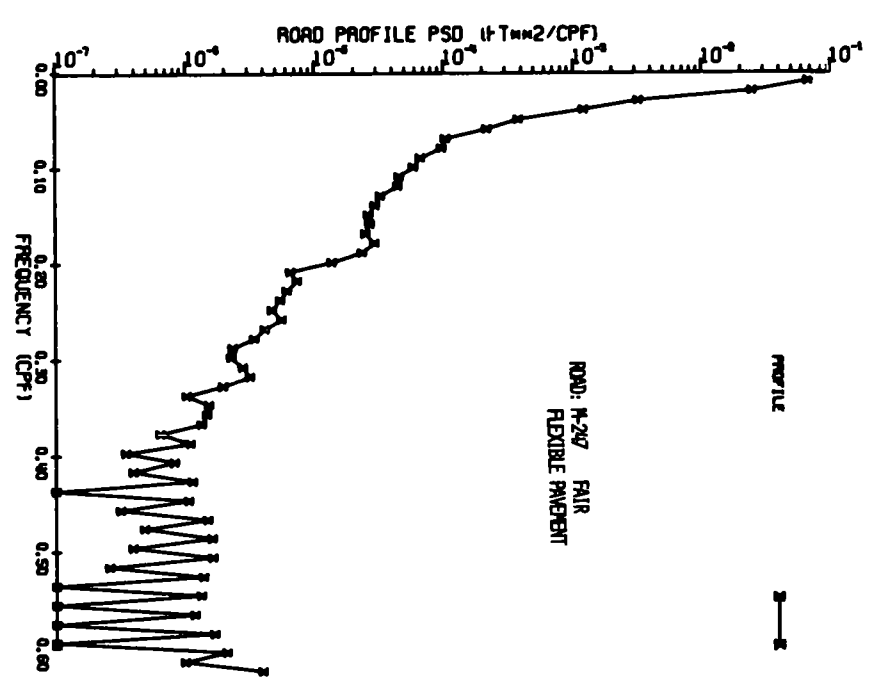
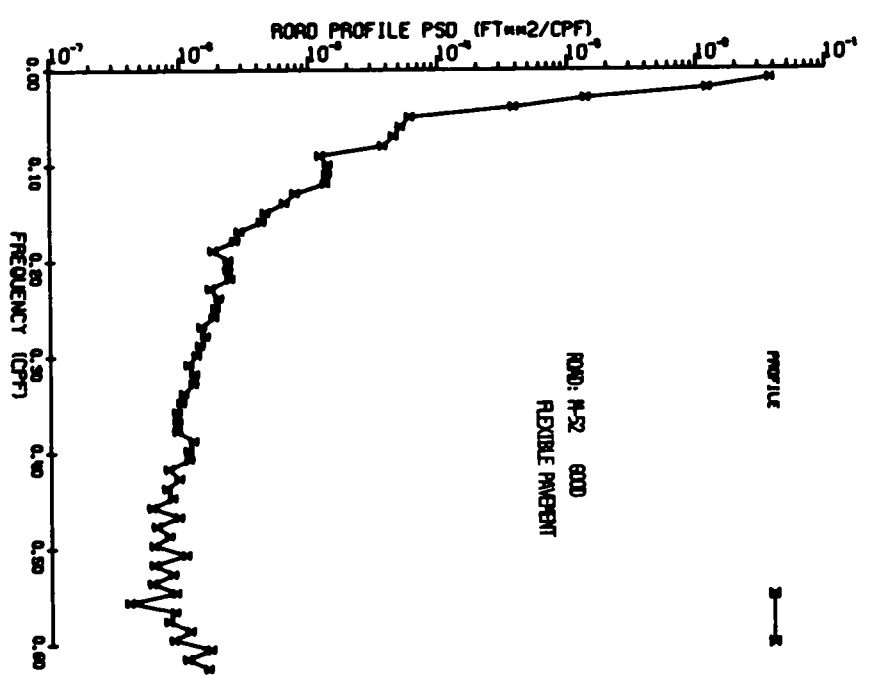
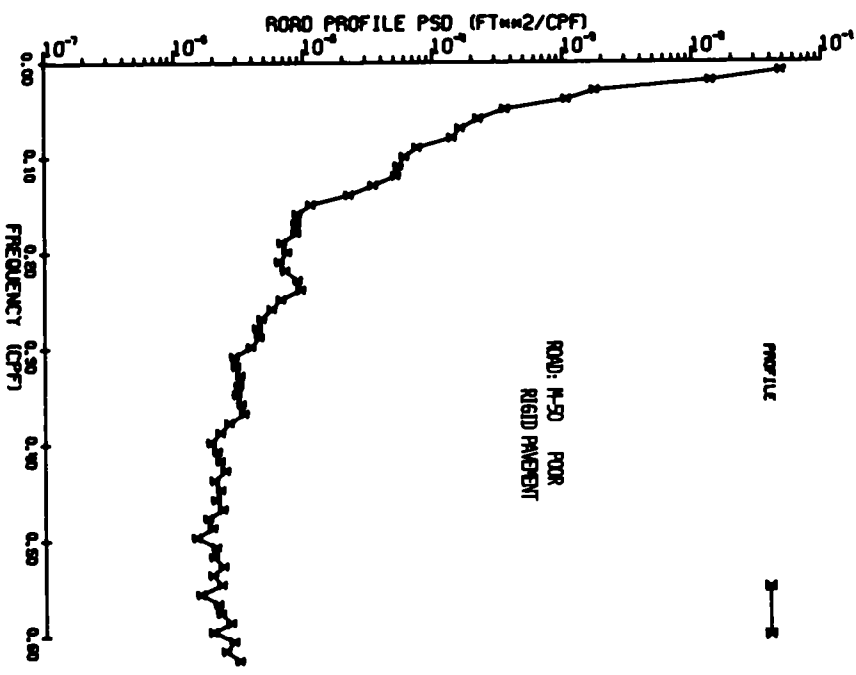
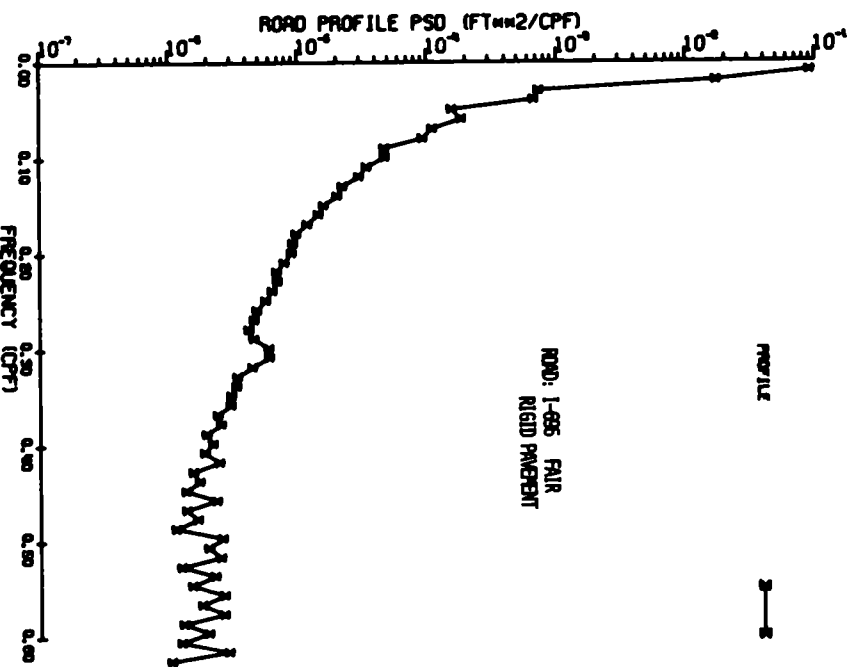
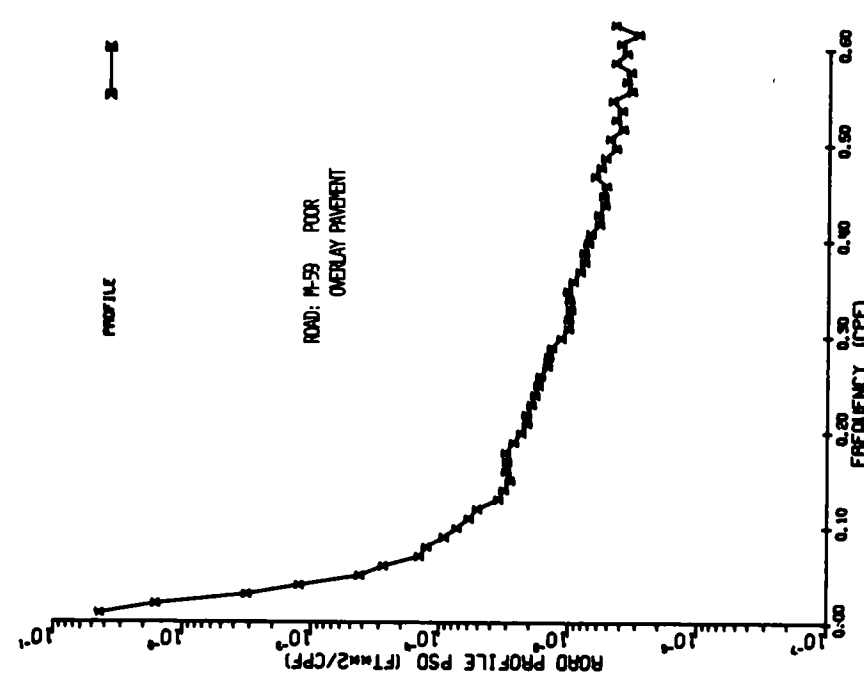
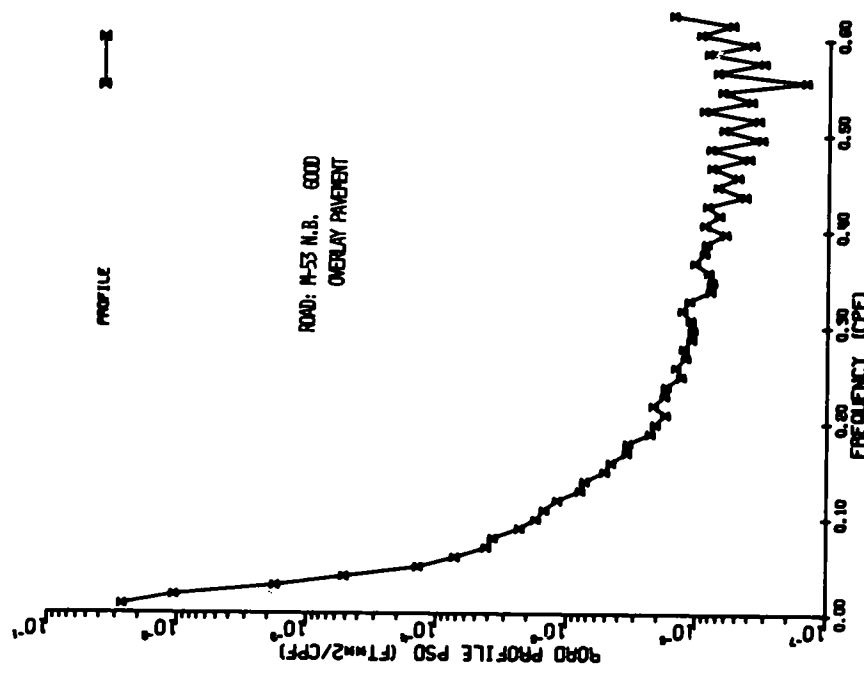
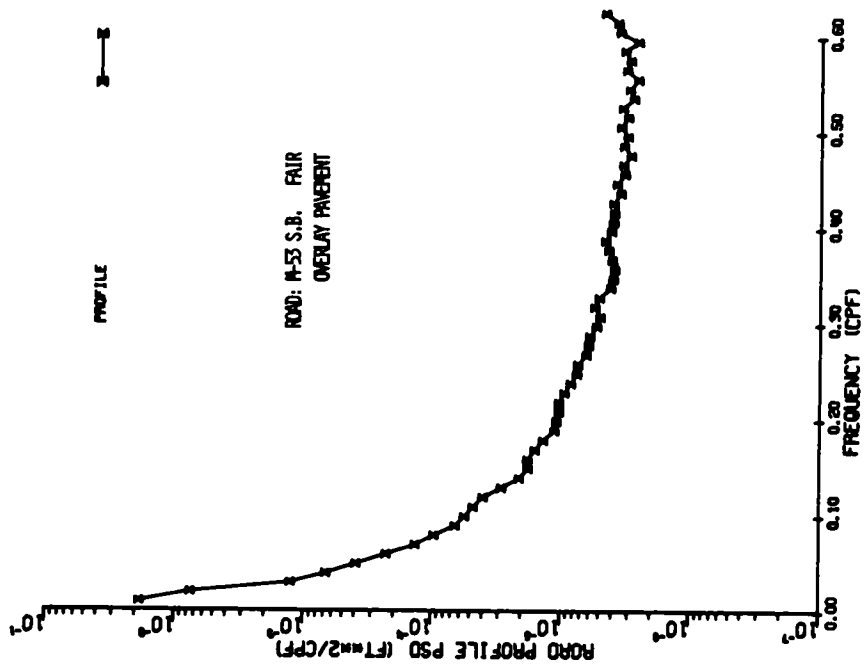
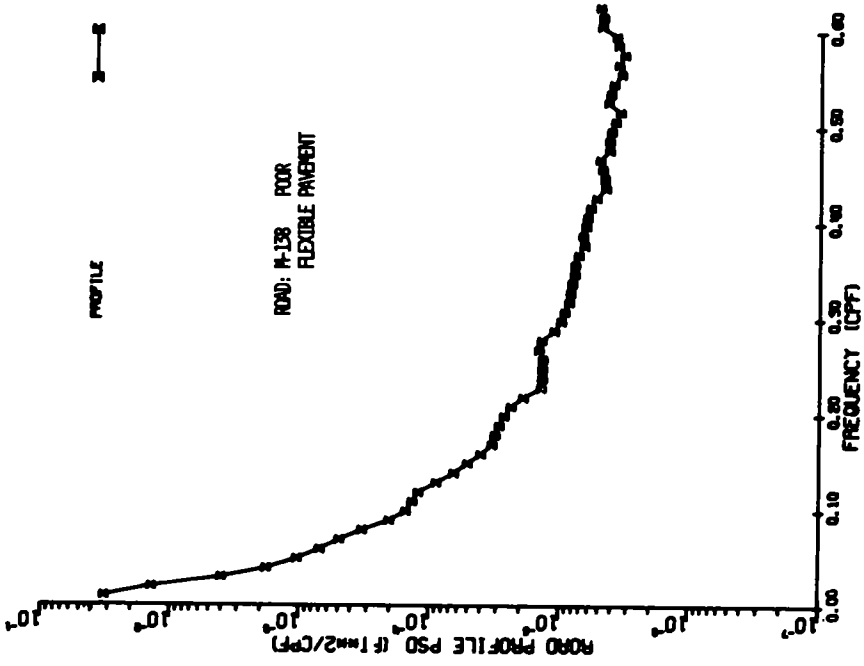


Figure G-1 (Continued)





## APPENDIX H

### TIRE PRESSURE TRANSDUCER SYSTEM

Measurement of tire pressure changes to indicate dynamic pavement loads was considered to be the least complex and most convenient of several potential systems. Some studies to evaluate the relationship of tire pressure changes versus dynamic pavement load were made using a light panel truck equipped with Goodyear 8:15 × 15 4-ply (8-ply rating) tires.

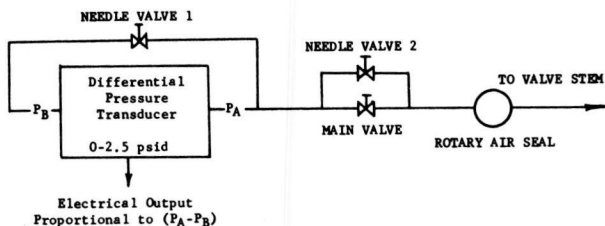
Tire pressure changes in the right rear tire (loaded to 1,100 lb) were monitored using a Statham 0- to 2.5-psi differential pressure transducer, connected as shown in Figures H-1 and H-2. The needle valves were provided for convenience during tire inflation and were closed during all of the rather short-term tests that were run.

#### SYSTEM RESPONSE

By using a reference transducer installed directly in the rim, the time delay due to the connecting lines of the test transducer was determined to be about 0.002 sec. A sharp impact on the inflated tire showed the measurement system first resonance to be about 300 cps.

#### PRESSURE VERSUS LOAD—NONROLLING

A force transducer was placed under the instrumented tire and the axle housing was excited vertically with an electrohydraulic servo ram to produce a 300-lb peak-to-peak force at the tire patch. In the frequency range from 1 to 12 cps, the tire pressure change resulting from the force input varied only  $\pm 5\%$ . Above 12 cps, however, the tire pressure change sensitivity in psi/lb increased rapidly, nearly doubling at 27 cps (Fig. H-3).



#### VALVE SETTINGS:

- During Tire Inflation: Needle valves 1 & 2 open, main valve closed to avoid large pressure variations.
- Before Test: Needle valve 1 and main valve open; needle valve 2 closed.
- During Test: Main valve open; both needle valves closed.

Figure H-1. Tire pressure transducer system schematic.

#### PRESSURE VERSUS LOAD—ROLLING

Rolling tires respond quite differently than do nonrolling tires. Not only do the tire's spring rate and damping characteristics change significantly, but the tire also has some "enveloping" capability when it crosses a bump. A rolling, dynamic evaluation of the tire pressure measurement was required to adequately evaluate the technique.

Wooden bumps  $\frac{1}{2}$  in. high × 18 in. long were attached to an embedded scale and the truck was driven across the scale at speeds of 5 to 15 mph. Test speeds were limited because the vehicle pressure measurement system was connected via a long lead wire to a stationary oscillograph simultaneously recording the embedded scale output.

The pressure and force traces were generally similar; however, the traces indicate a definitely nonlinear and phase-shifted relationship between pressure change and pavement load (Fig. H-4).

The sensitivity of the pressure transducer to acceleration was checked by shutting off the air pressure to the transducer and repeating the runs. Signals observed were less than 5% of those previously seen.

#### CONCLUSIONS

The observed nonlinearities and frequency response limitations were not considered acceptable for a precision pavement load measurement system. However, because the tire

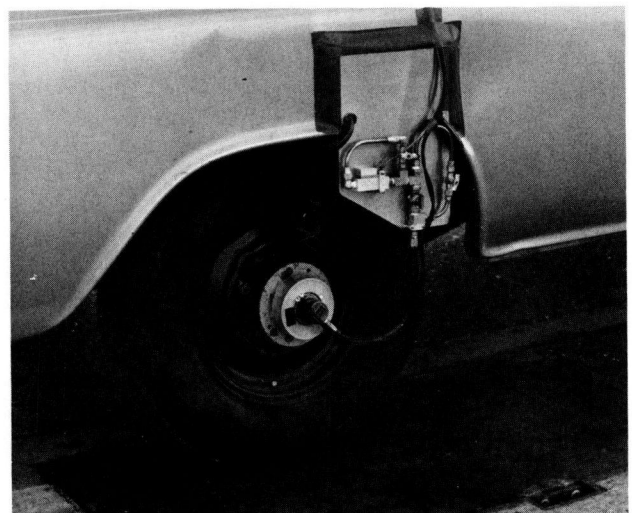


Figure H-2. Tire pressure transducer system installation.

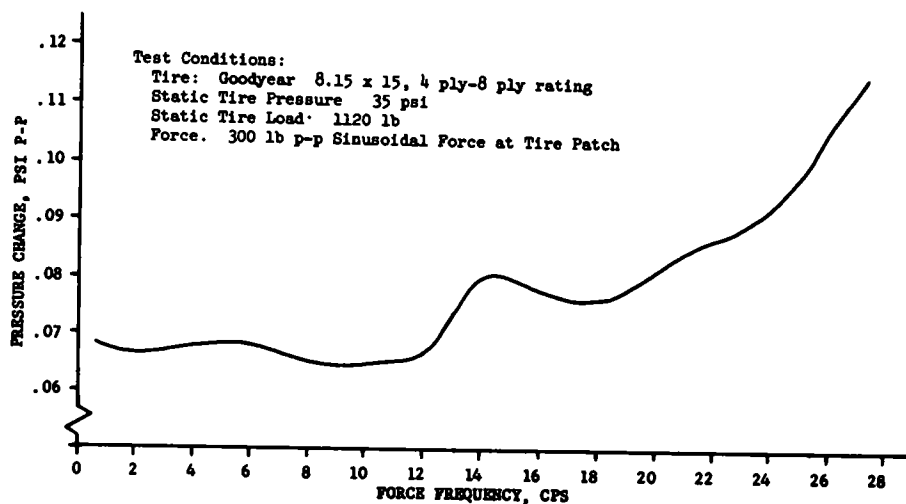


Figure H-3. Tire pressure versus force frequency, nonrolling tire.

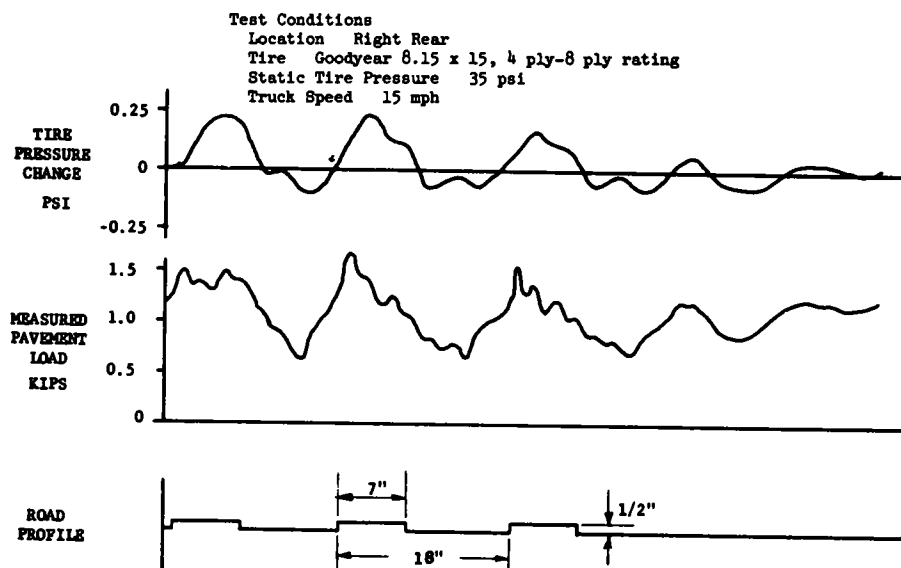


Figure H-4 Tire pressure transducer system correlation data

pressure system is relatively convenient and inexpensive to adapt to any vehicle, it is appealing and might be adequate for obtaining pavement load data in limited frequency and amplitude ranges under specific test conditions.

Because the tire air pressure technique employs the tire as a transducer element, some tires may yield far better results than the one used for this test. Other researchers have found more useful pressure/force relationships with certain larger tires.

If the tire air pressure technique is to be used, the tire transducer properties (including the effects of factors such as inflation pressure, tire temperature, and static load) should be established. It may be necessary to apply corrections for these factors.

## APPENDIX I

### STRAIN-GAGED AXLE HOUSING TRANSDUCER SYSTEM

The strain-gaged axle housing pavement load measurement system differed from previously reported strain-gaged axle housing systems in that an inertial force component, detailed later, was added to the force measured in the axle housing to obtain the pavement load. This system, adapted from a General Motors Proving Ground automotive pavement load measurement system, was installed on Test Vehicle No. 1 (Fig. I-1). Some features of the strain-gaged axle housing system were:

1. Both left side, right side, and total axle pavement loads were measured.
2. Front (steer) axle pavement loads, as well as rear (drive) axle pavement loads, were measured.
3. The strain-gaged axle housing system was available much sooner than the wheel force transducer.
4. The strain-gaged axle housing pavement load measurement system did not require resolvers, as did the rotating wheel force transducer.

However, the strain-gaged axle housing system was much less sensitive than the wheel force transducer and was not transferable to other test vehicles.

#### FORCE MEASUREMENT CHANNELS

Both the front and rear axle housings were strain-gaged to measure vertical shear forces between the outboard wheel and bearing assembly and the spring pad locations on the axle. The right rear axle housing was also gaged to measure fore-and-aft forces. Micro Measurements EA-06-125-TH-120 shear gage pairs were installed using Eastman "910" adhesive. Stress relief lead wire loops were connected to terminal strips, and the gage installations were coated with

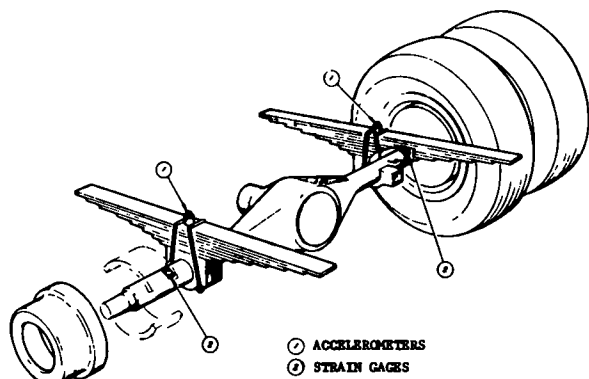


Figure I-1 Axle housing transducer system

William T. Bean & Co. Gagecote No. 1 and Gagecote No. 5. A nickel-chrome sheet-metal shield was spot-welded over the entire installation.

#### Rear-Axle Force Channels

All three bridges had a sensitivity of about 20 lb/ $\mu\epsilon$  (lb/microstrain). Individual calibrations are shown in Figures I-2, I-3, and I-4. Crosstalk checks showed:

1. 1.7% of fore-and-aft force was indicated on the vertical channel
2. 0.0% of the vertical load was indicated on the right fore-and-aft channel.
3. A 2,500-lb lateral load applied 18 in. below the axle center line produced:
  - a. 63-lb indication on the right fore-and-aft channel (2.5%).
  - b. 125-lb indication on the right vertical channel (5%).
  - c. 162-lb indication on the left vertical channel (6.5%).

#### Front-Axle Force Channels

The two front-axle vertical force bridges were found to be about 30 lb/ $\mu\epsilon$  less sensitive than the rear. Their calibration curves are shown in Figures I-5 and I-6. Crosstalk due to directions of force input other than vertical was not checked.

#### ACCELERATION CHANNELS

Vertical accelerations of both axle assemblies were also measured. Consolidated Electrodynamics strain-gage accelerometers, Type 4-202-0001, were mounted on the front and rear axles.

#### Rear-Axle Acceleration

Rear axle vertical accelerations were measured as shown in Figure I-1 at the rear spring pad locations, 21 in. from the geometric center of the axle, providing a 42-in. spacing between accelerometers. The fore-and-aft acceleration on the right side was measured at the spring pad location.

#### Front-Axle Acceleration

Accelerations of the top of the front axle were measured at a location 15½ in. from the geometric center of the axle, providing a spacing of 31 in. between accelerometers.

#### Acceleration Computation

The wheel assembly center line spacings for this vehicle are 72 in. (rear) and 75 in. (front). The vertical acceleration channels combined electronically yield the following computed accelerations:

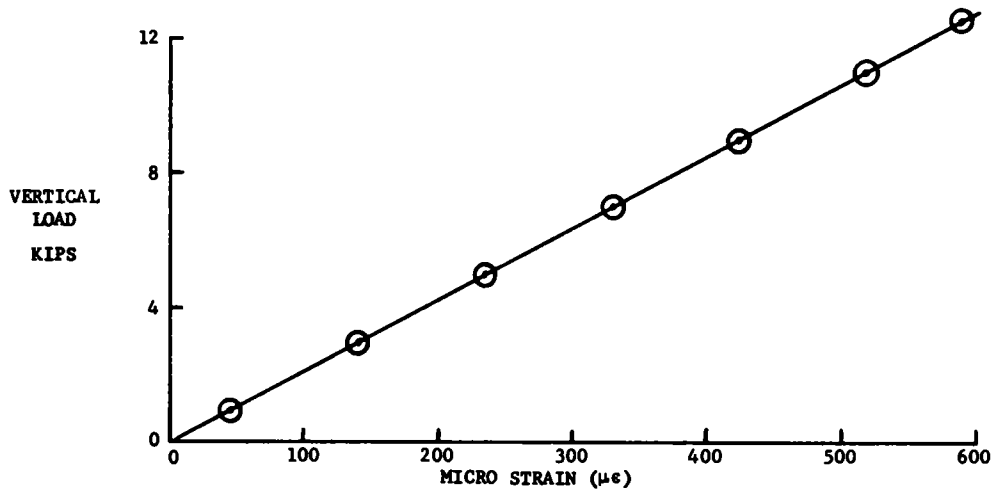


Figure 1-2. Right rear vertical calibration curve 100K  $\Omega$  equivalent load equals 12.8 kips

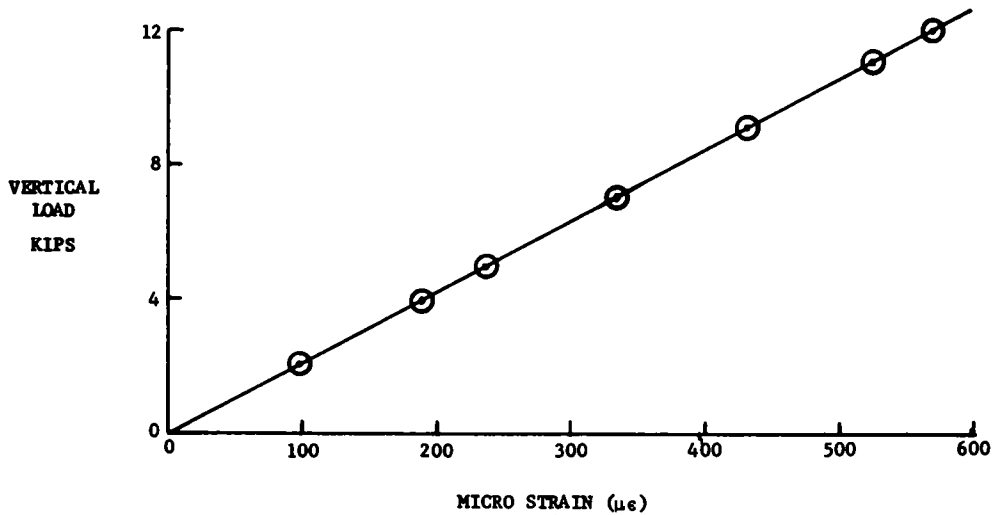


Figure 1-3 Left rear vertical calibration curve 100K  $\Omega$  equivalent load equals 12.6 kips.

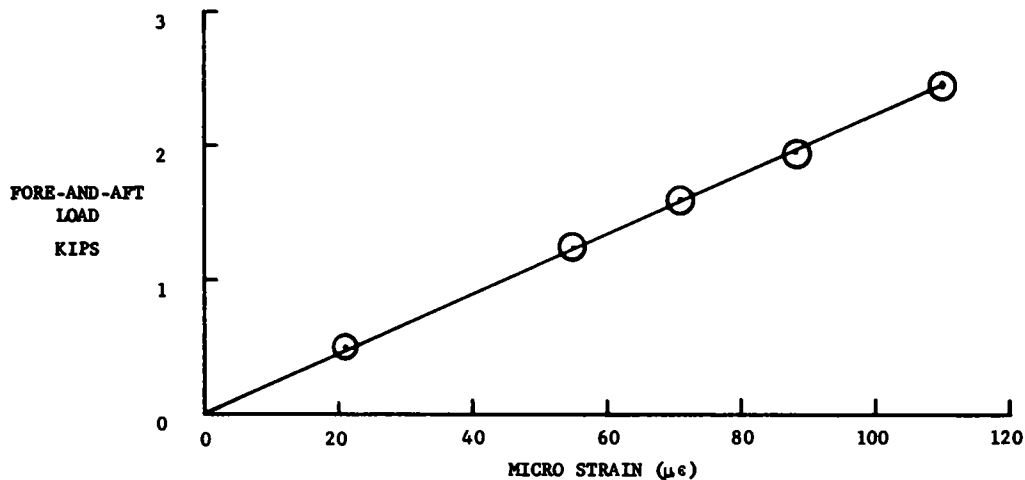


Figure 1-4. Right rear fore-and-aft calibration curve 100K  $\Omega$  equivalent load equals 12.8 kips.

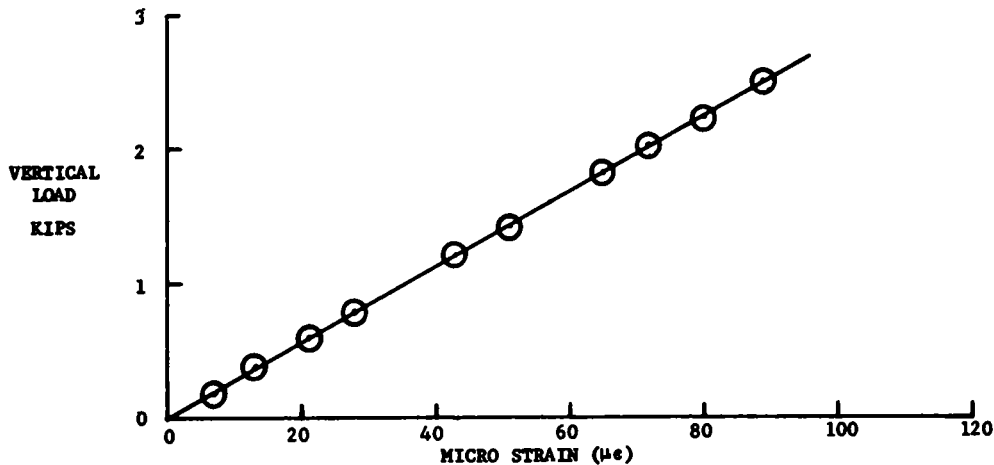


Figure 1-5 Right front vertical calibration curve 100K Ω equivalent load equals 16.9 kips.

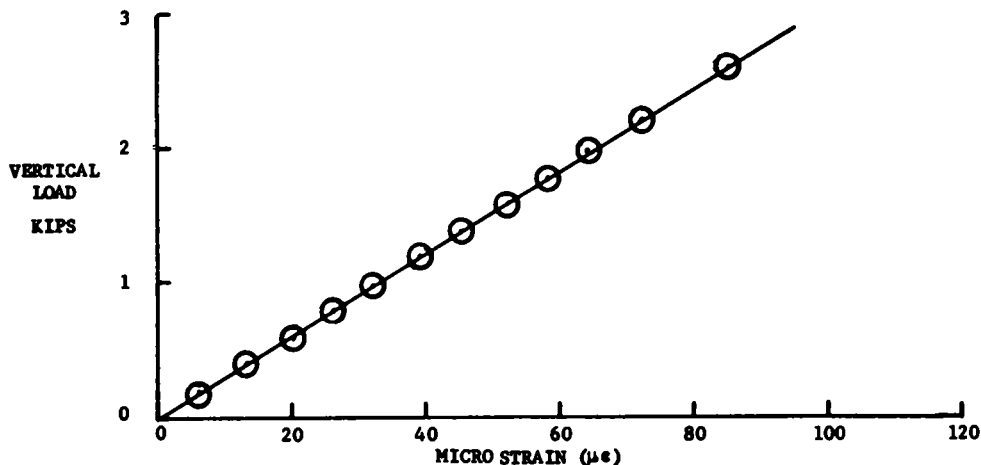


Figure 1-6 Left front vertical calibration curve 100K Ω equivalent load equals 18.6 kips

$$A_{RR} = \frac{a_{RR} + a_{LR}}{2} + \frac{72}{42} \left( \frac{a_{RR} - a_{LR}}{2} \right)$$

$$A_{LR} = \frac{a_{RR} + a_{LR}}{2} - \frac{72}{42} \left( \frac{a_{RR} - a_{LR}}{2} \right)$$

$$A_{RF} = \frac{a_{RF} + a_{LF}}{2} + \frac{75}{31} \left( \frac{a_{RF} - a_{LF}}{2} \right)$$

$$A_{LF} = \frac{a_{RF} + a_{LF}}{2} - \frac{75}{31} \left( \frac{a_{RF} - a_{LF}}{2} \right)$$

in which

$a_{RR}$  = acceleration at right rear accelerometer, g's; and  
 $A_{RR}$  = computed acceleration at right rear wheel assembly center line, g's.

#### PAVEMENT LOAD COMPUTATION

The tires, rims, wheels, brake drums and shoe assemblies, and axle housing stubs outboard of the gaged sections on each axle constitute a mass of significant inertia. When

the tires contact a bump, the part of the developed pavement load required to accelerate this "outboard mass" is not transmitted across the strain-gaged sections and therefore is not measured. To measure the total pavement load, a force component equal to the product of this outboard mass and its acceleration must be summed with the forces measured by the strain-gaged sections.

The following equations relate the pavement load variables of the front and rear axle assemblies:

$$L_{RR} = F_{RR} + W_{RR} A_{RR}$$

$$L_{LR} = F_{LR} + W_{LR} A_{LR}$$

Total rear axle pavement load  $L_R = L_{RR} + L_{LR}$

$$L_{RF} = F_{RF} + W_{RF} A_{RF}$$

$$L_{LF} = F_{LF} + W_{LF} A_{LF}$$

Total front axle pavement load  $L_F = L_{RF} + L_{LF}$



in which

- $F_{RR}$  = force measured in right rear strain-gaged section;
- $W_{RR}$  = weight outboard of right rear strain-gaged section; and
- $L_{RR}$  = computed pavement load exerted by the right rear wheel assembly.

These pavement load equations are valid in frequency ranges where the axle assemblies and the components comprising the outboard masses behave essentially as rigid bodies.

Pavement loads may be computed from the force and acceleration data channels either during a test using an on-board analog summing amplifier or in the laboratory using an analog computer to process the data from magnetic tape.

**SYSTEM EVALUATION**

The rear axle pavement load measurement system was evaluated by comparing its output to the signal from the embedded electronic scales at the Grass Lake weigh sta-

tion of the Michigan Department of State Highways. A 1/2-in. x 18-in.-long step bump was placed on the 9-ft electronic scale. The pavement loads induced by the rear wheels contacting the bump were measured using the electronic scales and the rear axle housing pavement load measurement system. Loads were measured while both rear wheels traversed the bump at several different speeds. Typical results (Fig. I-7) showed that the strain-gaged axle housing transducer system compared very well with the electronic scale system at Grass Lake. The only significant difference in the measurements was due to a 65-cps mechanical resonance of the Grass Lake scales. These measurements also verified the necessity of including the inertial force component. For some maximum pavement load peaks, the inertial force component exceeded the vertical axle housing shear force component.

**OUTBOARD MASS WEIGHTS**

The weight outboard of the strain-gaged sections was originally estimated at 500 lb on each side at the rear and

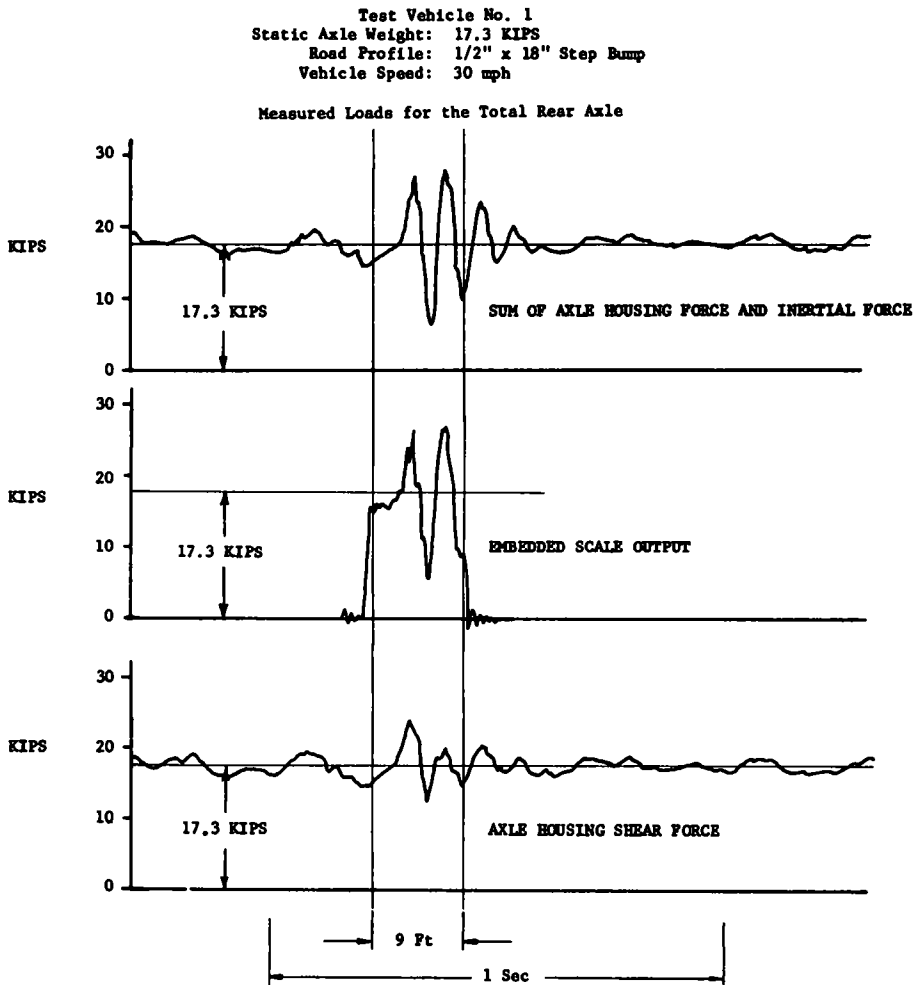


Figure I-7 Axle housing transducer system correlation data.

250 lb on each side at the front. These estimates were based primarily on a known 182-lb weight for a 10:00 × 20 tire and rim assembly (there are two wheel assemblies in a rear dual wheel set). The outboard mass at the rear wheel assemblies was measured later and was found to be 597 lb. All data published in this report were computed using the measured value of 597 lb.

## SUMMARY

These pavement load measurement systems did not offer quite as much precision as the planned wheel force transducer system, and the "910" shear gage installations were only temporary. However, the gaged axle systems allowed many tests to be run much earlier than planned, and provided a comprehensive look at pavement loads developed by Test Vehicle No. 1.

## APPENDIX J

### WHEEL FORCE TRANSDUCER SYSTEM

#### SYSTEM REQUIREMENTS

Accurate, instantaneous measurement of the radial plane (vertical fore-and-aft) pavement load vector was required.

Convenient installation of system components on several test vehicles, without requiring intermediate recalibration and reverification, was considered essential. Maximum interchangeability was desired, inasmuch as the system was required to fit any heavy truck with cast wheels and 20-in. or larger rims. Application to both dual and single wheel sets, with various tire sizes and spacer widths, was required.

A design load of 20,000 lb in the radial plane was established based on the maximum legal static weight of 9,000 lb, plus dynamic loads of about 6,000 lb indicated by embedded-scale tests. A design torque of 6,700 lb-ft was expected when the tires were sliding with the maximum legal static load, assuming a coefficient of friction of 1.00. Safety factors would provide design loads considerably lower than failure loads.

It was desirable for the measurement system to have a minimum effect on the vehicle properties. Small weight increases were acceptable, but tire and wheel geometry, spacings, etc., were not to be altered.

#### FORCE TRANSDUCER LOCATION

A force transducer was required to measure loads transmitted between the tire/road interface and the truck body. It was desirable to locate the force transducer as close to the tire/road interface as possible. A brief survey of heavy trucks showed that although the rims and rim clamping techniques were fairly standard on cast wheels, similarities in physical layout or size between various vehicles ended at the bearing hub. Numbers of spokes, brake drum size, shape, and location; bearing diameters and spacings; and dual wheel center lines vary greatly. Sizes and shapes of suspension components were very dissimilar. Clearly, a universal transducer system would have to be located out-

board of the bearing hub. Because variations in rim size and spacing were required, the force transducer location had to be between the bearing hub and the rims.

Major manufacturers of cast wheels, truck tire rims, and brake drums were contacted to obtain dimensions of their "worst case" designs. A space envelope was determined, allowing clearance for the largest bearing hub, the smallest diameter 20-in. rim, and the largest brake drum (located as far outboard as possible).

#### MECHANICAL LAYOUT

The force transducer shown in Figure J-1 was designed within the established space limitations. The rims attach to the outer ring, while the inner ring provides a bolt circle for attaching the transducer to bearing hub adaptors. The symmetric layout of the transducer is suggested by the dual wheel arrangement, with the rims back to back and separated by a spacer. The rim clamping techniques and adaptors are discussed later.

#### MATERIAL SELECTION

Good sensitivity requires that transducer sensing elements be stressed highly at the design load, yet stresses at this load should be well below the yield point of the material—sufficiently low to ensure an essentially infinite fatigue life. These contradictory requirements can be satisfied by using a material with a very high yield stress. Practical high yield materials are all alloy steels.

Use of alloy steels, however, brings up two potential problems. In the high-strength, heat-treated condition, alloy steels do not allow practical machining of the complex shapes and the high accuracies required for transducer applications. If the steel is machined in the annealed condition, however, high-temperature heat treating may cause dimensional changes and warping.

In a long-term outdoor application like a truck wheel force transducer, most alloy steels experience surface

corrosion. In spite of the most careful plating or coating techniques, surface corrosion eventually will reach underneath strain gages, causing gage failures.

Material requirements were satisfied by a precipitation-hardening stainless steel (trade name: "Almar 362"). This steel is reasonably machinable in the annealed condition, and, being stainless, is highly corrosion-resistant. More important, however, machined parts may be treated to achieve high-tensile-strength levels (180,000 psi yield) with a relatively low-temperature heat-aging process that does not cause significant distortion.

### SENSING ELEMENTS

Determination of the radial plane pavement load involves measurement of two radial plane force components. The outer ring (rim support) was connected to the inner ring bearing hub support solely through four pairs of laterally oriented beams (Fig. J-2). The 1-in.-long beams (actually 1/2-in.-wide sections of a cylinder 16 1/2 in. in diameter and 1/2-in. thick) were treated as 1/2-in.-square  $\times$  1-in.-long beams for the purpose of design calculations (Fig. J-3). Orthogonal radial plane coordinate axes, perpendicular to the beam surfaces, were defined by lines through the beam centers and the center of the transducer (Fig. J-4). To positively eliminate confusion in identifying rotating radial measurements, the two axes were designated "red" and "yellow."

Owing to the lateral orientation of the beams, radial plane forces and torque loads produced bending in the beams, while lateral forces and moments about radial axes produced tension and compression in the beams.

The theoretical stress-load relationships, assuming equal load distribution among the eight beams, are:

$$\text{Radial force} = F \text{ lb, } \sigma_{\max} = 3(F) \text{ psi (at each end of the beam, at the beam surface);}$$

$$\text{Torque} = T \text{ lb-ft, } \sigma_{\max} = 4.5(T) \text{ psi (at each end of the beam, at the beam surface);}$$

$$\text{Lateral force} = F' \text{ lb, } \sigma_{\max} = F'/2 \text{ psi (uniform tension-compression); and}$$

$$\text{Lateral moment} = M \text{ lb-ft, } \sigma_{\max} = 1.5(M) \text{ psi (uniform tension-compression).}$$

A force in the radial direction produces up to six times as much peak stress as the same force in the lateral direction, and a torque moment produces three times as much peak stress as moments about radial axes. These relationships demonstrate that laterally oriented beams offer good sensitivity and selectivity with respect to input force direction.

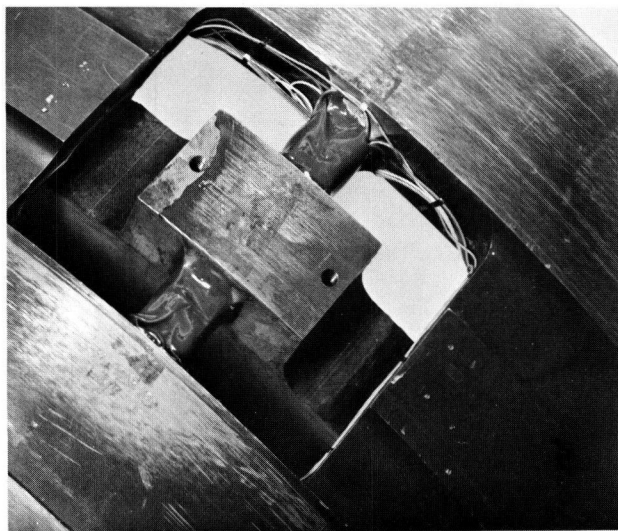


Figure J-2. Wheel force transducer element.

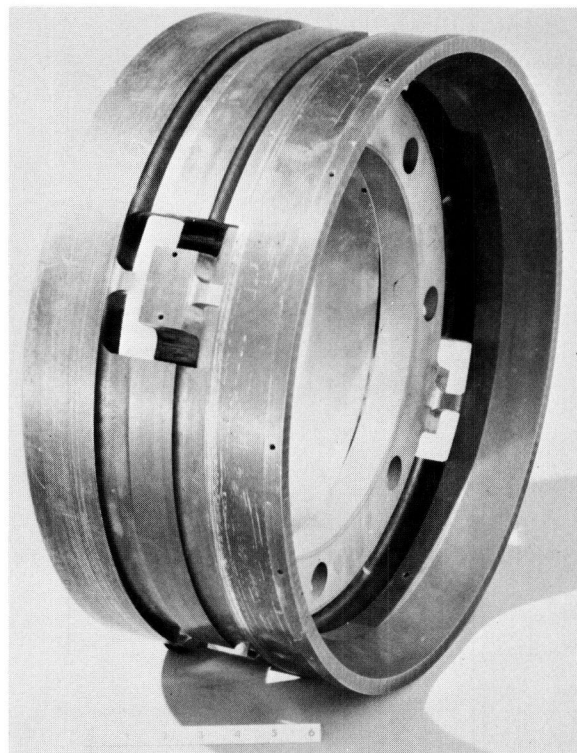


Figure J-1. Wheel force transducer.

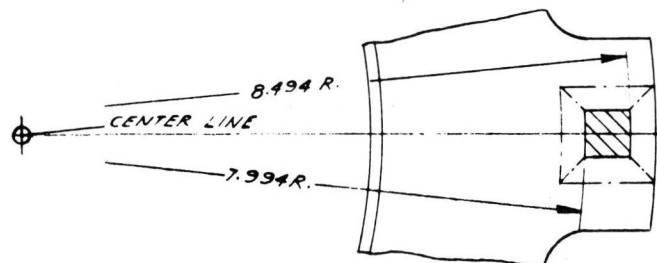


Figure J-3. Sensing element cross-section.

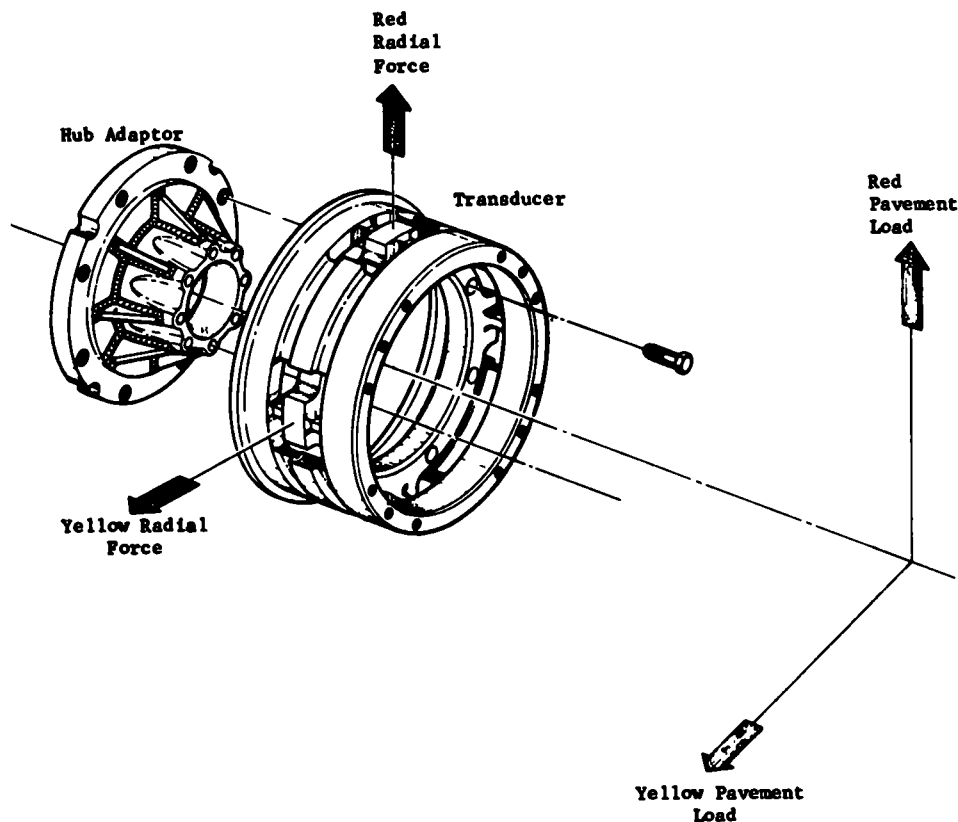


Figure J-4. Force measurement axes.

At the design loads:

Radial: 20,000 lb,  $\sigma_{max} = 60,000$  psi.

Torque: 6,667 lb-ft,  $\sigma_{max} = 60,000$  psi.

The computed maximum stress, at the design limits, provides excellent sensitivity, and yet is well below the material yield stress of over 180,000 psi (equivalent to a radial load of 60,000 lb, or seven times the 9,000-lb maximum static load). As steel may be considered to have an infinite life at cyclic stress levels less than 50% of yield, maximum design stress of 30% of yield should avoid fatigue problems.

The preceding stress calculations were useful for establishing design geometry and predicting approximate stress values. In actual practice, because of stress concentration, the beams cannot be abruptly terminated, and maximum stresses were somewhat lower due to the 0.250-in. fillets at the bases of each beam. The strain gage locations were at the base of the 0.250 fillets, near the point of maximum bending stress.

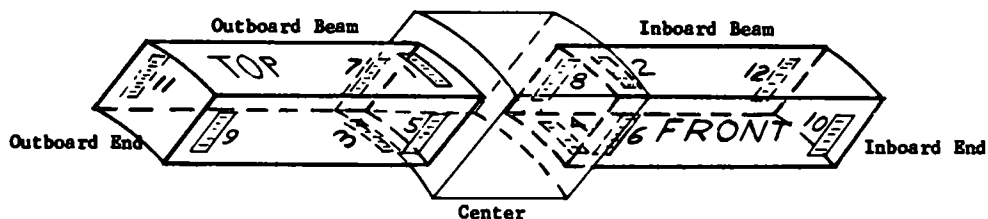
In this transducer, 120-ohm,  $\frac{1}{16}$ -in.-square Micro-Measurements EA-06-062-AA-120 gages were located at the base of the fillets, 0.312 in. from the centers of the beams. The gages were attached using Micro-Measurements 610 adhesive, cured by baking for 10 hr at 240°F. The installations were then coated with layers of William T. Bean & Co. Gagecote No. 1 and Gagecote No. 5 for protection from moisture and mechanical damage.

#### BRIDGE WIRING

Gage location identifications are shown in Figure J-5. A 4-gage bridge (8-gage for torque) wiring setup, based on the assumption that loads were equally shared among the eight beams, is shown in Figure J-6.

Initial calibration checks of the 4-gage bridges showed, however, that some deformation did occur in the inner and/or outer rings, causing variations in the load sharing between the eight beams. These variations in load sharing required that loads in each direction be determined by summing components from all eight beams. Inasmuch as two opposite polarity gages were provided on each beam to ensure proper matching, the 16-gage bridges shown in Figure J-7 resulted. The series-parallel wiring arrangement shown resulted in a net bridge impedance of 120 ohms, as with a conventional 4-gage bridge. Excitation voltage for these bridges should not exceed 12 volts RMS.

The "truth tables" in Figure J-8 were prepared to aid in determining the response of each of the three bridges to loads in the various directions. By applying these stress conditions to the wiring diagrams in Figure J-7, responses of the bridges to various inputs were predicted. In every case, the idealized predicted crosstalk response was zero.



	Outboard Center	Inboard Center	Outboard End	Inboard End
Top	1	2		
Front	5	6	9	10
Bottom	3	4		
Back	7	8	11	12

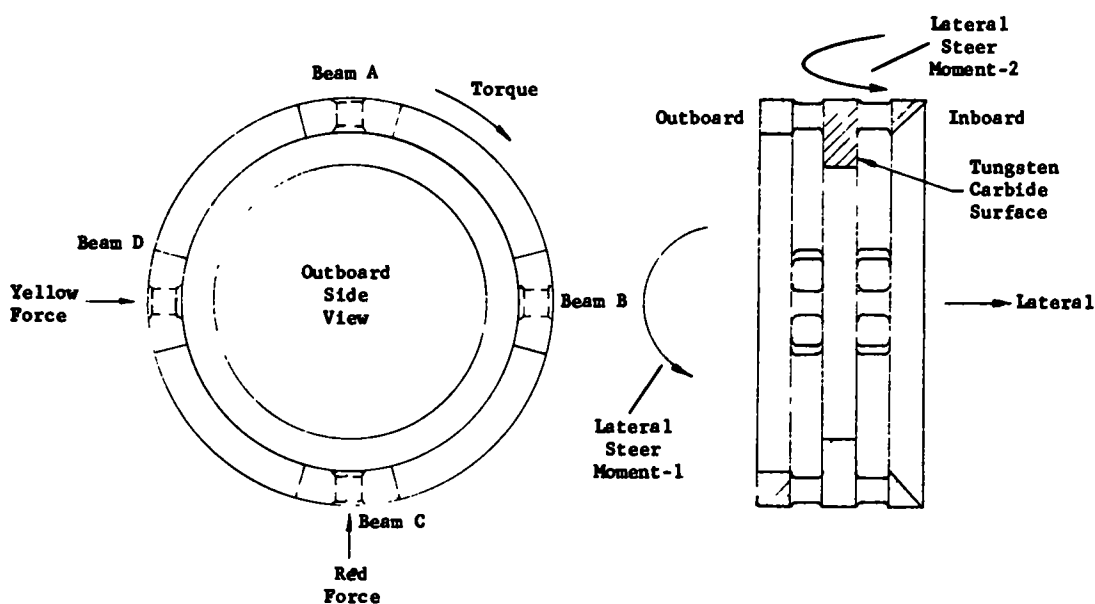


Figure J-5. Gage location and force input direction identifications

**RIM ATTACHMENT**

Dual wheel sets were attached to the transducer using 16 clamps (8 per rim) in a manner similar to the conventional cast wheel wedge clamping technique (Fig. J-9). Because tension forces in the wheel produced by clamping are distributed through steel webs connecting the two sides of the outer ring, and because the cross-sectional area of the webs is 18 times that of the beam, the effect of clamping stresses on the beam is small. The corresponding effects due to changes in clamping forces are very small. Rim pilots were provided on the wheel force transducer clamps. The existing set of clamps was designed for 20-in. standard (19.550 pilot diameter) rims and a 4-in. spacer. Additional

sets of clamps, with varied geometry, allow the transducer to accept 20-in. medium-duty rims, 20-in. heavy-duty rims, 22.5-in. rims, or a 22.5-in. "super single" duplex rim, and to accommodate spacer widths up to 6 in. Single wheels are mounted by installing a dummy rim and spacer.

**BEARING HUB ADAPTORS**

Standard cast wheels were modified to accept the 13.375-in.-diameter eight-hole bolt circle on the wheel force transducer (Fig. J-10). The surface of this bolt circle was placed 0.625 in. inboard of the dual wheel center line to maintain the same wheel position. Brake drums were attached to the adaptor as with the standard cast wheel.

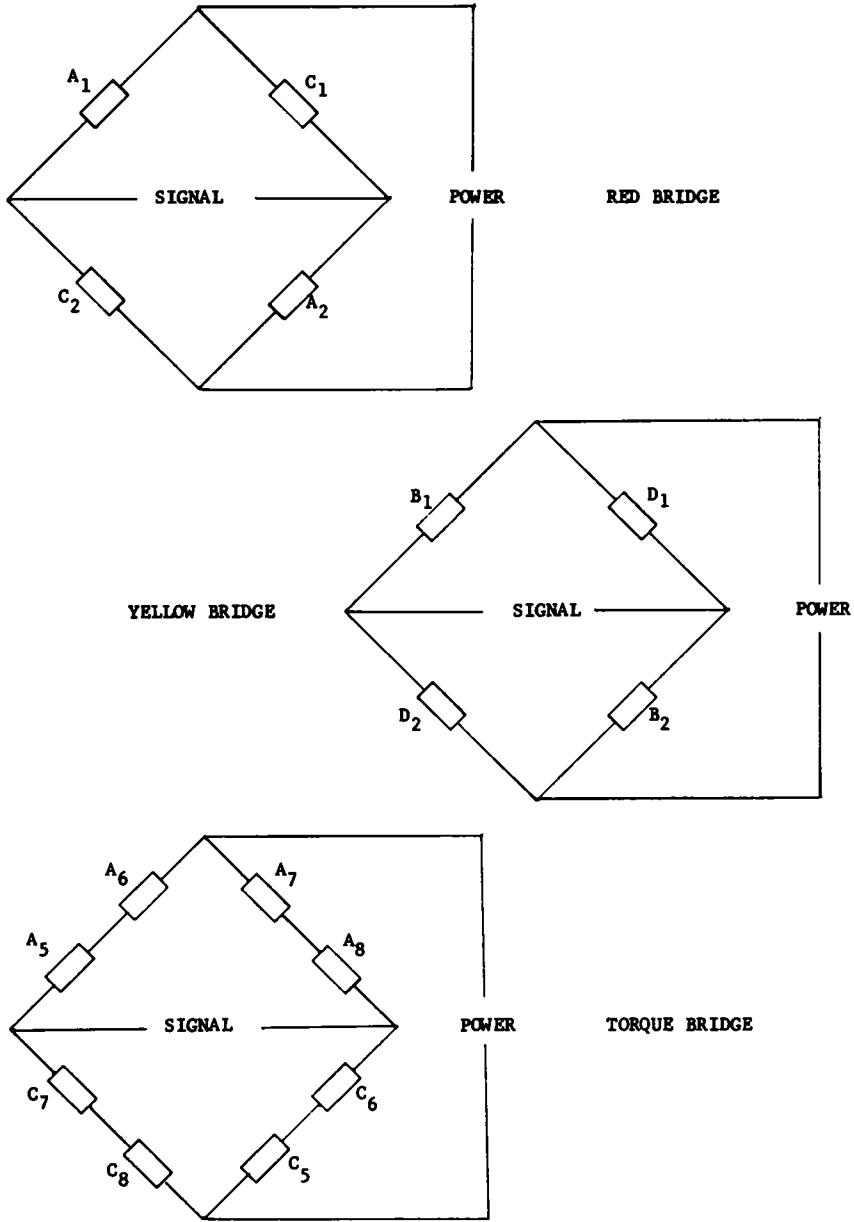


Figure J-6. Original bridge wiring

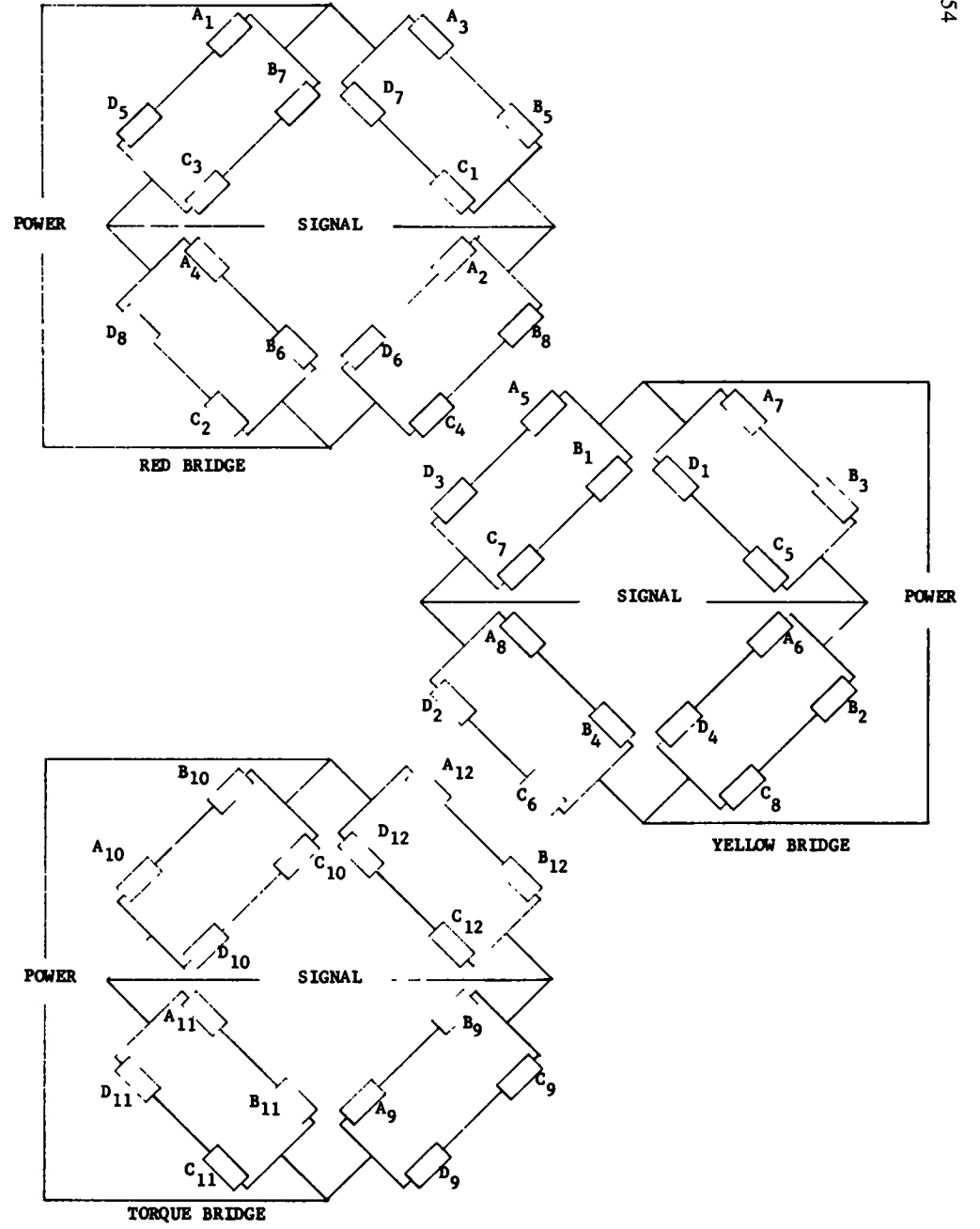


Figure J-7 Final bridge wiring

<u>Red Bridge</u>		<u>Gage Location</u>															
<u>Load Direction</u>	A1	A2	A3	A4	B5	B6	B7	B8	C1	C2	C3	C4	D5	D6	D7	D8	
*Red Radial	C	C	T	T	T	T	C	C	T	T	C	C	C	C	T	T	
Yellow Radial	NS	NS	NS	NS	C	C	T	T	NS	NS	NS	NS	C	C	T	T	
Torque	NS	NS	NS	NS	C	C	T	T	NS	NS	NS	NS	C	C	T	T	
Lateral	C'	T'	C'	T'	C'	T'	C'	T'	C'	T'	C'	T'	C'	T'	C'	T'	
Lateral-Steer Moment 1	T'	C'	T'	C'	NS	NS	NS	NS	C'	T'	C'	T'	NS	NS	NS	NS	
Lateral-Steer Moment 2	NS	NS	NS	NS	C'	T'	C'	T'	NS	NS	NS	NS	T'	C'	T'	C'	

<u>Yellow Bridge</u>		<u>Gage Location</u>															
<u>Load Direction</u>	A5	A6	A7	A8	B1	B2	B3	B4	C5	C6	C7	C8	D1	D2	D3	D4	
Red Radial	NS	NS	NS	NS	NS	NS	NS	NS	NS	NS	NS	NS	NS	NS	NS	NS	
*Yellow Radial	C	C	T	T	C	C	T	T	T	T	C	C	T	T	C	C	
Torque	C	C	T	T	NS	NS	NS	NS	C	C	T	T	NS	NS	NS	NS	
Lateral	C'	T'	C'	T'	C'	T'	C'	T'	C'	T'	C'	T'	C'	T'	C'	T'	
Lateral-Steer Moment 1	T'	C'	T'	C'	NS	NS	NS	NS	C'	T'	C'	T'	NS	NS	NS	NS	
Lateral-Steer Moment 2	NS	NS	NS	NS	C'	T'	C'	T'	NS	NS	NS	NS	T'	C'	T'	C'	

<u>Torque Bridge</u>		<u>Gage Location</u>															
<u>Load Direction</u>	A9	A10	A11	A12	B9	B10	B11	B12	C9	C10	C11	C12	D9	D10	D11	D12	
Red Radial	NS	NS	NS	NS	C	C	T	T	NS	NS	NS	NS	T	T	C	C	
Yellow Radial	T	T	C	C	NS	NS	NS	NS	C	C	T	T	NS	NS	NS	NS	
*Torque	T	T	C	C	T	T	C	C	T	T	C	C	T	T	C	C	
Lateral	C'	T'	C'	T'	C'	T'	C'	T'	C'	T'	C'	T'	C'	T'	C'	T'	
Lateral-Steer Moment 1	T'	C'	T'	C'	NS	NS	NS	NS	C'	T'	C'	T'	NS	NS	NS	NS	
Lateral-Steer Moment 2	NS	NS	NS	NS	C'	T'	C'	T'	NS	NS	NS	NS	T'	C'	T'	C'	

C = Compression, Bending  
 T = Tension, Bending  
 C' = Compression, Axial  
 T' = Tension, Axial  
 NS = No Stress Produced in Neutral Axis Plane

\* Sensitive Axis

Figure J-8. Individual gage stress "truth tables"

An 11.500-in.-diameter pilot was provided on the adaptor for the wheel force transducer, but this pilot was not intended to carry radial loads. Small motions at a pilot interface could cause changes in the sensing element stress distribution that result in zero shift and hysteresis in the bridge outputs. To prevent even minor slippage of the bolted interface, the mating surfaces on both the transducer and adaptor were flame-sprayed with a 0.003-in.-thick

tungsten carbide coating. (Flame spraying was provided by Union Carbide, Materials Systems Division.) A 0.005-in. brass gasket was used between the two surfaces. When the two surfaces were pressed together by torquing the eight bolts, irregularities in the very hard tungsten carbide surfaces penetrated the brass gasket, providing a friction interface approaching a mechanical bond. This friction value is limited by the shear strength of the brass gasket



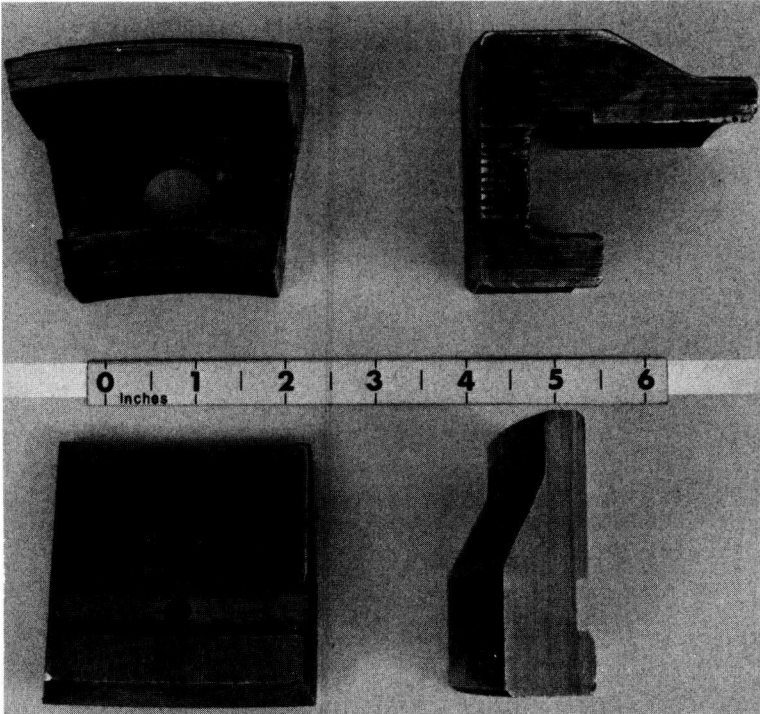


Figure J-9. Rim clamps. Outboard (upper). Inboard (lower).

which is very high owing to its large area. Three bearing hub adaptors, fitting at least 10 axle types, were made during the project:

TEST VEHICLE	AXLE TYPE	APPLICATION TO AXLE TYPE
No. 1	Eaton 166221	Eaton 16121, Eaton 30 DSC (tandem) and possibly equivalent Timken axles
No. 2	Timken SLHD	SUDD, Eaton 34 DCS, Eaton 17121, Eaton 17221, and some Timken single axles
No. 3	Fruehauf I-beam	No others known

Factors determining the interchangeability of adaptors are bearing size and spacing, wheel center line locations, axle size and attachment methods, and brake drum configuration.

#### CALIBRATION

The three bridges were calibrated with the transducer element installed on a test vehicle to ensure that all practical limitations due to installation procedure, mounting techniques, etc., were reflected in the calibration. A precision mechanical scale and an electrical torque transducer, both traceable to the National Bureau of Standards, were used as calibration load references. Each bridge was calibrated with the load applied along its sensitive axis, and

loading was repeated along 45° radial lines, to ensure that both radial bridges correctly indicated the load component along their sensitive axes. Calibration results are shown in Figures J-11, J-12, and J-13.

#### CROSSTALK CHECKS

Crosstalk, a bridge output due to a load change in an axis other than the sensitive axis, was minimized in this transducer by:

1. Designing the beam layout in such a way that loads of interest produced much higher stresses than loads not to be measured.
2. Very accurate and symmetrical machining of the sensing elements.
3. Wiring the bridges in such a way that the gage outputs cancel except for loads in the sensitive axis.

Crosstalk measurements were typically less than 1% (Table J-1).

Lateral force and radial moment crosstalk checks were combined because in practice lateral forces can be developed only at the tire/road interface. This off-center loading applied the only significant moments about radial axes.

#### OFF-CENTER LOADING

Radial plane calibrations were repeated with the loads applied through only one tire. This caused a center of load offset of about 7 in. from the transducer center line. No changes were observed in the linearity or crosstalk performance of the transducer.

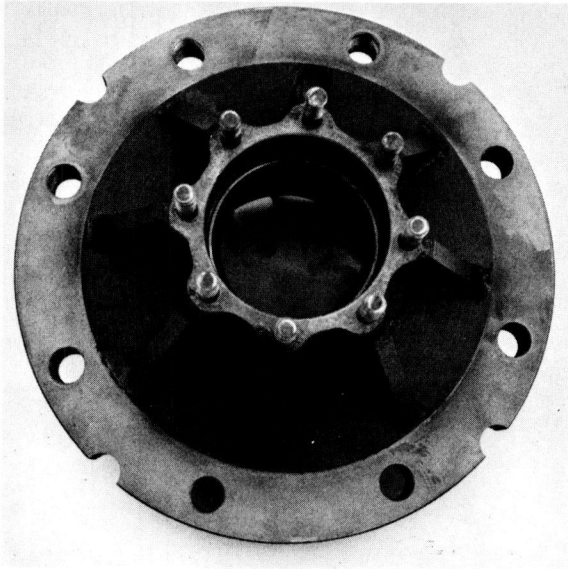


Figure J-10. Bearing hub adaptor.

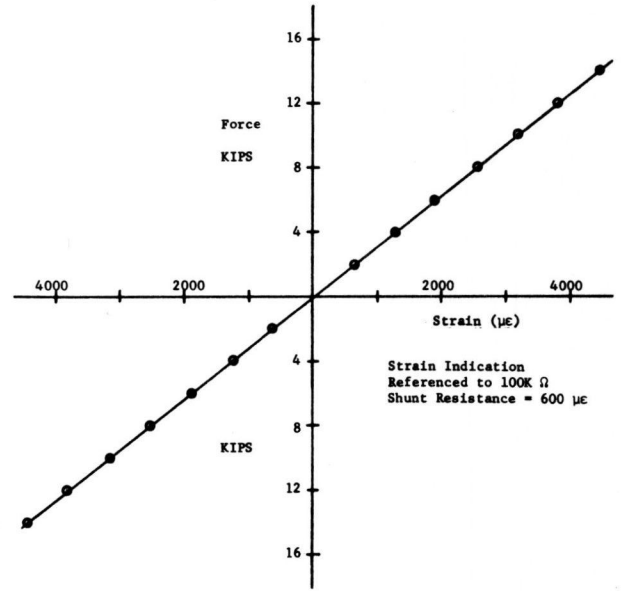


Figure J-11. Wheel force transducer, red radial force bridge calibration curve. 100K Ω equivalent load equals 1.92 kips.

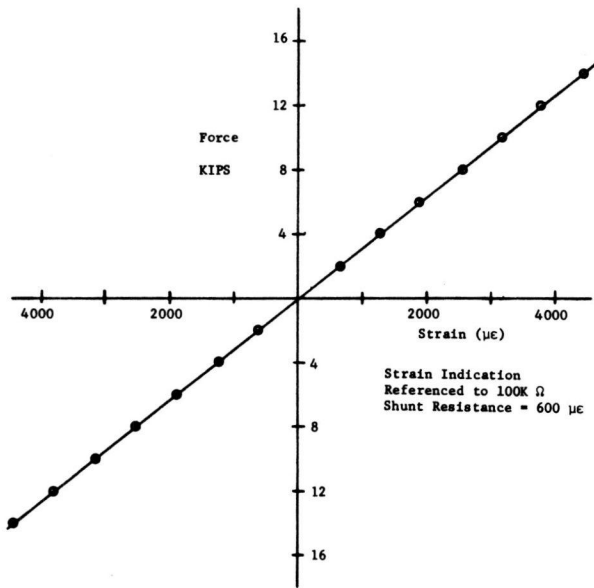


Figure J-12. Wheel force transducer, yellow radial force bridge calibration curve. 100K Ω equivalent load equals 1.94 kips.

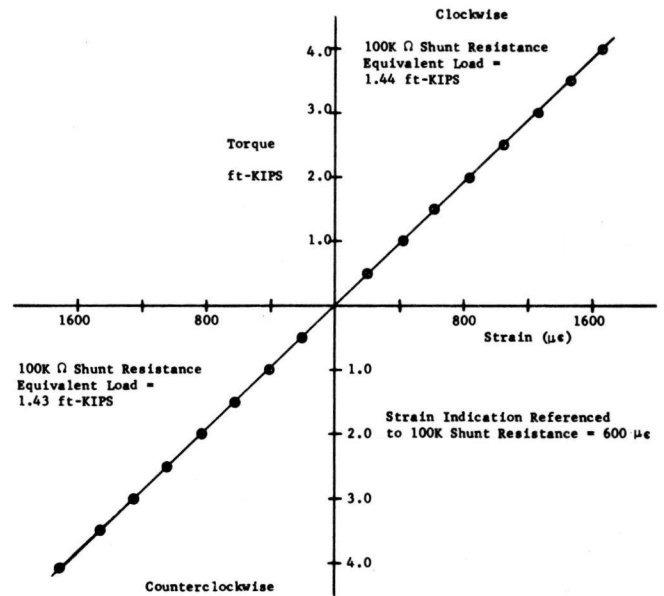


Figure J-13. Wheel force transducer, torque bridge calibration curve.

TABLE J-1  
SUMMARY OF CROSSTALK MEASUREMENTS

LOAD APPLICATION DIRECTION	MAXIMUM BRIDGE SENSITIVITY (COMPARED TO DESIGN AXIS SENSITIVITY)		
	YELLOW RADIAL	RED RADIAL	TORQUE
Radial (yellow)	1.000 lb/lb	0.0063 lb/lb	0.0017 lb-ft/lb
Radial (red)	0.0120 lb/lb	1.000 lb/lb	0.0071 lb-ft/lb
Torque (rear axle)	0.0363 lb/lb-ft	0.0056 lb/lb-ft	1.000 lb-ft/lb-ft
Lateral <sup>a</sup>	0.0086 lb/lb	0.0043 lb/lb	0.0032 lb-ft/lb

<sup>a</sup> Lateral force was applied at the tire contact patch location, 20 in. from the wheel center line. This also produced a moment about a radial axis equal to 1.83 lb-ft/lb of lateral force. Moments were applied in this manner first about the red and then the yellow radial axes.

## PROOF LOAD

Both radial axes were loaded to  $\pm 30,000$  lb (150% design load). The bridge outputs at this load were accurate and no indications of material yielding were observed

## ACCELERATION MEASUREMENTS

The pavement load vector may be thought of as being in two parts. One component of the load is transmitted from the tire-rim assemblies to the axle assembly. This transmitted force is measured by the wheel force transducer. A second part of the pavement load is an inertial force component that varies with the acceleration of the mass elements between the force transducer and the tire/road interface. In the case of the wheel force transducer, this mass included the tires, rims, outer ring of the wheel force transducer, and the rim clamps.

To measure this inertial force, radial plane accelerations were measured along the same rotating axes as the wheel transducer forces. The two acceleration components were designated "red" and "yellow" (Fig. J-14).

Commercial strain gage accelerometers, Consolidated Electroynamics Type 4-202-0001,  $\pm 100g$  range were used. The primary features of these accelerometers were 0.75% maximum nonlinearity, 1,000 cps frequency response, and  $0.01g/g$  maximum cross-axis sensitivity.

Because the accelerometers were to be located on the rotating wheel, they were subjected to centrifugal acceleration components along the sensitive axis. The accelerome-

ters were mounted as near the center of rotation as possible, to minimize this acceleration component. In the mounted position, the accelerometer sensing elements were only 1 in. from the center of rotation of the wheel (Fig. J-15). At 65 mph the  $10:00 \times 20$  tire rotation speed of 9 rps produced about  $9g$ 's centrifugal acceleration at a 1-in radius. This acceleration component was a function of wheel speed, and acceleration measurements varying as a function of wheel speed were not acceptable. In each axis, therefore, two accelerometers were mounted back to back, symmetric about the center of rotation, and the outputs were wired to add radial acceleration components and cancel centrifugal acceleration components. By use of input line padding resistors, accelerometer sensitivities were matched well enough for  $\pm 10g$  centrifugal acceleration to produce less than  $0.1g$  output. The accelerometer pair was calibrated dynamically at  $\pm 10g @ 15$  cps to determine an equivalent 100K shunt acceleration. The accelerometer pairs were carefully checked to ensure that acceleration in the direction of positive force axes produced positive output voltages (i.e., that force and acceleration polarities were compatible).

## SLIP RING

A Noise and Vibration Laboratory 20-channel instrumentation slip ring assembly was used to make electrical connections with the force and acceleration strain-gage bridges on the rotating wheel assembly (Fig. J-15). This slip ring,

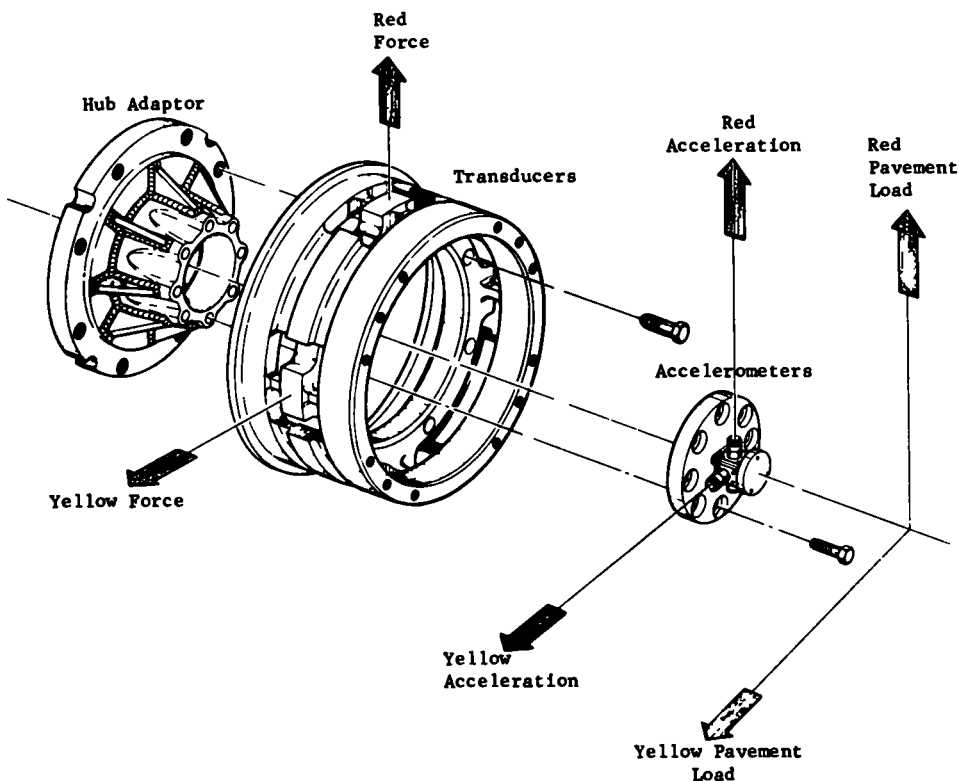


Figure J-14 Accelerometer axis definition

capable of operating acceptably under very high-level accelerations, features noise levels low enough not to significantly affect strain-gage measurements.

### COMPUTATION AND RESOLUTION

The inertial pavement load component along each radial axis, assuming the outboard mass moves as a rigid body, is computed as follows:

$$F_{RI} = W_I A_R$$

The pavement load component along this axis is:

$$L_R = F_{RT} + F_{RI}$$

in which

- $F_{RI}$  = the "red" axis inertial force component;
- $W_I$  = the outboard mass weight in lb;
- $A_R$  = the "red" axis acceleration in g's;
- $L_R$  = the "red" axis pavement load; and
- $F_{RT}$  = the "red" axis transducer force.

Because the radial axes rotate with the wheel, neither radial pavement load component is referenced to a stationary axis (Fig. J-14). To obtain the resultant pavement load,  $L(t)$ , the vector resultant of the two components must be taken:

$$\sqrt{L_R^2 + L_Y^2} = \sqrt{[L(t)]^2 [\sin^2\theta + \cos^2\theta]} = L(t)$$

because  $L_R = L(t) \sin\theta$ ; and  $L_Y = L(t) \cos\theta$ ; in which  $\theta$  is the instantaneous angle between the pavement load vector and the "yellow" radial axis.

This radial plane pavement load vector resultant is not referenced to the true vertical, as fore-and-aft components can shift the radial load away from the vertical. Work with the strain-gaged axle (Appendix I) showed, however, that fore-and-aft loads under constant speed conditions are typically less than 5% of vertical loads, and the 2.5° angle of the resultant from the vertical will cause much less than 1% difference between vertical loads and radial plane resultant loads. Under conditions of braking or acceleration, the wheel force transducer output is the resultant total radial plane pavement load, including the effects of fore-and-aft shear pavement loads.

The analog computer program shown in Figure J-16 was used to scale raw data channels, compute "red" and "yellow" load components, and compute the instantaneous pavement load resultant,  $L(t)$ . The "resolver" circuit is of interest in that it has built-in calibration and zero capability. Because pavement loads appeared as amplitude modulations  $L(t)$  of  $\sin \omega t$  and  $\cos \omega t$  (in which  $\omega$  is wheel rotation speed), and because  $\omega$  is always greater than 2 cps at speeds above 15 mph, the "red" and "yellow" load components were capacitance-coupled (high-pass filtered,  $\omega_n = 0.25$  cps) to eliminate dc offsets without losing information about the truck static weight. The resolver circuit then provides an accurate zero reference, and because the average output must equal the truck wheel weight, calibration value accuracy may be easily checked. Because dc (static) voltage offsets on the resolver input cause dynamic output errors, accurately established zeros on the raw data chan-



Figure J-15. Wheel force transducer system.

nels are essential. Zeros are most easily achieved using the high-pass filtering techniques described.

In this study, the scaling and electronic summing, both scalar and vector, were performed by an analog computer operating on recorded magnetic tape data. However, commercially available operational amplifier summing devices and resolvers could accomplish on-board computations prior to recording.

### ACCURACY CONSIDERATIONS

Three factors could limit the accuracy of the wheel force transducer system.

#### Outboard Mass Errors

Although the weight of the outboard mass was determined, this weight is an accurate measure of the effective outboard mass only for rigid body motions. Local bending of the tires and/or rims or other nonrigid body actions would result in pavement load measurement errors.

#### Tramp Acceleration Errors

The accelerometer system was slightly offset from the outboard mass center line, but accelerations measured were assumed to be on the center line. If significant tramp accelerations are present, some error can be introduced in the inertial part of the pavement load measurement.

#### Fore-and-Aft Loads

The wheel force transducer measures total pavement loads, whether the loads are vertical or fore-and-aft. If the load resultant is assumed to be vertical, braking (or acceleration when applied to a drive axle) can cause an "apparent

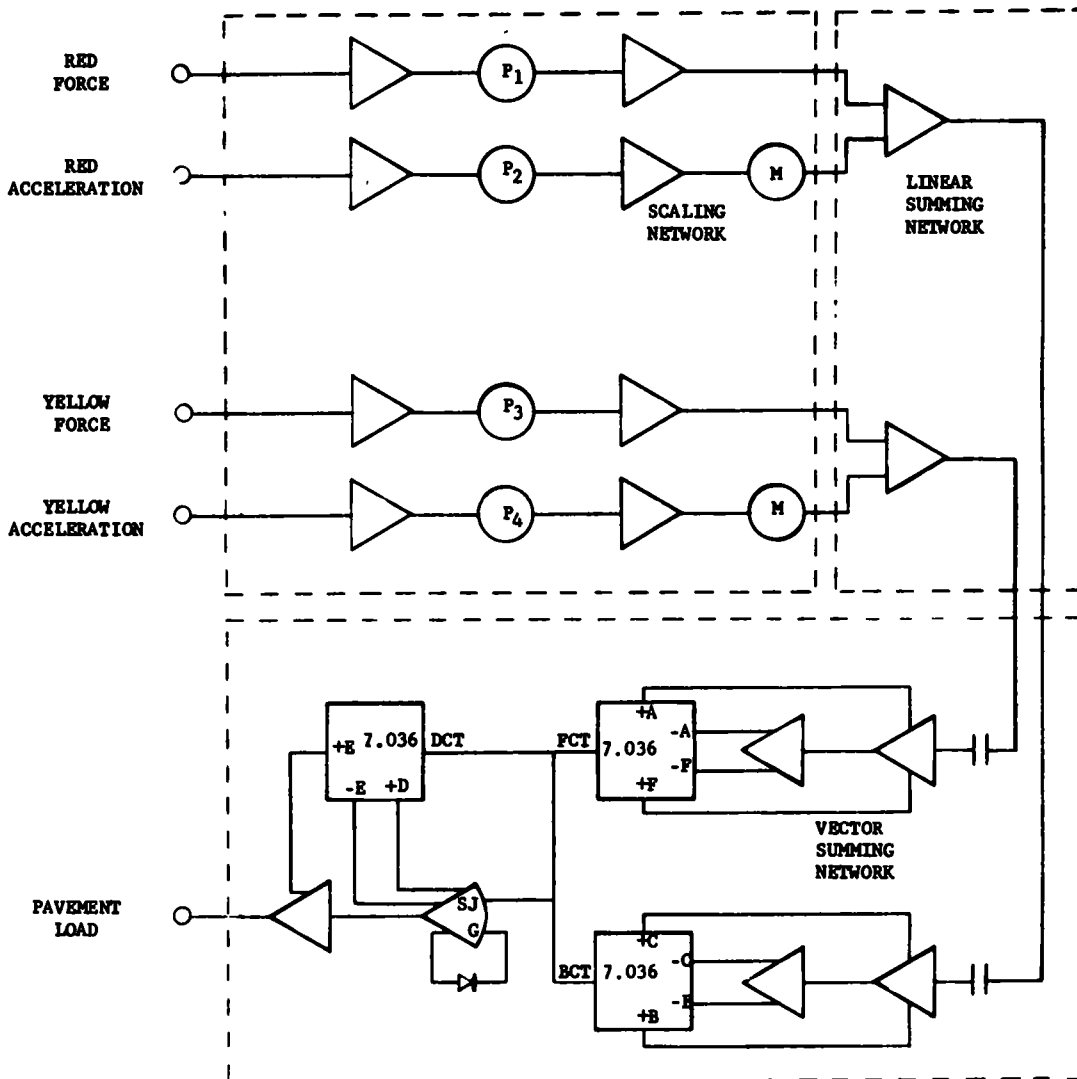


Figure J-16. Wheel force transducer, analog computation networks.

error" by shifting the load vector away from true vertical. Care should be exercised to ensure large shear pavement loads are not present if measured loads are to be treated as vertical loads.

#### SYSTEM CHECKOUT

Although the force transducer and accelerometers had been calibrated separately, the accuracy of the pavement load system had to be demonstrated. Three types of dynamic tests, using reference transducers traceable to the National Bureau of Standards, were run.

#### Laboratory Dynamic Test (Nonrolling)

Test Vehicle No. 1, with the wheel force transducer installed, was set up on four hydraulic servo rams (Fig. J-17 and Appendix K). Each pair of shakers was set on a Noise and Vibration Laboratory load cell to measure shaker input forces to the rear tires. Because the moving mass between

these load cells and the tire/road interface was very small, the load cell output was an accurate reference.

Loads measured by the wheel force transducer system, the strain-gaged axle system (Appendix I), and the reference load cells were recorded while the vehicle was excited sinusoidally, in both hop and tramp, at frequencies from 1 to 19 cps. Step inputs of several sizes, both positive and negative, also were applied to both wheels and then to one wheel. Loads measured during these tests demonstrated that pavement loads measured by the wheel force transducer system and the strain-gaged axle systems agreed very well with input forces measured by the reference load cell.

#### Embedded Scale Test (Rolling)

Loads developed by Test Vehicle No. 1 hitting a ½-in. × 3-ft haversine bump at speeds of 17, 34, and 55 mph were recorded. The bump was mounted on the No. 1 embedded electronic scale at the Grass Lake weigh station, so the embedded scale could be used as a reference transducer.

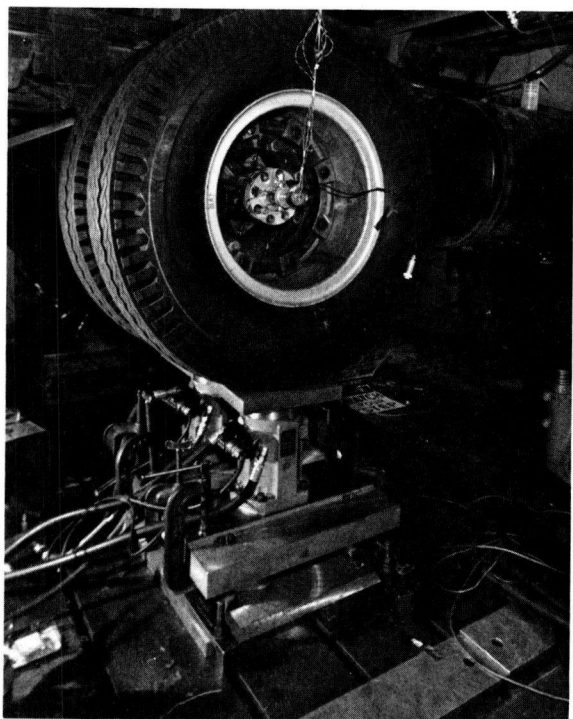


Figure J-17. Test Vehicle No. 1 on hydraulic shakers.

Comparison of load records from the transducer systems showed very good agreement between the wheel force transducer system and the embedded scale (Fig. J-18).

#### Road Test Evaluation

Pavement loads developed by Test Vehicle No. 1 on a 1-mi section of "good" and "poor" pavements were measured using both on-board load measurement systems—the strain-gaged axle system and wheel force transducer system.

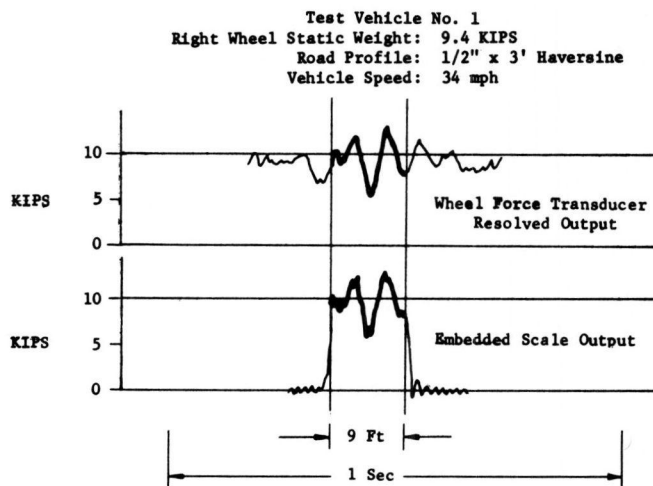


Figure J-18. Wheel force transducer system correlation data.

Studies of the time domain data traces (Fig. J-19), as well as power spectral density analysis displays (Fig. J-20), show good agreement between loads measured by both systems.

On the basis of these checkout tests it was concluded that the wheel force transducer system accurately measured pavement loads.

#### PROBLEMS AND FUTURE IMPROVEMENTS

In the event that a second wheel force transducer were built, some improvements should be included.

#### Gage Fatigue

The selected design stress of 60,000 psi, or 2,000  $\mu\epsilon$ , is too high to permit good strain-gage life. Although the steel transducer is not subject to fatigue problems at this stress level, the strain gages used on this model have a specified

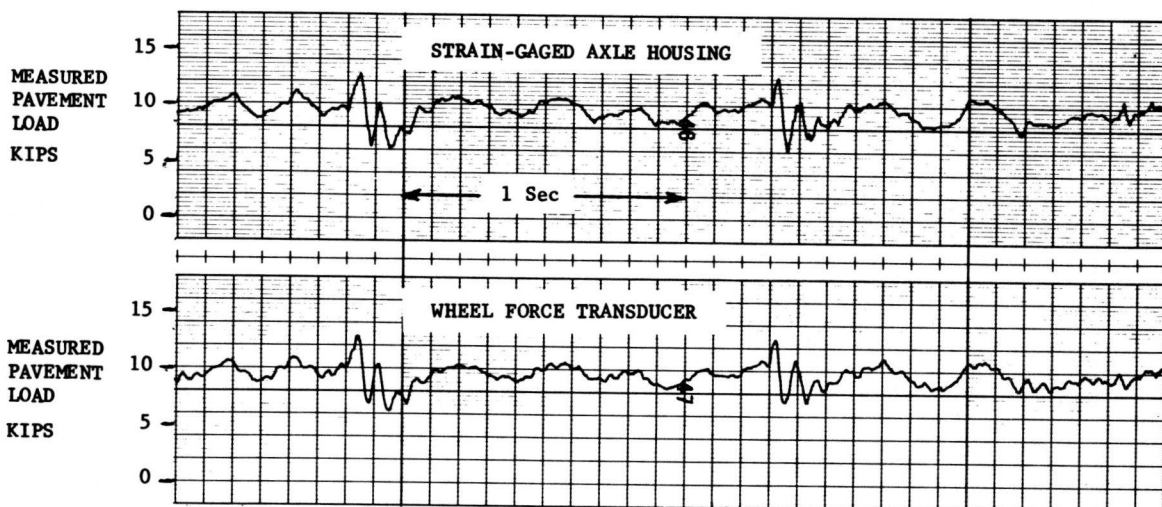


Figure J-19. Comparison of strain-gaged axle housing and wheel force transducer.



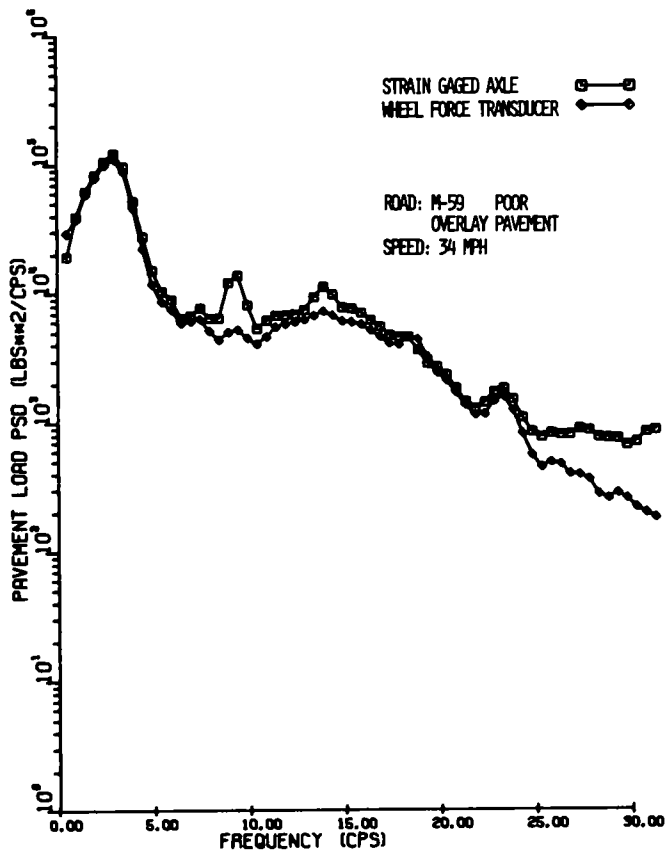


Figure J-20 Pavement load power spectral density

fatigue life of only 1 million cycles at strain levels of  $\pm 1,500 \mu\epsilon$  and 10 million cycles at  $\pm 1,400 \mu\epsilon$ . By itself the typical static wheel load on the rotating transducer causes  $\pm 720 \mu\epsilon$ , cycled 496 times per mile. Additional stresses induced by nonuniform loading and by dynamic

pavement loads, when added to the once-per-revolution load change due to the vehicle static weight, makes strain-gage fatigue a potentially serious problem.

In fact, six gage failures (of 48 gages) were experienced during the experimental tests. This inconvenience should be eliminated in future models by reducing the design stress to 30,000 psi. In the current transducer, regaging with a higher fatigue limit strain gage and gaging the out-board fillets (where peak stresses are lower) would reduce the frequency of gage failures. However, high fatigue strain gages are less accurate for a variety of reasons.

#### Integral Accelerometer

Strain-gaged beams similar to the load-carrying beams connected between the transducer and an inertial mass element would measure wheel accelerations. A ring-shaped element would be insensitive to centrifugal forces and would fit well with the general transducer layout. This possibility of including an accelerometer as an integral part of the transducer should not be overlooked in future designs.

#### Varied Accelerometer Locations

Two nonrotating accelerometers installed on the vehicle axle could be substituted for the four rotating accelerometers used with this system. Wheel center line accelerations could be computed as discussed in Appendix I, and the inertial force component could be added to the resolved wheel force transducer output.

Although this technique requires two less accelerometers than the rotating accelerometer system, the accelerometer installation becomes more involved, and vehicle suspension geometry must be considered in load computation. In addition, errors can now be introduced due to nonrigid body motions of the axle assembly, and the frequency response of the system may be reduced. Most important, the measurement characteristics of the transducer system are no longer independent of the test vehicle characteristics.

## APPENDIX K

### HYDRAULIC SHAKER TESTS

Test Vehicle No 1 was installed on electro-hydraulic servo rams (Fig. K-1) with one ram driving the truck through each of the four rear tires. Each pair of hydraulic rams was set on a reference load cell to measure input forces to each dual wheel set. Input forces also were measured using the wheel force transducer and the strain-gaged axle housing assembly on this vehicle.

Oscilloscope comparisons between outputs from the

wheel force transducer system, the strain-gaged axle housing system, and the reference load cells clearly demonstrated good dynamic performance of both measurement systems.

The reader is cautioned that, although the hydraulic servo ram studies are useful for instrumentation checkout, the extension of this technique to suspension dynamic response studies is not straightforward. Tire enveloping

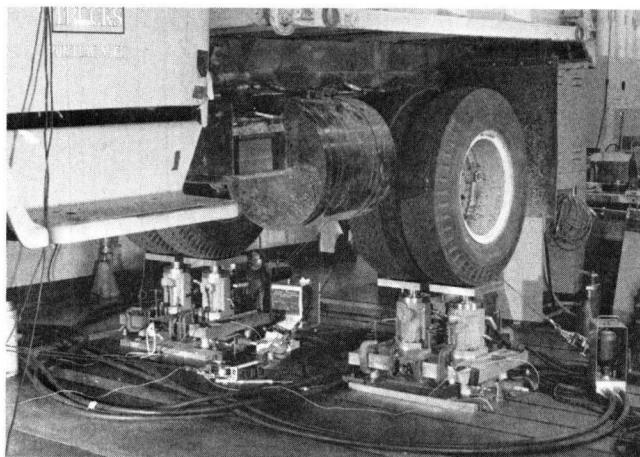
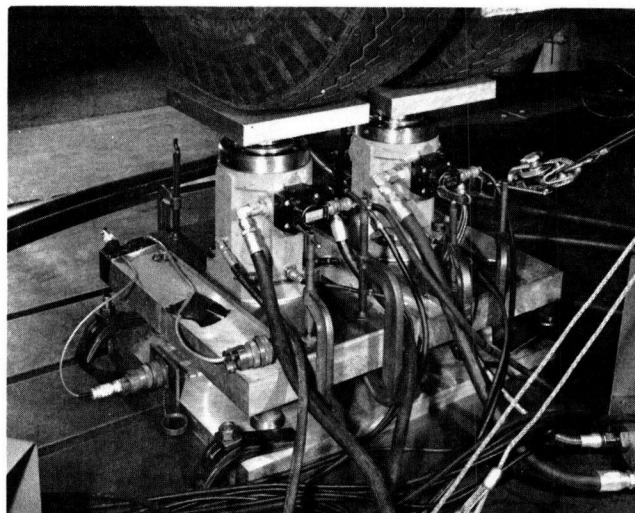
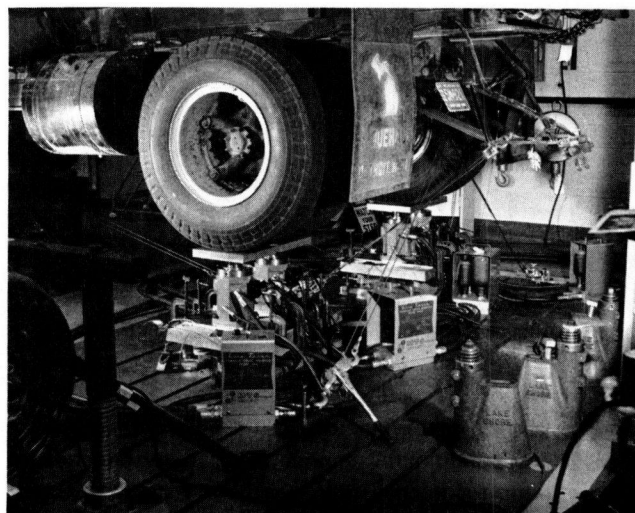


Figure K-1. Test Vehicle No. 1 on electro-hydraulic servo rams.



characteristics, stiffness properties, and damping properties are significantly different for rolling and nonrolling tires. Meaningful information on pavement loads developed by deterministic profiles is best obtained by directing the test vehicle over fabricated bumps attached to a smooth road.



## APPENDIX L

### INITIAL ROAD TESTS

Two General Motors Proving Ground roads, both previously profiled, were selected for initial road testing. A rough road (Proving Ground Oval Track) and a smooth road (Proving Ground Circular Track) were traveled using Test Vehicle No. 1 to furnish data for analytical prediction technique development and also to establish test procedures and data analysis techniques.

#### TEST RUNS

Axle shear forces and accelerations were recorded on FM magnetic tape while the fully loaded test vehicle (18.8 kips

rear axle static weight) traversed 1-mi sections of each track at speeds of 20, 30, 40, and 50 mph. A tire inflation pressure of 75 psi-cold was used for these tests. The recorded quantities were played back to an analog computer data reduction system. Pavement load data were computed, scaled, and recorded on strip charts. Computed variables on each axle were:

1. Pavement load, vertical, total (right and left).
2. Pavement load, fore-and-aft, right side (rear axle only).
3. Sum of forces, vertical ( $\text{hop} \times 2$ ).



4. Difference of forces, vertical (tramp  $\times 2$ ).
5. Hop acceleration, vertical.
6. Tramp acceleration, vertical.

**RESULTS**

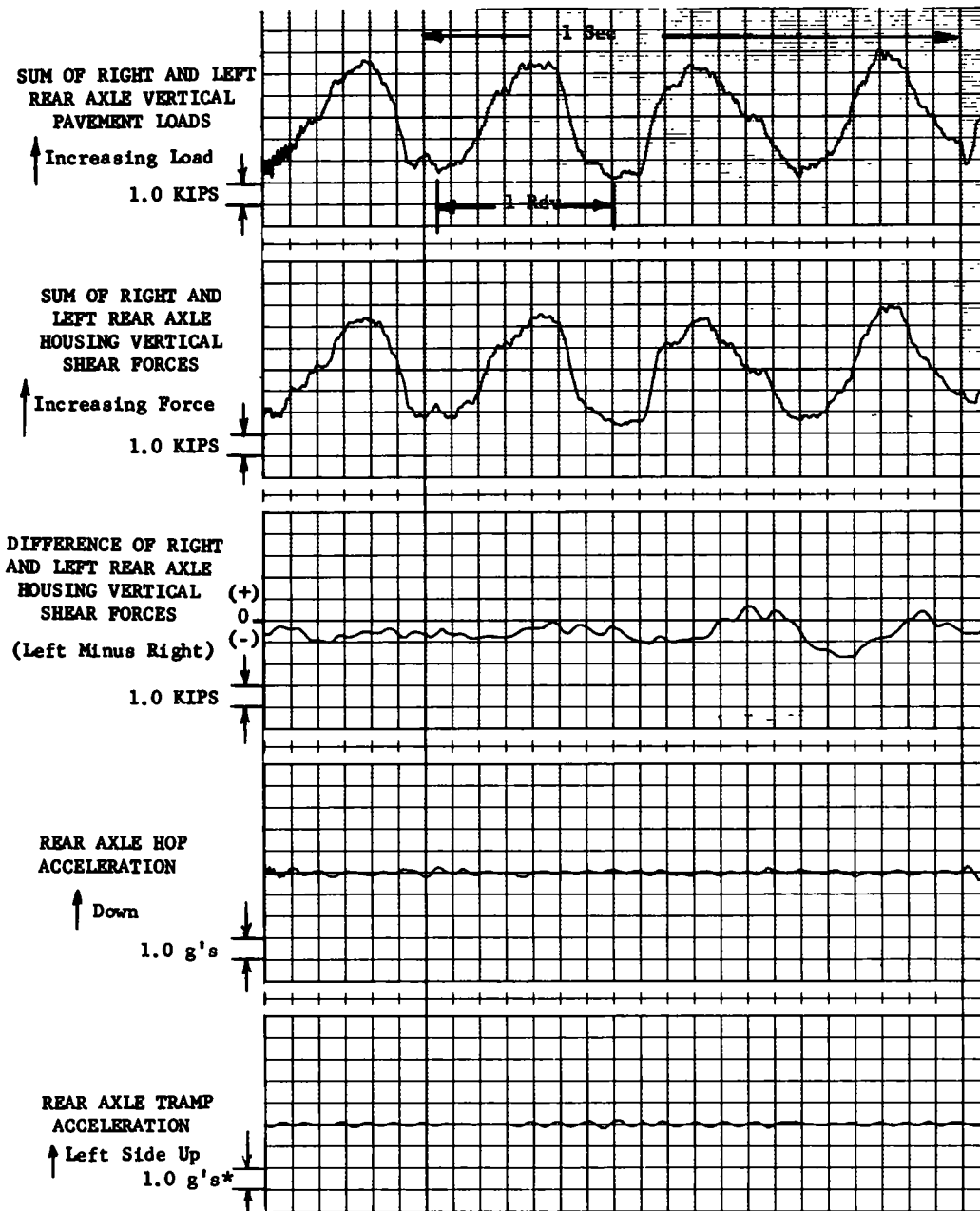
The following observations were made from these road data.

1. On the smooth road, the major rear axle pavement load variations were found to be unassociated with the road

profile. These loads occurred at a rate of once-per-wheel revolution (Fig. L-1). A detailed study of these loads is discussed in Appendix M.

2. For the constant-speed conditions, maximum fore-and-aft pavement loads on the rough road were less than 1,000 lb, or 10% of corresponding vertical loads (Fig. L-2) Because the fore-and-aft loads are small in comparison to the vertical loads, the difference between the vertical and resultant loads is less than 1%.

3 Front axle dynamic pavement loads were very small,



\* At the Accelerometer Location  
 Where  $1.0g = 2.75 \text{ rad/sec}^2$

Figure L-1. Rear axle pavement load, smooth road. Vehicle speed: 20 mph.

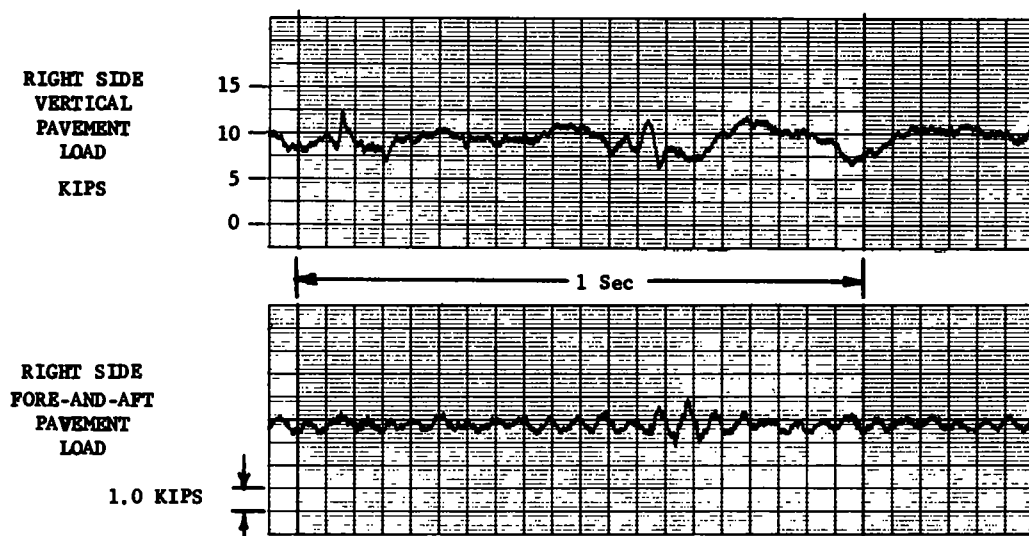


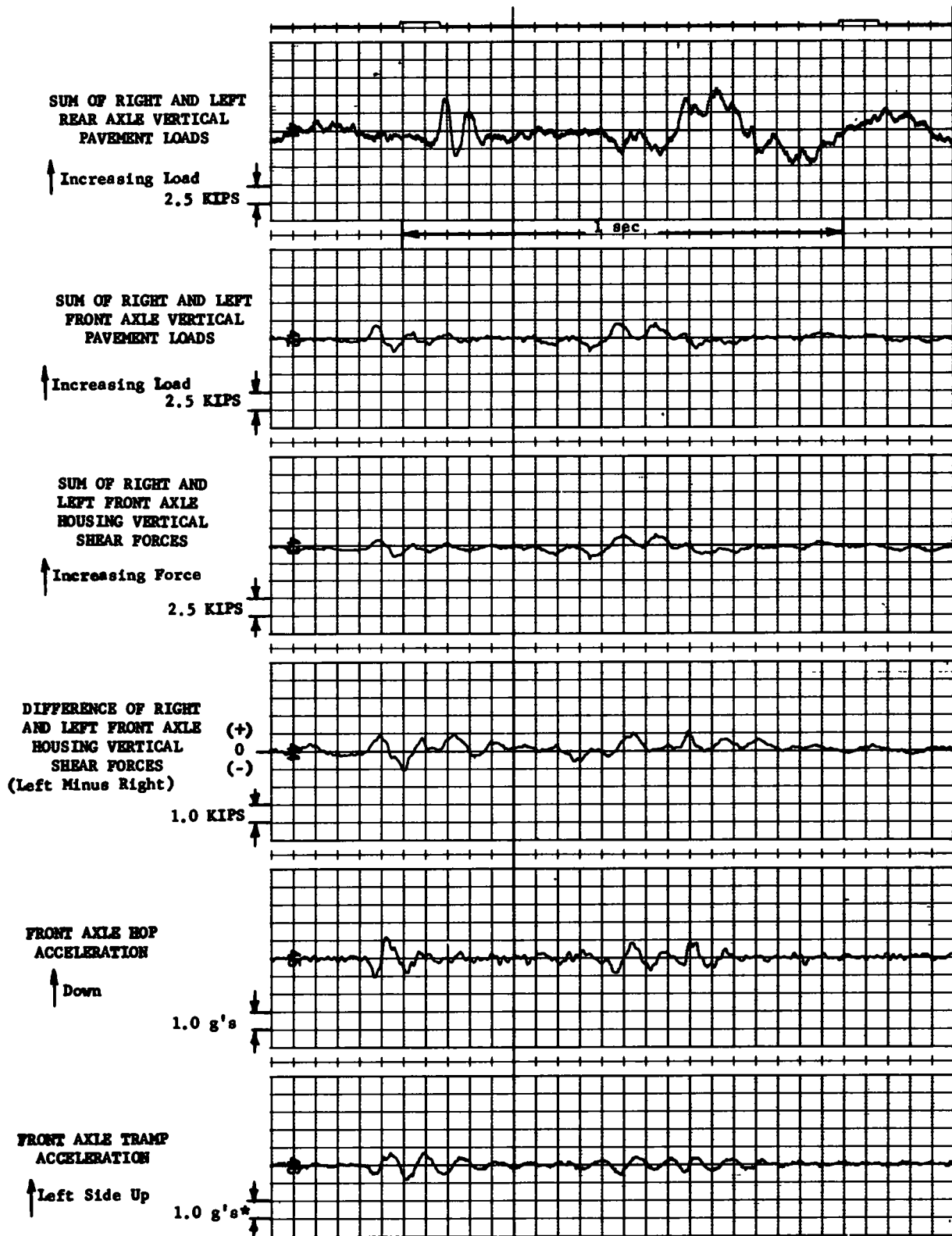
Figure L-2. Simultaneous vertical and fore-and-aft pavement loads at right rear wheel. Vehicle speed: 50 mph.

seldom over 2,000 lb (zero-to-peak), even on the rough road at high speeds (Fig. L-3). On severe sharp bumps, front dynamic loads never exceed 30% of corresponding rear loads (Fig. L-4). Front dynamic load peaks are not time-correlated with rear dynamic load peaks, either for low- or high-frequency loads, indicating pitch coupling is not a significant factor in pavement load development with this vehicle. Because of the small degree of pitch coupling, front axle interactions can be neglected in the study of high-level rear axle pavement loads.

4. Hop and tramp axle motions and forces occur in about equal proportions, indicating that significant data may be overlooked by considering only total axle pavement loads (Fig. L-5). The effects of tramp coupling were therefore considered in more detail during the deterministic input tests discussed in Appendix N.

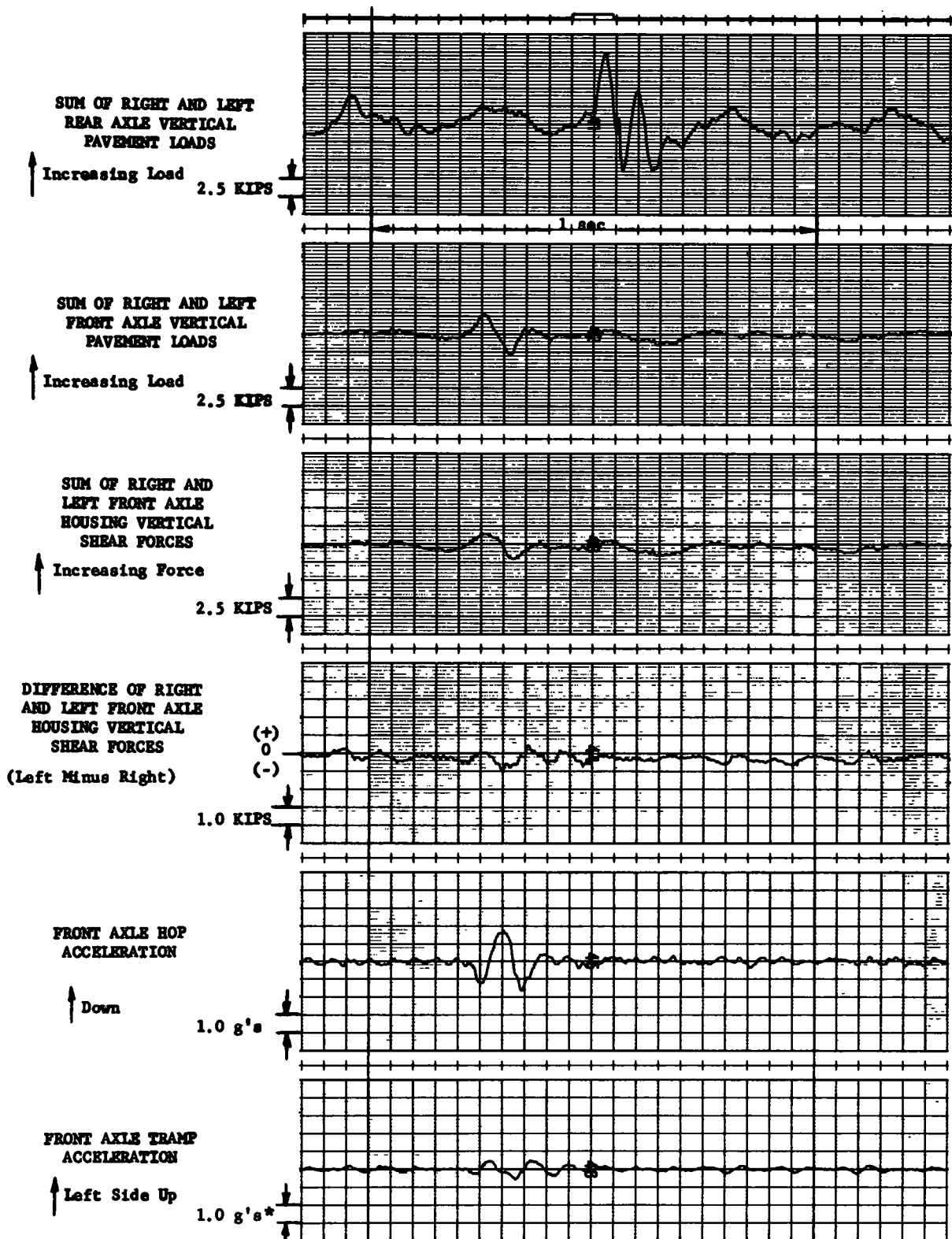
#### CONCLUSION

These test data proved very useful for initial analyses, simulation development, and correlation work. Owing to the dominance of wheel rotation frequency loads, publication of large amounts of these data was not considered useful.



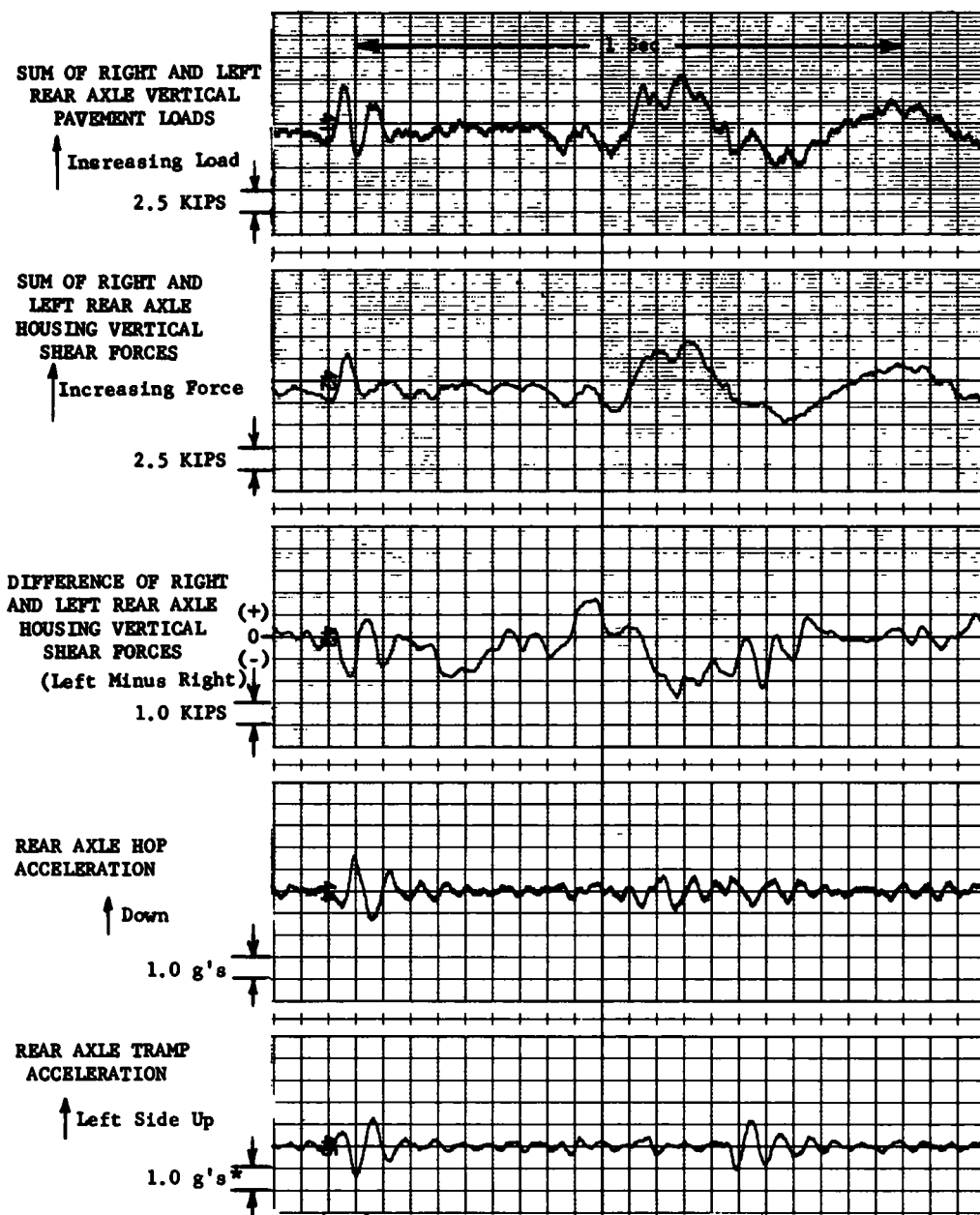
\* At the Accelerometer Location  
 Where 1.0g = 2.02 rad/sec<sup>2</sup>

Figure L-3. Typical front axle pavement load, rough road. Vehicle speed: 50 mph.



\* At the Accelerometer Location  
 Where 1.0g = 2.02 rad/sec<sup>2</sup>

Figure L-4. Peak front axle pavement load, rough road. Vehicle speed: 30 mph.



\* At the Accelerometer Location  
 Where  $1.0g = 2.75 \text{ rad/sec}^2$

Figure L-5 Rear axle pavement load, rough road. Vehicle speed: 50 mph.

## APPENDIX M

### STUDY OF PAVEMENT LOADS RELATED TO WHEEL ROTATION

When Test Vehicle No. 1 was run on a smooth road (Proving Ground Circular Track), low-frequency sinusoidal variations in the rear axle pavement load were observed (Fig. M-1). Comparison of these pavement loads with a corresponding road profile showed that the loads were not related to road inputs, but were related to wheel rotation frequency. A power spectral density analysis of the pavement load confirms the presence of several orders of wheel rotation frequency (Fig. M-2).

First-order forces are often associated with wheel unbalance. However, at 65 mph a 1-lb unbalance at the rim location would produce less than  $\pm 100$  lb of force variation. Therefore, rim assembly runout and/or tire nonuniformity were the probable causes of these forces.

To more fully evaluate the causes of these self-generated first-order loads, the test vehicle was installed on a chassis dynamometer (Fig. M-3). The chassis dynamometer rolls provided a very smooth "road" [0.003 in. total indicated runout (TIR)].

The rear axle strain-gaged axle housing transducer system (Appendix I) was used to measure "pavement" loads. A TR-20 portable analog computer was used to compute the loads, and the results were displayed on a Brush two-channel recorder.

When the vehicle wheel speed was swept from 20 to 60 mph, rear axle load variations of over 5,000 lb peak-to-peak were observed at some speeds (Fig. M-4). When the vehicle was run at constant speed, the peak load variation amplitude was observed to increase to a maximum and then decrease to a minimum (Fig. M-5). About 90 sec were required for the amplitude variation to complete a full cycle.

Observation of the truck body motion at 25 mph indicated that the truck body was in a bounce mode when maximum load variations occurred. When the load variation was near a minimum the body appeared to be rolling.

Because load amplitude variations made speed sweeps unrepeatable, loads were recorded at speeds of 20, 25, 30, 35, 40, 45, 50, 55, and 60 mph. At each speed, sufficient

time was allowed for the amplitude to vary through a complete cycle. Both the sum (hop) and difference (tramp) of the individual rear wheel loads were recorded (Table M-1).

The amplitude variation was found to be associated with a mode transition from bounce to roll (Fig. M-5). When hop loads were minimum, tramp loads were maximum. Apparently slight differences in individual rear wheel circumferences caused the force excitation phase relationship between right- and left-side inputs to vary, resulting in wheel rotation frequency excitation which gradually changed from hop to tramp. The particularly high load variation at 20 mph occurred because wheel rotation frequency (approximately 3 cps) was very near the body-suspension bounce frequency. Body roll motions did not peak at any particular speed in the 20- to 60-mph range.

TABLE M-1  
REAR AXLE LOADS—HOP AND TRAMP

SPEED (MPH)	SUM (HOP LOAD) (LB P-P)		DIFFERENCE (TRAMP LOAD) (LB P-P)	
	MAX	MIN.	MAX.	MIN.
20	5200	1200	1400	400
25	4100	1600	1600	400
30	2800	1000	1800	500
35	2200	700	1600	400
40	2200	900	1400	400
45	2000	700	1400	400
50	2200	200	1000	500
55	2000	1000	1000	600
60	2200	1400	1100	600

P-p = peak-to-peak

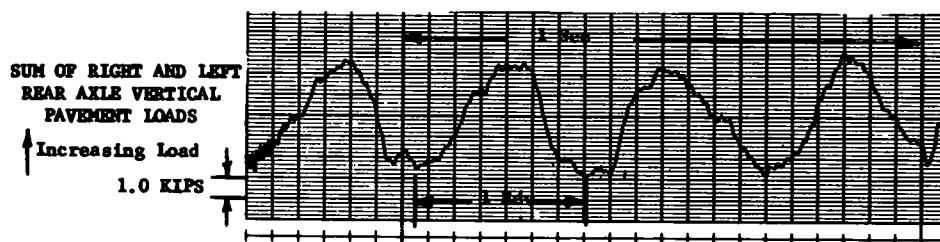


Figure M-1 Smooth road pavement load variations. Vehicle speed: 20 mph.

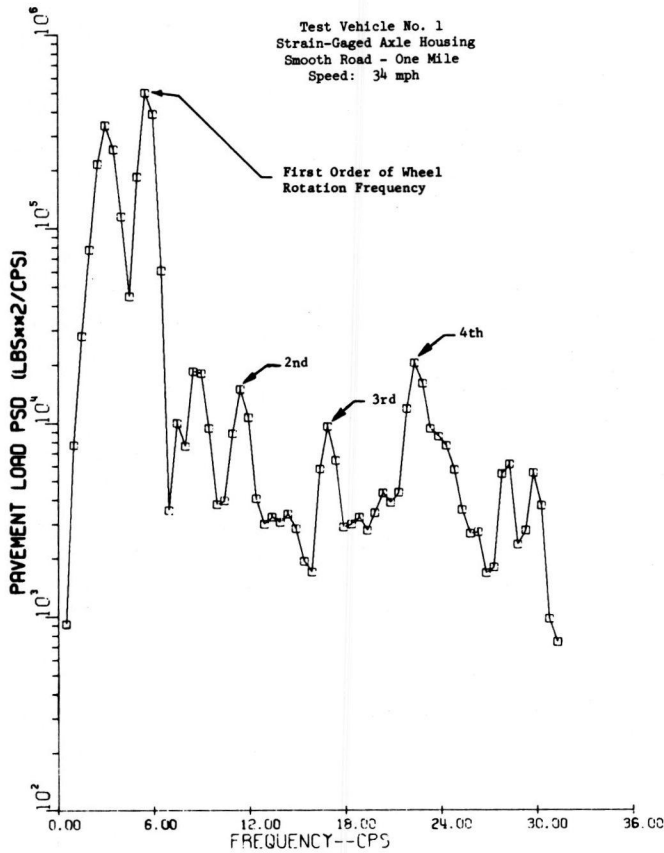


Figure M-2. Pavement load power spectral density.

To more effectively study the cause of the once-per-revolution excitation, individual right and left "pavement" loads were measured for the same test speeds. These loads are given in Table M-2.

Peak loads on each side were found to be synchronized with wheel "wobble" (lateral runout). Although tire irregularities could have produced these loads, in this case the



Figure M-3. Test Vehicle No. 1 on chassis dynamometer.

primary cause was rim assembly installation misalignment (Fig. M-6). The misalignment was caused by nonsymmetrical clamping around the circumference of the wheel. Low-speed checks with dial indicators showed that maximum radial runout and maximum lateral runout occurred at the same position on the wheel.

The runout-induced loads in this test vehicle were considered typical of those experienced with heavy trucks with "clamp-on" rims. For purposes of correlating computed pavement loads based on road profiles with measured pavement loads, runout-induced load variation constituted an extraneous signal that tended to mask the profile-induced loads of interest. To reduce these variations, a custom installation procedure, involving measurement of the radial runout during the rim installation, was made. The resultant radial runout values were 0.050 in. TIR for the right side

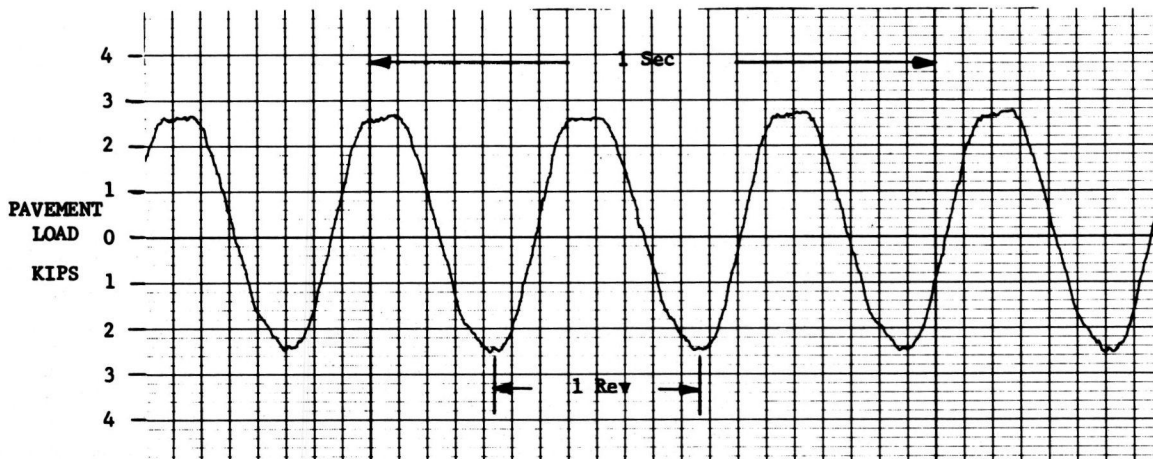


Figure M-4. Rear axle pavement load, 20 mph on chassis dynamometer.

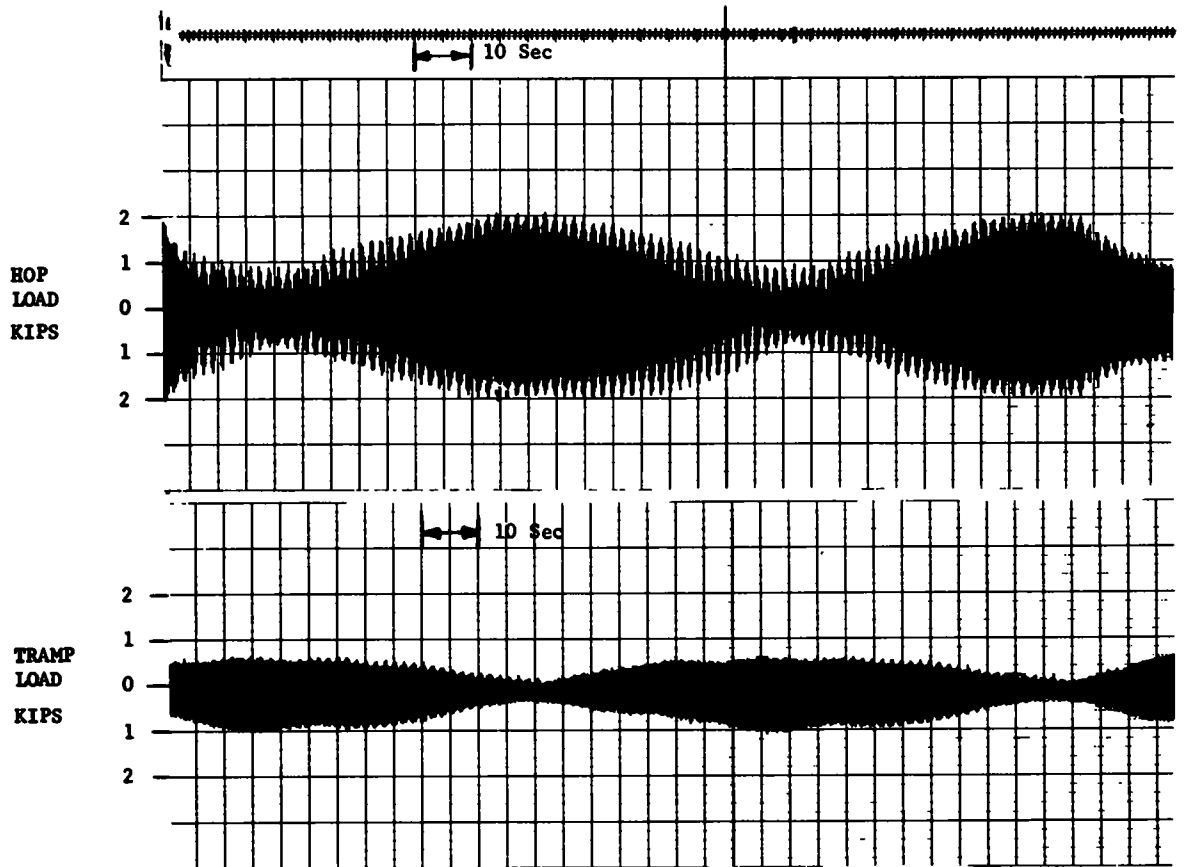


Figure M-5. Rear axle hop load versus tramp load, 20 mph on chassis dynamometer.

and 0.090 in. TIR for the left side. The pavement load variations after this realignment are given in Table M-3.

Most of the remaining load variation, particularly at the higher speeds, occurred at frequencies higher than first-order tire rotation frequency. The residual load variation of less than 800 lb peak-to-peak per side at speeds above 30 mph was considered low enough not to interfere with

measurement of road-profile-induced pavement loads (Fig. M-7).

A PSD plot of pavement loads recorded on a "good" road (I-75) further verified the reduction of excitation at first order of wheel rotation frequency (Fig. M-8). The first order content of Figure M-2 should be compared with Figure M-8.

TABLE M-2  
REAR WHEEL LOADS

SPEED (MPH)	RIGHT SIDE (LB P-P)		LEFT SIDE (LB P-P)	
	MAX.	MIN.	MAX.	MIN.
20	2800	600	2700	700
25	2200	800	2200	1200
30	1600	1100	1600	1200
35	1300	1000	1300	1100
40	1100	800	1300	1000
45	1200	800	1200	900
50	1300	700	1200	800
55	1200	1000	1200	600
60	1400	1100	1200	800

P-p = peak-to-peak

TABLE M-3  
REAR WHEEL LOADS AFTER REALIGNMENT

SPEED (MPH)	RIGHT SIDE (LB P-P)		LEFT SIDE (LB P-P)	
	MAX.	MIN.	MAX.	MIN.
20	1600	1200	1600	800
25	1000	800	1000	600
30	800	500	700	400
35	700	500	600	400
40	600	400	600	300
45	600	400	600	400
50	700	400	800	300
55	800	500	700	300
60	700	600	700	500

P-p = peak-to-peak



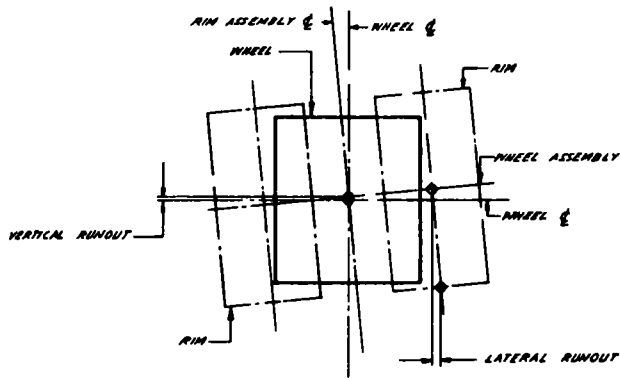


Figure M-6. Rim assembly installation misalignment schematic

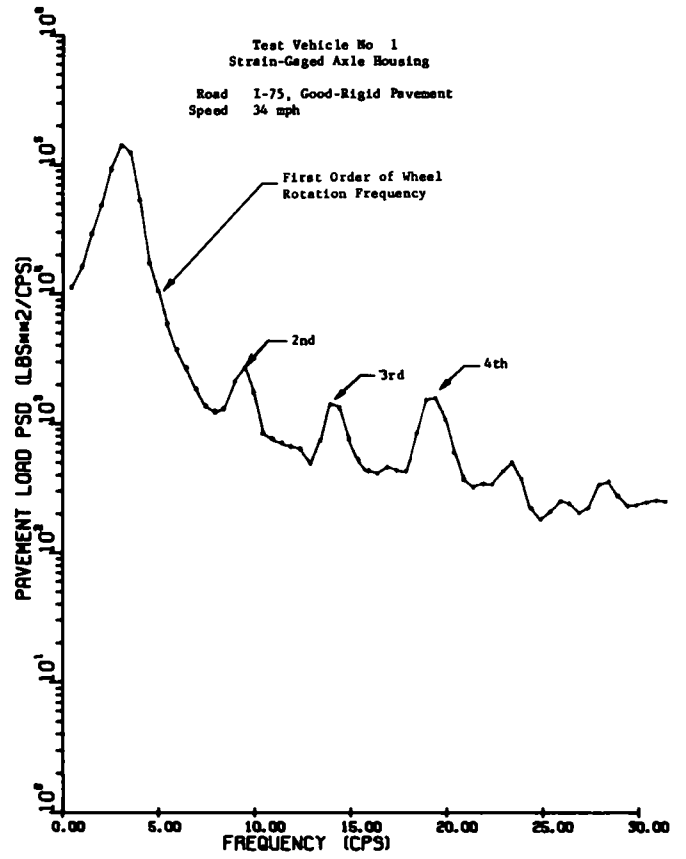


Figure M-8 Pavement load power spectral density.

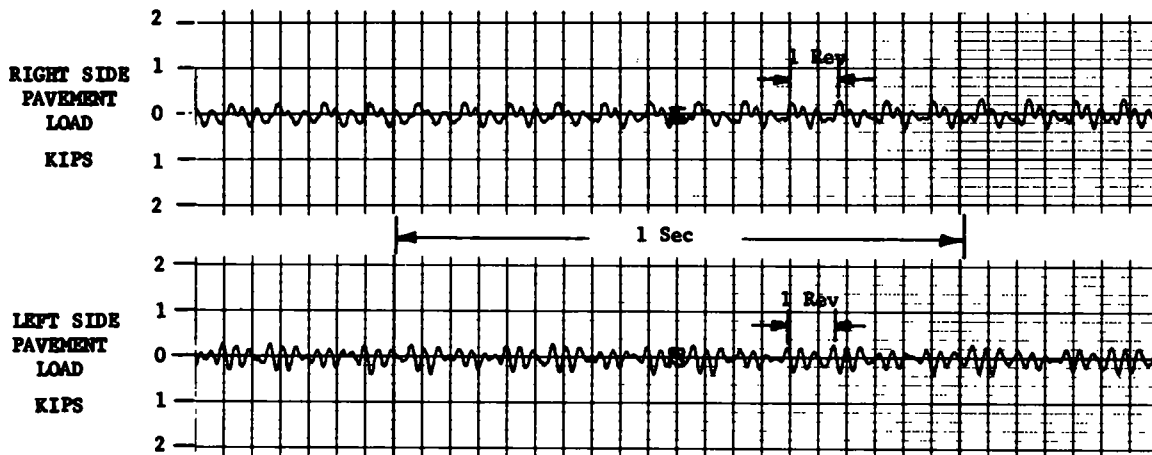


Figure M-7. Rear axle pavement load with improved wheel alignment, 50 mph on chassis dynamometer.

# APPENDIX N

## DETERMINISTIC PROFILE TESTS

A series of road tests were performed using road profiles of deterministic shape to gain knowledge in two areas. First, it was desired to determine the effect of tramp coupling on rear-wheel pavement loads. Second, the determination of tire enveloping magnitude and rear suspension damping characteristics was required for load prediction model development. Twelve plywood "bumps" on 88-ft spacings were set up on a very smooth test road. Bump profiles are given in Table N-1.

The bumps were traversed at 17, 34, and 55 mph, first with both rear wheel sets contacting the bumps, and then with only the right wheel set contacting the bumps.

### TRAMP COUPLING

Left wheel dynamic loads measured when only the right wheels traversed the bumps were typically 30% of the dynamic loads developed at the right wheels. Right wheel

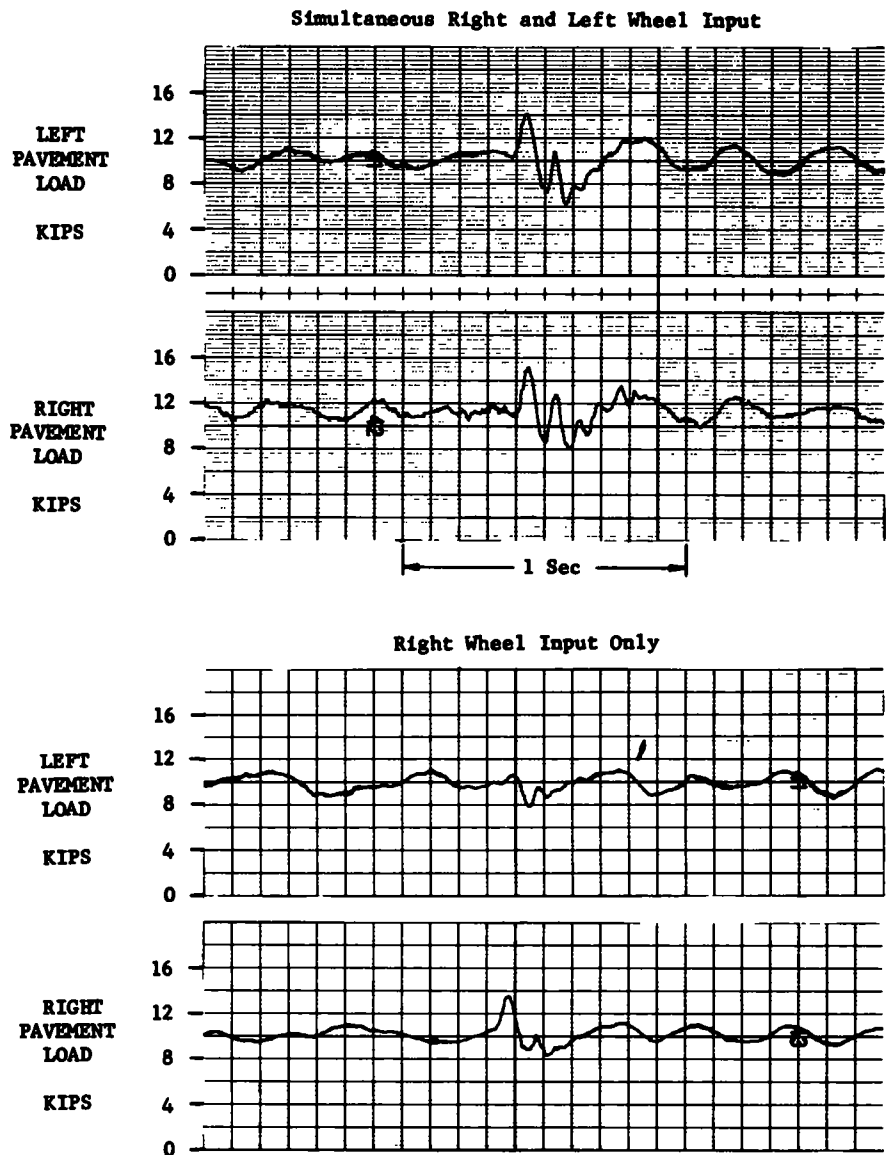


Figure N-1 Evaluation of tramp coupling One-in  $\times$  3-ft haversine bump Speed. 17 mph

TABLE N-1  
DETERMINISTIC PROFILE SPECIFICATIONS

Profile	Height(h)	Length	Side View
Haversine	1/2"	3'	
Haversine	1"	3'	
Step	1/4"	16'	
Step	1/2"	16'	
Step	3/4"	16'	
Ramp	1/4"	3' taper, 16'	
Ramp	1/2"	3' taper, 16'	
Ramp	3/4"	3' taper, 16'	
Impulse	1/4"	1"	
Impulse	1/2"	1"	
Impulse	3/4"	1"	
Impulse	1"	1"	

dynamic loads developed when only the right wheels traversed the bumps were 70% to 85% of right wheel dynamic loads developed when both wheels traversed the bumps (Fig. N-1). This corresponded to a difference in peak pavement load of less than 12%.

#### TIRE ENVELOPING AND SUSPENSION DAMPING

The determination of tire enveloping and suspension damping from deterministic profile data is discussed in Appendix S.

## APPENDIX O

### REPEATABILITY STUDIES

A 1/2-in.-high  $\times$  18-in.-long step bump was placed on the Grass Lake embedded scales. Test Vehicle No. 1 traversed the bump six times at apparently the same speed (30 mph). A typical load trace is shown in Figure O-1. Loads measured during the six runs are given in Table O-1. Load variations were about  $\pm 3\%$  of the peak load and  $\pm 10\%$  of the dynamic load.

In Table O-1 the second peak exceeds the initial peak. The initial peak is the response to one step input (the leading edge of the bump). The second peak is the sum

of responses to two sequential inputs (the 1/2-in. up step at the leading edge and the 1/2-in. down step at the trailing edge). For this particular combination of bump length, vehicle speed, and vehicle wheel hop resonant frequency, the two responses are additive, resulting in a particularly high second peak.

TABLE O-1  
PAVEMENT LOAD MEASUREMENT  
REPEATABILITY DATA

RUN NO.	SPEED (MPH)	INITIAL PEAK (KIPS)	MINIMUM (KIPS)	SECOND PEAK (KIPS)
1	28.3	23.5	14.5	26.0
2	28.5	24.0	15.0	25.5
3	29.0	24.0	14.0	26.0
4	29.5	24.5	13.0	27.0
5	28.8	24.0	15.0	26.0
6	30.0	25.0	13.5	27.0
Mean value	29.0	24.2	14.2	26.3
Variation	1.7	1.5	1.5	1.5

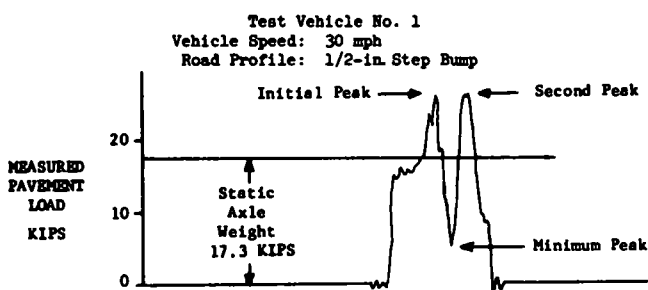


Figure O-1 Embedded scale output.

## APPENDIX P

### PAVEMENT LOAD DATA—STRIP CHARTS AND PROBABILITY DENSITIES

Right-wheel load data for the instrumented axle on each test vehicle were collected for the test conditions listed in Table P-1. Figure P-1 shows data representative of that collected for each run. Similar data for all other tests are available on request to the Program Director, NCHRP. A single data sheet was prepared for each run. Low-speed

time domain charts of load and vehicle speed were plotted for each of the 1-mi runs, and high-speed strip charts of sections of each run show a high-level load on an expanded time scale. Arrows identify the same high-level load with both low and high strip chart speeds. The same point on a 1-mi test road was noted for all tests conducted on that

TABLE P-1  
TEST CONDITIONS FOR MEASURED PAVEMENT LOAD DATA

TEST CONDITION		
VEHICLE NO. 1, 2-D, DRIVE AXLE	VEHICLE NO. 2, 3S2, FORWARD DRIVE AXLE	VEHICLE NO. 3, 3S1, TRAILER AXLE
I-75, good-rigid 34 mph 55 mph Sweep 63 mph 34 mph—vehicle unloaded 65 mph—vehicle unloaded	I-75, good-rigid 34 mph 55 mph Sweep	I-75, good-rigid 34 mph 54 mph Sweep
I-696, fair-rigid 34 mph 55 mph Sweep	I-696, fair-rigid 34 mph 54 mph Sweep	I-696, fair-rigid 34 mph 55 mph Sweep
M-50, poor-rigid 34 mph 53 mph Sweep	M-50, poor-rigid 34 mph 55 mph Sweep	M-50, poor-rigid 34 mph 55 mph Sweep
M-52, good-flexible 34 mph 46 mph Sweep	M-52, good-flexible 34 mph 55 mph Sweep	M-52, good-flexible 34 mph 55 mph Sweep
M-247, fair-flexible 34 mph 47 mph Sweep	M-247, fair-flexible 34 mph 47 mph Sweep	M-247, fair-flexible 34 mph 48 mph Sweep
M-138, poor-flexible 34 mph 44 mph Sweep	M-138, poor-flexible 34 mph 55 mph—not available Sweep	M-138, poor-flexible 34 mph 42 mph Sweep
M-53 NB, good-overlay 34 mph 54 mph Sweep	M-53 NB, good-overlay 34 mph 55 mph Sweep	M-53 NB, good-overlay 34 mph 53 mph Sweep
M-53 SB, fair-overlay 34 mph 55 mph Sweep	M-53 SB, fair-overlay 34 mph 55 mph Sweep	M-53 SB, fair-overlay 34 mph 55 mph Sweep
M-59, poor-overlay 34 mph 53 mph Sweep 64 mph 34 mph—vehicle unloaded 65 mph—vehicle unloaded	M-59, poor-overlay 34 mph 48 mph Sweep	M-59 NB, poor-overlay 34 mph 55 mph Sweep

NB—northbound, SB—southbound

Vehicle No. 1, 2-D  
 Instrumented Wheel: Right Side of Drive Axle  
 Static Weight on Wheel: 9.4 KIPS  
 Road: I-75, Good-Rigid  
 Speed: 34 mph

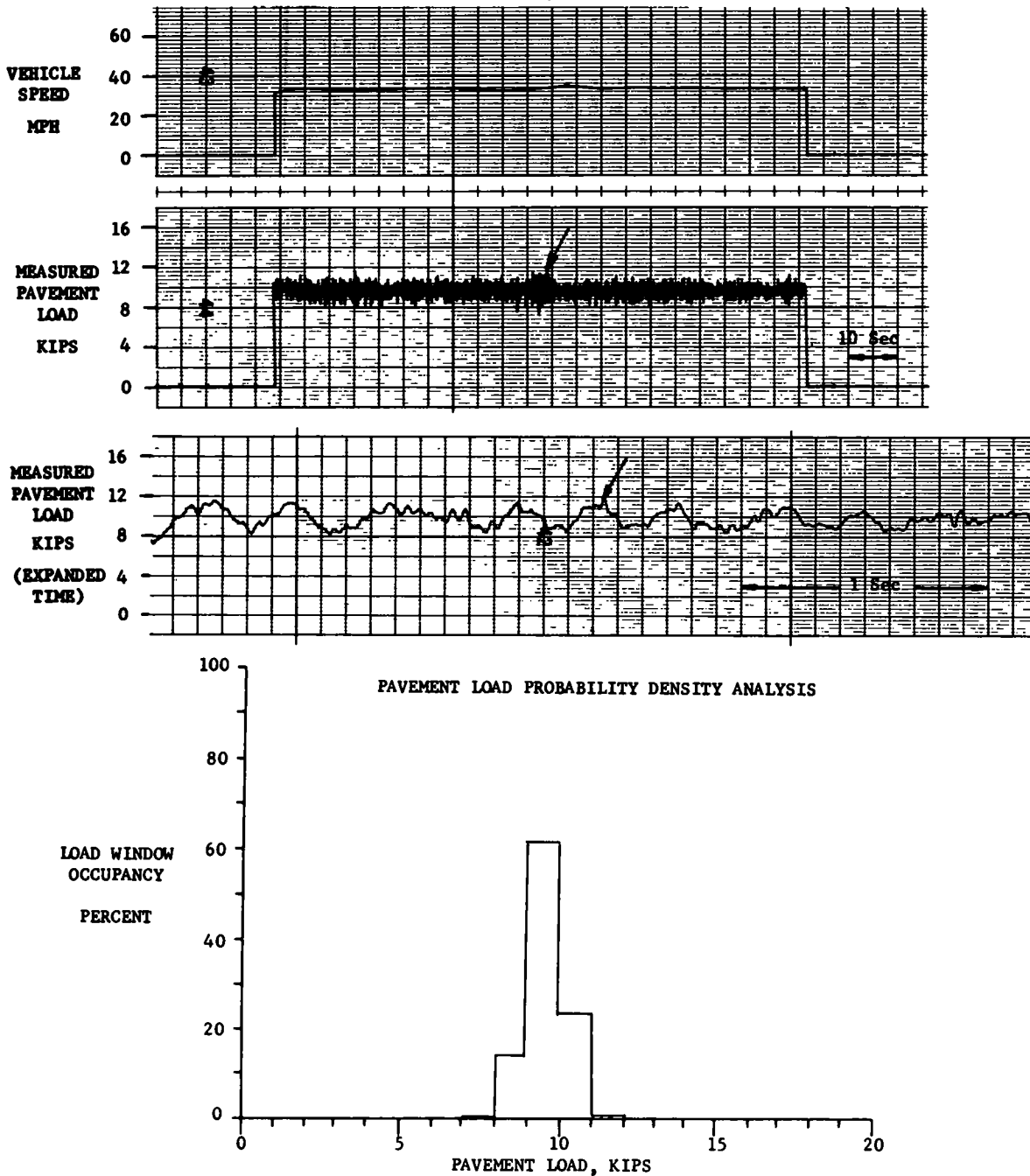


Figure P-1 Measured pavement load.

road. The road profiles that caused the high-level loads are shown in Appendix T. A probability density plot of the load is shown for each 1-mi run. Representative power spectral density and load-occurrence analyses for one of the test conditions run with Test Vehicle No 1 are included in Appendix T

## APPENDIX Q

### FREQUENCY DOMAIN PREDICTION TECHNIQUES

This appendix describes methods of defining a frequency-domain model of a linear vehicle system (6, 8) by considering a road profile as its input and the corresponding tire/road interface force as its output. Model definition would permit pavement load prediction from any measured road profile. Two methods of model definition and subsequent pavement load prediction are discussed.

#### POWER SPECTRAL DENSITY (PSD) METHOD

Model definition by this method requires computation of power spectral density (PSD) functions as a measured road profile and the corresponding pavement load. The pavement load PSD is divided by the road profile PSD and the square root taken to form the magnitude of the frequency response function describing the vehicle system (Fig. Q-1). The square of this vehicle frequency response function can then be multiplied by the PSD of any road profile to determine the corresponding pavement load PSD for that particular road.

#### CROSS SPECTRAL DENSITY (CSD) METHOD

Model definition by this method requires computation of the road profile PSD and the road profile/pavement load CSD function. The CSD is divided by the road profile PSD to form the complete frequency response function describing the vehicle system. Because the CSD has both magnitude and phase, the resulting vehicle frequency response function also contains both magnitude and phase information (Fig. Q-2). Prediction of a pavement load PSD is accomplished in the same way as stated in the PSD method. Also, because the complete (magnitude and phase) frequency response function is computed, the pavement load time history can be predicted using convolution techniques.

#### IMPLEMENTATION OF PSD AND CSD METHODS

Some preliminary attempts were made to compute vehicle frequency response functions by both methods. Both methods encountered difficulties because of low signal-to-noise ratios for short-wavelength (high-frequency) road profile data. Inspection of any of the road profile PSD functions in Appendix G shows that the PSD amplitude is very low at higher frequencies. This made the quotient (vehicle response function) very unreliable.

If further research is to be fruitful in this area, methods must be devised to improve the road profile signal-to-noise ratio at frequencies of interest. This can be done by selecting or physically constructing a road profile with substantial excitation at all frequencies of interest. If this is impractical, a usable road profile PSD can be constructed from low signal-to-noise ratio data by a process known as "pre-whitening."

"Pre-whitening" consists of multiplying the road profile PSD by a frequency response function, which will make the resulting PSD essentially flat and of significant content at all frequencies of interest. Then, when the division is performed, the denominator will be more reliable and will provide a more meaningful quotient. However, a frequency response function derived in this manner must be "post-darkened"; in other words, it must be multiplied by a frequency response function with opposite characteristics to the "pre-whitening" function.

#### DISCUSSION OF SYSTEM LINEARITY ASSUMPTION

Both methods of computing frequency response functions just described are based on the important assumption of system linearity. In a nonlinear system, the vehicle system characteristics change with the amplitude of the input. Therefore, frequency response functions calculated by the PSD and CSD methods can at best be only linear approxi-

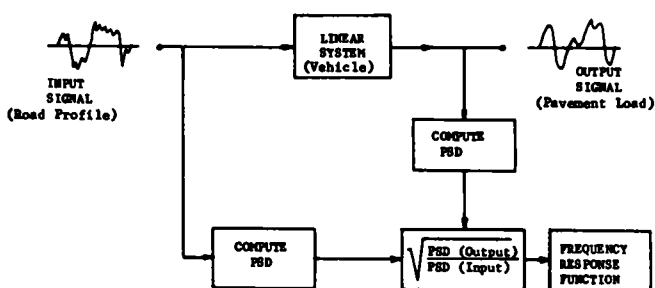


Figure Q-1. Power spectral density method for computing frequency response function.

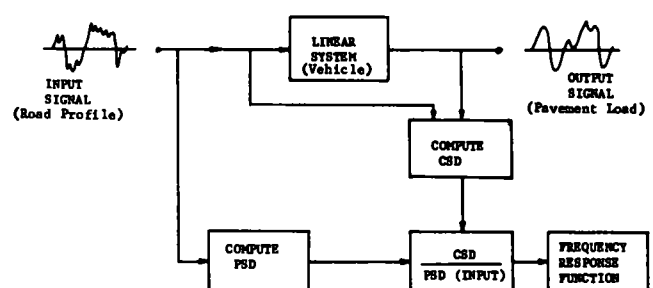


Figure Q-2. Cross spectral density method for computing frequency response function.

mations of the true nonlinear system. They may, however, be adequate for a certain range of input amplitudes, and so could be useful in prediction of dynamic pavement loads.

It should be emphasized that frequency domain studies were by no means exhaustive, and further work in this area may produce valuable findings.

## APPENDIX R

### SIMULATION OF TIRE ENVELOPING

Analog simulations of vehicles for use in computing dynamic pavement loads from road profile inputs must include an adequate representation of tire enveloping effects. The ability of the tire to conform to road irregularities reduces the severity of loading with respect to both the pavement and the vehicle. If tire enveloping effects are ignored, the computed loads are consistently too high. The following discussion outlines approaches to analog simulation of these effects.

#### THE CONCEPT OF AN EFFECTIVE ROAD PROFILE

Figure R-1 shows a simple model of a truck that lacks tire enveloping. Analog voltages proportional to road profile displacements were introduced to an analog simulation of the model through the simple linear tire spring. The computed loads were too high when compared to experimental loads. If the recorded profile was passed through appropriate signal-conditioning circuits prior to introduction to the tire spring, favorable load agreement was achieved. The road profile generated by passing the analog signal through the tire enveloping circuits is called the *effective road profile* (Fig. R-2). Two methods of generating effective road profiles are described as follows.

#### FORCES DEVELOPED BY 1-IN. CLEATS

The first method simulates tire enveloping effects by generating effective road profiles as suggested by experimental evidence (9). Vertical forces produced by a slowly rolling tire (2.5 mph) passing over a 1-in.-wide cleat have a waveform as shown in Figure R-3. Furthermore, the amplitude of the force is reasonably linear with respect to the height of the cleat. In view of these results, the road profile could be thought of as a series of 1-in.-wide cleats, each of appropriate height, as shown in Figure R-4.

Each cleat in contact with the tire contributes a component of vertical force of the same form, as shown in Figure R-3. The total force can be approximated as a sum of the contributions of all cleats in contact with the tire. For example, if the tire patch is 10 in. long (Fig. R-5) the total load consists of the contributions of 10 1-in.-wide cleats. These load contributions are properly phased to account for relative displacement along the traveled direction and of amplitude proportional to the relative displacement between the road profile and suspension mass.

Figure R-6 shows the relative position of load components and their sum for a tire traveling over a smooth road. The resultant ripple in the total load is artificial in the case of the smooth road but must be tolerated if this

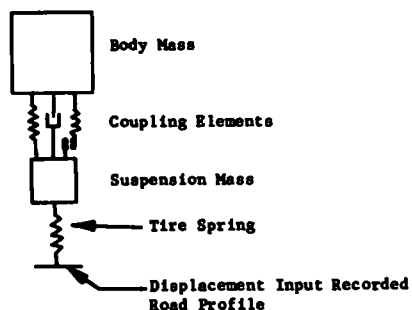


Figure R-1. Analog truck model without tire enveloping.

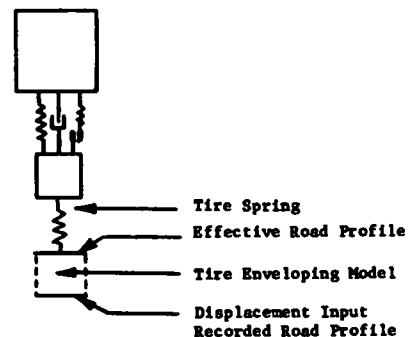


Figure R-2. Truck model with simulated tire enveloping properties.

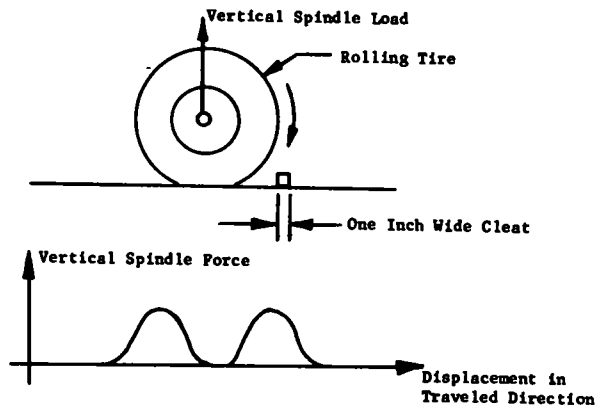


Figure R-3. Vertical spindle force produced by 1-in-wide cleat.

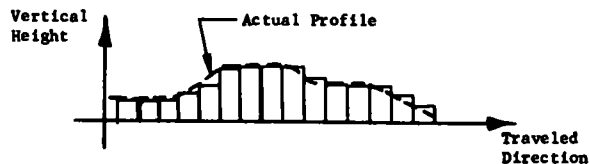


Figure R-4. Road profile approximated by series of 1-in. cleats.

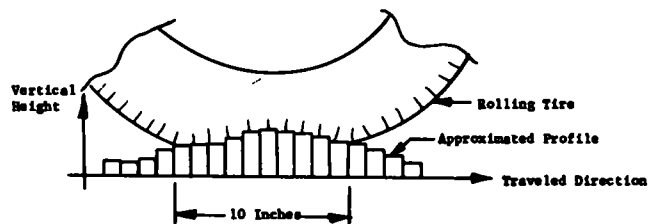


Figure R-5. Tire with 10-in. patch in contact with cleats.

synthesis is to be used. For a 10-in. contact patch at 30 mph, the ripple frequency is about 1 kHz—much higher than significant vehicle response frequencies.

**CONVOLUTED CLEAT SIMULATION OF TIRE ENVELOPING**

The analog simulation of tire enveloping effects consisted of a circuit that generated an effective road profile to produce loads in accordance with the foregoing cleat description. Because the waveform for a single 1-in. cleat was approximately sinusoidal, it was generated by a conventional three-amplifier oscillator (Fig. R-7). The outputs of 10 such oscillators were used to synthesize the enveloping effects of a 10-in. tire patch. The analog voltage proportional to road profile was applied to the initial condition inputs of the 10 oscillators. This input provided a sequential updating of each oscillator's amplitude.

One oscillator at a time was initialized to the current road profile amplitude by a rapid scanning multiplex scheme. The initializing commands were timed by a 10-station binary ring counter. To clarify the timing involved, Figure R-8 shows the outputs of three adjacent oscillators. Each frequency was set so that two cycles of oscillation were completed in the time required to move forward 10 in. The analog wiring diagram for the tire enveloping simulation is shown in Figure R-9.

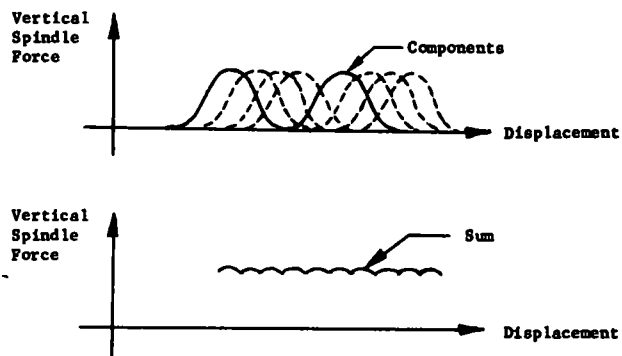


Figure R-6. Spindle load components and their sum.

**FIRST-ORDER LAG SIMULATION OF TIRE ENVELOPING**

Although the cleat approach produced satisfactory performance, it required many analog components arranged in a complex circuit. Operationally, the cleat circuit produced results similar to low-pass filtering of the road profile. Consequently, the search for a simpler, more efficient analog simulation of tire enveloping led to the least complex of all low-pass filters; that is, the first-order lag circuit, as shown in Figure R-10.

The effective road profile generated by two lag circuits performed as well as the cleat representation when used as an input to the analog truck model.

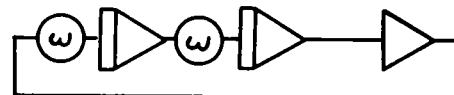


Figure R-7 Simple three amplifier analog oscillator.

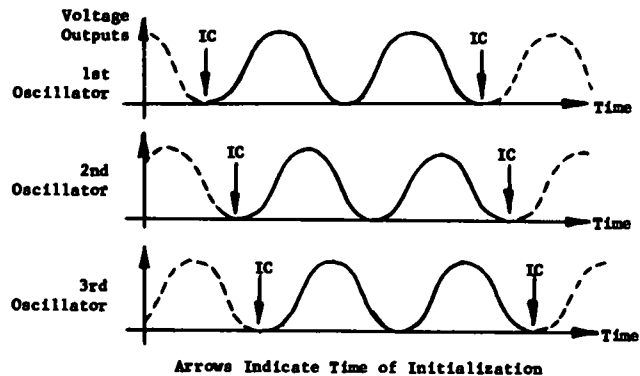


Figure R-8. Timing diagram showing sequential initialization of three adjacent oscillators.



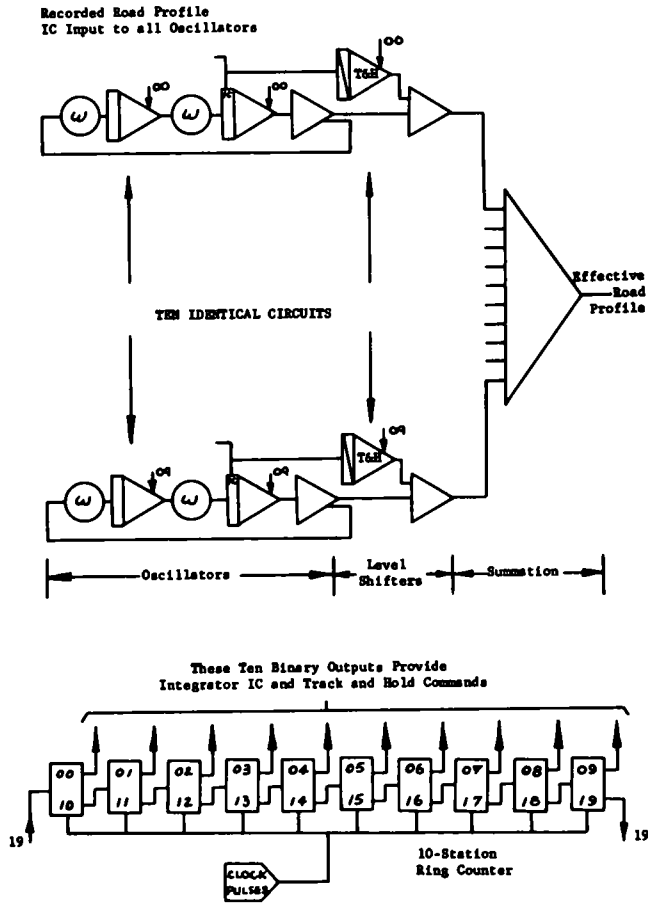


Figure R-9 Analog wiring diagram, convoluted cleat model

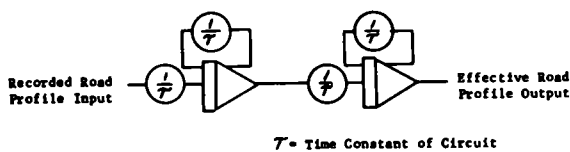


Figure R-10 Cascaded first-order lag circuits

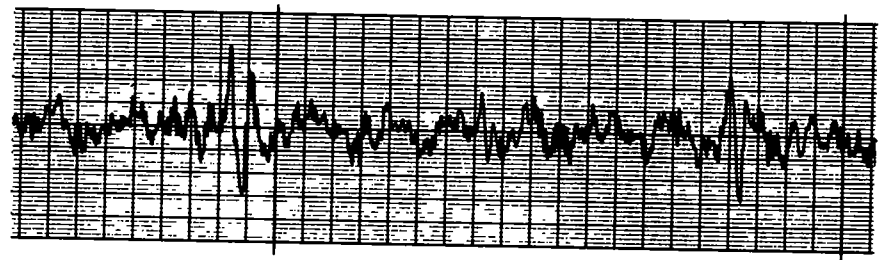
### ANALOG TIME FUNCTIONS SIMULATE DISTANCE FUNCTIONS

Both the convoluted model and lag circuits are time functions, whereas tire enveloping is a distance function. In the foregoing analog models, time and distance are equivalent at only one speed. For other speeds, the model parameters would require adjustment to maintain the equivalence. For example, in the convoluted model the frequency of clock pulses is proportional to vehicle speed, in the lag simulation the circuit time constant would be adjusted. If vehicle speed information is available for use as a control signal, the parameter adjustments could be done automatically. Thus, continuous tracking of vehicle speed could be achieved.

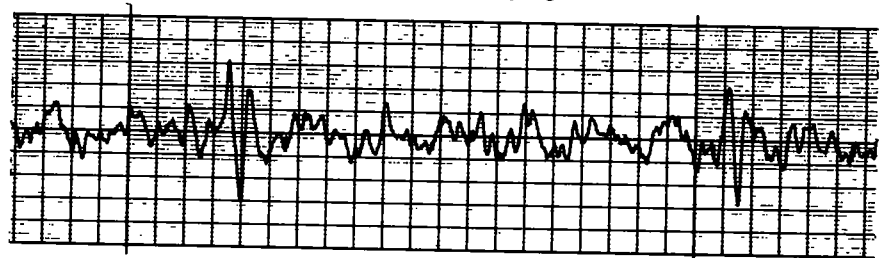
### CONCLUSION

Performance of the tire enveloping simulations was evaluated by comparing computed pavement loads with experimentally measured loads. Time history recordings of dynamic pavement loads are shown in Figure R-11. Referring to the figure, loads computed with no tire enveloping (a) are higher than experimental loads (d). Better correlation is seen in both the convoluted cleat model (b) and the simple lag model (c). Because both circuits performed about the same, the convoluted cleat model was abandoned in favor of the simpler lag representation for the load prediction work.

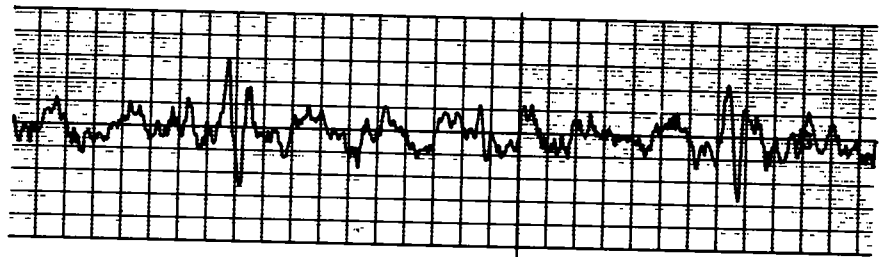
In future work, however, the convoluted model could be expanded in two ways. First, the model could be modified to account for change in size of contact patch resulting from vertical motion. Second, the circuit timing pulse rate could be made to track tire rotational speed



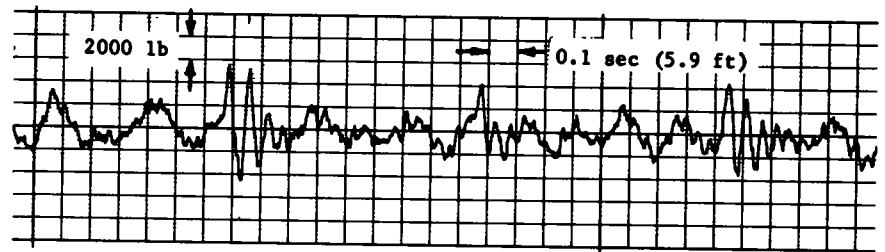
(a) Computed Dynamic Pavement Load  
No Tire Enveloping



(b) Computed Dynamic Pavement Load  
Complex Tire Enveloping Model



(c) Computed Dynamic Pavement Load  
Simple Tire Enveloping Model



(d) Experimental Dynamic Pavement Load  
Truck No. 1 at 40 mph on Moderately  
Rough Road (Oval Test Track)

Figure R-11 Performance of tire enveloping models

## APPENDIX S

### DEVELOPMENT OF A QUARTER-VEHICLE ANALOG SIMULATION

Development of the quarter-vehicle simulation required selection and measurement of significant vehicle properties to construct an analog computer vehicle model. This

appendix discusses the steps necessary to accomplish these objectives.

The basic quarter-vehicle model (Fig S-1) was devel-

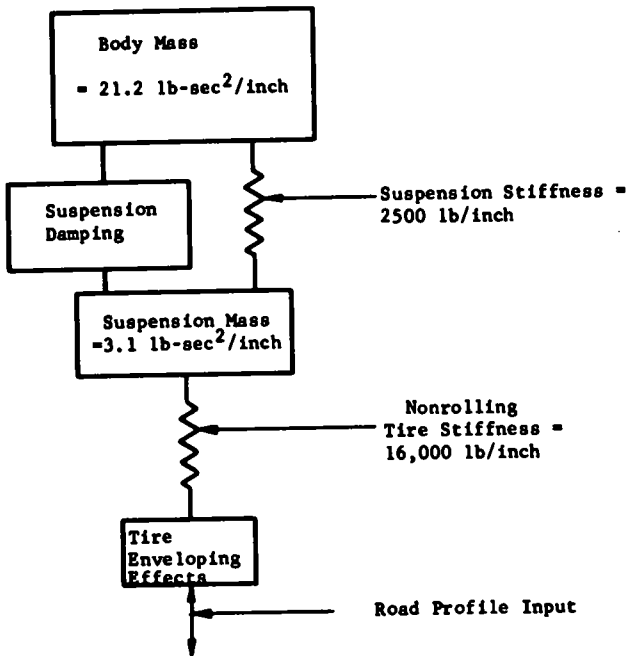


Figure S-1 Basic schematic of quarter-vehicle model

oped from static laboratory measurements and a physical examination of Test Vehicle No. 1. The vehicle body mass and the unsprung mass were determined from static weight measurements. Approximate suspension spring stiffness was

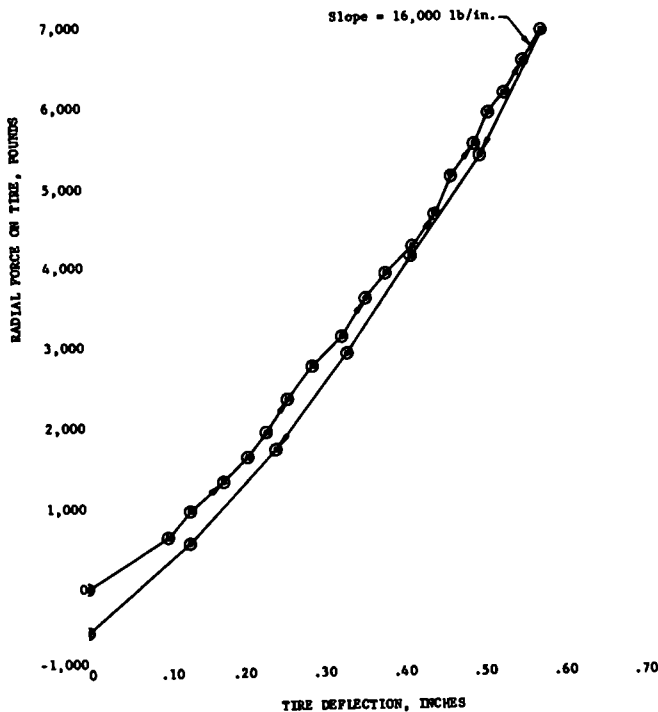


Figure S-3. Nonrolling load-deflection curve for a rear dual tire set on Test Vehicle No. 1.

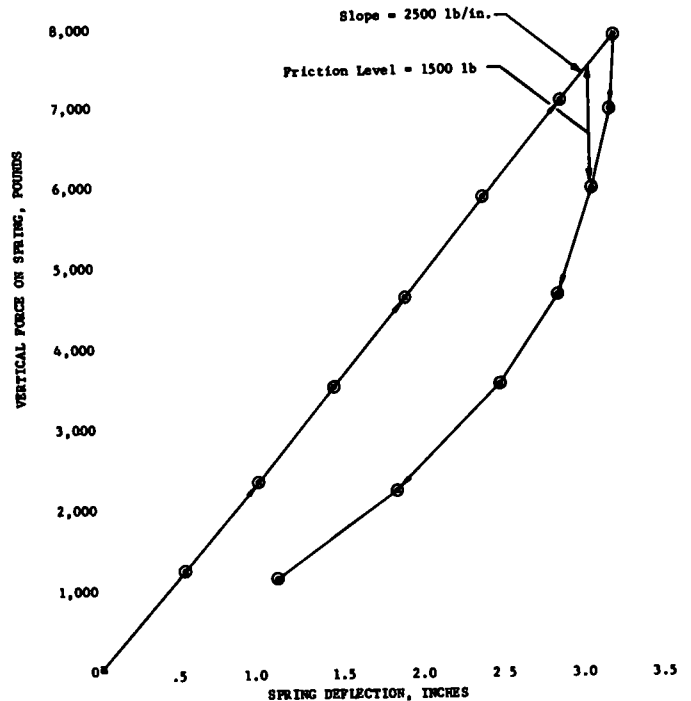


Figure S-2 Load-deflection curve for rear leaf spring on Test Vehicle No 1.

determined using the load-deflection curve in Figure S-2. It was recognized that differences exist between nonrolling and rolling tire spring rates. The more easily measured nonrolling rate (determined from Fig. S-3) was used in this model. As indicated in Appendix T, a model using the nonrolling rate showed good correlation with measured data. This indicated that the difference between rolling and nonrolling tire rates was not a controlling factor in the accuracy of the simulation.

Areas of this model that required further definition were the magnitude of tire enveloping (Appendix R) and the magnitude and character of the damping in the suspension leaf spring. Because the prediction technique involved solution of time-dependent differential equations, the need for *dynamic* testing to define these areas was evident.

The following methods of vehicle property definition were available:

1. The vehicle rear suspension could be physically disassembled, and separate laboratory tests could be conducted to define each parameter.

2. The vehicle could be driven over bumps of deterministic shape and experimental measurements of pavement load could be made. The same shapes could then be simulated as inputs to the basic model, and the correct parameter values could be determined by adjusting each value for the best match between experimental and computed pavement loads.

The second method was used in this project for two reasons. First, systems for measurement of dynamic pavement loads were readily available. Secondly, the study of

pavement loads caused by deterministic profile bumps contributed to the over-all understanding of dynamic pavement loads

### EXPERIMENTAL TESTS TO DEFINE VEHICLE PROPERTIES

Dynamic pavement loads were measured as Test Vehicle No. 1 was driven over several bumps of deterministic shape. A complete listing of the bump profiles and test conditions is included in Appendix N. Only the experimental results for the 34-mph tests were used in determining the magnitude of model parameters. Figure S-4 shows examples of loads developed for some of the fabricated bump inputs.

### DETERMINATION OF MODEL PARAMETERS

Determination of tire enveloping and suspension damping from a single set of test results was possible because of the independent effect of each parameter. Changes in tire enveloping significantly affected the *initial peak* in the computed dynamic response curves similar to those in Figure S-4. In contrast, the *decay* of the trace was significantly affected by suspension spring rate and damping. This degree of independence allowed the magnitude of tire enveloping to be defined almost independently of suspension damping.

#### Determination of Tire Enveloping Magnitude

Tire enveloping allows the tire to absorb sharp changes in road profile without equally sharp changes in pavement load. A discussion of tire enveloping and two methods of analog simulation are included in Appendix R. The first-order lag method was used in the quarter-vehicle model. By matching the initial peaks of the experimental and computed pavement load traces for the deterministic bumps run at 34 mph, a tire enveloping constant of 0.008 sec was determined. Strictly, this time constant is optimum only at 34 mph; however, reasonable results at other speeds were achieved (Appendix T).

### Determination of Suspension Spring and Damping Characteristics

In selecting a suitable simulation for the leaf spring between the suspension and body of the vehicle, a linear viscous element in parallel with a linear spring was used as a first approximation. It was found that a good match between experimental and computed responses for fabricated bump impacts could be achieved with viscous damping of approximately 100 lb-sec/in. and spring rate of 2,500 lb/in. However, when real road profile inputs were applied to the simulation, the low-frequency oscillation evident in measured load traces was nearly absent in the computed loads, as shown in Figure S-5. Load computations, based only on viscous damping, could not match measured loads in both amplitude and frequency because of the basic nonlinearity of the suspension damping.

Measured load data from all nine roads showed that the low-frequency oscillation occurred anywhere between approximately 1.6 and 4.1 cps. These frequencies define two different modes of oscillation. Intermediate frequencies are due to mixing of the two modes.

The 1.6-cps mode was the lowest natural frequency for the body (21.2 lb-sec<sup>2</sup>/in.) and suspension masses (3.1 lb-sec<sup>2</sup>/in.) in resonance on the suspension spring (2,500 lb/in.) and tire spring (16,000 lb/in.). The calculation of this frequency is included in many vibration texts (10).

The 4.1-cps mode occurred as both masses moved in phase and deflected only the tire spring. Locking up of the suspension spring (due to friction) made this mode possible. In this mode the vehicle responds as a single degree of freedom system. The natural frequency is calculated as follows:

$$f = \frac{1}{2\pi} \sqrt{\frac{K_T}{M_B + M_S}} = \frac{1}{2\pi} \sqrt{\frac{16,000}{21.2 + 3.1}} = 4.1 \text{ cps}$$

Several experiments with combinations of viscous and friction damping led to the suspension spring model shown in Figure S-6. Three friction elements, set at different

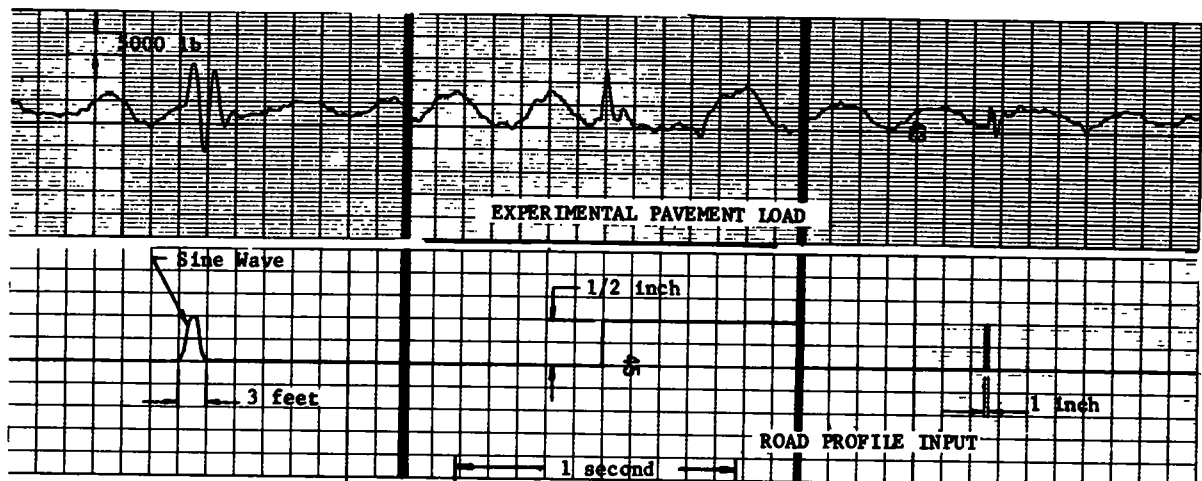


Figure S-4. Dynamic pavement loads generated by fabricated bumps Vehicle speed. 34 mph.

Viscous Damping: 200 lb-sec/in.  
 Road Section: M-59  
 Vehicle Speed: 34 mph

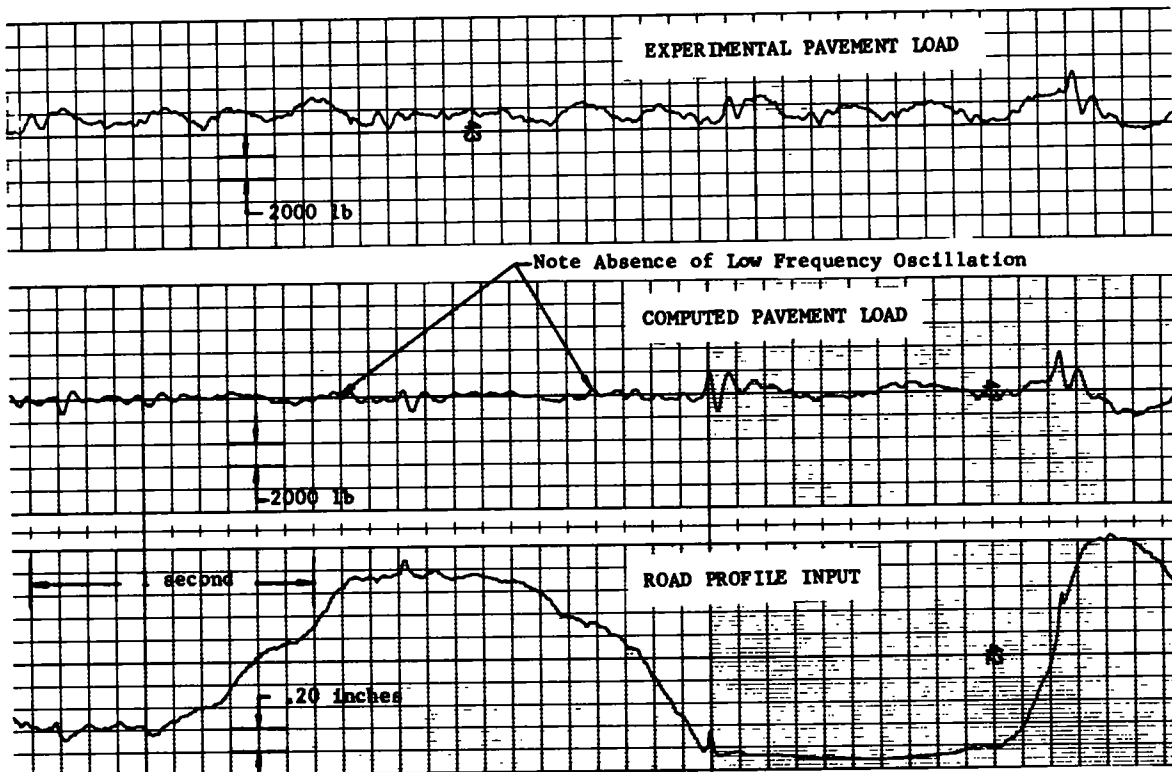
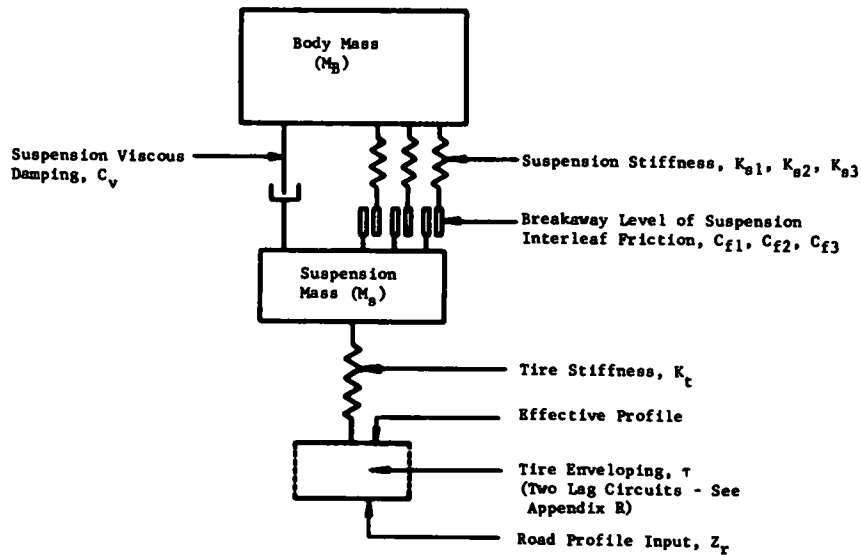


Figure S-5 Pavement loads computed using linear viscous damping in suspension leaf spring.

breakaway levels, allowed the low-frequency modes (1.6 and 4.1 cps) to be excited at correct levels for small profile inputs and the wheel hop mode (approximately 19 cps) to be excited at correct levels for sharp inputs. The 375-lb and 175-lb friction levels primarily controlled the amplitude of the low-frequency modes, whereas decay of all three modes was a function of all three levels, plus the level of viscous damping. In a physical sense, these individual friction levels represented the friction coupling between leaf elements of the suspension spring.

It was also determined that the stiffness of the spring elements in series with each friction element (7,500 lb/in.) could not be related directly to the suspension spring stiffness as measured statically (2,500 lb/in.). However, these spring elements may be defined in a more detailed simulation of the leaf spring (Fig. S-7). Stiffness of the model spring elements was determined by adjustment to get the best match with measured responses. The adjustment procedure consisted of varying the spring rate of the three elements simultaneously. An analog computer circuit diagram of the final model and a list of potentiometer settings are shown in Figures S-8 and S-9.

Figure S-10 shows the measured and computed pavement loads for several deterministic bumps traversed at 34 mph. As shown, the agreement for haversine and step inputs was good, with less agreement for impulse inputs.



LISTING OF PARAMETER VALUES

Parameter	Value Used in Simulation
$M_B$	21.2 lb-sec <sup>2</sup> /in. (Equivalent to 8.2 KIPS)
$C_V$	50 lb-sec/in.
$K_{s1}, K_{s2}, K_{s3}$	7500 lb/in.
$C_{f1}$	750 lb
$C_{f2}$	375 lb
$C_{f3}$	175 lb
$M_s$	3.1 lb-sec <sup>2</sup> /in. (Equivalent to 1.2 KIPS)
$K_t$	16,000 lb/in.
$\tau$	.008 sec

Figure S-6 Schematic of quarter-vehicle model used in simulation

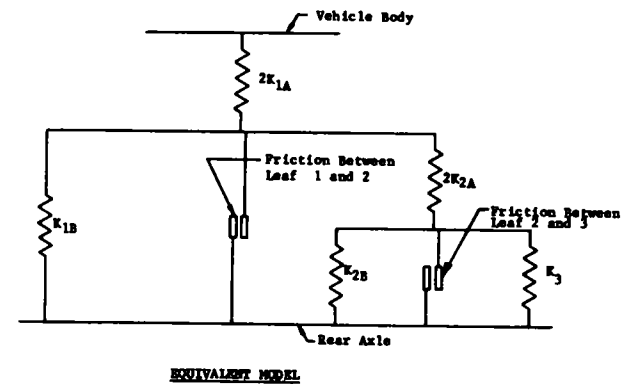
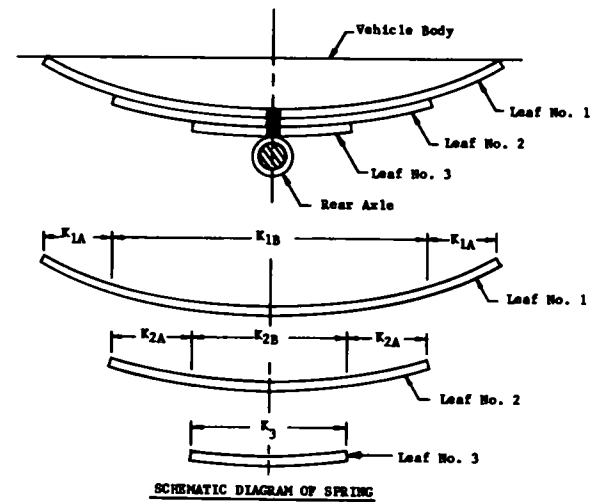


Figure S-7 Detailed model of suspension leaf spring

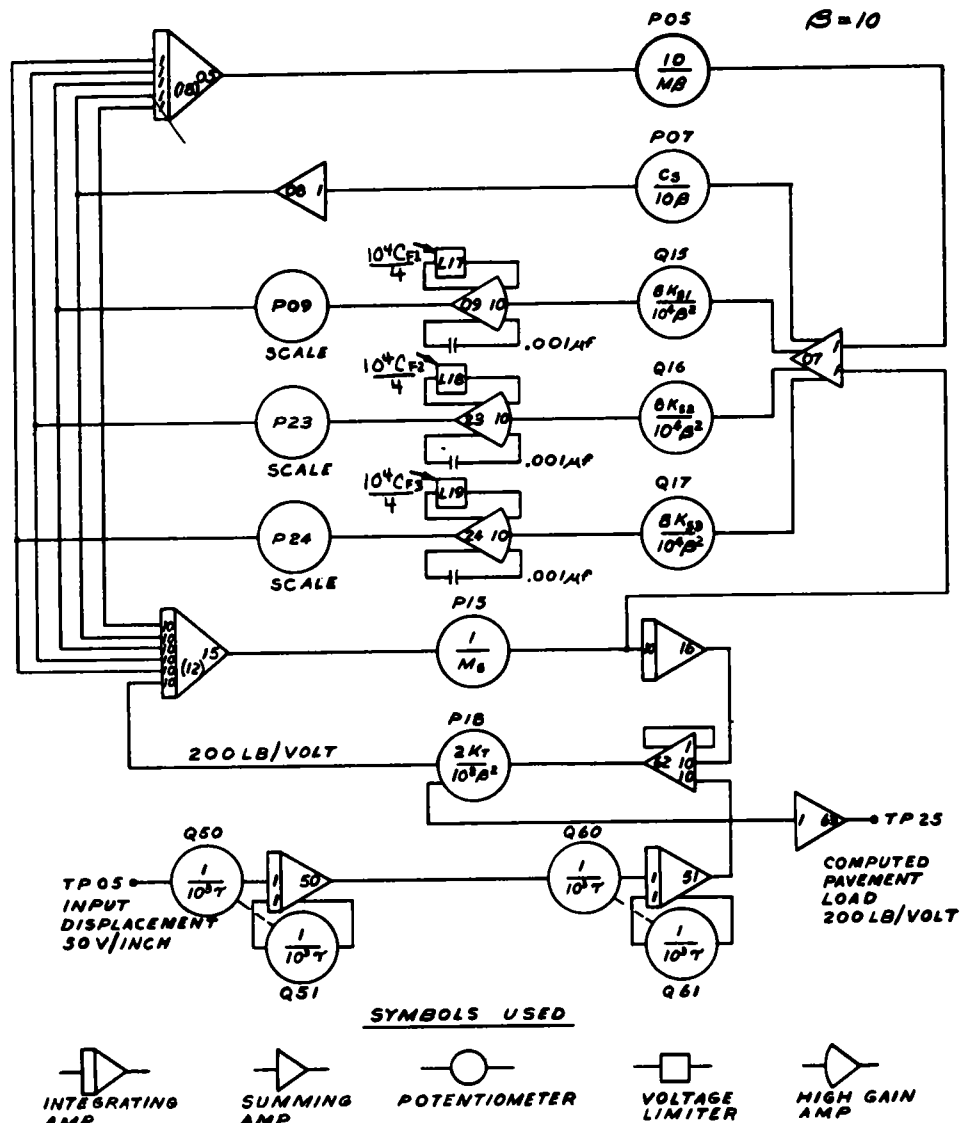


Figure S-8. Analog computer circuit for quarter-vehicle model.

NO.	SUMMING POINT	PARAMETER	SETTING	POTENTIOMETER	PARAMETER	SETTING
P1						
P2						
P3						
P4						
P5						
P6						
P7						
P8	.6720	$10/M\beta$				
P9						
P10	.2500	$C_3/10\beta$				
P11	.1250	Friction Scale				
P12						
P13						
P14						
P15						
P16						
P17						
P18						
P19						
P20	.3220	$1/M\beta$	.0600	$\frac{8K_{11}}{10^4\beta^2}$		
P21			.0600	$\frac{8K_{22}}{10^4\beta^2}$		
P22			.0600	$\frac{8K_{33}}{10^4\beta^2}$		
P23	.3200	$2K_T/10^3\beta^2$				
P24						
P25						
P26						
P27						
P28	.1250	Friction Scale				
P29	.1250	Friction Scale				
P30						
P31						
P32						
P33						
P34						
P35						
P36						
P37						
P38						
P39						
P40						
P41						
P42						
P43						
P44						
P45						
P46						
P47						
P48						
P49						
P50						
P51						
P52						
P53						
P54						
P55						
P56						
P57						
P58						
P59						
P60						
P61						
P62						
P63						
P64						
P65						
P66						
P67						
P68						
P69						
P70						
P71						
P72						
P73						
P74						
P75						
P76						
P77						
P78						
P79						
P80						
P81						
P82						
P83						
P84						
P85						
P86						
P87						
P88						
P89						
P90						
P91						
P92						
P93						
P94						
P95						
P96						
P97						
P98						
P99						
P100						

Figure S-9. Potentiometer settings for quarter-vehicle model simulation.

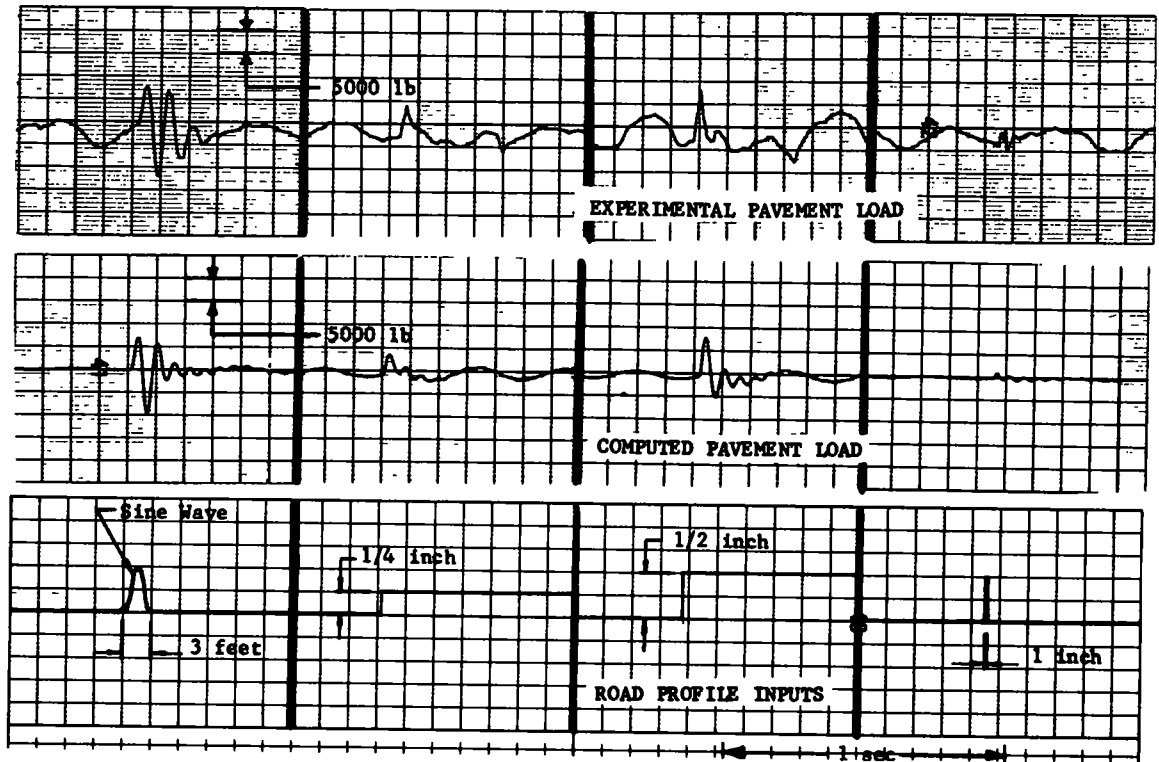


Figure S-10. Computed and experimental dynamic loads for deterministic inputs. Vehicle speed 34 mph

## APPENDIX T

### CORRELATION DATA FOR MEASURED AND COMPUTED PAVEMENT LOADS

Pavement load data for the nine test road sections were measured and computed. These data allowed evaluation of prediction technique accuracy. The following methods of comparison were used:

1. Load versus time strip charts.
2. Number of occurrences of peak loads.
3. Probability density analyses.
4. Power spectral density analyses.

Table T-1 gives the particular road section on which data were collected. Vehicle operating conditions were:

1. Vehicle speed = 34 mph (constant).
2. Static weight on right rear wheel set = 9.4 kips.
3. Tire pressure = 75 psi-cold.

Figures T-1 through T-3 show data representative of that collected for the various road sections and conditions. Similar data for all other tests are available on request to the Program Director, NCHRP.

Tables T-2, T-3, and T-4 are summaries of differences between computed and measured loads for several methods

of comparison. The observations in the section of Chapter Two entitled "Dynamic Pavement Load Prediction Using Analog Computation Techniques" were drawn from these summaries. In all cases, percentage of nonagreement was calculated as follows:

$$\text{Percentage of Nonagreement} = \frac{\text{Measured Value} - \text{Computed Value}}{\text{Measured Value}} \times 100$$

In addition to the foregoing test conditions, comparative data were collected for the following additional conditions on M-59 and I-75 road sections (Table T-1):

1. An unloaded vehicle was simulated by reducing the quarter-vehicle body mass from 8.2 kips to 2.0 kips. This was equivalent to reducing the weight on the right rear wheel from 9.4 kips to 3.2 kips. All other parameters were held constant.
2. Vehicle speed was increased to 65 mph. All other parameters were held constant.



Vehicle No. 1, 2-D  
 Instrumented Wheel: Right Side of Drive Axle  
 Static Weight on Wheel: 9.4 KIPS  
 Road: I-75, Good-Rigid  
 Speed: 34 mph

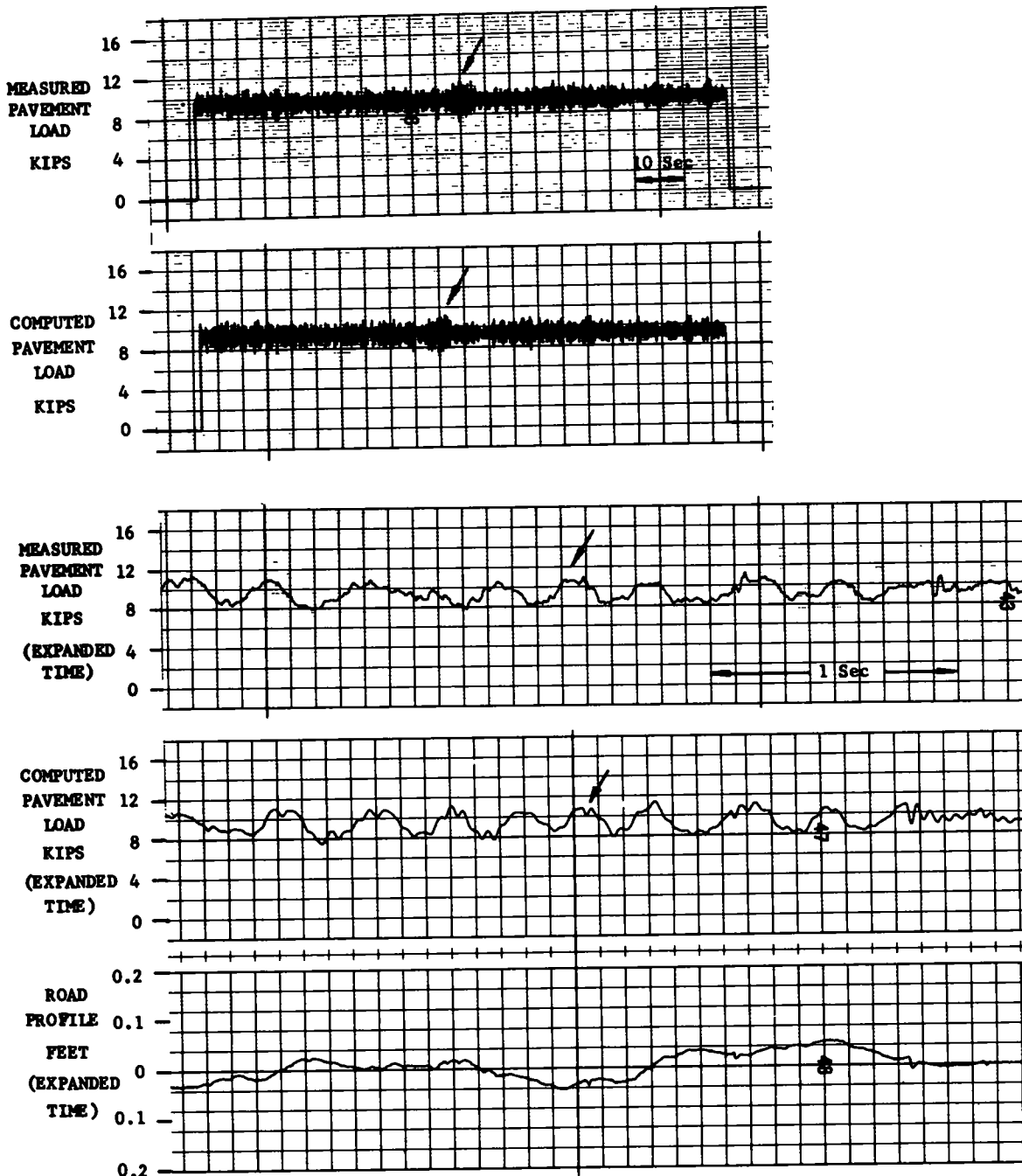


Figure T-1 Load versus time comparisons.

It should be noted that differences up to about 10% existed between the "apparent" static weight measured on the moving vehicle and the static weight on the instrumented wheel. The reasons for these differences are discussed in the section of Chapter Two entitled "Pavement Load Measurements."

When computed and measured load data were compared, it was desired to have measured data reflect the static

measured weight on the instrumented wheel. Consequently, measured load data signals were passed through a signal-conditioning circuit to eliminate all static (or dc) load components. Then, a dc voltage proportional to 9.4 kips static load was added to the resulting signal. This process allowed meaningful comparisons to be made between computed and measured load data. All measured load data in this appendix were processed in the foregoing manner

Vehicle No. 1, 2-D  
 Instrumented Wheel Right Side of Drive Axle  
 Static Weight on Wheel 9.4 KIPS  
 Road I-75, Good-Rigid  
 Speed 34 mph

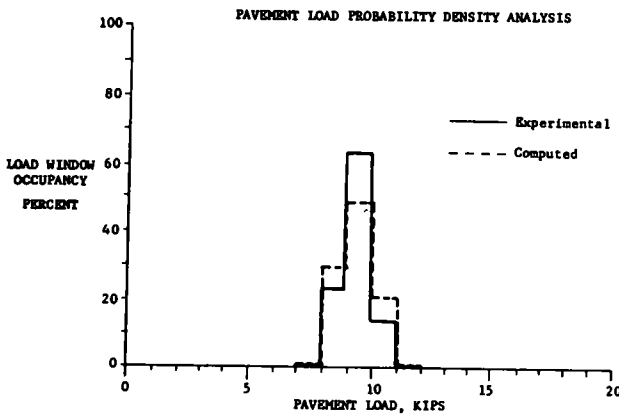
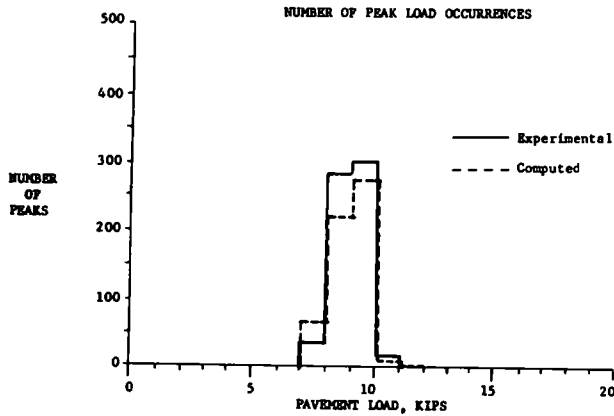


Figure T-2 Statistical comparisons

TABLE T-1

ROAD SECTIONS ON WHICH DATA WERE COLLECTED

ROAD SECTION
(a) Original Conditions
I-75, good-rigid
I-696, fair-rigid
M-50, poor-rigid
M-52, good-flexible
M-247, fair-flexible
M-138, poor-flexible
M-53 NB, good-overlay
M-53 SB, fair-overlay
M-59, poor-overlay
(b) Additional Condition No. 1; static wheel weight reduced to 3.2 kips
I-75, good-rigid
M-59, poor-overlay
(c) Additional Condition No. 2: vehicle speed increased to 65 mph
I-75, good-rigid
M-59, poor-overlay

NB = northbound, SB = southbound

Vehicle No. 1, 2-D  
 Instrumented Wheel Right Side of Drive Axle  
 Static Weight on Wheel 9.4 KIPS  
 Road I-75, Good-Rigid  
 Speed 34 mph

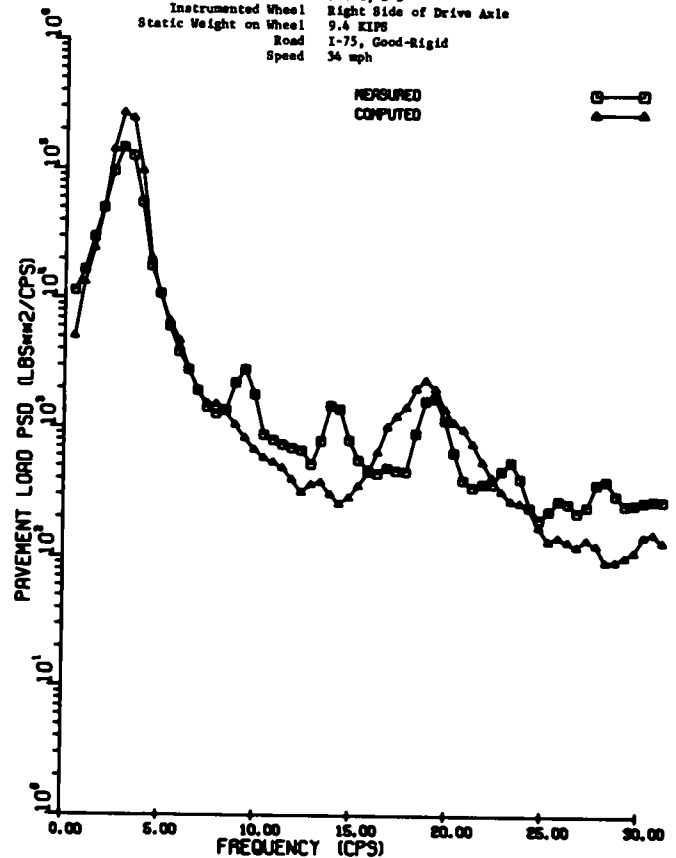


Figure T-3. Pavement load power spectral density

TABLE T-2

PEAK PAVEMENT LOADS ON NINE TEST ROAD SECTIONS \*

ROAD SECTION	PEAK LOAD (KIPS)		%
	MEASURED	PREDICTED	
I-75	11.2	11.2	0
I-696	12.6	11.3	-10
M-50	11.4	12.0	+5
M-52	11.2	10.8	-4
M-247	12.9	13.1	+2
M-138	13.5	12.4	-8
M-53 NB	11.7	13.1	+12
M-53 SB	12.7	12.2	-4
M-59	13.6	13.2	-3
Average	12.3	12.1	-2

\* Peak pavement load values, taken from load versus time strip charts, are maximums or near-maximums for each road

TABLE T-3

MAXIMUM DIFFERENCES BETWEEN MEASURED AND COMPUTED LOADS ABOVE 10 KIPS, BASED ON PROBABILITY DENSITY ANALYSES

ROAD SECTION	MAXIMUM DIFF. (KIPS) <sup>a</sup>
I-75	1
I-696	1
M-50	1
M-52	1
M-247	1
M-138	2
M-53 NB	1
M-53 SB	1
M-59	1

<sup>a</sup> Maximum differences of less than 1 kip appear as 1 kip owing to the resolution of load levels for these analyses

TABLE T-4

PERCENTAGE OF ERROR IN PREDICTING 3-CPS AND 19-CPS PEAKS IN POWER SPECTRAL DENSITY CURVES

ROAD SECTION	% NONAGREEMENT <sup>a</sup>	
	3 CPS	19 CPS
I-75	5	17
I-696	4	4
M-50	3	14
M-52	16	9
M-247	2	14
M-138	2	10
M-53 NB	4	4
M-53 SB	3	9
M-59	5	12
Average	5	10

<sup>a</sup> Percentage of nonagreement in predicting logarithm of power spectral density function.

## APPENDIX U

### FACTORS THAT LIMITED PREDICTION TECHNIQUE ACCURACY

Correlation between measured and computed pavement loads is shown in Appendix T. Although this degree of correlation is adequate for many purposes, a future use might require better agreement. This appendix discusses the disparities and suggests how correlation might be improved.

#### POTENTIAL MODIFICATIONS TO COMPUTER SIMULATION

Better correlation probably would result if the computer simulation was modified to include the following items.

##### Effect of Rear Axle Tramp

The use of a quarter-vehicle simulation requires the assumption that right and left rear wheel pavement loads are independent. Experimental tests with Test Vehicle No. 1 showed that the right side dynamic load when only the right wheel passed over a bump was only 70% to 85% of the right side dynamic load when both rear wheels passed over the same bump. This corresponded to a difference in *peak* pavement load of less than 12%. These tests are discussed in the section of Chapter Two entitled "Identification of Factors Affecting Dynamic Pavement Loads." A half-vehicle model that included tramp effects probably would exhibit better correlation to measured loads.

##### Suspension Spring and Damping Properties

As shown by the experimental load trace in Figure U-1, high peaks in dynamic load were followed by ringing and decay. The decay time of this oscillation was controlled on the analog model by the magnitude of suspension friction level and suspension stiffness. Thus, the approximate modeling of these parameters adversely affected the level of correlation. A more detailed modeling of the suspension spring probably would improve correlation (Fig. S-7).

##### Tire Spring Rate and Enveloping Quality

Tire spring rate and enveloping quality were assumed to be linear quantities. Although the linearity assumption produced good correlation, inclusion of a nonlinear tire spring element, as well as use of a more sophisticated simulation of tire enveloping, probably would improve correlation. A detailed discussion of tire enveloping and analog simulation methods appears in Appendix R.

#### REPEATABILITY OF EXPERIMENTAL LOAD MEASUREMENTS

As discussed in Appendix O, dynamic load measurements made during six identical passes over fabricated bumps showed *dynamic load* variations of approximately  $\pm 10\%$ . This degree of nonrepeatability probably resulted from the effects of vehicle pitch and roll, rim assembly runout, and tire nonuniformity.

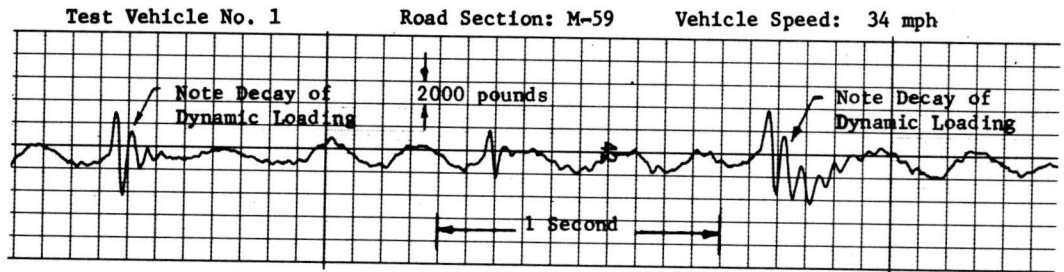


Figure U-1. Experimental load trace showing decay of dynamic loading.

These factors also influenced the measurement of pavement loads on the nine test road sections. Correlation between computed and measured *dynamic* loads better than about  $\pm 10\%$  could not be expected when the nonrepeatability of experimental measurements is considered.

#### ACCURACY OF ROAD PROFILES

The ability to accurately measure road profiles as simulation input data was fundamental to the accuracy of the prediction technique. The road profiles measured by the profilometer differed slightly from the profile experienced by Test Vehicle No. 1 for two reasons.

##### Effect of Profile Width

The total tread width of a rear dual tire set is much greater than the 2-in. width of the profilometer following wheel (Fig. U-2). Therefore, the measured pavement loads were excited by an average profile over the width of a dual tire set, whereas the computed pavement loads were excited by only a 2-in. wide profile.

##### Effect of Difference in Vehicle and Profilometer Wheel Paths

The difference in the wheel paths of the profilometer and test vehicle as they traveled the test road sections constitutes

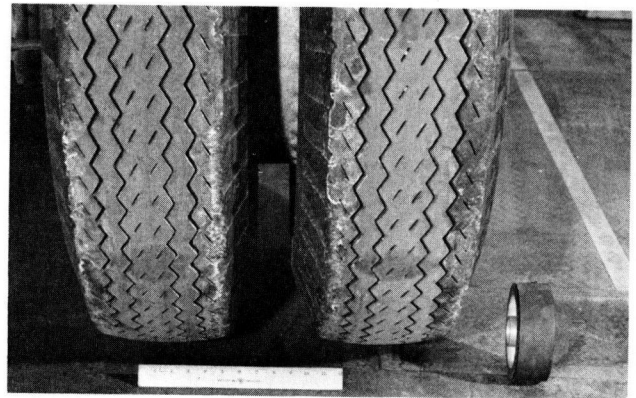


Figure U-2. Comparison of test vehicle and profile wheel widths.

another approximation. Neither vehicle could maintain a fixed distance from the edge of the road but "wandered" from side to side in its traffic lane. Thus, the wheel paths coincided only a fraction of the time.

Both these effects could be corrected if the test vehicle itself was instrumented as a profiling device.

## APPENDIX V

### VARIATION OF PARAMETERS STUDY

A parameter sensitivity study was conducted using the analog model that correlated well with experimental data for Test Vehicle No. 1. The schematic of this model and its parameters appear in Figure S-6. For this study, the parameters of the foregoing model were designated reference parameters.

Input to the model was a step displacement in road profile. This input was chosen because it simplified the

study by eliminating bump wavelength as a parameter. The parameter sensitivity study consisted of an orderly change of one parameter at a time. The parameter varied was first reduced by a factor of two and then increased by the same factor. Time history recordings of instantaneous dynamic pavement load produced by a  $\frac{1}{2}$ -in. displacement input were computed for each parameter condition. The time history charts appear in Figure V-1.

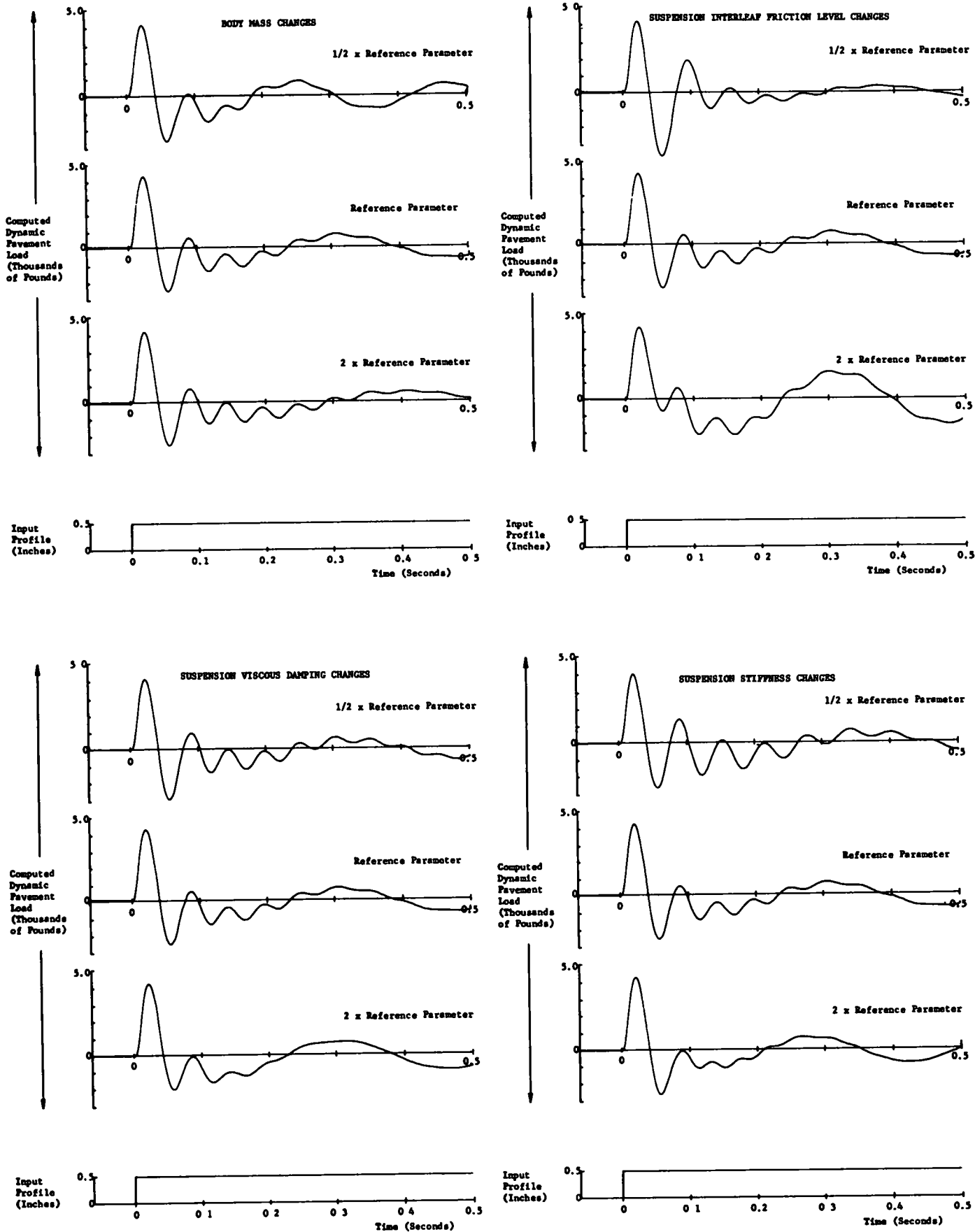
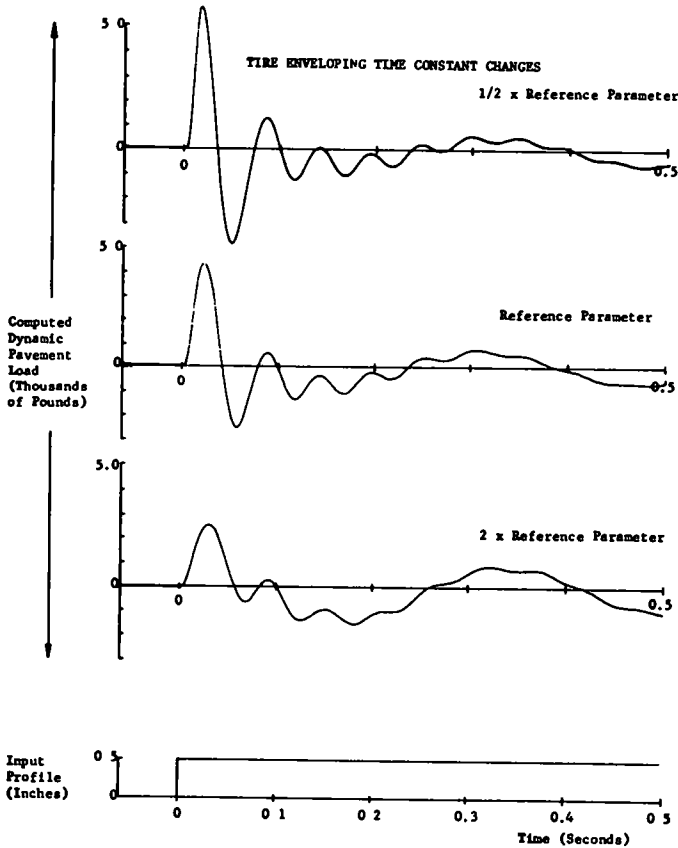
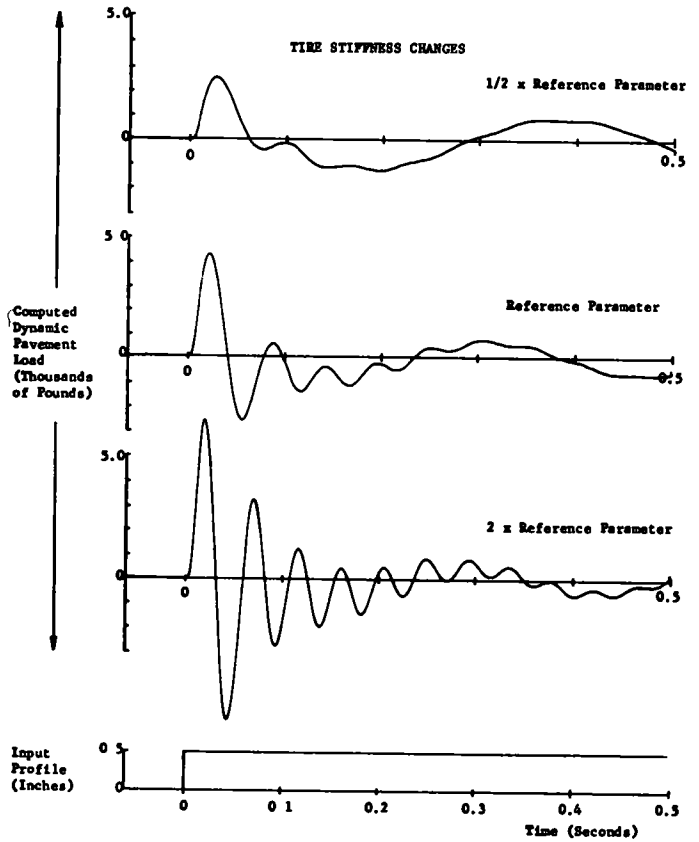
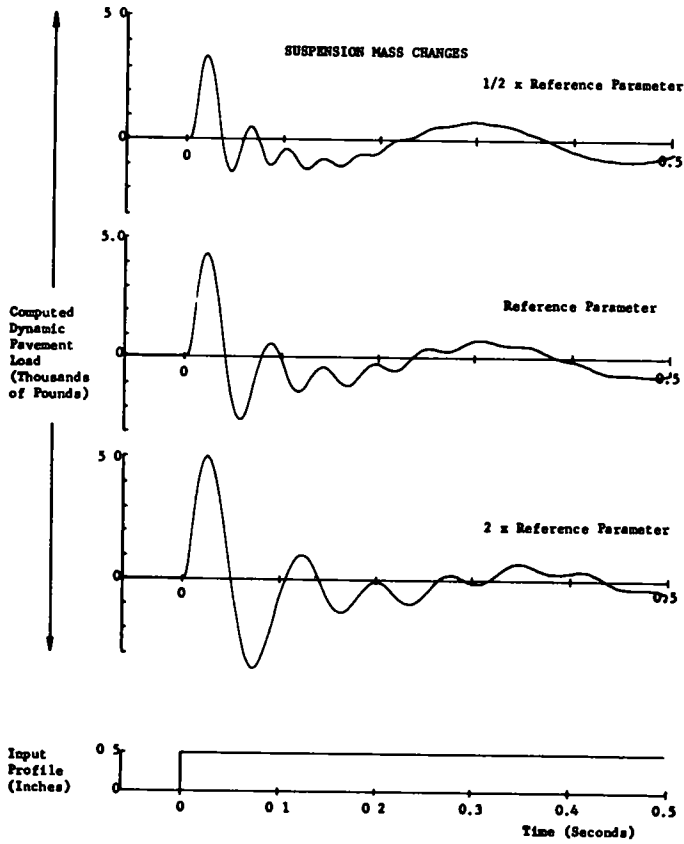


Figure V-1. Computed effects of parameter variations



**TABLE V-1**  
SUMMARY OF PARAMETER VARIATION COMPUTATIONS

MODEL PARAMETER VARIED	CHANGE IN MAXIMUM DYNAMIC PAVEMENT LOAD (%) <sup>a</sup>	
	2 X REF. PARAMETER	1/2 X REF. PARAMETER
Body mass	0	0
Breakaway level of suspension interleaf friction	0	0
Suspension viscous damping	0	0
Suspension stiffness	+3	-2
Suspension mass	+19	-19
Tire stiffness	+55	-40
Tire enveloping	-40	+39

<sup>a</sup> Data taken from Fig V-2

Referring to the charts, the origin of computed dynamic pavement load is the static vehicle weight. The origin of time is the initiation of the ½-in. step.

Throughout all of the figures, two basic frequencies exist in the reference response: one near 19 cps, the other about 3 cps. The higher frequency results from suspension motions; the lower is caused by body motions.

Although many such character changes occurred in the responses, interest was limited to noting how peak loads were affected. The percentage change in dynamic pave-

ment load for each parameter condition is summarized in Table V-1. The percentages were calculated based on the computed model response with the reference parameter.

One interesting observation was made relative to an upper limit on dynamic pavement load. For suspensions with normal amounts of damping (10% of critical or more), an apparent limit for maximum dynamic pavement load is the product of road bump height and tire spring rate. This limit was not exceeded either by experimentally measured or computed pavement load data.

Published reports of the

**NATIONAL COOPERATIVE HIGHWAY RESEARCH PROGRAM**

are available from.

Highway Research Board  
National Academy of Sciences  
2101 Constitution Avenue  
Washington, D.C. 20418

Rep.

No. Title

- \* A Critical Review of Literature Treating Methods of Identifying Aggregates Subject to Destructive Volume Change When Frozen in Concrete and a Proposed Program of Research—Intermediate Report (Proj. 4-3(2)), 81 p., \$1.80
- 1 Evaluation of Methods of Replacement of Deteriorated Concrete in Structures (Proj. 6-8), 56 p., \$2.80
  - 2 An Introduction to Guidelines for Satellite Studies of Pavement Performance (Proj. 1-1), 19 p., \$1.80
  - 2A Guidelines for Satellite Studies of Pavement Performance, 85 p.+9 figs., 26 tables, 4 app., \$3.00
  - 3 Improved Criteria for Traffic Signals at Individual Intersections—Interim Report (Proj. 3-5), 36 p., \$1.60
  - 4 Non-Chemical Methods of Snow and Ice Control on Highway Structures (Proj. 6-2), 74 p., \$3.20
  - 5 Effects of Different Methods of Stockpiling Aggregates—Interim Report (Proj. 10-3), 48 p., \$2.00
  - 6 Means of Locating and Communicating with Disabled Vehicles—Interim Report (Proj. 3-4), 56 p., \$3.20
  - 7 Comparison of Different Methods of Measuring Pavement Condition—Interim Report (Proj. 1-2), 29 p., \$1.80
  - 8 Synthetic Aggregates for Highway Construction (Proj. 4-4), 13 p., \$1.00
  - 9 Traffic Surveillance and Means of Communicating with Drivers—Interim Report (Proj. 3-2), 28 p., \$1.60
  - 10 Theoretical Analysis of Structural Behavior of Road Test Flexible Pavements (Proj. 1-4), 31 p., \$2.80
  - 11 Effect of Control Devices on Traffic Operations—Interim Report (Proj. 3-6), 107 p., \$5.80
  - 12 Identification of Aggregates Causing Poor Concrete Performance When Frozen—Interim Report (Proj. 4-3(1)), 47 p., \$3.00
  - 13 Running Cost of Motor Vehicles as Affected by Highway Design—Interim Report (Proj. 2-5), 43 p., \$2.80
  - 14 Density and Moisture Content Measurements by Nuclear Methods—Interim Report (Proj. 10-5), 32 p., \$3.00
  - 15 Identification of Concrete Aggregates Exhibiting Frost Susceptibility—Interim Report (Proj. 4-3(2)), 66 p., \$4.00
  - 16 Protective Coatings to Prevent Deterioration of Concrete by Deicing Chemicals (Proj. 6-3), 21 p., \$1.60
  - 17 Development of Guidelines for Practical and Realistic Construction Specifications (Proj. 10-1), 109 p., \$6.00
  - 18 Community Consequences of Highway Improvement (Proj. 2-2), 37 p., \$2.80
  - 19 Economical and Effective Deicing Agents for Use on Highway Structures (Proj. 6-1), 19 p., \$1.20
  - 20 Economic Study of Roadway Lighting (Proj. 5-4), 77 p., \$3.20
  - 21 Detecting Variations in Load-Carrying Capacity of Flexible Pavements (Proj. 1-5), 30 p., \$1.40
  - 22 Factors Influencing Flexible Pavement Performance (Proj. 1-3(2)), 69 p., \$2.60
  - 23 Methods for Reducing Corrosion of Reinforcing Steel (Proj. 6-4), 22 p., \$1.40
  - 24 Urban Travel Patterns for Airports, Shopping Centers, and Industrial Plants (Proj. 7-1), 116 p., \$5.20
  - 25 Potential Uses of Sonic and Ultrasonic Devices in Highway Construction (Proj. 10-7), 48 p., \$2.00
  - 26 Development of Uniform Procedures for Establishing Construction Equipment Rental Rates (Proj. 13-1), 33 p., \$1.60
  - 27 Physical Factors Influencing Resistance of Concrete to Deicing Agents (Proj. 6-5), 41 p., \$2.00
  - 28 Surveillance Methods and Ways and Means of Communicating with Drivers (Proj. 3-2), 66 p., \$2.60
  - 29 Digital-Computer-Controlled Traffic Signal System for a Small City (Proj. 3-2), 82 p., \$4.00
  - 30 Extension of AASHO Road Test Performance Concepts (Proj. 1-4(2)), 33 p., \$1.60
  - 31 A Review of Transportation Aspects of Land-Use Control (Proj. 8-5), 41 p., \$2.00
  - 32 Improved Criteria for Traffic Signals at Individual Intersections (Proj. 3-5), 134 p., \$5.00
  - 33 Values of Time Savings of Commercial Vehicles (Proj. 2-4), 74 p., \$3.60
  - 34 Evaluation of Construction Control Procedures—Interim Report (Proj. 10-2), 117 p., \$5.00
  - 35 Prediction of Flexible Pavement Deflections from Laboratory Repeated-Load Tests (Proj. 1-3(3)), 117 p., \$5.00
  - 36 Highway Guardrails—A Review of Current Practice (Proj. 15-1), 33 p., \$1.60
  - 37 Tentative Skid-Resistance Requirements for Main Rural Highways (Proj. 1-7), 80 p., \$3.60
  - 38 Evaluation of Pavement Joint and Crack Sealing Materials and Practices (Proj. 9-3), 40 p., \$2.00
  - 39 Factors Involved in the Design of Asphaltic Pavement Surfaces (Proj. 1-8), 112 p., \$5.00
  - 40 Means of Locating Disabled or Stopped Vehicles (Proj. 3-4(1)), 40 p., \$2.00
  - 41 Effect of Control Devices on Traffic Operations (Proj. 3-6), 83 p., \$3.60
  - 42 Interstate Highway Maintenance Requirements and Unit Maintenance Expenditure Index (Proj. 14-1), 144 p., \$5.60
  - 43 Density and Moisture Content Measurements by Nuclear Methods (Proj. 10-5), 38 p., \$2.00
  - 44 Traffic Attraction of Rural Outdoor Recreational Areas (Proj. 7-2), 28 p., \$1.40
  - 45 Development of Improved Pavement Marking Materials—Laboratory Phase (Proj. 5-5), 24 p., \$1.40
  - 46 Effects of Different Methods of Stockpiling and Handling Aggregates (Proj. 10-3), 102 p., \$4.60
  - 47 Accident Rates as Related to Design Elements of Rural Highways (Proj. 2-3), 173 p., \$6.40
  - 48 Factors and Trends in Trip Lengths (Proj. 7-4), 70 p., \$3.20
  - 49 National Survey of Transportation Attitudes and Behavior—Phase I Summary Report (Proj. 20-4), 71 p., \$3.20



- | <i>Rep. No.</i> | <i>Title</i>  | <i>Rep. No.</i> | <i>Title</i>   |
|-----------------|---|-----------------|--|
| 50              | Factors Influencing Safety at Highway-Rail Grade Crossings (Proj. 3-8), 113 p., \$5.20                                  | 76              | Detecting Seasonal Changes in Load-Carrying Capabilities of Flexible Pavements (Proj. 1-5(2)), 37 p., \$2.00               |
| 51              | Sensing and Communication Between Vehicles (Proj. 3-3), 105 p., \$5.00  | 77              | Development of Design Criteria for Safer Luminaire Supports (Proj. 15-6), 82 p., \$3.80                                    |
| 52              | Measurement of Pavement Thickness by Rapid and Nondestructive Methods (Proj. 10-6), 82 p., \$3.80                       | 78              | Highway Noise—Measurement, Simulation, and Mixed Reactions (Proj. 3-7), 78 p., \$3.20                                      |
| 53              | Multiple Use of Lands Within Highway Rights-of-Way (Proj. 7-6), 68 p., \$3.20   | 79              | Development of Improved Methods for Reduction of Traffic Accidents (Proj. 17-1), 163 p., \$6.40                            |
| 54              | Location, Selection, and Maintenance of Highway Guardrails and Median Barriers (Proj. 15-1(2)), 63 p., \$2.60           | 80              | Oversize-Overweight Permit Operation on State Highways (Proj. 2-10), 120 p., \$5.20  |
| 55              | Research Needs in Highway Transportation (Proj. 20-2), 66 p., \$2.80  | 81              | Moving Behavior and Residential Choice—A National Survey (Proj. 8-6), 129 p., \$5.60                                       |
| 56              | Scenic Easements—Legal, Administrative, and Valuation Problems and Procedures (Proj. 11-3), 174 p., \$6.40              | 82              | National Survey of Transportation Attitudes and Behavior—Phase II Analysis Report (Proj. 20-4), 89 p., \$4.00              |
| 57              | Factors Influencing Modal Trip Assignment (Proj. 8-2), 78 p., \$3.20  | 83              | Distribution of Wheel Loads on Highway Bridges (Proj. 12-2), 56 p., \$2.80   |
| 58              | Comparative Analysis of Traffic Assignment Techniques with Actual Highway Use (Proj. 7-5), 85 p., \$3.60                | 84              | Analysis and Projection of Research on Traffic Surveillance, Communication, and Control (Proj. 3-9), 48 p., \$2.40         |
| 59              | Standard Measurements for Satellite Road Test Program (Proj. 1-6), 78 p., \$3.20  | 85              | Development of Formed-in-Place Wet Reflective Markers (Proj. 5-5), 28 p., \$1.80   |
| 60              | Effects of Illumination on Operating Characteristics of Freeways (Proj. 5-2) 148 p., \$6.00                             | 86              | Tentative Service Requirements for Bridge Rail Systems (Proj. 12-8), 62 p., \$3.20   |
| 61              | Evaluation of Studded Tires—Performance Data and Pavement Wear Measurement (Proj. 1-9), 66 p., \$3.00                   | 87              | Rules of Discovery and Disclosure in Highway Condemnation Proceedings (Proj. 11-1(5)), 28 p., \$2.00                       |
| 62              | Urban Travel Patterns for Hospitals, Universities, Office Buildings, and Capitols (Proj. 7-1), 144 p., \$5.60           | 88              | Recognition of Benefits to Remainder Property in Highway Valuation Cases (Proj. 11-1(2)), 24 p., \$2.00                    |
| 63              | Economics of Design Standards for Low-Volume Rural Roads (Proj. 2-6), 93 p., \$4.00                                     | 89              | Factors, Trends, and Guidelines Related to Trip Length (Proj. 7-4), 59 p., \$3.20  |
| 64              | Motorists' Needs and Services on Interstate Highways (Proj. 7-7), 88 p., \$3.60   | 90              | Protection of Steel in Prestressed Concrete Bridges (Proj. 12-5), 86 p., \$4.00  |
| 65              | One-Cycle Slow-Freeze Test for Evaluating Aggregate Performance in Frozen Concrete (Proj. 4-3(1)), 21 p., \$1.40        | 91              | Effects of Deicing Salts on Water Quality and Biota—Literature Review and Recommended Research (Proj. 16-1), 70 p., \$3.20 |
| 66              | Identification of Frost-Susceptible Particles in Concrete Aggregates (Proj. 4-3(2)), 62 p., \$2.80                      | 92              | Valuation and Condemnation of Special Purpose Properties (Proj. 11-1(6)), 47 p., \$2.60                                    |
| 67              | Relation of Asphalt Rheological Properties to Pavement Durability (Proj. 9-1), 45 p., \$2.20                            | 93              | Guidelines for Medial and Marginal Access Control on Major Roadways (Proj. 3-13), 147 p., \$6.20                           |
| 68              | Application of Vehicle Operating Characteristics to Geometric Design and Traffic Operations (Proj. 3-10), 38 p., \$2.00 | 94              | Valuation and Condemnation Problems Involving Trade Fixtures (Proj. 11-1(9)), 22 p., \$1.80                                |
| 69              | Evaluation of Construction Control Procedures—Aggregate Gradation Variations and Effects (Proj. 10-2A), 58 p., \$2.80   | 95              | Highway Fog (Proj. 5-6), 48 p., \$2.40   |
| 70              | Social and Economic Factors Affecting Intercity Travel (Proj. 8-1), 68 p., \$3.00                                       | 96              | Strategies for the Evaluation of Alternative Transportation Plans (Proj. 8-4), 111 p., \$5.40                              |
| 71              | Analytical Study of Weighing Methods for Highway Vehicles in Motion (Proj. 7-3), 63 p., \$2.80                          | 97              | Analysis of Structural Behavior of AASHTO Road Test Rigid Pavements (Proj. 1-4(1)A), 35 p., \$2.60                         |
| 72              | Theory and Practice in Inverse Condemnation for Five Representative States (Proj. 11-2), 44 p., \$2.20                  | 98              | Tests for Evaluating Degradation of Base Course Aggregates (Proj. 4-2), 98 p., \$5.00                                      |
| 73              | Improved Criteria for Traffic Signal Systems on Urban Arterials (Proj. 3-5/1), 55 p., \$2.80                            | 99              | Visual Requirements in Night Driving (Proj. 5-3), 38 p., \$2.60  |
| 74              | Protective Coatings for Highway Structural Steel (Proj. 4-6), 64 p., \$2.80   | 100             | Research Needs Relating to Performance of Aggregates in Highway Construction (Proj. 4-8), 68 p., \$3.40                    |
| 74A             | Protective Coatings for Highway Structural Steel—Literature Survey (Proj. 4-6), 275 p., \$8.00                          | 101             | Effect of Stress on Freeze-Thaw Durability of Concrete Bridge Decks (Proj. 6-9), 70 p., \$3.60                             |
| 74B             | Protective Coatings for Highway Structural Steel—Current Highway Practices (Proj. 4-6), 102 p., \$4.00                  | 102             | Effect of Weldments on the Fatigue Strength of Steel Beams (Proj. 12-7), 114 p., \$5.40                                    |
| 75              | Effect of Highway Landscape Development on Nearby Property (Proj. 2-9), 82 p., \$3.60                                   | 103             | Rapid Test Methods for Field Control of Highway Construction (Proj. 10-4), 89 p., \$5.00                                   |
|                 |   | 104             | Rules of Compensability and Valuation Evidence for Highway Land Acquisition (Proj. 11-1), 77 p., \$4.40                    |

*Rep.*

*No. Title*

**105** Dynamic Pavement Loads of Heavy Highway Vehicle (Proj. 15-5), 94 p., \$5.00

**Synthesis of Highway Practice**

- 1** Traffic Control for Freeway Maintenance (Proj. 20-5, Topic 1), 47 p., \$2.20
- 2** Bridge Approach Design and Construction Practices (Proj. 20-5, Topic 2), 30 p., \$2.00
- 3** Traffic-Safe and Hydraulically Efficient Drainage Practice (Proj. 20-5, Topic 4), 38 p., \$2.20
- 4** Concrete Bridge Deck Durability (Proj. 20-5, Topic 3), 28 p., \$2.20



**THE NATIONAL ACADEMY OF SCIENCES** is a private, honorary organization of more than 700 scientists and engineers elected on the basis of outstanding contributions to knowledge. Established by a Congressional Act of Incorporation signed by President Abraham Lincoln on March 3, 1863, and supported by private and public funds, the Academy works to further science and its use for the general welfare by bringing together the most qualified individuals to deal with scientific and technological problems of broad significance.

Under the terms of its Congressional charter, the Academy is also called upon to act as an official—yet independent—adviser to the Federal Government in any matter of science and technology. This provision accounts for the close ties that have always existed between the Academy and the Government, although the Academy is not a governmental agency and its activities are not limited to those on behalf of the Government.

**THE NATIONAL ACADEMY OF ENGINEERING** was established on December 5, 1964. On that date the Council of the National Academy of Sciences, under the authority of its Act of Incorporation, adopted Articles of Organization bringing the National Academy of Engineering into being, independent and autonomous in its organization and the election of its members, and closely coordinated with the National Academy of Sciences in its advisory activities. The two Academies join in the furtherance of science and engineering and share the responsibility of advising the Federal Government, upon request, on any subject of science or technology.

**THE NATIONAL RESEARCH COUNCIL** was organized as an agency of the National Academy of Sciences in 1916, at the request of President Wilson, to enable the broad community of U. S. scientists and engineers to associate their efforts with the limited membership of the Academy in service to science and the nation. Its members, who receive their appointments from the President of the National Academy of Sciences, are drawn from academic, industrial and government organizations throughout the country. The National Research Council serves both Academies in the discharge of their responsibilities.

Supported by private and public contributions, grants, and contracts, and voluntary contributions of time and effort by several thousand of the nation's leading scientists and engineers, the Academies and their Research Council thus work to serve the national interest, to foster the sound development of science and engineering, and to promote their effective application for the benefit of society.

**THE DIVISION OF ENGINEERING** is one of the eight major Divisions into which the National Research Council is organized for the conduct of its work. Its membership includes representatives of the nation's leading technical societies as well as a number of members-at-large. Its Chairman is appointed by the Council of the Academy of Sciences upon nomination by the Council of the Academy of Engineering.

**THE HIGHWAY RESEARCH BOARD**, organized November 11, 1920, as an agency of the Division of Engineering, is a cooperative organization of the highway technologists of America operating under the auspices of the National Research Council and with the support of the several highway departments, the Federal Highway Administration, and many other organizations interested in the development of transportation. The purpose of the Board is to advance knowledge concerning the nature and performance of transportation systems, through the stimulation of research and dissemination of information derived therefrom.



**HIGHWAY RESEARCH BOARD**  
NATIONAL ACADEMY OF SCIENCES—NATIONAL RESEARCH COUNCIL  
2101 Constitution Avenue Washington, D. C. 20418

NON-PROFIT ORG.  
U.S. POSTAGE  
PAID  
WASHINGTON, D.C.  
PERMIT NO. 42970

ADDRESS CORRECTION REQUESTED

LIBRARIAN  
003901  
NATL ACADEMY SCIENCES  
P.O. STOP 44





1789930